



## 저작자표시-비영리-변경금지 2.0 대한민국

이용자는 아래의 조건을 따르는 경우에 한하여 자유롭게

- 이 저작물을 복제, 배포, 전송, 전시, 공연 및 방송할 수 있습니다.

다음과 같은 조건을 따라야 합니다:



저작자표시. 귀하는 원저작자를 표시하여야 합니다.



비영리. 귀하는 이 저작물을 영리 목적으로 이용할 수 없습니다.



변경금지. 귀하는 이 저작물을 개작, 변형 또는 가공할 수 없습니다.

- 귀하는, 이 저작물의 재이용이나 배포의 경우, 이 저작물에 적용된 이용허락조건을 명확하게 나타내어야 합니다.
- 저작권자로부터 별도의 허가를 받으면 이러한 조건들은 적용되지 않습니다.

저작권법에 따른 이용자의 권리는 위의 내용에 의하여 영향을 받지 않습니다.

이것은 [이용허락규약\(Legal Code\)](#)을 이해하기 쉽게 요약한 것입니다.

[Disclaimer](#)

**Doctor of Philosophy**

DEVELOPMENT OF TERMINAL SLIDING MODE  
CONTROL METHODS FOR UNCERTAIN  
NONLINEAR SYSTEMS AND THEIR  
APPLICATIONS TO ROBOTIC MANIPULATORS

The Graduate School of the University of Ulsan  
Department of Electrical Engineering  
Vo, Anh-Tuan

공학박사 학위논문

불확실 비선형 시스템의 터미널 슬라이딩 모드 제어  
방법 개발 및 로봇 매니퓰레이터에 대한 적용

DEVELOPMENT OF TERMINAL SLIDING MODE  
CONTROL METHODS FOR UNCERTAIN  
NONLINEAR SYSTEMS AND THEIR  
APPLICATIONS TO ROBOTIC MANIPULATORS

지도교수     강희준

이 논문을 공학박사 학위논문으로 제출함

2020 년 11 월

울산대학교 대학원  
전기전자보시스템공학부  
Vo, Anh-Tuan

Vo, Anh-Tuan 의 공 학박사학위 논문을 인준함

심사위원장 김한실



심사위원 조강현



심사위원 서영수



심사위원 강현덕



심사위원 강희준



울산대학교 대학원  
전기전자보시스템공학부  
2020 년 11 월





Doctor of Philosophy

Development of Terminal Sliding Mode  
Control Methods for Uncertain Nonlinear  
Systems and Their Applications to Robotic  
Manipulators



# Supervisory Committee

This certifies that the dissertation of Anh Tuan Vo is approved

**Professor Han-Sil Kim**

*Committe Chair*

**Professor Kang-Hyun Jo**

*Committe Member*

**Professor Young Soo Suh**

*Committe Member*

**Professor Hyun-Deok Kang**

*Committe Member*

**Professor Hee-Jun Kang**

*Committe Member*

**Department of Electrical Engineering**

**Ulsan, Korea**

**November 2020**



# VITA

Vo, Anh Tuan was born in Dong Nai City, Vietnam on April 22, 1984. He received his B.S. degree in Electrical Engineering from Danang University of Technology, DaNang city, Vietnam, in 2008. In March 2016, he began working full time towards his Ph.D. degree in the School of Electrical Engineering, University of Ulsan, Ulsan, Korea under the guidance of Professor Kang, Hee-Jun. Since then, he has concentrated researches in nonlinear control systems, intelligent controls, terminal sliding mode controls, fault-tolerant controls, adaptive controls, and robotic manipulators.



# Acknowledgments

It is my pleasure to take this chance to thank all those who made this thesis possible. First of all, I would like to express my hearty gratitude to my supervisor, Professor Kang, Hee-Jun whose insight and knowledge into the subject matter steered me through this research. thanks for all his constant support, continuous encouragement, technical instructions, beneficial suggestion, and great patience through my research work.

I would like to thank my doctoral committee members for their precious time and tremendously helpful feedback to evaluate the progress of my work.

I would like to acknowledge other faculty members of Electrical Engineering Department, Computer Engineering Department, and Mechanical Engineering Department at University of Ulsan for their dedicated help and valuable lectures during my academic work.

I would also like to thank all my colleagues in Intelligent Robotic System Lab, friends in University of Ulsan for the valuable discussion and help. The financial support of the BK21+ program is also gratefully acknowledged.

Last but not least my gratitude go to my dearest family and my wife Nguyen Ngoc Hoai An for their love, support, and concern.

Ulsan, November 2020

Anh Tuan Vo

# Abstract

The study reported in this thesis develops TSMCs for uncertain nonlinear systems and their applications to robotic manipulators that plays a very critical role in modern control technology. The central motivation of this thesis is to significantly improve trajectory tracking precision and to overcome the limitations of SMC-based methods and TSMC-based methods for several classes of uncertain nonlinear systems in presence of external disturbances and uncertain dynamics, or even undesired faults. These proposed control methodologies are developed based on SMC, SC, TSMC, NFTSMC, FLS, STA, NNs, observer-based controllers, and AC. The fundamental theoretical procedure is the foundation of the asymptotic stability based Lyapunov theory underpinned by the Lipschitz condition in the ordinary differential equations and finite time control method. The main applications of the proposed control methodologies are to apply to uncertain mechanical systems and robotic systems, in which external disturbances and uncertain dynamics are required to be bounded and to satisfy the suitable condition.

The proposed control algorithms are designed to achieve the following major advantages such as simple design, fast transient response, defined time convergence, robustness against uncertainties, high tracking accuracy, and stabilization with small steady-state errors. These proposed control algorithms can reject some/all of the limitations in conventional SMC or TSMC such as reaching phase glitch and the singularity problem. They can also avoid/ eliminate/ attenuate the effects of chattering behavior and the requirement for prior information about the upper bound of external disturbances and uncertain dynamics as well as the necessity for an exact mathematical model. Especially, some the designed controllers have estimate ability and fault tolerance.

The proposed control algorithms were applied for trajectory tracking control and FTC of parallel and serial robotic manipulators, or synchronization problem in motion controlling. The computer numerical simulation and experiment results are performed for 2-DOF planar parallel manipulator, 3-DOF planar parallel manipulator, 2-DOF serial robotic manipulator, and 3-DOF Puma560 robot manipulator to demonstrate the effectiveness and applicability of the proposed systems and to validate the theoretical derivation. Moreover, the designed control methodologies can be extended their applications to uncertain high-order MIMO systems.





# Contents

<b>Supervisory Committee</b>	<b>iii</b>
<b>VITA</b>	<b>v</b>
<b>Acknowledgments</b>	<b>vii</b>
<b>Abstract</b>	<b>i</b>
<b>Abbreviations</b>	<b>xiii</b>
<b>1 Introduction</b>	<b>1</b>
1.1 Introduction . . . . .	1
1.2 Objective of the Thesis . . . . .	4
1.3 Outline of the Thesis . . . . .	4
<b>2 A Chattering-Free, Adaptive, Robust Tracking Control Scheme for Non-linear Systems with Uncertain Dynamics</b>	<b>7</b>
2.1 Introduction . . . . .	7
2.2 Preliminaries and Problem Statements . . . . .	9
2.3 Design a Chattering-Free, Adaptive Robust Controller Using The PID-NFTSM Function . . . . .	10
2.4 Numerical Simulations . . . . .	16
2.5 Conclusions . . . . .	21
<b>Appendix A</b>	<b>27</b>
Design PID-SMC. . . . .	27
Design TSMC . . . . .	28
<b>3 Adaptive Neural Integral Full-Order Terminal Sliding Mode Control for an Uncertain Nonlinear System</b>	<b>31</b>
3.1 Introduction . . . . .	31
3.2 Problem Formulations . . . . .	32

iii

3.3	Design Synthesis of The Control System . . . . .	33
3.3.1	Design of IFOTSM Surface . . . . .	33
3.3.2	Design of IFOTSMC . . . . .	34
3.3.3	Radial Basis Function Neural Network . . . . .	35
3.3.4	Design of ARBFNN-IFOTSMC . . . . .	36
3.4	Numerical Simulation Results . . . . .	39
3.5	Conclusions . . . . .	43
<b>Appendix B</b>		<b>47</b>
	DESIGN RBFNN-SMC . . . . .	47
	DESIGN RBFNN-TSMC . . . . .	48
<b>4</b>	<b>An Adaptive Terminal Sliding Mode Control for Robot Manipulators with Non-singular Terminal Sliding Surface Variables</b>	<b>51</b>
4.1	Introduction . . . . .	51
4.2	Problem Formulations . . . . .	53
4.3	Design Procedure of the Control Algorithm . . . . .	55
4.3.1	Design of NTSM Surface . . . . .	55
4.3.2	Design of the Proposed Control Algorithm . . . . .	58
4.4	Numerical Simulation Results . . . . .	63
4.5	Conclusions . . . . .	69
<b>Appendix C</b>		<b>75</b>
<b>5</b>	<b>A New Finite-time Control Solution for Robotic Manipulators Based on Non-singular Fast Terminal Sliding Variables and the Adaptive Super-Twisting Scheme</b>	<b>79</b>
5.1	Introduction . . . . .	79
5.2	Problem Statement . . . . .	81
5.3	Design Procedure of the Control Scheme . . . . .	82
5.3.1	Design of NFTSM Variables . . . . .	83
5.3.2	Design of a New Finite-time Control Solution Based on NFTSM Variables and the ASTA . . . . .	85
5.4	Numerical Simulation Studies . . . . .	89
5.5	Conclusions . . . . .	92
<b>Appendix D</b>		<b>95</b>
	The design procedure of SMC . . . . .	95

The design procedure of NTSMC . . . . .	96
<b>6 An Adaptive Neural Non-Singular Fast-Terminal Sliding-Mode Control for Industrial Robotic Manipulators</b>	<b>99</b>
6.1 Introduction . . . . .	99
6.2 Problem Statements . . . . .	101
6.2.1 Radial Basis Function Neural Network . . . . .	101
6.2.2 Dynamic Model of the Robot Manipulator . . . . .	102
6.3 Design Procedure of the Control Strategy . . . . .	103
6.3.1 Design of NFTSM Variable . . . . .	103
6.3.2 Design an ANNFTSMC for Robotic Manipulators . . . . .	106
6.4 Numerical Simulation Studies . . . . .	111
6.5 Conclusions . . . . .	116
<b>7 Neural Integral Non-singular Fast Terminal Synchronous Sliding Mode Control for Uncertain 3-DOF Parallel Robotic Manipulators</b>	<b>119</b>
7.1 Introduction . . . . .	119
7.2 Problem Formulations and Preliminaries . . . . .	122
7.2.1 Dynamic Model Description of 3-DOF parallel robot manipulators .	122
7.2.2 Error Definitions in Synchronization Control . . . . .	124
7.3 Proposed NINFTSSMC Design . . . . .	125
7.3.1 Design of SINFTSM Surface . . . . .	125
7.3.2 Design of the proposed NINFTSSMC . . . . .	126
7.3.3 Feed Forward Neural Network Structural Design . . . . .	127
7.4 Numerical Simulation Studies . . . . .	131
7.5 Conclusions . . . . .	136
<b>Appendix E</b>	<b>141</b>
Design of the SMC . . . . .	141
Design of the SSMC . . . . .	142
Design of the NFTSMC . . . . .	142
<b>8 A Novel Fault-Tolerant Control Method for Robot Manipulators Based on Non-Singular Fast Terminal Sliding Mode Control and Disturbance Observer</b>	<b>145</b>
8.1 Introduction . . . . .	145
8.2 Statement of the Problem . . . . .	148
8.2.1 The Problem Statement . . . . .	148

8.3	FTCM for Robot Manipulators based on NFTSMC, DO, and STRCL . . .	150
8.3.1	Design of the new FTSMS . . . . .	150
8.3.2	Design of NFTSMC . . . . .	151
8.3.3	Stability Analysis of NFTSMC . . . . .	153
8.3.4	Design of DO . . . . .	153
8.3.5	Stability Analysis of DO . . . . .	154
8.3.6	Design of the proposed FTCM . . . . .	154
8.3.7	Stability Analysis of The Proposed FTCM . . . . .	155
8.4	Simulation Results and Discussion . . . . .	157
8.5	Conclusion . . . . .	164
<b>9</b>	<b>Conclusions and Future Works</b>	<b>165</b>
9.1	Conclusions . . . . .	165
9.2	Future works . . . . .	169
	<b>Publications</b>	<b>171</b>
	SCI (E) Journals . . . . .	171
	International Conference . . . . .	172
	<b>Bibliography</b>	<b>173</b>

# List of Figures

2.1	Tracking Positions in situation 1: (a) at Joint 1, (b) at Joint 2, and (c) at Joint 3. . . . .	19
2.2	Tracking Errors in situation 1: (a) at Joint 1, (b) at Joint 2, and (c) at Joint 3. . . . .	20
2.3	Control Input Signals in situation 1: (a) at Joint 1, (b) at Joint 2, and (c) at Joint 3. . . . .	21
2.4	Tracking Positions in situation 2: (a) at Joint 1, (b) at Joint 2, and (c) at Joint 3. . . . .	22
2.5	Tracking Errors in situation 2: (a) at Joint 1, (b) at Joint 2, and (c) at Joint 3. . . . .	23
2.6	Control Input Signals in situation 2: (a) at Joint 1, (b) at Joint 2, and (c) at Joint 3. . . . .	24
2.7	The response time of the estimating parameter. . . . .	24
2.8	The response time of the proposed Sliding Surfaces: (a) at Joint 1, (b) at Joint 2, and (c) at Joint 3. . . . .	25
3.1	The architecture of an RBFNN. . . . .	36
3.2	Block diagram of the proposed control scheme. . . . .	39
3.3	Block diagram of the proposed control scheme. . . . .	40
3.4	The desired trajectory and real trajectory of the end-effector. . . . .	43
3.5	The tracking errors of the end-effector in the X-direction. . . . .	44
3.6	The tracking errors of the end-effector in the Y-direction. . . . .	44
3.7	Control input signals: (a) RBFNN-SMC, (b) RBFNN-TSMC, and (c) ARBFNN-IFOTSMC. . . . .	45
3.8	Variation of the adaptive gains at Joint 1 and Joint 2. . . . .	45
4.1	Block diagram of the proposed control method. . . . .	64
4.2	3-DOF PUMA560 robot manipulator. . . . .	65
4.3	Tracking Positions with a sign function: (a) at Joint 1, (b) at Joint 2, and (c) at Joint 3. . . . .	66

4.4	Tracking Errors with a sign function: (a) at Joint 1, (b) at Joint 2, and (c) at Joint 3. . . . .	67
4.5	Control inputs with a sign function: (a) at Joint 1, (b) at Joint 2, and (c) at Joint 3. . . . .	68
4.6	Tracking positions with a saturation function: (a) at Joint 1, (b) at Joint 2, and (c) at Joint 3. . . . .	69
4.7	Tracking errors with a saturation function: (a) at Joint 1, (b) at Joint 2, and (c) at Joint 3. . . . .	70
4.8	Control inputs with a saturation function: (a) at Joint 1, (b) at Joint 2, and (c) at Joint 3. . . . .	71
4.9	Non-singular terminal sliding surfaces with a sign function: (a) at Joint 1, (b) at Joint 2, and (c) at Joint 3. . . . .	72
4.10	Non-singular terminal sliding surfaces with a saturation function: (a) at Joint 1, (b) at Joint 2, and (c) at Joint 3. . . . .	73
4.11	The response time of the estimating parameters with a sign function: (a) at Joint 1, (b) at Joint 2, and (c) at Joint 3. . . . .	73
4.12	The response time of the estimating parameters with a saturation function: (a) at Joint 1, (b) at Joint 2, and (c) at Joint 3. . . . .	74
5.1	3-DOF PUMA560 robot manipulator. . . . .	89
5.2	Tracking positions: (a) at Joint 1, (b) at Joint 2, and (c) at Joint 3 . . . .	91
5.3	Tracking errors: (a) at Joint 1, (b) at Joint 2, and (c) at Joint 3 . . . . .	92
5.4	Control input signals: (a) at Joint 1, (b) at Joint 2, and (c) at Joint 3 . . .	93
5.5	Sliding variables: (a) at Joint 1, (b) at Joint 2, and (c) at Joint 3. . . . .	94
6.1	Structure of radial basis function neural network. . . . .	101
6.2	Block diagram of the proposed control method. . . . .	111
6.3	Trajectory tracking positions: (a) at Joint 1, (b) at Joint 2, and (c) at Joint 3. . . . .	114
6.4	Trajectory tracking errors: (a) at Joint 1, (b) at Joint 2, and (c) at Joint 3.	115
6.5	Control input signals: (a) FNTSMC, (b) classical SMC, and (c) the suggested control methodology. . . . .	116
6.6	Time history of adaptive gain. . . . .	117
7.1	The kinematic illustration of the 3-DOF planar parallel robot manipulators.	123
7.2	The architecture of the FNN. . . . .	128
7.3	Diagram of the proposed control system. . . . .	132
7.4	3-D computer-aided design of the 3-DOF planar parallel robot manipulator.	134

7.5	The prescribed path and actual path of the end-effector under the four different control methods. . . . .	135
7.6	The response time of the end-effector in control error comparison (X-axis). . . . .	137
7.7	Response time of the end-effector in control error comparison (Y-axis). . . . .	137
7.8	Response time of the rotary angle in control error comparison. . . . .	138
7.9	Control errors of Joints (a) at Joint 1, (b) at Joint 2, and (c) at Joint 3. . . . .	138
7.10	Synchronization Error and Coupling Position Error of Joints (a) at Joint 1, (b) at Joint 2, and (c) at Joint 3. . . . .	139
7.11	Control input actions: (a) SMC, (b) SSMC, (c) NFTSMC, and (d) NIN-FTSSMC. . . . .	139
8.1	Diagram of the proposed FTCM. . . . .	155
8.2	Assumed and estimated value of disturbance, uncertainty, and fault: (a) at the first Joint, (b) at the second Joint, and (c) at the third Joint. . . . .	159
8.3	Tracking positions are provided by SMC, NFTSMC, and proposed controller: (a) at the first Joint, (b) at the second Joint, and (c) at the third Joint. . . . .	160
8.4	Positional control errors are provided by SMC, NFTSMC, and proposed controller: (a) at the first Joint, (b) at the second Joint, and (c) at the third Joint. . . . .	161
8.5	Velocity control errors are provided by SMC, NFTSMC, and proposed controller: (a) at the first Joint, (b) at the second Joint, and (c) at the third Joint. . . . .	162
8.6	Response time of the sliding mode manifolds: (a) at the first Joint, (b) at the second Joint, and (c) at the third Joint. . . . .	162
8.7	Control input signals are provided by SMC, NFTSMC, and proposed controller: (a) at the first Joint, (b) at the second Joint, and (c) at the third Joint. . . . .	163





# List of Tables

3.1	Parameters of the Mechanical Model . . . . .	41
3.2	Selected Parameters of the Control Methods. . . . .	42
5.1	Averaged tracking errors under the control signals of the control schemes. .	94
6.1	The control parameter selection for the varying control strategies. . . . .	113
6.2	Averaged tracking errors under the control signals of the control schemes. .	113
7.1	The parameters of the robotic system . . . . .	133
7.2	Parameters the different control systems . . . . .	136
8.1	Control parameter selection of control algorithms . . . . .	158
8.2	The average control errors are provided by control systems . . . . .	158



# Abbreviations

SISO	Single-Input/Single-Output
MIMO	Multi-Input/Multi-Output
AC	Adaptive Control
OC	Optimal Control
DOF	Degree of Freedom
RC	Robust Control
SC	Synchronization Control
PD	Proportional-Derivative
PID	Proportional-Integral-Derivative
ASL-PD	Adaptive Switching Learning-Proportional-Derivative
CTC	Computed Torque Control
DO	Disturbance Observer
VSS	Variable Structure System
BLT	Boundary Layer Technique
STA	Super Twisting Algorithm
ASTA	Adaptive Super Twisting Algorithm
NN	Neural Network
NNs	Neural Networks
RBFNN	Radial Basis Function NN
ARBFNN	Adaptive Radial Basis Function NN
FNN	Feed Forward NN
FL	Fuzzy Logic
FLS	Fuzzy Logic System
FLSs	Fuzzy Logic Systems
FTC	Fault-Tolerant Control
AFTC	Active FTC
PFTC	Passive FTC
SMC	Sliding Mode Control
SMCs	Sliding Mode Controls
ISMC	Integral SMC

## ABBREVIATIONS

---

TSM	Terminal Sliding Mode
TSMC	Terminal SMC
TSMCs	Terminal SMCs
ITSMC	Integral TSMC
ATSMC	Adaptive TSMC
FOSMC	Full-Order SMC
FOTSMC	Full-Order TSMC
TSMO	Terminal Sliding Mode Observer
HOSM	High-Order Sliding Mode
HOSMC	High-Order SMC
SOSMC	Second-Order SMC
IFOTSM	Integral Full-Order Sliding Mode
IFOTSMC	Integral Full-Order SMC
NTSM	Nonsingular TSM
NTSMC	Nonsingular TSMC
FTSM	Fast TSM
FTSMC	Fast TSMC
NFTSM	Nonsingular Fast TSM
NFTSMC	Nonsingular Fast TSMC
INFTSMC	Integral Nonsingular Fast TSMC
RBFNN-SMC	Radial Basis Function NN-SMC
RBFNN-TSMC	Radial Basis Function NN-TSMC
ARBFNN-IFOSMC	Adaptive Radial Basis Function NN-Integral Full-Order SMC
SINFTSM	Synchronous Integral Non-singular Fast TSM
PID-FTSM	Proportional-Integral-Derivative-Fast TSM
ANNFTSMC	Adaptive Neural Non-singular Fast Terminal Synchronous SMC
NINFTSSMC	Neural Integral Non-singular Fast Terminal Synchronous SMC
ANNFTSMC	Adaptive Neural Non-singular Fast TSMC

# Chapter 1

## Introduction

### 1.1 Introduction

The faster the development of modern production systems is, the greater the requirements are for speed, accuracy, reliability, and safety. Further, the more complex a technology is, the more it needs to adopt more advanced technical systems, especially in mechanical structures, sensor systems, electronic systems, and a significant drawback worthy of concern is the delay of the mechanical system generated by friction. If uncertainty parameters of a system are not accurately calculated and thoroughly resolved, they can reduce the system performance [1–3]. Moreover, almost real applications express nonlinear dynamic behavior, thus, the certainty is a subject that continues to challenge researchers and is of practical promising importance for instantaneous and extensive applications. To deal with all of the above constraints is a difficult challenge, requiring researchers to propose solutions for performance enhancement. In detail, robust controllers with the ability to counteract or compensate for undesirable terms disturbing the system needs to be developed. Once developed, the system's performance, reliability, and safety will be enhanced. The control problem of nonlinear systems is difficult for SISO. For MIMO nonlinear systems, the design of a controller is very complex due to the couplings among various inputs and outputs. In general view, it is a real challenge to handle because of the effects of external disturbances and uncertain dynamics, which is not easy to know in advance [1–3]. During recent decades, considerable research efforts have been devoted to investigating nonlinear control systems, and it has become an important topic. As reported in the literature, several control algorithms have been successfully adopted to control uncertain nonlinear systems. Noteworthy examples such as PD, PID controllers [4], [5], or CTC [6, 7] for robotic manipulators. Those mentioned controllers were highlighted as simple and monotonic methods for robot control. Unfortunately, those controllers do not exhibit good control performance of highly nonlinear and uncertain control systems. Ac-

cordingly, to handle external disturbances and uncertain dynamics and to improve the control performance, recently, many nonlinear control methods have been proposed for nonlinear systems such as the intelligent controllers [8–10], AC [11, 12], SC [13, 14], and SMC [15–17] have been cited. These methods have the capability to achieve the control target in spite of the existence of external disturbances and uncertain dynamics in the controlled systems. Among these control approaches, SMC has the best properties to control strongly against external disturbances and system uncertainties.

The SMC has been launched from VSS theory and developed by many researchers [18–20]. The SMC has been a useful and impressive robust control methodology to correct deficiency from any kind of uncertainties or external disturbances for both linear and nonlinear systems. Moreover, it has a fast dynamic response and a simple design. Consequently, it has been widely applied in various real applications such as motors, DC-DC converters, helicopter, aircraft, and robotic manipulators [21–24]. The design of SMC control method includes two steps [16, 18]: firstly perform suitable sliding surfaces that ensure the desired dynamics and then build up a discontinuous control principle that obligates the controlled variables to attain and maintain the sliding surface. Generally, the operation of the conventional SMC includes two phases. In the first phase, the system is forced to reach the sliding surface; this phase is usually called as reaching phase. Then, in the second phase, the system is kept to maintain in the sliding surface in infinite time. With the reaching phase in conventional SMC, the system state is driven from any initial values to approach the sliding surface, in which the system is formed into the sliding motion on the sliding surface. In this processing stage, the tracking control performance can be reduced because the invariance properties against parameter variations cannot be assumed during the reaching phase [18, 20]. Furthermore, this algorithm only stabilizes the system asymptotically in the sliding phase following a linear sliding manifold methodology. From this point of view, the controlled variables cannot obtain the desired values within a finite amount of time.

In 1990s, a new category of SMC called TSMC was originally published by Venkataraman and Gulati [25] and then advanced by Zhihong et al. [26] and Wu et al. [27]. Contrary to linear sliding surfaces, nonlinear sliding hyperplanes have exposed some advanced properties in terms of high robustness, fast transient response, high tracking positional accuracy, and finite-time convergence. Therefore, many applications have been developed based on the TSMC method such as robotic control [26, 28], motor control [29], DC-AC converter [30], spacecraft [31], TSMO [32], SOSMC, and so on [33–35]. Nonetheless, this control algorithm does not exhibit good convergence when the controlled variables are distant from the desired values. Specifically, the TSMC algorithm has encountered the singularity drawback that causes complex-value, exponent, and a greater control ef-

fort. Both of the above problems have been resolved in [36, 37]. The method in [38] not only avoids the singular problem, but also entirely eliminates the reaching phase problem [18, 20] regardless of the initial states. Therefore, the system always in the sliding mode, and the invariance property is guaranteed at all time. Moreover, the tracking error convergence time to zero in a finite time that can be set arbitrarily. However, this method has never been implemented in any real system.

Over the past decade, the finite-time control methods have attracted a great deal of attention in the research community. To increase convergence speed once the controlled variables are significantly different from the desired values, Yu and Zhihong [39] and Yang and Yang [36] presented FTSMC. However, both of the above methods still encounter the singularity drawback. So, to deal with this obstacle, several Non-singular TSM (NTSM) methods [36, 37, 40] based on TSMC have been established. These techniques give faster and finite-time convergence, and also impart advanced properties such as better robustness against external disturbances and uncertain dynamics and higher precision performance [41, 42]. Some control method have been proposed based on TSMC techniques [43, 44] in addition, the combination of asymptotic stability and homogeneous properties results in control methods with the finite-time stability [45, 46]. Practically, however, methods based on FTSMC or NTSMC have only addressed one limitation, skipping the other issues that limit conventional SMC. Therefore, NFTSMC [47–49] has been introduced. With NFTSMC, the system states achieve fast finite-time convergence and avoid the singularity problem. Another approach to improve the transient response of conventional SMC is to use ISMC [50, 51]. One of the goals of this research is to achieve both finite time convergences and fast transient response speed. Therefore, ISMC and TSMC can be combined to establish ITSMC [52, 53]. However, ITSMC still has the drawbacks of conventional SMC because the TSMC scheme is still included in the design of ITSMC.

It should be mentioned that two of the major challenges in designing a control system according to SMC or TSMC is knowing the bounds of modelling disturbances and dynamic uncertainties and computing an exact dynamic model, which is not known in advance for practical systems. However, in traditional SMC and traditional TSMC, the drawbacks have been considered individually or ignored. To approximate this unknown model, several computing attempts have been proposed, such as NNs [8, 54–56] and FLSs [57, 58], due to their approximation abilities. Moreover, many kinds of SMC and TSMC methods using adaptive control have been introduced for the estimation of sliding gains [59–61] because of the estimated ability of the adaptive laws without the need for unrealistic assumptions.

Chattering behavior is an undesired issue in practical applications that rely on TSMC, FTSMC, NTSMC, or NFTSMC with a high-frequency switching control term. This chat-



tering behavior affects the control performance or can lead to instability of the control system [20, 62, 63]. Therefore, some methods have been proposed to address this problem such as BLT [60, 64], HOSMC [64, 65], and DO [66] have been reported to cause a reduction in chattering. Some of the techniques cause the loss of robustness and degrade performance when eliminating the effects of the chattering behavior. And some other intelligent control-based techniques are even quite complicated and only suitable to simple systems. Accordingly, the selection of suitable methods in rejecting the chattering phenomenon is a significant challenge in this thesis.

## 1.2 Objective of the Thesis

Motivated by the above discussion, this thesis presents some advanced control methods for nonlinear systems in presence of uncertainties and external disturbances based on TSMC/ NN/ SC/ STA/ FOSMC/ ISMC/ HOSMC/ AC/ FTC and Lyapunov theory to solve the main purpose like "tracking error convergence/stabilization/error synchronization of zero" and simultaneously some/ all the following purposes:

- Avoiding the reaching phase problem as well as the singularity issue;
- Avoiding/Eliminating/Attenuating the effects of the chattering phenomena;
- Eliminating the need for a priori knowledge of the upper bounds of the system uncertainties and an exact mathematical model;
- Applying the proposed control methods for various robotic manipulators;
- Estimate ability and fault tolerance.
- Designing the active, robust, simple, and adaptive control methodologies for real applications.
- Extends the applicability for some classes of uncertain nonlinear systems;
- The convergence, the defined time stability, and the stability of the control system can be confirmed by the Lyapunov criterion.

## 1.3 Outline of the Thesis

The thesis is organized as follows

- **In chapter 1**, Introduction, the research objectives and contributions are outlined.

- **Chapter 2** introduces a chattering-free, adaptive, robust tracking control scheme for a class of second-order nonlinear systems with uncertain dynamics.
- **Chapter 3** reports an adaptive neural integral full-order terminal sliding mode control for an uncertain nonlinear system.
- **Chapter 4** presents an adaptive terminal sliding mode control for robot manipulators with non-singular terminal sliding surface variables.
- **Chapter 5** suggests a new finite-time control solution for robotic manipulators based on non-singular fast terminal sliding variables and the adaptive super-twisting scheme.
- **Chapter 6** proposes an adaptive neural non-singular fast-terminal sliding-mode control for industrial robotic manipulators.
- **Chapter 7** designs a neural integral non-singular fast terminal synchronous sliding mode control for uncertain 3-DOF parallel robotic manipulators.
- **Chapter 8** develops a novel fault-tolerant control method for robot manipulators based on non-singular fast terminal sliding mode control and disturbance observer.
- **Chapter 9** contains the conclusion of the thesis and further directions for future research are suggested.



## Chapter 2

# A Chattering-Free, Adaptive, Robust Tracking Control Scheme for Nonlinear Systems with Uncertain Dynamics

### 2.1 Introduction

As reported in the literature, several control algorithms have been successfully adopted to control uncertain nonlinear systems. Noteworthy examples such as PD or PID controllers [4, 5], intelligent controllers [8, 10], adaptive controllers [11, 12], synchronization controllers [13, 14], and SMC [15, 16] have been cited. Among these control approaches, SMCs have the best properties to control strongly against perturbations and system uncertainties. However, the classical SMC still has several weaknesses (e.g., significant chattering behavior due to the way to eliminate the chattering in SMC is still missing, undefined time convergence, and ineffective adaptation with rapid variations of perturbations or faults). To treat those obstacles, several recently improved controllers have been suggested and adopted using a nonlinear sliding function in place of a linear sliding function. Those control methodologies are called as TSMC [25, 26, 40]. Technically, TSMC carries a defined time convergence but attaches a singularity matter. Additionally, when the state variables are far from the desired path, TSMC provides a slower convergence time than SMC. To treat the singularity matter thoroughly, NTSMC was established and successfully adopted in an effort to control nonlinear systems [37, 67]. The remaining weak point was fast convergence time, which led to FTSMC being applied to controlling uncertain, nonlinear second-order systems [39, 68, 69]. Unfortunately, the methods based on NTSMC and FTSMC only treat specific systems. Hence, to treat both singularity and fast con-

vergence time simultaneously, NFTSMC system has been developed [36, 48, 59, 70]. As a special consideration, undesired chattering occurred in practical systems whenever all the above control approaches (e.g., TSMC, FTSMC, NTSMC, NFTSMC) were applied with a large control gain in the corresponding reaching control law. A large amount of chattering can limit the robust behavior of the control system and attenuate performance significantly. For this reason, several capable algorithms such as BLT [60, 64], HOSMC [64, 65], and DO [66] have been reported to cause a reduction in chattering. The weaknesses of the above-mentioned techniques sometimes present a challenging trade-off between chattering behavior attenuation and trajectory tracking accuracy, or else demanding an unrealistic magnitude of initial control input. However, there is an effective method to eliminate chattering behavior without the attenuation of the precision of the controlled system; the method applies an integral of a switching term to give chattering-free behavior such as FOSM [71]. It should be mentioned that all of the above-stated methods require prior knowledge of the bounded value of the uncertainties. To overcome this dependence, many kinds of SMC and TSMC methods using adaptive control have been introduced for the estimation of sliding gains [60, 61] because of the estimated ability of the adaptive laws without the need for unrealistic assumptions. Consequently, the motivation of our article is to propose a chattering-free, robust tracking control method that simultaneously eliminates the disadvantages of SMC and TSMC methods. In detail, a robust controller for uncertain nonlinear second-order systems must perform as follows:

- Removes the singularity weakness, provides fast convergence time, and states error with small oscillation along with robust behavior.
- Removes the dependency on essential knowledge of the upper bounded constants of unknown, uncertain terms.
- Gives chattering-free behavior without losing the robust behavior by adopting an integral of a switching term and an adaptive updating law.
- The convergence, the defined time stability, and the suggested adaptive adjustment law of the control system can be confirmed by the Lyapunov criterion.

The rest of this chapter is presented as follows. The problem statements facilitated for the proposed PID-NFTSM function and the control law are presented in Section 2. Section 3 explains the design process of the suggested control method to obtain the desired output performance and to reject chattering behavior from the classic SMC. In Section 4, the suggested control method is applied to an uncertain nonlinear system [72]. Its simulated performance tracks a desired path to be compared to those methods based on the classical SMC [15], [16] and TSMC [40] methods to investigate positional errors, convergence

time, rapid response, and chattering behavior reduction. Finally, Section 5 gives some conclusions of this paper.

## 2.2 Preliminaries and Problem Statements

This section presents some preliminary information and the problem statement, which is necessary for the controlling design.

**Lemma 2.1:** [41]: Suppose that a continuous positive-definite function  $\Lambda(t)$  satisfies the following inequality:

$$\dot{Z}(t) \leq -\alpha Z(t), \quad \forall t \geq t_0, \quad Z(t) \geq 0, \quad (2.1)$$

in which  $\alpha > 0, 0 < \gamma < 1$  are positive coefficients. Then for any given  $t_0, Z(t_0)$  the following inequality is satisfied:

$$Z^{1-\gamma}(t) \leq Z^{1-\gamma}(t_0) - \alpha(1-\gamma)(t-t_0), \quad t_0 \leq t \leq t_1 \quad (2.2)$$

with  $Z(t) = 0, \quad \forall t \geq t_1$ , and  $t_1$  is computed by:

$$t_1 = t_0 + \frac{1}{\alpha(1-\gamma)} Z^{1-\gamma}(t_0). \quad (2.3)$$

**Lemma 2.2:** ([73], Jensen's inequality). The following expression holds:

$$\left( \sum_{i=1}^k \vartheta_i^{\beta_2} \right)^{1/\phi_2} \leq \left( \sum_{i=1}^k \vartheta_i^{\beta_1} \right)^{1/\phi_1}, \quad 0 < \phi_1 < \phi_2 \quad (2.4)$$

with  $\vartheta_i \geq 0, 1 \leq i \leq k$ .

Consider the following general nonlinear second-order system with disturbances and/or uncertainties ([71]):

$$\begin{cases} \dot{X} = X_2 \\ \dot{X}_2 = \Pi(X, t) + \Phi(X, t) u^*(t) + \delta(X, t) \end{cases}, \quad (2.5)$$

where  $X = \begin{bmatrix} X_1 & X_2 \end{bmatrix} \in R^n$  denotes the system state vector.  $\Pi(X, t) \in R^n$  and  $\Phi(X, t) \in R^{n \times n}$  are dynamic nonlinear smooth functions that have the corresponding expression as  $\Pi(X, t) = \Pi_n(X, t) + \Delta\Pi(X, t)$  with  $\Pi(0) = 0$ , and  $\Phi(X, t) u^*(t) = \Phi(X, t) u(t) + \Phi(X, t) \Delta u(t)$ . The term  $\Delta\Pi(X, t)$  indicates structural variation of the dynamic system, which is an uncertain term. The term of  $\delta(X, t)$  indicates the disturbances and uncertainties,  $u^*(t)$  is the actuation control input,  $u(t)$  is the designed control

value, and  $\Delta u$  is the input signal uncertainty.

In this chapter, all anonymous terms are a function  $L(X, \Delta u, \delta, t)$ , which is termed as the lumped system uncertainty and defined as:

$$L(X, \Delta u, \delta, t) = \Delta \Pi(X, t) + \Phi(X, t) \Delta u(t) + \delta(X, t). \quad (2.6)$$

From Eq. (2.6), the dynamics system of Eq. (2.5) can be represented as:

$$\begin{cases} \dot{X}_1 = X_2 \\ \dot{X}_2 = \Pi_n(X, t) + \Phi(X, t) u(t) + L(X, \Delta u, \delta, t) \end{cases} \quad (2.7)$$

The central motivation of this chapter is that the proposed control system can provide high tracking precision for the system (2.7). Here, stated variables in Eq.(2.7) can approach the sliding function in a defined time. Then, those variables converge along the sliding function to the stable point regardless of disturbances and uncertainties.

The following constraint is assumed for the control approach design.

**Assumption 2.1:** There exists a known positive coefficient  $\Gamma_d$  such that the derivative of the  $\Omega(X, \Delta u, \delta, t)$  function is bounded by

$$\left\| \frac{d}{dt} (\Omega(X, \Delta u, \delta, t)) \right\| \leq \Gamma_d, \quad (2.8)$$

where  $\Omega(X, \Delta u, \delta, t)$  will be explained after Eq. (2.15).

## 2.3 Design a Chattering-Free, Adaptive Robust Controller Using The PID-NFTSM Function

This section presents the approach to investigate the good features of both the PID and the NFTSM controllers as well as adaptive controllers. First, a new form of the sliding function is introduced. Second, a control method with an integral of a switching term and an adaptive updating law is designed to obtain the desired performance.

In this work, the PID sliding function is proposed as:

$$\sigma = K_P s + K_I \int_0^t s d\phi + K_D \dot{s}, \quad (2.9)$$

where  $K_P$ ,  $K_I$ , and  $K_D$  correspond to the proportional, integral, and derivative gain, respectively.  $\sigma \in R^n$  is the PID-NFTSM sliding function,  $s$  is the first order NFTSM variable, and  $s$  is defined as [40]:

$$s = X_2 + \kappa_1 X_1 + \kappa_2 (X_1)^{[\varphi]} \quad (2.10)$$

with  $0 < \varphi < 1$  a constant,  $\kappa_1 = \text{diag} \begin{pmatrix} \kappa_{11} & \dots & \kappa_{1n} \end{pmatrix}$ ,  $\kappa_2 = \begin{pmatrix} \kappa_{21} & \dots & \kappa_{2n} \end{pmatrix}$ ,  $(X_1)^{[\varphi]} = \text{sign}(X_1)^\varphi$ , and  $\text{sign}(X_1)^\varphi$  is defined as [40]:  
 $\text{sign}(X)^{\varphi_i} = \begin{bmatrix} |X_1|^{\varphi_1} \text{sign}(X_1) & \dots & |X_n|^{\varphi_n} \text{sign}(X_n) \end{bmatrix}$ ,  $i = 1, 2$ .

The  $k^{\text{th}}$  element of the sliding surface of Eq. (2.10) is expressed as:

$$s_k = X_{2k} + \kappa_{1k} X_{1k} + \kappa_{2k} |X_{1k}|^{\varphi_k} \text{sign}(X_{1k}). \quad (2.11)$$

The first derivative of the first order NFTSM variable (2.10) is calculated as:

$$\dot{s}_k = \dot{X}_{2k} + \kappa_{1k} X_{2k} + \kappa_{2k} X_{qk}, \quad (2.12)$$

where

$$X_{qk} = \begin{cases} \varphi_k |X_{1k}|^{\varphi_k-1} \dot{X}_{1k}, & \text{if } X_{1k} \neq 0 \\ 0, & \text{if } X_{1k} = 0 \end{cases}. \quad (2.13)$$

Furthermore, Eq. (2.12) can be rewritten in the vector form as  $\dot{s} = \dot{X}_2 + \kappa_1 X_2 + \kappa_2 X_q$ .

The PID sliding function (2.9) is based on the NFTSM variables of Eq. (2.10), and thus it owns the values of both algorithms such as non-singularity, quick response, defined time convergence, robustness with uncertainties, and small steady-state error. These features are suitable and crucial for the controlling design because of its capability to compensate and quickly stabilize uncertain systems.

Substituting the derivative of the NFTSM variable (2.11) into (2.9) gives:

$$\sigma = K_P s + K_I \int s + K_D \left( \dot{X}_2 + \kappa_1 X_2 + \kappa_2 X_q \right). \quad (2.14)$$

Substituting system (2.7) into (2.14) gives:

$$\begin{aligned} \sigma &= K_P s + K_I \int s + K_D \left( \begin{matrix} \Pi_n(X, t) + \Phi(X, t) u(t) \\ + L(X, \Delta u, \delta, t) + \kappa_1 X_2 + \kappa_2 X_q \end{matrix} \right) \\ &= K_P s + K_I \int s + K_D (\kappa_1 X_2 + \kappa_2 X_q) + K_D (\Pi_n(X, t) + \Phi(X, t) u(t) + L(X, \Delta u, \delta, t)) \\ &= \Xi(X, s) + \Omega(X, \Delta u, \delta, t) + K_D (\Pi_n(X, t) + \Phi(X, t) u(t)) \end{aligned} \quad (2.15)$$

where  $\Xi(X, s) = K_P s + K_I \int s + K_D (\kappa_1 X_2 + \kappa_2 X_q)$ , and  $\Omega(X, \Delta u, \delta, t) = K_D L(X, \Delta u, \delta, t)$  indicates the anonymous terms in the system.



The following control law is developed for system (2.7) to achieve the desired performance:

$$u = -\Phi^*(X, t) (u_{eq} - K_D^{-1} u_{re}), \quad (2.16)$$

where  $\Phi^*(X, t) = \Phi^T(X, t) [\Phi(X, t) \Phi^T(X, t)]^{-1}$  is pseudoinverse. The equivalent control law is constructed as:

$$u_{eq} = K_D^{-1} \Xi(X, s) + \Pi_n(X, t), \quad (2.17)$$

and the continuous reaching control law is

$$\dot{u}_{re} + \Lambda u_{re} = \omega, \quad (2.18)$$

and

$$\omega = -(\Gamma_d + \Gamma_T + \rho) \text{sign}(\sigma). \quad (2.19)$$

The initial value of  $u_{re}(0)$  is chosen to be zero,  $\Gamma_d$  is a constant value which was stated as (2.8), and  $\rho$  is a small positive coefficient.  $\Lambda > 0$  and  $\Gamma_T$  are chosen such that:

$$\Gamma_T \geq \Lambda L_d. \quad (2.20)$$

**Remark 2.1:** From (2.18)–(2.19),  $u_{re}$  is obtained by adopting an integral of a switching term. Accordingly, the control system will achieve the chattering-free behavior.

Regarding the upper-bounded constants of both disturbances and uncertainties, an adaptive adjustment law is adopted to estimate those upper bounded values. Therefore, the system performance is always assured regardless of disturbances, uncertainties, and unknown terms influencing the control system.

A continuous adaptive reaching control law is designed as:

$$\dot{u}_{re} + \Lambda u_{re} = \omega_a, \quad (2.21)$$

and

$$\omega_a = -(\hat{\Gamma}_a + \rho) \text{sign}(\sigma), \quad (2.22)$$

in which  $\hat{\Gamma}_a$  is the estimating value of the bounded constants  $\Gamma_d + \Gamma_T$ .  $\hat{\Gamma}_a$  is adopted by the following updating law:

$$\dot{\hat{\Gamma}}_a = \frac{1}{\mu} |\sigma|, \quad (2.23)$$

where  $\mu > 0$  indicates the adaptive gain.

**Theorem 2.1:** The uncertain nonlinear system (2.7) will quickly approach the sliding function in the defined time and then stabilize around zero within the defined time  $(T \leq 2V_2^{1/2}(0)/\gamma)$ ; if the satisfactory sliding function is proposed as (2.9), the control input signal is designed as (2.16)–(2.17), (2.21)–(2.22) with its corresponding adaptive adjustment law as (2.23), and there exist a bounded constant satisfying the constraint (2.24).

$$\hat{\Gamma}_a \leq \Gamma^* \quad (2.24)$$

This means that the robustness stability and the desired performance of the system (2.7) are always assured.

**Proof:** Adopting the control laws (2.16)–(2.17) and (2.21)–(2.22) to the sliding function (2.15) obtains:

$$\begin{aligned} \sigma &= \Xi(X, s) + \Omega(X, \Delta u, \delta, t) + K_D \left( \begin{aligned} &\Pi_n(X, t) - \Phi(X, t) \Phi^*(X, t) \\ &\times (K_D^{-1} \Xi(X, s) + \Pi_n(X, t) - K_D^{-1} u_{re}) \end{aligned} \right). \quad (2.25) \\ &= u_{re} + \Omega(X, \Delta u, \delta, t) \end{aligned}$$

The result of Eq. (2.18) is presented by:

$$u_{re}(t) = (u_{re}(t_0) + (1/\Lambda)(\Gamma_d + \Gamma_T + \rho) \text{sign}(\sigma)) e^{t-t_0} - (1/\Lambda)(\Gamma_d + \Gamma_T + \rho) \text{sign}(\sigma). \quad (2.26)$$

Considering (2.20), (2.25)–(2.26) and the condition  $u_{re}(0) = 0$ , the following inequalities are achieved:

$$\Gamma_T \geq \Lambda L_d \geq \Lambda |u_{re}(t)|_{\max} \geq \Lambda |u_r(t)|. \quad (2.27)$$

With (2.21)–(2.22), the derivative of the sliding variable (2.25) gives:

$$\dot{\sigma} = -(\hat{\Gamma}_a + \rho) \text{sign}(\sigma) - \Lambda u_{re} + \dot{\Omega}(X, \Delta u, \delta, t). \quad (2.28)$$

The estimated error is described as:

$$\tilde{\Gamma}_a = \hat{\Gamma}_a - (K_d + K_T). \quad (2.29)$$

The positive-definite Lyapunov functional is defined as:

$$V_1 = \frac{1}{2}\sigma^T\sigma + \frac{\mu\tilde{\Gamma}_a^T\tilde{\Gamma}_a}{2}. \quad (2.30)$$

Utilizing the adaptive adjustment law (2.23), the derivative of sliding function (2.28), and the estimated error (2.29), the time derivative of the Lyapunov function (2.30) gives:

$$\begin{aligned} \dot{V}_1 &= \sigma^T\dot{\sigma} + \mu\left(\hat{\Gamma}_a - (\Gamma_d + \Gamma_T)\right)\dot{\hat{\Gamma}}_a \\ &\quad \sigma^T \begin{pmatrix} -\left(\hat{\Gamma}_a + \rho\right) \text{sign}(\sigma) \\ -\Lambda u_{re} + \dot{\Omega}(X, \Delta u, \delta, t) \end{pmatrix} + \left(\hat{\Gamma}_a - (\Gamma_d + \Gamma_T)\right)|\sigma| \\ &= (-\Lambda u_{re}\sigma - \Gamma_T|\sigma| - \rho|\sigma|) + \begin{pmatrix} \dot{\Omega}(X, \Delta u, \delta, t)\sigma \\ -\Gamma_d|\sigma| \end{pmatrix} \\ &\leq -\rho|\sigma| \end{aligned} \quad (2.31)$$

The parameter  $\rho$  is assigned to be greater than zero, and thus,  $\dot{V}_1$  will be negative. According to the Lyapunov principle, because  $\dot{V}_1$  is negative  $\sigma$  and  $\tilde{\Gamma}_a$  will reach zero. This means that the estimated value of  $\hat{\Gamma}_a$  has a bounded constant in Eq. (2.24). Next, it will be proved that system (2.7) will approach the sliding function within the defined time.

Consider the following Lyapunov function candidate as:

$$V_2 = \frac{\sigma^T\sigma}{2} + \frac{\xi\tilde{\Gamma}_a^T\tilde{\Gamma}_a}{2}, \quad (2.32)$$

where  $\xi$  is a positive coefficient. With Eq. (2.24), the time derivative of Eq. (2.32) is derived similarly to obtain  $\dot{V}_1$  as:

$$\begin{aligned} \dot{V}_2 &= \sigma^T\dot{\sigma} + \mu\left(\hat{\Gamma}_a - \Gamma^*\right)\dot{\hat{\Gamma}}_a \\ &= \sigma^T \begin{pmatrix} -\left(\hat{\Gamma}_a + \rho\right) \text{sign}(\sigma) \\ -\Lambda u_{re} + \dot{\Omega}(X, \Delta u, \delta, t) \end{pmatrix} + \frac{\xi}{\mu}\left(\hat{\Gamma}_a - \Gamma^*\right)|\sigma| \\ &= (-\Lambda u_{re}\sigma - \Gamma_T|\sigma| - \rho|\sigma|) + \left(\dot{\Omega}(X, \Delta u, \delta, t)\sigma - \Gamma_d|\sigma|\right) + \frac{\xi}{\mu}\left(\hat{\Gamma}_a - \Gamma^*\right)|\sigma| \\ &\leq -\rho|\sigma| + \frac{\xi}{\mu}\left(\hat{\Gamma}_a - \Gamma^*\right)|\sigma| \end{aligned} \quad (2.33)$$

Because the estimated value  $\hat{\Gamma}_a$  is bounded by  $\Gamma^*$ , 2.33 yields:

$$\dot{V}_2 \leq -\rho|\sigma| + \frac{\xi}{\mu}\left(\hat{\Gamma}_a - \Gamma^*\right)|\sigma| \leq 0. \quad (2.34)$$

The parameters  $\rho$ ,  $\xi$  are assigned to be greater than zero, so  $\dot{V}_2$  will be negative:

$$\begin{aligned}\dot{V}_2 &\leq -\rho|\sigma| - \rho_1 \left| \hat{\Gamma}_a - \Gamma^* \right| \\ &\leq -\sqrt{2}\rho \frac{|\sigma|}{\sqrt{2}} - \rho_1 \sqrt{\frac{2}{\xi}} \sqrt{\xi} \frac{\left| \hat{\Gamma}_a - \Gamma^* \right|}{\sqrt{2}}, \\ &\leq -\min \left\{ \sqrt{2}\rho, \rho_1 \sqrt{\frac{2}{\xi}} \right\} \cdot \left( \frac{|\sigma|}{\sqrt{2}} + \sqrt{\xi} \frac{\left| \hat{\Gamma}_a - \Gamma^* \right|}{\sqrt{2}} \right)\end{aligned}\quad (2.35)$$

where  $\rho_1 = \frac{\xi}{\mu} |\sigma|$ .

By using Jensen's inequality in Lemma 2.2 and assigning  $\Upsilon = \min \left\{ \sqrt{2}\rho, \rho_1 \sqrt{\frac{2}{\xi}} \right\}$ , the following inequality can be achieved:

$$\begin{aligned}\dot{V}_2 &\leq -\Upsilon \left( \frac{\sigma^T \sigma}{(\sqrt{2})^2} + \left( \sqrt{\xi} \right)^2 \frac{\left( \hat{\Gamma}_a - \Gamma^* \right)^T \left( \hat{\Gamma}_a - \Gamma^* \right)}{(\sqrt{2})^2} \right)^{\frac{1}{2}} \\ &\leq -\Upsilon V_2^{1/2}\end{aligned}\quad (2.36)$$

Based on Lemma 2.1, it can be proved that the sliding variables in Eq. 2.9 will approach the PID-NFTSM function within the defined time  $\left( T \leq 2V_2^{1/2}(0)/\Upsilon \right)$ . Additionally, when the PID-NFTSM function approaches zero, then the state variable system 2.10 will also stabilize around 0 in the defined time. This completes the proof of Theorem 2.1.

**Remark 2.2:** Once the PID-NFTSM function quickly approaches the stable point, the NFTSM variables will approach zero. For sliding variables defined by 2.10  $s = X_2 + \kappa_1 X_1 + \kappa_2 (X_1)^{[\varphi]}$ ,  $X_1$  is the system's terminal attractor. The attaining time  $t_s$  that is taken to travel from  $X_1(t_r) \neq 0$  to  $X_1(t_r + t_s) = 0$  has been defined as [40]:

$$t_s = \frac{1}{\kappa_1(1-\varphi)} \ln \frac{\kappa_1 V^{1-\varphi}(X_0) + \kappa_2}{\kappa_2}, \quad (2.37)$$

where  $V$  is an extended Lyapunov description of the finite-time convergence, which can be given by  $\dot{V}(X) + \kappa_1 V(X) + \kappa_2 V^\varphi(X) \leq 0$ ,  $0 < \varphi < 1$ , with  $t_r$  defined as in [36].

**Remark 2.3:** In practical systems, the parameter drift matter has usually happened under the updating law 2.23. Therefore, the bounded method is performed to set up the updating law as:

$$\dot{\hat{\Gamma}}_a = \begin{cases} 0 & \text{if } |\sigma| \leq v \\ \frac{1}{\mu} |\sigma| & \text{if } |\sigma| > v \end{cases}, \quad (2.38)$$

whereas  $v > 0$  is an arbitrary positive value.

**Remark 2.4:** In this work, two control methodologies (PID-SMC and TSMC [40] shown in Appendix) used a boundary layer technique [60, 64, 74] to reject chattering behavior. This technique adopts a saturation function in the reaching control law instead of adopting a function:

$$\text{sat} \left( \frac{\sigma}{\chi} \right) = \begin{cases} \text{sign}(\sigma) & \text{if } |\sigma| \geq \chi \\ \frac{\sigma}{\chi} & \text{if } |\sigma| < \chi \end{cases}, \quad (2.39)$$

in which  $\chi$  is a minor positive coefficient. However, in some cases, the tracking error accuracy will be significantly reduced by using this technique. This technique will be analyzed in detail with numerical simulations.

## 2.4 Numerical Simulations

The suggested control algorithm can be applied to many systems, such as robotic manipulators, magnetic levitation systems, chaotic systems, etc. In the simulation section, some position tracking computer simulations for a three-link robot manipulator have been performed to confirm the effectiveness of the proposed methodology.

For an  $n$ -link rigid robotic manipulator, the corresponding dynamic equation is given as ([75], [40]):

$$M(\theta) \ddot{\theta} + C_m(\theta, \dot{\theta}) \dot{\theta} + G(\theta) = \tau(t) + \tau_d(t), \quad (2.40)$$

where  $\theta(t)$ ,  $\dot{\theta}(t)$ ,  $\ddot{\theta}(t) \in R^n$  denote the system's state vectors.  $M(\theta) = M_0(\theta) + \Delta M(\theta) \in R^{n \times n}$  is the positive definite inertia matrix and is symmetric,  $C_m(\theta, \dot{\theta}) = C_0(\theta, \dot{\theta}) + \Delta C_m(\theta, \dot{\theta}) \in R^{n \times 1}$  indicates Coriolis and centrifugal forces,  $G(\theta) = G_0(\theta) + \Delta G(\theta) \in R^{n \times 1}$  indicates gravitational force terms,  $\tau(t) \in R^{n \times 1}$  indicates the control input torque, and  $\tau_d(t) \in R^{n \times 1}$  indicates unknown disturbances. Here  $M_0(\theta)$ ,  $C_0(\theta, \dot{\theta})$ ,  $G_0(\theta)$  are nominal terms, whereas  $\Delta M(\theta)$ ,  $\Delta C_m(\theta, \dot{\theta})$ ,  $\Delta G(\theta)$  are dynamic uncertainties. Then, Eq. (2.40) can be represented as:

$$M_0(\theta) \ddot{\theta} + C_0(\theta, \dot{\theta}) \dot{\theta} + G_0(\theta) = \tau(t) + \tau_d(t) + F(\theta, \dot{\theta}, \ddot{\theta}), \quad (2.41)$$

whereas  $F(\theta, \dot{\theta}, \ddot{\theta}) = -\Delta M(\theta) \ddot{\theta} - \Delta C_m(\theta, \dot{\theta}) \dot{\theta} - \Delta G(\theta) \in R^n$ .

Eq. (2.41) can be rewritten as:

$$\ddot{\theta} = M^{-1}(\theta) \left[ -C_0(\theta, \dot{\theta}) \dot{\theta} - G_0(\theta) \right] + M^{-1}(\theta) \tau(t) + M^{-1}(\theta) \left[ \tau_d(t) + F(\theta, \dot{\theta}, \ddot{\theta}) \right]. \quad (2.42)$$

To simplify the analysis and design in subsequent development, (2.42) can be expressed as:

$$\ddot{\theta} = \Pi(\theta, \dot{\theta}) + \Phi(\theta) \tau(t) + \delta(\theta, \dot{\theta}, t), \quad (2.43)$$

where  $\Pi(\theta, \dot{\theta}) = M^{-1}(\theta) \left[ -C_0(\theta, \dot{\theta}) \dot{\theta} - G_0(\theta) \right]$ ,  $\Phi(\theta) = M^{-1}(\theta)$ , and  $\delta(\theta, \dot{\theta}, t) = M^{-1}(\theta) \left[ \tau_d(t) + F(\theta, \dot{\theta}, \ddot{\theta}) \right]$ .  $u^*(t) = \tau(t)$  is assigned to be the control input torque, and  $X = [X_1, X_2]^T$  is the state variable vector with  $X_1, X_2$  corresponding to  $\theta, \dot{\theta} \in R^{n \times 1}$ . Therefore, the robotic dynamic system (2.43) can be presented as:

$$\begin{cases} \dot{X}_1 = X_2 \\ \dot{X}_2 = \Pi(X, t) + \Phi(X, t) u^*(t) + \delta(X, t) \end{cases}, \quad (2.44)$$

where  $\Phi(X, t) \in R^{n \times n}$  and  $\Pi(X, t)$  are the smooth nonlinear vector fields and  $\delta(X, t)$  represents the disturbances and uncertainties.

It can be seen that (2.44) is exactly the same form of the general nonlinear second-order system (2.5). Consequently, the proposed control method can be directly applied to the robotic system (2.40).

In this work some position tracking computer simulations for a three-link robot manipulator were performed to show practicality and effectiveness of the suggested methodology. The dynamical model and crucial parameters of the robot was reported previously [72]. All simulation studies were implemented in the MATLAB/Simulink software with a fixed-step size of  $10^{-3}s$ . The Robot was only inspected when the first three joints and the last three joints were locked.

The reference joint paths for the position tracking are

$$\begin{cases} \theta_{d1} = \cos\left(\frac{t}{5\pi}\right) - 1 \\ \theta_{d2} = \sin\left(\frac{t}{5\pi} + \frac{\pi}{2}\right) - 1 \\ \theta_{d3} = \sin\left(\frac{t}{5\pi} + \frac{\pi}{2}\right) - 1 \end{cases}. \quad (2.45)$$

Disturbances  $\tau_d(t)$  and the dynamic uncertainties  $F(\theta, \dot{\theta}, \ddot{\theta})$  at each joint are assumed to be

$$\begin{cases} \tau_{d1} + F_1 = 7.3 \sin(\dot{\theta}_1) + 7.5 \operatorname{sign}(3\dot{\theta}_1) + 6.2\dot{\theta}_1 \\ \tau_{d2} + F_2 = 6.5 \sin(\dot{\theta}_2) + 8.3 \operatorname{sign}(2\dot{\theta}_2) + 9.3\dot{\theta}_2 \\ \tau_{d3} + F_3 = 5.5 \sin(\dot{\theta}_3) + 3.5 \operatorname{sign}(2\dot{\theta}_3) + 4.5\dot{\theta}_3 \end{cases} \quad (2.46)$$

The initial state variables of the robotic system were chosen as  $\theta_1(0) = -0.5; \theta_2(0) = -0.5; \theta_3(0) = -0.5, \dot{\theta}_1(0) = \dot{\theta}_2(0) = \dot{\theta}_3(0) = 0$ . The parameters of the PID-FTSM function (2.9)-(2.10) were experimentally chosen as  $K_P = 15, K_I = 0.1, K_D = 0.5, \kappa_1 = 0.1, \kappa_2 = 2.2$ , and  $\varphi = 0.5$ . The controlling input (2.16)-(2.17) and (2.21)-(2.22) are experimentally chosen with  $\rho = 0.02, \Lambda = 0.5$  and other related parameters of the controller were chosen as same as the PID-FTSM function. The initial value of adaptive control law was chosen as  $\hat{\Gamma}_a(0) = 0, \mu = 0.05$ , and  $v = 0.01$  to compensate and quickly stabilize uncertain systems.

To present the best capability of the proposed control algorithm, its reference trajectory performances were compared with PID-SMC that was based on the classical SMC [15], [16] and the TSMC [40] to inspect positional errors, convergence time, rapid response, and chattering-free behavior. These controllers for comparison have been briefly presented in Appendix.

The parameters of the sliding function and the PID-SMC were suitably selected from the simulated experiment as  $K_P = 6.5, K_I = 0.01, K_D = 0.5, \Gamma = 10$ , and  $\rho = 0.02$  to similarly assign the initial control input magnitude and to achieve good simulation performance.

The parameters of the control method in [40] were suitably selected from the simulated experiment as  $\beta = \operatorname{diag}(0.5, 0.5, 0.5), \gamma = 1.67, k_1 = \operatorname{diag}(38, 65, 15), \Gamma = 10$ , and  $\rho = 0.02$  to similarly assign the initial control input magnitude and to achieve good simulation performance.

The examples were simulated in two situations to analyze the effectiveness of the control methods in terms of both their chattering phenomenon and positional accuracies.

Situation 1: Each of three control methods has the  $\operatorname{sign}(\cdot)$  function in its reaching control term.

Situation 2: The proposed control methodology has the  $\operatorname{sign}(\cdot)$  function in its the reaching control law compared to both PID-SMC and TSMC [40] adopting Remark 2.4.

In Situation 1, the reference tracking positions and the corresponding tracking errors of the first three joints under all controllers are shown in Figs. 2.1-2.2. From Figures 2.1-2.2, it can be observed that all three control methods can reach and maintain the desired path. However, TSMC [40] and PID-SMC are less robust against large assumption

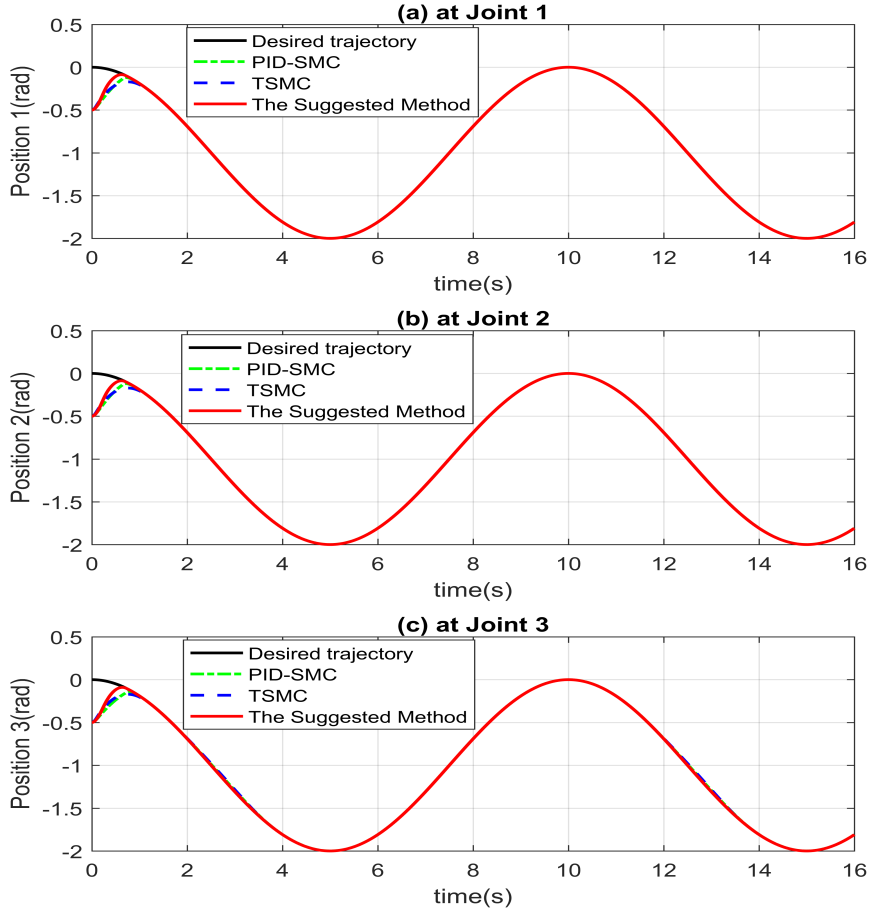


Figure 2.1: Tracking Positions in situation 1: (a) at Joint 1, (b) at Joint 2, and (c) at Joint 3.

uncertainties, while the suggested methodology has smaller position errors, (with  $10^{-6} - 10^{-7}$  rad) compared to both mentioned controllers, by an order of  $10^{-3} - 10^{-4}$  rad. Regarding chattering issues, a comparison of the control inputs in terms of the chattering phenomena is shown in Fig. 2.3. To obtain good simulation performance with the TSMC [40] and PID-SMC, the reaching control term required a large sliding gain that led to a significant chattering behavior. The chattering behavior from the suggested methodology was eliminated because this method applies a PID-FTSM function and an integral of a switching term.

The simulation results of Situation 2 verify the expected results illustrated in Figs. 2.4-2.5-2.6. In this Situation, the saturation function has been adopted in two control algorithms (PID-SMC and TSMC [40]) instead of the function to reduce the chattering phenomena while the proposed methodology still adopts an integral of a switching term.



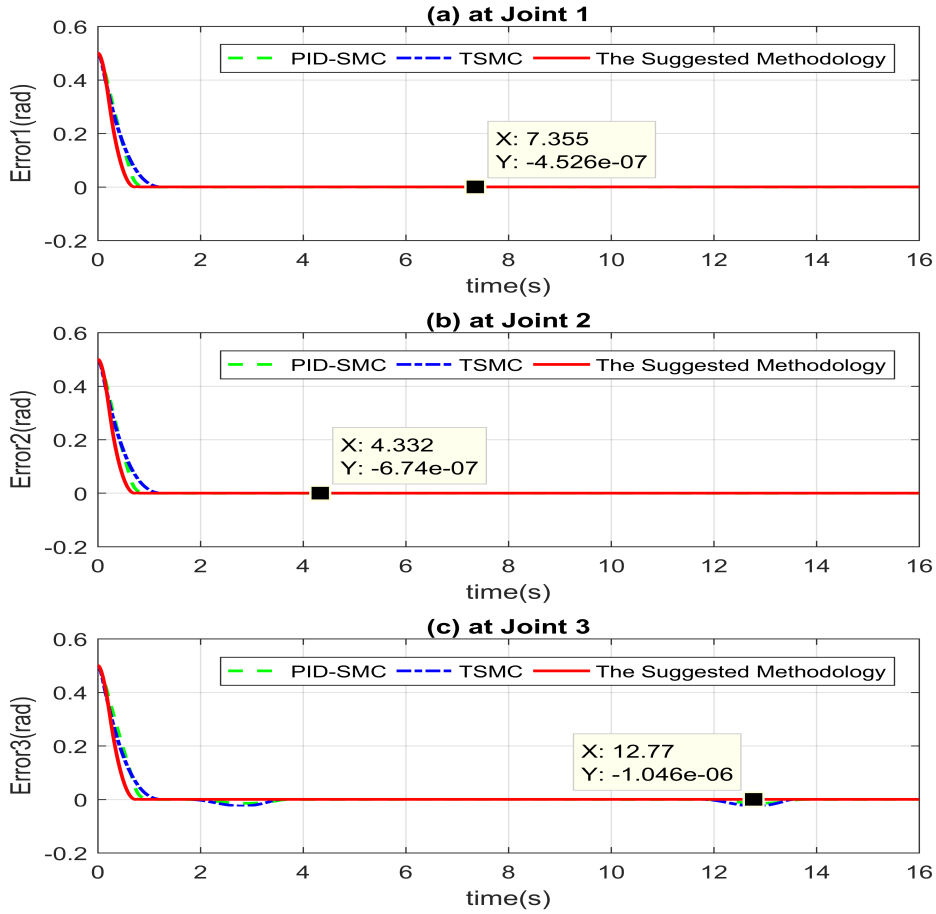


Figure 2.2: Tracking Errors in situation 1: (a) at Joint 1, (b) at Joint 2, and (c) at Joint 3.

However, as stated above, this technique decreases chattering behavior along with decreasing the robustness of the controllers. From Figs. 2.4-2.5-2.6, it is easy to anticipate that all three controllers will have a continuous control signal. It is noteworthy that the suggested control algorithm guarantees robustness with small steady-state errors, which are on the order of rad, and chattering-free behavior, while those of the other controllers are worse, on the order of  $10^{-2} - 10^{-3}$  rad.

Considering the bounded value of the uncertainties, the PID-SMC and TSMC control methods require prior knowledge of those bounded constants, but our suggested methodology does not. Therefore, the suggested methodology will be more optimal than the other controllers. The variations of the approximated value are shown in Fig. 2.7. It can be observed that the values are approximated according to the variation of the unknown disturbances and uncertainties, and these approximated values will approach constant

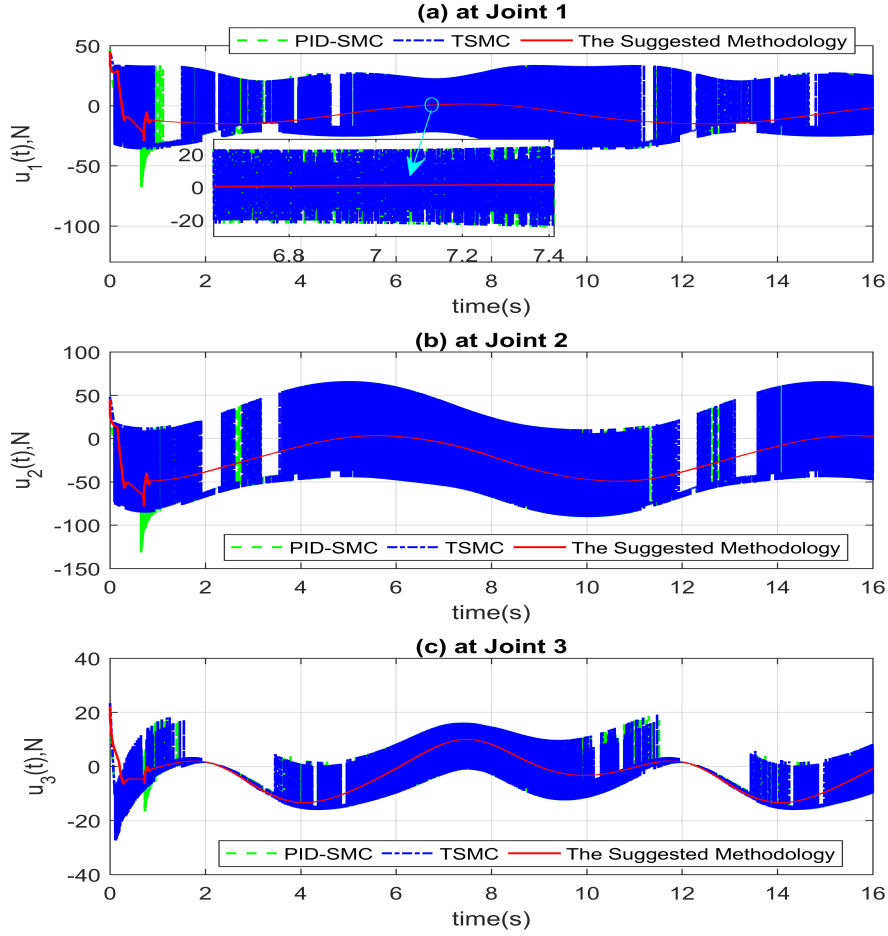


Figure 2.3: Control Input Signals in situation 1: (a) at Joint 1, (b) at Joint 2, and (c) at Joint 3.

values along with the state variables reach to the PID-FTSM function.

The response time of the sliding surface is shown in Fig. 2.8.

From the simulation results, it is concluded that the suggested control methodology exhibits the best performance among the three control methods, including higher position precision, lower steady-state error, faster response, and chattering-free behavior.

## 2.5 Conclusions

This chapter develops a chattering-free, adaptive, robust tracking control algorithm for a class of second-order nonlinear systems. In our algorithm, a novel sliding function, termed as a PID-NFTSM function, is proposed to incorporate the good features of both the PID and the NFTSM approaches. Our proposed sliding function inherits some ap-

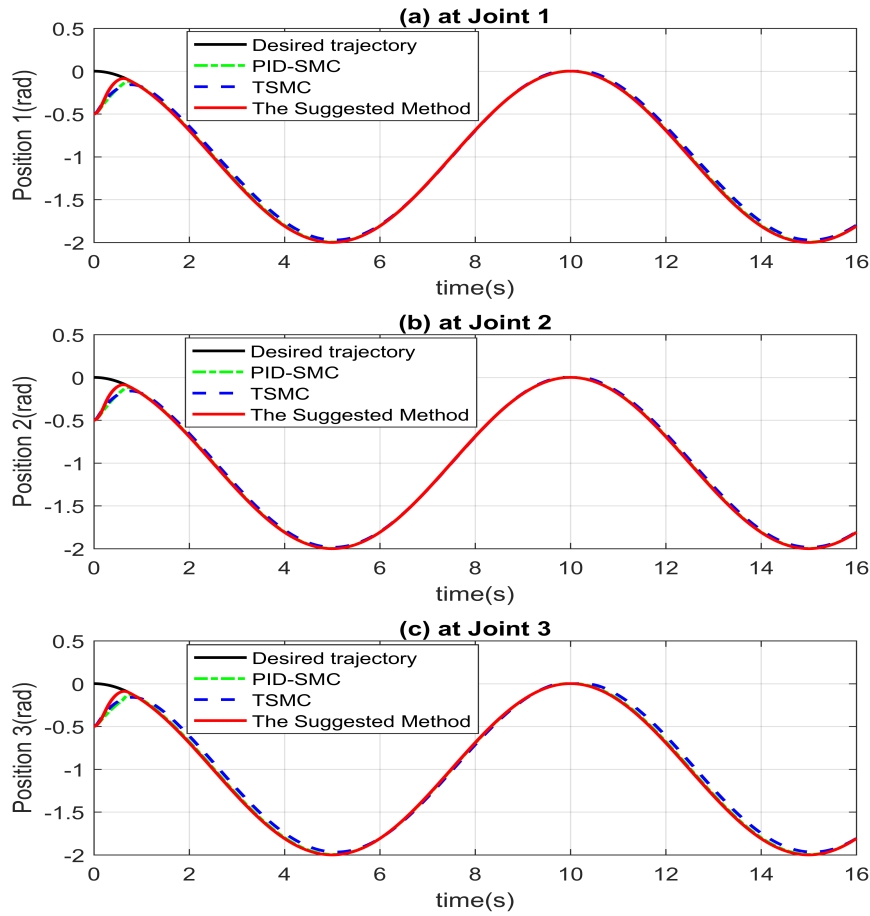


Figure 2.4: Tracking Positions in situation 2: (a) at Joint 1, (b) at Joint 2, and (c) at Joint 3.

proaches in the field such as PID, NTSMC, and FTSMC to achieve non-singularity, fast response, defined time convergence, and stability with small steady-state error. To obtain a chattering-free behavior, a continuous method (with an integral of a switching term and adaptive updating law) have been applied to compensate for all of the anonymous uncertain components in the control system, such as disturbances, unmodeled dynamics, nonlinearities, and unmeasurable noise. Accordingly, the suggested method does not need prior information about the bound values of those anonymous components, along with chattering-free behavior, compared to other controllers. The experimental results for a PUMA560 robot manipulator confirm that the suggested methodology has more capability to adapt to many uncertain nonlinear systems with high accuracy.

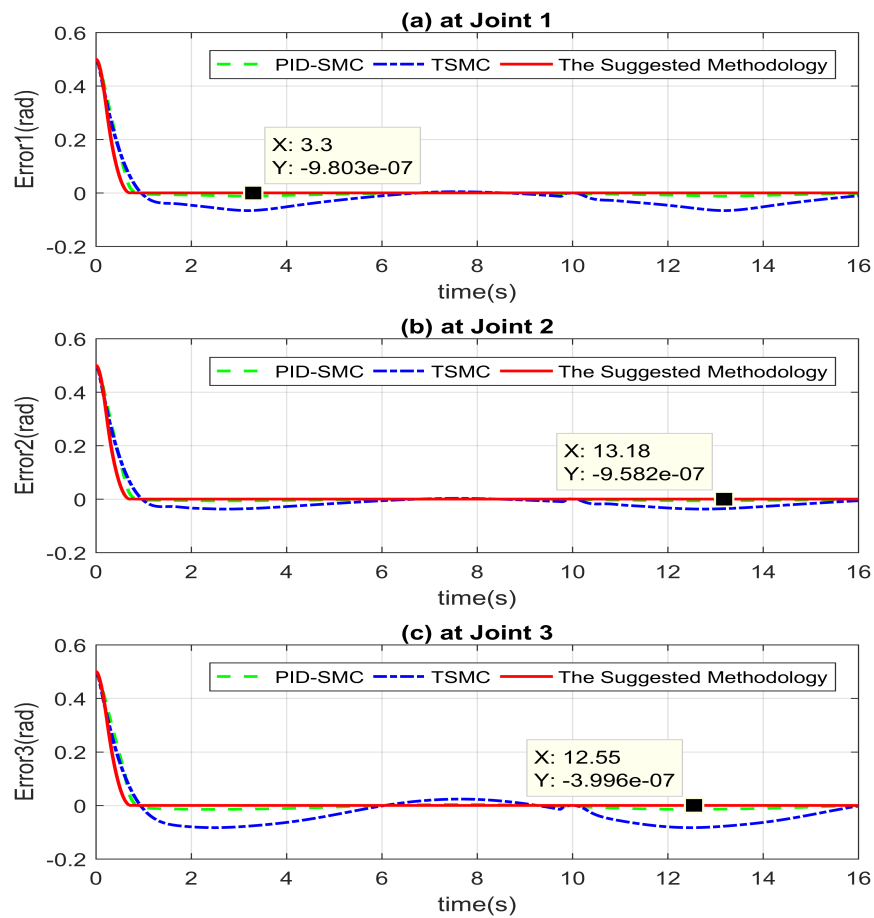


Figure 2.5: Tracking Errors in situation 2: (a) at Joint 1, (b) at Joint 2, and (c) at Joint 3.

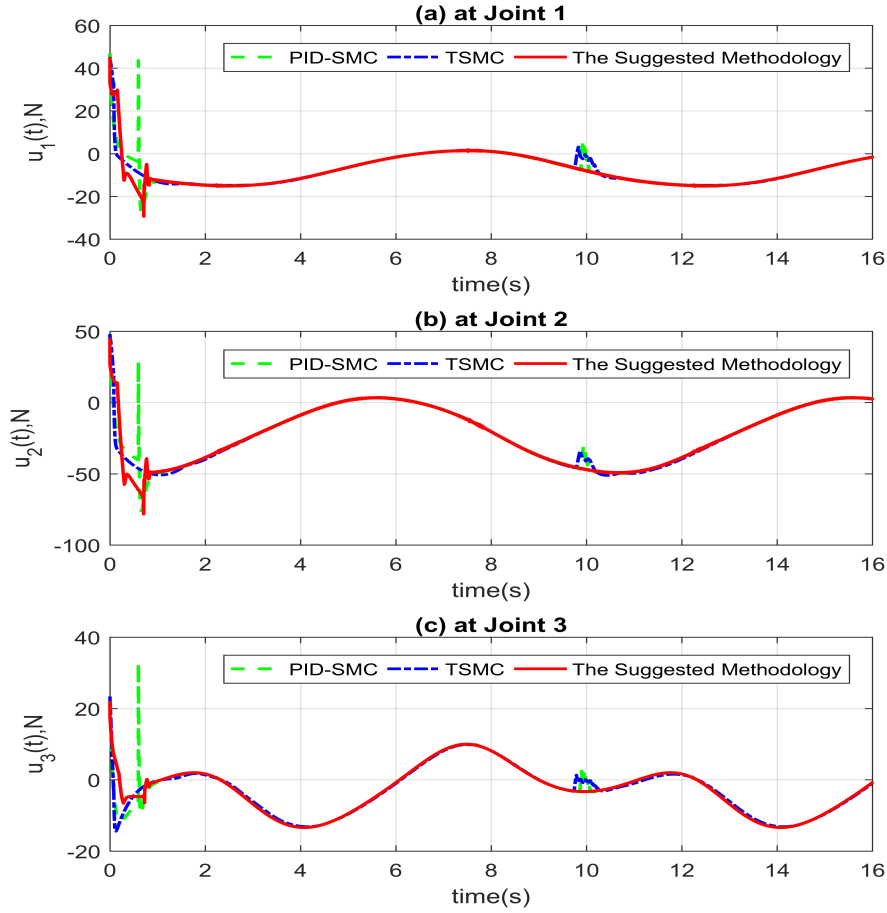


Figure 2.6: Control Input Signals in situation 2: (a) at Joint 1, (b) at Joint 2, and (c) at Joint 3.

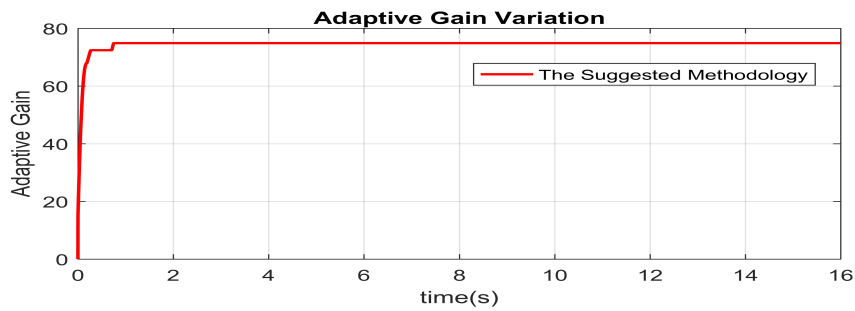


Figure 2.7: The response time of the estimating parameter.

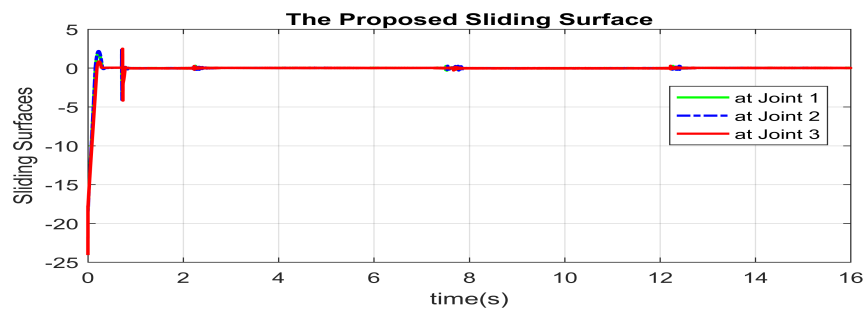


Figure 2.8: The response time of the proposed Sliding Surfaces: (a) at Joint 1, (b) at Joint 2, and (c) at Joint 3.



# Appendix A

## Design PID-SMC.

The PID based on SMC for the robotic manipulator (2.40) can be constructed as follows [15, 16].

Let  $e(t) = \theta(t) - \theta_d(t)$  be the tracking positional error,  $\theta_d$  with indicating the desired reference trajectory.

The following sliding function is considered as:

$$s = K_P e + K_I \int_0^t e(t) dt + K_D \dot{e}, \quad (\text{A.1})$$

in which  $K_p$ ,  $K_I$ , and  $K_D$  are proportional gain, integral gain, and derivative gain matrices, respectively. The time derivative of Eq. (A.1) is computed as:

$$\dot{s} = K_P \dot{e} + K_I e + K_D \ddot{e}. \quad (\text{A.2})$$

To guarantee that the controlled variables of Eq. (A.1) converge to sliding variables, the following relations must be satisfied:  $s = 0$  and  $\dot{s} = 0$ . The following proposed controller is based on the sliding mode design procedure:

$$\tau(t) = \tau_{eq}(t) + \tau_{re}(t). \quad (\text{A.3})$$

The term of the equivalent control of  $\tau_{eq}(t)$  holds the trajectory of the error state variables on the sliding function, and it is computed with  $\dot{s} = 0$  and  $\delta(\theta, \dot{\theta}, t) = 0$ .

$$\dot{s} = K_P \dot{e} + K_I e + K_D \left( \Pi(\theta, \dot{\theta}) + \Phi(\theta) \tau(t) + \delta(\theta, \dot{\theta}, t) - \ddot{\theta}_d \right) = 0. \quad (\text{A.4})$$

Therefore, the term of the equivalent control of  $\tau_{eq}(t)$  is designed as:

$$\tau_{eq}(t) = -\Phi^{-1}(\theta) \left( \left( \Pi(\theta, \dot{\theta}) - \ddot{\theta}_d \right) + \frac{K_I}{K_D} e + \frac{K_P}{K_D} \dot{e} \right), \quad (\text{A.5})$$

and the reaching control term is designed as:



$$\tau_{re}(t) = -\Phi^{-1}(\theta)(\Gamma + \rho) \operatorname{sign}(s). \quad (\text{A.6})$$

## Design TSMC

The control algorithm based on TSMC [40] for the robotic manipulator (2.40) can be constructed as follows [40, 76]. Let  $e(t) = \theta(t) - \theta_d(t)$  be the tracking positional error, with  $\theta_d$  indicating the desired reference trajectory. The sliding function can be considered as:

$$s = e + \beta \operatorname{sig}(\dot{e})^\gamma, \quad (\text{A.7})$$

where  $\beta = \operatorname{diag}(\beta_1, \beta_2, \dots, \beta_n)$  with  $\beta_i > 0$  and  $1 < \gamma < 2$  and  $\operatorname{sig}(\dot{e})^\gamma = (|\dot{e}_1|^\gamma \operatorname{sign}(\dot{e}_1), |\dot{e}_2|^\gamma \operatorname{sign}(\dot{e}_2), \dots, |\dot{e}_n|^\gamma \operatorname{sign}(\dot{e}_n))$ .

The time derivative of Eq. (A.7) is computed as:

$$\dot{s} = \dot{e} + \beta\gamma |\dot{e}|^{\gamma-1} \ddot{e}. \quad (\text{A.8})$$

To guarantee that the controlled variables of Eq. (A.7) converge to sliding variables, the following relations must be satisfied:  $s = 0$  and  $\dot{s} = 0$ .

The following proposed controller is based on the sliding mode design procedure:

$$\tau(t) = \tau_{eq}(t) + \tau_{re}(t). \quad (\text{A.9})$$

The term of the equivalent control of  $\tau_{eq}(t)$  holds the trajectory of the error state variables on the sliding function, and it is computed with  $\dot{s} = 0$  and  $\delta(\theta, \dot{\theta}, t) = 0$ .

$$\begin{aligned} \dot{s} &= \dot{e} + \beta\gamma |\dot{e}|^{\gamma-1} \ddot{e} \\ &= \dot{e} + \beta\gamma |\dot{e}|^{\gamma-1} \left( \Pi(\theta, \dot{\theta}) + \Phi(\theta) \tau(t) + \delta(\theta, \dot{\theta}, t) - \ddot{\theta}_d \right). \end{aligned} \quad (\text{A.10})$$

Therefore, the term of  $\tau_{eq}(t)$  the equivalent control of is designed as:

$$\tau_{eq}(t) = -\Phi^{-1}(\theta) \left( \Pi(\theta, \dot{\theta}) - \ddot{\theta}_d + \frac{\beta^{-1}}{\gamma} |\dot{e}|^{2-\gamma} \right), \quad (\text{A.11})$$

and the fast TSM reaching control term is designed as:

$$\tau_{re}(t) = -\Phi^{-1}(\theta) (k_1 s + (\Gamma + \rho) \operatorname{sign}(s)) \quad (\text{A.12})$$

in which  $k_1 = \operatorname{diag}(k_{11}, k_{12}, k_{13})$ ,  $k_{1i}$ ,  $\Gamma$ , and  $\rho$  are positive coefficients.

Therefore, the TSM controller has the control input as:

$$\tau(t) = -\Phi^{-1}(\theta) \left( \Pi(\theta, \dot{\theta}) - \ddot{\theta}_d + \frac{\beta^{-1}}{\gamma} |\dot{e}|^{2-\gamma} + k_1 s + (\Gamma + \rho) \text{sign}(s) \right). \quad (\text{A.13})$$



## Chapter 3

# Adaptive Neural Integral Full-Order Terminal Sliding Mode Control for an Uncertain Nonlinear System

### 3.1 Introduction

The increasingly rigorous performance requirements of industrial applications highlight the importance of enhanced control systems developed for uncertain nonlinear systems that are normally subject to various nonlinearities, external disturbances, and uncertainties. Studies on the class of general nonlinear second-order systems have proposed many control methods focused on attaining the desired performance against various uncertainties, including external disturbances. SMC has been validated to provide high robustness against uncertainties and disturbances for nonlinear systems [77, 78]. Accordingly, SMC is usually applied to industrial application systems [8, 15, 16, 58]. Nonetheless, several challenges of the traditional SMC still exist such as the requirement of an exact dynamic model, singularity, chattering occurrence, and unidentified convergence time. Various studies have focused on treating these challenges. For the system state variables to reach the prescribed SMC surface within a definite time, TSMC, based on the nonlinear sliding mode function, has been used [27, 79]. However, the TSMC convergence time is slower than the traditional SMC convergence time, and still encompasses a singularity phenomenon. To handle convergence time and a singularity glitch, numerous FTSMC [68, 69] and NTSMC [80] systems have been applied to magnetic levitation systems [81], chaos control [67, 82], and robotic manipulators [49, 83, 84]. Private control manners such as FTSMC or NTSMC have only focused on the resolution of individual weaknesses or neglected to handle the other weaknesses of the traditional SMC. For that reason, NFTSMC has been developed for controlling uncertain nonlinear second-order

systems [8, 83, 85–87]. NFTSMC can deal with several drawbacks of the traditional SMC or other control systems based on TSMC. Nonetheless, chattering is not removed by applying a high-frequency reaching control term to the control input of the above systems, which include TSMC, FTSMC, NTSMC, and NFTSMC. As a result, several useful control systems have been proposed by applying FOSMC [71, 88], or HOSMC [64, 89].

Two of the major challenges in designing a control system according to SMC or TSMC is knowing the bounds of modelling disturbances and dynamic uncertainties and computing an exact dynamic model, which is not known in advance for practical systems. To approximate this unknown model, several computing attempts have been proposed, such as NNs [8, 54–56] and FLSs [57, 58], due to their approximation abilities. In traditional SMC and traditional TSMC, the drawbacks have been considered individually or ignored. In response, this work focuses on the synchronized resolve of SMC and TSMC drawbacks, including the condition for an exact dynamic model, the existence of a singularity, chattering occurrence, and finite-time convergence.

Consequently, the objective is to develop a controller for the class of general nonlinear second-order systems. The suggested system has the following major advantages: 1) it inherits the benefits of RBFNN and IFOSMC, including good performance with minimum position errors, robustness against uncertainties, and work without a precise dynamic model; 2) it consists of a control input system with chattering reduction; 3) compared to RBFNN-SMC and RBFNN-TSMC, ARBFNN-IFOSMC provides better performance and stronger resistance against disturbances and uncertainties; and 4) stability and tracking error convergence of the class of general nonlinear second-order systems was fully confirmed by the Lyapunov benchmark.

The remainder of this chapter is arranged as follows. After the introduction, the preliminaries and problem formulations are stated, followed by the design approach for the proposed controller, where the proposed system is applied to allow position pathway tracking control simulation for a 2-DOF parallel manipulator. The tracking performance is compared with those of the RBFNN-SMC and RBFNN-TSMC to evaluate the effectiveness of the proposed control system. Finally, conclusions are provided.

## 3.2 Problem Formulations

A class of general nonlinear second-order systems is considered as follows:

$$\begin{cases} \dot{x}_1 = x_2 \\ \dot{x}_2 = F(x, t) + D(x, t) + Q(x, t) u_{in} \end{cases}, \quad (3.1)$$

where  $x = \begin{bmatrix} x_1 & x_2 \end{bmatrix}^T$  represents the system state vector,  $F(x, t) \in R^{n \times 1}$ ,  $Q(x, t) \in R^{n \times n}$  are the smooth nonlinear vector fields, and  $D(x, t) \in R^{n \times 1}$  represents the disturbances and uncertainties.

The target of this chapter is to develop a control system such that the controlled variables of the system follow the designated trajectory with minimum position errors, robustness against uncertainties, and work without a precise dynamic model. Accordingly, the tracking positional error is defined as:

$$e_1 = x_1 - x_d. \quad (3.2)$$

The following assumption is essential for developing the control algorithm in the next part.

**Assumption 3.1:** We assume that the lumped uncertain components are first-order differentiable and have the existence of the defined positive constant satisfying the following condition:

$$\left\| \dot{D}(x, t) \right\| \leq \Xi \quad (3.3)$$

where  $\Xi$  is the defined positive constant.

### 3.3 Design Synthesis of The Control System

In this part, a control method is developed for the class of general nonlinear second-order systems, which is described by in the two following steps.

#### 3.3.1 Design of IFOTSM Surface

First, with the tracking position error from Eq. (3.2), an IFOTSM surface is proposed as:

$$s = \dot{e}_2 + \int_0^t \left( \omega_1 e_1^{[\mu_1]} + \omega_2 e_2^{[\mu_2]} \right) d\sigma, \quad (3.4)$$

where  $s = [s_1, s_2, \dots, s_n]^T \in R^{n \times 1}$  is a sliding variable,  $\omega_1, \omega_2$  are positive constants,  $0 < \mu < 1$ ,  $\mu_2 = 2\mu_1 / (1 + \mu_1)$ ,  $e_1 = [e_{11}, e_{12}, \dots, e_{1n}]^T \in R^{n \times 1}$  represents the tracking position errors,  $e_2 = [e_{21}, e_{22}, \dots, e_{2n}]^T \in R^{n \times 1}$  represents the tracking velocity error,  $\dot{e}_2$  is the time derivative of  $e_2$ , and  $e^{[\mu(\bullet)]}$  is defined as follows:

$$e^{[\mu(\bullet)]} = |e|^{\mu(\bullet)} \text{sign}[e] \quad (3.5)$$

where  $\mu_1 > 0$ ,  $\mu_2 > 0$  and  $\text{sign}[e] = \begin{cases} 1 & \text{if } e > 0 \\ -1 & \text{if } e < 0 \\ 0 & \text{if } e = 0 \end{cases}$ .

With Eq. (3.2), Eq. (3.1) can be expressed in the following error state space form as:

$$\begin{cases} \dot{e}_1 = e_2 \\ \dot{e}_2 = F(x, t) + D(x, t) + Q(x, t) u_{in} - \ddot{x}_d \end{cases}. \quad (3.6)$$

Substituting Eq. (3.6) into the IFOTSM surface (3.4) yields:

$$s = F(x, t) + D(x, t) + Q(x, t) u_{in} - \ddot{x}_d + \int_0^t \left( \omega_1 e_1^{[\mu_1]} + \omega_2 e_2^{[\mu_2]} \right) d\sigma. \quad (3.7)$$

### 3.3.2 Design of IFOTSMC

For system (3.1) to operate with quality performance, the control input system is designed as follows:

$$u_{in} = -Q^{-1}(x, t) (u_{eq} + u_{sw}). \quad (3.8)$$

Here, the equivalent control term is designed as:

$$u_{eq} = F(x, t) - \ddot{x}_d + \int_0^t \left( \omega_1 e_1^{[\mu_1]} + \omega_2 e_2^{[\mu_2]} \right) d\sigma, \quad (3.9)$$

and the switching control term is designed as:

$$\dot{u}_{sw} = (\Xi + \varpi) \text{sign}(s). \quad (3.10)$$

Accordingly, the following theorem is formed to complete the proof.

**Theorem 3.1:** Consider a class of general nonlinear second-order systems (3.1). If the proposed control input system is designed for system (3.1) as Eqs. (3.8)–(3.10), then system (3.1) is guaranteed to have stability.

**Proof:** Applying the control input system (3.8)–(3.10) to Eq. (3.7) gives:

$$\begin{aligned} s &= F(x, t) + D(x, t) - \left( u_{sw} + F(x, t) - \ddot{x}_d + \int_0^t \left( \omega_1 e_1^{[\mu_1]} + \omega_2 e_2^{[\mu_2]} \right) d\sigma \right) - \ddot{x}_d + \int_0^t \left( \omega_1 e_1^{[\mu_1]} + \omega_2 e_2^{[\mu_2]} \right) d\sigma \\ &= D(x, t) - u_{sw} \end{aligned} \quad (3.11)$$

Taking the time derivative of Eq. (3.11) gives:

$$\begin{aligned}\dot{s} &= \dot{D}(x, t) - \dot{u}_{sw} \\ &= \dot{D}(x, t) - (\Xi + \varpi) \text{sign}(s)\end{aligned}\quad (3.12)$$

Consider the following Lyapunov function as follows:

$$L = \frac{s^T s}{2}. \quad (3.13)$$

With the result of Eq. (3.12), the time derivative of Eq. (3.13) is derived as:

$$\begin{aligned}\dot{L} &= s^T \dot{s} \\ &= s^T \left( \dot{D}(x, t) - (\Xi + \varpi) \text{sign}(s) \right) \\ &= \left( \dot{D}(x, t) s - \Xi |s| \right) - \varpi |s| \leq -\varpi |s|\end{aligned}\quad (3.14)$$

Based on Eq. (3.14), the requirement for the Lyapunov stability benchmark [90] is guaranteed, wherein proof of stability is confirmed.

Nonetheless, the design approach requires an exact dynamic mode of  $F(x, t)$  and satisfies Assumption 1. It is not trivial to precisely estimate dynamic uncertainties, external disturbances, and provide an exact dynamic function in the control system. To handle these challenges, a robust control approach will be developed for the class of general nonlinear second-order systems based on an IFOTSM surface and RBFNN. Here, two nonlinear terms in the IFOTSM surface and an adaptive compensator will be used to compensate for the effects of the dynamic uncertainties, disturbances, and error from the RBFNN, while an RBFNN will be utilized to approximate an unknown dynamic model.

### 3.3.3 Radial Basis Function Neural Network

RBFNNs have major advantages, including a highly parallel structure, robust tolerance to external disturbances and uncertainties, nonlinear function approximation [91], and online adaptation capability. Compared to other neural networks, RBFNN has a simpler and quicker convergence rate. An RBFNN includes three layers, input, hidden and output, which are shown in Figure. 3.1

The following RBFNN output is defined as:

$$H(\mu) = \theta^T \Psi(\mu) + \varepsilon(\mu), \quad (3.15)$$

where  $\mu \in R^n$  and  $H(\mu)$  correspond to the RBFNN input and output.  $\theta^T \in R^{n \times m}$  represents the weight matrix linking the hidden layer and the output layer,  $\Psi(\mu)$  represents the nonlinear function of the hidden nodes, and  $\varepsilon(\mu) \in R^n$  represents an approximation



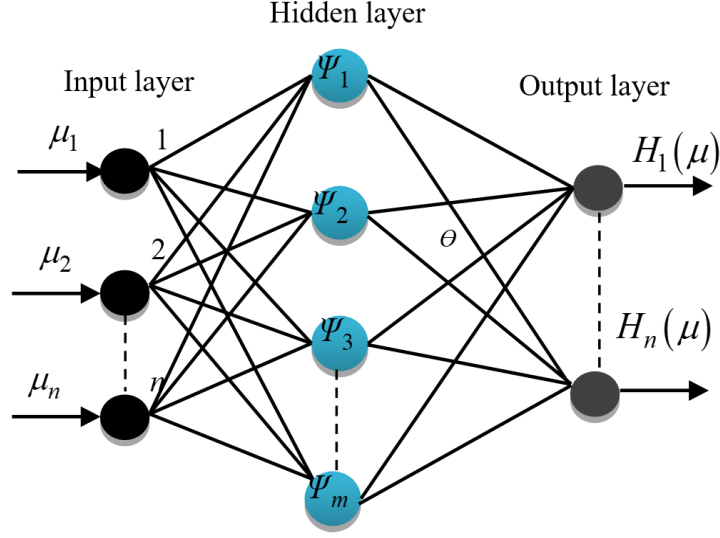


Figure 3.1: The architecture of an RBFNN.

error.

A Gaussian function is defined for the nonlinear function as follows:

$$\Psi(\mu) = \exp\left(-(\mu - \eta_l)^T(\mu - \eta_l)/d_l^2\right), l = 1, 2, \dots, m, \quad (3.16)$$

where  $d$  and  $\eta$  correspond to the width and center of the Gaussian function.

### 3.3.4 Design of ARBFNN-IFOTSMC

In this report, RBFNN is used to approximate the unknown dynamic model as follows:

$$h(x) = F(x, t). \quad (3.17)$$

Define  $\hat{h}(x)$  as an approximated function of  $h(x)$ .  $\hat{h}(x)$  can be described by a RBFNN, as follows:

$$\hat{h}(x) = \int_0^t \hat{\theta}^T \Psi(x) dt. \quad (3.18)$$

Here,  $\hat{\theta}$  is the adaptable parameter vector.

The optimal parameter can be described as follows:

$$\theta_H^* = \arg \min \left\{ \sup_{x \in \Theta_x} \left| h(x) - \hat{h}(x, \hat{\theta}) \right| \right\}. \quad (3.19)$$

Accordingly, RBFNN (3.18) can exactly approximate the arbitrary value of  $h(x)$ , which

is given by the following Lemma [91].

**Lemma 3.1:** For arbitrary positive constant  $\varepsilon > 0$  and any real continuous function  $h(X)$  on the compact set  $\Theta_X \in R^n$ , there is a neural approximator existence  $\hat{h}(X)$  that holds a similar form as Eq. (3.18), such that:

$$\sup_{X \in \Theta_X} |h(X) - \hat{h}(X, \hat{\theta})| < \varepsilon. \quad (3.20)$$

Consequently, the unknown dynamic model can be described as:

$$\dot{e}_2 = \int_0^t \theta^{*T} \Psi(x) dt + Q(x, t) u_{in} - \ddot{x}_d + \Gamma, \quad (3.21)$$

where  $\Gamma = D(x, t) + \varepsilon$  is the lumped uncertainty, including disturbances, dynamic uncertainties, and NN approximation error. To facilitate the next design step, the time derivative of the lumped uncertainty is assumed to be bounded by an unknown positive constant,  $\|\dot{\Gamma}\| \leq \Pi$ .

The proposed control law is designed as follows:

$$u_{in} = -Q^{-1}(x, t) (u_{eq} + u_{asw}). \quad (3.22)$$

Here, the equivalent control law is constructed as:

$$\tau_{eq}(t) = \int_0^t \hat{\theta}^T \Psi(x) dt - \ddot{x}_d + \int_0^t (\omega_1 e_1^{[\mu_1]} + \omega_2 e_2^{[\mu_2]}) d\sigma, \quad (3.23)$$

and  $u_{asw}$  is an adaptive compensator for substituting the control term of  $u_{sw}$  in Eq. (3.12), describing  $u_{asw}$  as:

$$\dot{u}_{asw} = (\hat{\Pi} + \varpi) \text{sign}(s). \quad (3.24)$$

The adaptive laws are designed as:

$$\dot{\hat{\Pi}} = \gamma^{-1} |s|, \quad (3.25)$$

$$\dot{\hat{\theta}} = \kappa^{-1} s \Psi(x), \quad (3.26)$$

where  $\hat{\Pi}$  is the estimated value of the design parameter  $\Pi$ ,  $\varpi$  is a positive constant, and  $\gamma, \kappa$  indicate the adaptive parameters.

The control design approach for the robot system is described in Theorem 3.2 below.

**Theorem 3.2:** For the system (3.1), if suitable IFOTSM surfaces are proposed as (3.4) and the control input signal is constructed as (3.22)–(3.24) with its parameter updating

rules designed as (3.25) and (3.26), then the stability of the system (3.1) is secured with the desired performance, and the tracking errors reach zero.

**Proof:** Identify the adaptive estimation error and NN weight approximation error, respectively, as follows:

$$\tilde{\Pi} = \hat{\Pi} - \Pi, \quad (3.27)$$

$$\tilde{\theta} = \theta^* - \hat{\theta}. \quad (3.28)$$

The sliding surface in Eq. (3.7) is rewritten as:

$$s = \int_0^t \theta^{*T} \Psi(x) dt + Q(x, t) u_{in} - \ddot{x}_d + \Gamma + \int_0^t \left( \omega_1 e_1^{[\mu_1]} + \omega_2 e_2^{[\mu_2]} \right) d\sigma. \quad (3.29)$$

Substituting control laws (3.22)–(3.24) into Eq. (3.29) provides:

$$s = \int_0^t \tilde{\theta}^T \Psi(x) dt - u_{asw} + \Gamma. \quad (3.30)$$

Taking the time derivative of Eq. (3.30) gives:

$$\dot{s} = \tilde{\theta}^T \Psi(x) - \left( \hat{\Pi} + \varpi \right) \text{sign}(s) + \dot{\Gamma}. \quad (3.31)$$

The positive-definite Lyapunov functional is selected as:

$$L_2 = \frac{s^T s}{2} + \frac{\gamma \tilde{\Pi}^T \tilde{\Pi}}{2} + \frac{\kappa \tilde{\theta}^T \tilde{\theta}}{2}. \quad (3.32)$$

With the result of Eq. (3.31), the time derivative of Eq. (3.32) is derived as:

$$\begin{aligned} \dot{L}_2 &= s^T \dot{s} + \gamma \tilde{\Pi}^T \dot{\tilde{\Pi}} - \kappa \tilde{\theta}^T \dot{\tilde{\theta}} \\ &= s^T \left( \tilde{\theta}^T \Psi(x) - \left( \hat{\Pi} + \varpi \right) \text{sign}(s) + \dot{\Gamma} \right) + \gamma \left( \hat{\Pi} - \Pi \right) \dot{\hat{\Pi}} - \kappa \tilde{\theta}^T \dot{\tilde{\theta}} \\ &= s^T \tilde{\theta}^T \Psi(x) - \hat{\Pi} |s| - \varpi |s| + \dot{\Gamma} s + \gamma \left( \hat{\Pi} - \Pi \right) \dot{\hat{\Pi}} - \kappa \tilde{\theta}^T \dot{\tilde{\theta}} \end{aligned} \quad (3.33)$$

Applying the updating laws (3.25)–(3.26) to (3.33) yields:

$$\begin{aligned} \dot{L}_2 &= -\hat{\Pi} |s| - \varpi |s| + \Pi s + \left( \hat{\Pi} - \Pi \right) |s| \\ &= -\varpi |s| + \left( \dot{\Gamma} s - \Pi |s| \right) \\ &\leq -\varpi |s| \end{aligned} \quad (3.34)$$

As shown in Eq. (3.34), if the constant of  $\varpi$  is selected to be greater than zero,  $\dot{L}_2$  will

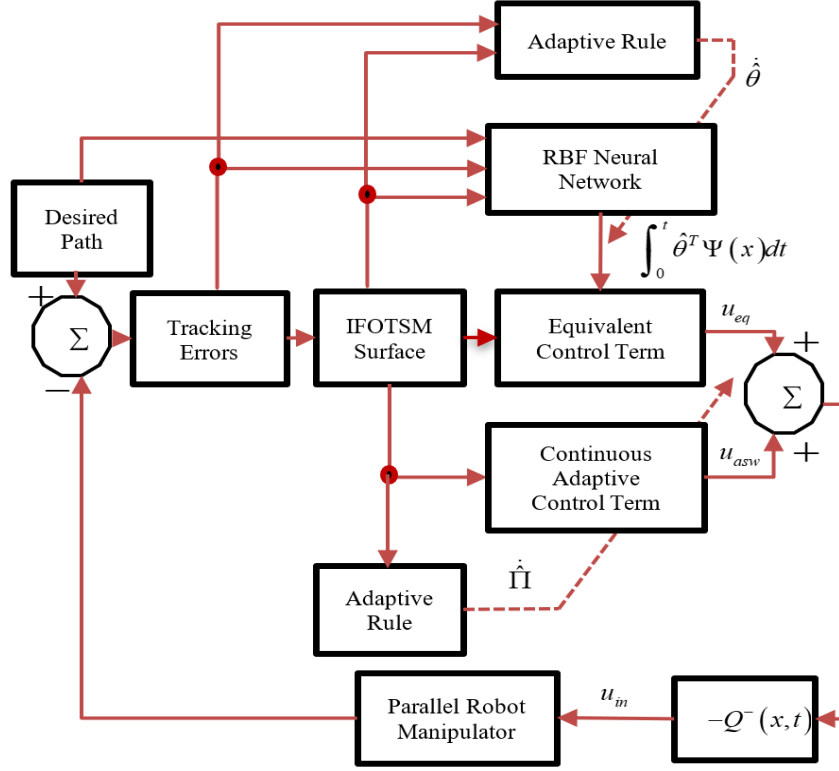


Figure 3.2: Block diagram of the proposed control scheme.

be negative-definite. According to the Lyapunov benchmark [90],  $\dot{L}_2$  becoming negative-definite implies that  $s$  and  $\tilde{\Gamma}$  reach zero, and the tracking error variables thus approach zero as well. Therefore, Theorem 3.2 is proven.

### 3.4 Numerical Simulation Results

While the ARBFNN-IFOTSMC can be applied for a class of second-order nonlinear system such as serial robotic manipulators, parallel robotic manipulators, spacecraft, we consider a five-bar manipulator acting on a horizontal plane as an example that was presented in [6, 92] and its kinematic illustration was shown in Fig. 3.3. The dynamic model of the planar five-bar manipulator is given by [92]:

$$\hat{M}_a \ddot{\theta}_a + \hat{C}_a \dot{\theta}_a + \Delta \tau_a = \tau_a, \quad (3.35)$$

where  $\theta_a = [\theta_{a1}, \theta_{a2}]^T$  is the active joint angle vector;  $\dot{\theta}_a = [\dot{\theta}_{a1}, \dot{\theta}_{a2}]^T$  is the active joint velocity vector;  $\ddot{\theta}_a = [\ddot{\theta}_{a1}, \ddot{\theta}_{a2}]^T$  is the active joint acceleration vector;  $\hat{M}_a \in R^{2 \times 2}$

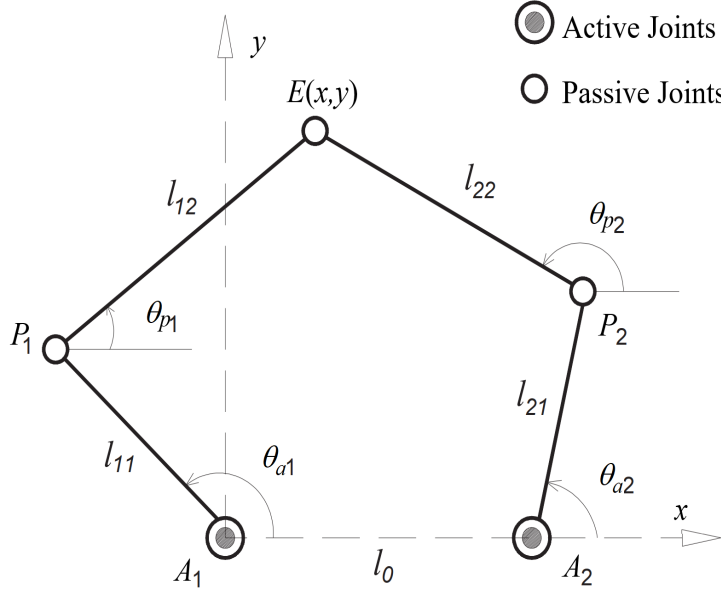


Figure 3.3: Block diagram of the proposed control scheme.

is the estimated inertia matrix;  $\hat{C}_a \in R^{2 \times 2}$  is the estimated centripetal Coriolis matrix;  $\Delta\tau_a$  is the vector of modeling errors and uncertainties; and  $\tau_a \in R^{2 \times 1}$  is the actuator output related to the control input  $u_{in}$ . The detailed computations of  $\hat{M}_a$  and  $\hat{C}_a$  were presented in [92]. The vector  $\Delta\tau_a$  from Eq. (3.35) is presented as the following:

$$\Delta\tau_a = \Delta M_a \ddot{\theta}_a + \Delta C_a \dot{\theta}_a + F_a, \quad (3.36)$$

where  $\Delta M_a$  and  $\Delta C_a$  are the bounded modeling errors and  $F_a$  is the friction force.

The robot in Eq. (3.35) is rewritten with the following expression:

$$\ddot{\theta}_a = \hat{M}^{-1}(\theta_a) [\tau_a - \hat{C}_a \dot{\theta}_a - \Delta\tau_a]. \quad (3.37)$$

Then, we assign  $u_{in} = \tau_a$  as the control input,  $x = [x_1, x_2]^T$  as the state vector in which  $x_1, x_2$  are corresponding to  $\theta_a, \dot{\theta}_a \in R^{2 \times 1}$ . The robotic dynamic of Eq. (3.35) can be described in the following state space form as:

$$\begin{cases} \dot{x}_1 = x_2 \\ \dot{x}_2 = F(x, t) + D(x, t) + Q(x, t) u_{in} \end{cases}, \quad (3.38)$$

where  $F(x, t) = \hat{M}^{-1}(\theta_a) [-\hat{C}_a \dot{\theta}_a] \in R^{2 \times 1}$ ,  $Q(x, t) = \hat{M}^{-1}(\theta_a) \in R^{2 \times 2}$  are the smooth nonlinear vector fields and  $D(x, t) = \hat{M}^{-1}(\theta_a) [-\Delta\tau_a] \in R^{2 \times 1}$  presents the disturbances and uncertainties.

To evaluate the effectiveness of ARBFNN-IFOTSMC, its performance is compared with

Table 3.1: Parameters of the Mechanical Model

Depiction	Parameters	Value
Link lengths	$l_{11} = l_{21}$	$0.102(m)$
	$l_{12} = l_{22}$	$0.18(m)$
	$l_0$	$0.132(m)$
Distances from the joint to the center of mass of the links	$r_{11}$	$0.05(m)$
	$r_{21}$	$0.055(m)$
	$r_{12} = r_{22}$	$0.09(m)$
Masses of the links	$m_{11}$	$0.8(kg)$
	$m_{21}$	$0.78(kg)$
	$m_{12}$	$1.17(kg)$
	$m_{22}$	$1.2(kg)$
Inertia tensors of the links	$I_{z11}$	$0.0027(kg.m^2)$
	$I_{z21}$	$0.0031(kg.m^2)$
	$I_{z12} = I_{z22}$	$0.0013(kg.m^2)$

those of RBFNN-SMC and RBFNN-TSMC. The design of RBFNN-SMC and RBFNN-TSMC are represented in Appendix B, respectively. Simulation studies were performed on a MATLAB–Simulink environment with a fixed-step size of  $10^{-3}s$  and the mechanical model of the 2-DOF parallel manipulator is built using a SimMechanics toolbox. This 2-DOF parallel manipulator operates on the horizontal plane. Hence, the end-effector of the parallel manipulator is controlled to track a circular path on the XY plane. The link parameters in the mechanical model are set as Table 3.1.

To establish the modeling errors  $\Delta M_a$ ,  $\Delta C_a$  simulations were performed with different parameters, both in the mechanical model of the robot as well as in the controllers:  $\hat{r}_{i1} = 0.9r_{i1}$  and  $\hat{r}_{i2} = 0.9r_{i2}$  in which  $\hat{r}_{i1}$ ,  $\hat{r}_{i2}$  ( $i = 1, 2$ ) are utilized for determining  $\hat{M}_a$ ,  $\hat{C}_a$ .

In the mechanical model, the frictions of the system involve viscous friction and Coulomb friction torques that are computed from the following formula:

$$f_{ai} = F_{ci} \text{sign}(\dot{\theta}_{ai}) + F_{vi} \dot{\theta}_{ai}, \quad (i = 1, 2), \quad (3.39)$$

where the coefficients are selected as  $F_{c1} = F_{c2} = 0.3$ , and  $F_{v1} = F_{v2} = 0.7$ .

In addition, the 2-DOF parallel manipulator system is also troubled by external distur-

Table 3.2: Selected Parameters of the Control Methods.

Control Method	Control Parameters	Control Parameter Values
RBFNN-SMC (B.7)	$\alpha, K, K_V$	10, 5, $\text{diag}(20, 20)$
RBFNN-TSMC (B.15)	$\alpha, (1/\beta)$	0.8, $\text{diag}(2, 2)$
	$K_V, \varpi, \Xi$	$\text{diag}(20, 20), 0.1, 5$
The Proposed Method (3.22)-(3.26)	$\omega_1, \omega_2, \mu_1, \mu_2$	20, 7, 0.5, 0.6
	$\varpi, \gamma, \kappa$	0.1, 0.05, $0.5I_{7 \times 7}$

bance forces  $d_a(t) = \begin{bmatrix} d_{a1}(t), d_{a2}(t) \end{bmatrix}^T = \begin{bmatrix} 2, 2 \end{bmatrix}^T$  at  $t = 3.0\text{s}$ .

The selected control parameters of three different control methodologies: RBFNN-SMC, RBFNN-TSMC, and ARBFNN-IFOTSMC are stated in Table 3.2.

The RBFNN had ten neurons in the input layer, seven neurons in the hidden layer, and two neurons in the output layer. The weight of RBFNN is initialed with a zero value.

The simulation studies were performed to compare the control methods in two terms of their positional accuracies and the resulting chattering phenomenon in their control input systems when the parallel manipulator tracked a desired circular path. Fig. 3.4 illustrates performance comparison of the position trajectory tracking when using three different control methodologies: RBFNN-SMC, RBFNN-TSMC, and ARBFNN-IFOTSMC. The end-effector of the robot manipulator has the initial position at the top of the designated circular path. For that reason, the initial position of the end effector of the robot manipulator is not on the specified circular trajectory, the real path of the robot in the operation had a malfunction at the starting of motion. The simulation results of the tracking errors of the end-effector on the X-direction and Y-direction are depicted in Figs. 3.5 and 3.6, respectively. These controllers can be used to track the specified trajectory. The tracking accuracy of the ARBFNN-IFOTSMC had the least amount of tracking errors, on the order of  $10^{-6} - 10^{-7}$  rad, in the presence of uncertainties and external disturbances.

The control input signals for all control types, including RBFNN-SMC, RBFNN-TSMC, and ARBFNN-IFOTSMC are depicted in Fig. 3.7. In Figs 3.7a and 3.7b, the RBFNN-SMC and RBFNN-TSMC offer a discontinuous control signal with serious chattering behavior. On the contrary, ARBFNN-IFOTSMC offers a continuous control signal for the robot manipulator, as depicted in Fig. 3.7c.

The adaptive parameters of the adaptive compensator in the proposed system are depicted in Fig. 3.8; alteration of the influences of external disturbances and uncertainties leads to adaptive parameters with corresponding alteration. These adaptive parameters

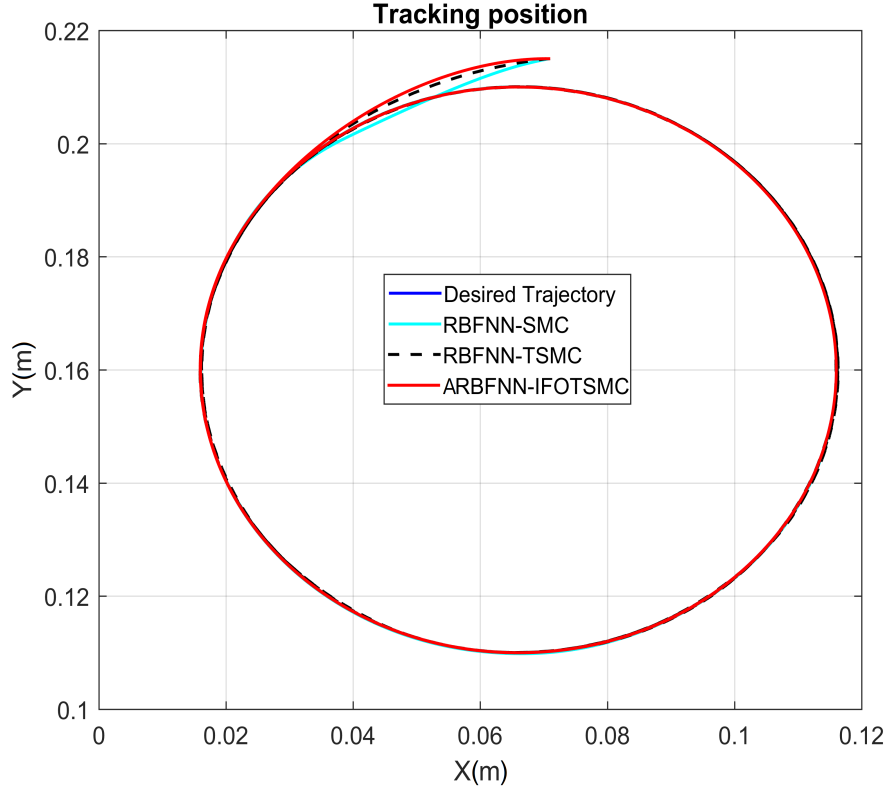


Figure 3.4: The desired trajectory and real trajectory of the end-effector.

will converge to constant values along with the system converging to the IFOTSM surface.

**Remark 3.1:** Throughout simulation analyses and comparison among those of RBFNN-SMC, RBFNN-TSMC, and ARBFNN-IFOTSMC, the simulated results and tracking performance comparison could be expected to exhibit the effectiveness and viability of our proposed control algorithm. In future studies, the ARBFNN-IFOTSMC will be applied to the real robot manipulator and compared with other state-of-the-art control systems to validate the effectiveness of this control methodology. We will also consider the effects of the measurement devices and errors associated with it.

### 3.5 Conclusions

This study reports the design of the control system for the class of general nonlinear second-order systems. The suggested system has the following major advantages: 1) it receives the advantages of both RBFNN and IFOSMC, including good performance with minimum position errors, robustness against uncertainties, and work with a precise dynamic model; 2) it consists of a control input system with chattering reduction; 3)





Figure 3.5: The tracking errors of the end-effector in the X-direction.

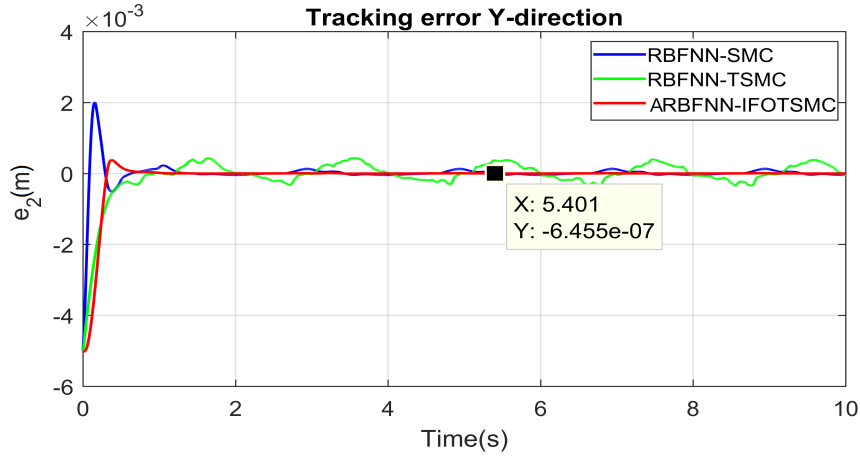


Figure 3.6: The tracking errors of the end-effector in the Y-direction.

ARBFNN-IFOSMC provides better performance and stronger resistance against disturbances and uncertainties compared to RBFNN-SMC and RBFNN-TSMC; and 4) stability and tracking error convergence of the class of general nonlinear second-order systems was fully confirmed by the Lyapunov benchmark.

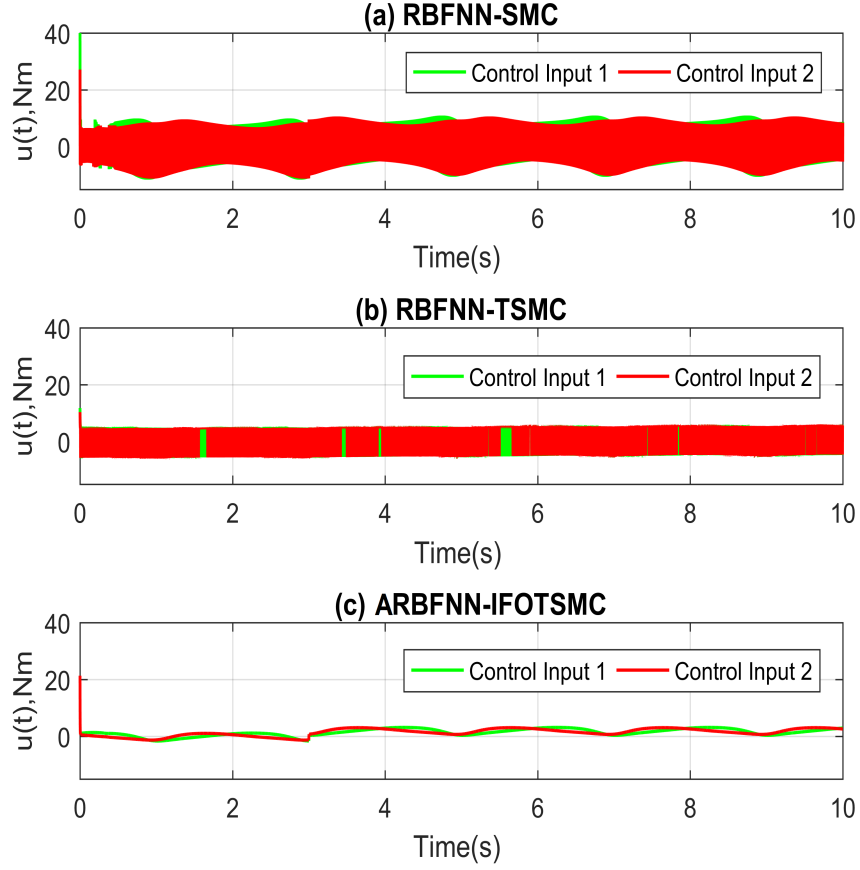


Figure 3.7: Control input signals: (a) RBFNN-SMC, (b) RBFNN-TSMC, and (c) ARBFNN-IFOTSMC.

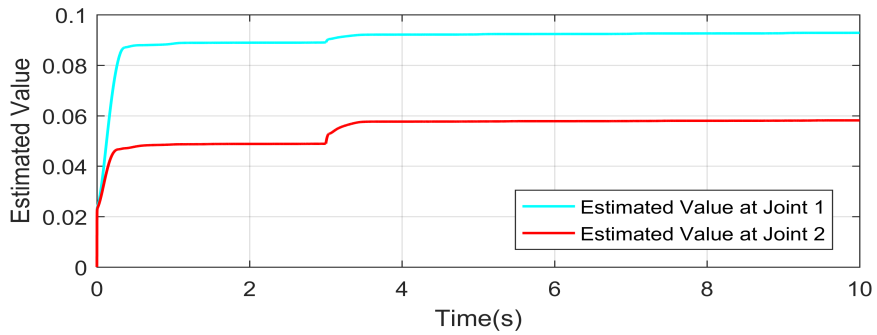


Figure 3.8: Variation of the adaptive gains at Joint 1 and Joint 2.



# Appendix B

## DESIGN RBFNN-SMC

Set  $e = x_1 - x_d$  as the tracking positional error and  $x_d$  as the desired trajectory values. Then, define the sliding variable and time derivative of the sliding variable as follows:

$$s = \dot{e} + \alpha e, \quad (\text{B.1})$$

$$\dot{s} = \ddot{e} + \alpha \dot{e}, \quad (\text{B.2})$$

where  $\alpha$  is a positive constant.

With Eq. (3.38), Eq. (B.2) can be expressed as follows:

$$\begin{aligned} \dot{s} &= \dot{x}_2 - \ddot{x}_d + \alpha (\dot{x}_1 - \dot{x}_d) \\ &= F(x, t) + D(x, t) + Q(x, t) u_{in} - \ddot{x}_d + \alpha (\dot{x}_1 - \dot{x}_d). \end{aligned} \quad (\text{B.3})$$

To obtain the desired performance for the robot system, the controller is designed as follows:

$$u_{in} = -Q^{-1}(x, t) (u_{eq} + u_{sw}). \quad (\text{B.4})$$

The equivalent control signal of  $u_{eq}$  is computed in the case of  $\dot{s} = 0$  and  $D(x, t) = 0$ . Consequently, the term of the equivalent control is designed as follows:

$$u_{eq} = F(x, t) - \ddot{x}_d + \alpha (\dot{x}_1 - \dot{x}_d) + K_V s, \quad (\text{B.5})$$

and the switching control term is designed as:

$$u_{sw} = K \text{sign}(s), \quad (\text{B.6})$$

where  $K$  is a positive constant and  $K_V$  is a diagonal matrix.

We will utilize a neural network to approximate the nonlinear unknown dynamic function of the robotic system  $F(x, t)$ . Accordingly, the controller of Eq. (B.4) becomes

$$u_{in} = -Q^{-1}(x, t) \left( \hat{\theta}^T \Psi(x) - \ddot{x}_d + \alpha(\dot{x}_1 - \dot{x}_d) + K_V s + g \operatorname{sgn}(s) \right). \quad (\text{B.7})$$

## DESIGN RBFNN-TSMC

The following is the design approach of RBFNN-TSMC.

$e = x_1 - x_d$  is the tracking error and  $\dot{e} = \dot{x}_1 - \dot{x}_d$  is the tracking velocity error. Then, the NFTSM surface was selected:

$$s = e + \beta^{-1} \operatorname{sig}(\dot{e})^\alpha, \quad (\text{B.8})$$

where  $s = \begin{bmatrix} s_1 & s_2 \end{bmatrix}^T \in R^{2 \times 1}$  is the sliding surface,  $\operatorname{sig}(\dot{e})^\alpha = (|\dot{e}_1|^\alpha \operatorname{sgn}(\dot{e}_1), \dots, |\dot{e}_n|^\alpha \operatorname{sgn}(\dot{e}_n))$ ,  $1 < \alpha < 2$ .

For system (3.35) to operate with the desired performance, the controller is designed as follows:

$$u_{in} = -Q^{-1}(x, t) (u_{eq} + u_{sw}). \quad (\text{B.9})$$

The equivalent control signal of  $u_{eq}$  is computed in the case of  $\dot{s} = 0$  and  $D(x, t) = 0$ . Therefore, the time derivative of the sliding surface is described as follows:

$$\dot{s} = \dot{e} + \alpha \beta^{-1} |\dot{e}|^{\alpha-1} \ddot{e}. \quad (\text{B.10})$$

From Eq. (3.38),  $\ddot{e}$  can be express as:

$$\ddot{e} = F(x, t) + D(x, t) + Q(x, t) u_{in} - \ddot{x}_d. \quad (\text{B.11})$$

Substituting (B.11) into (B.10) gives:

$$\dot{s} = \dot{e} + \alpha \beta^{-1} |\dot{e}|^{\alpha-1} (F(x, t) + D(x, t) + Q(x, t) u_{in} - \ddot{x}_d). \quad (\text{B.12})$$

Once the robot model  $F(x, t)$  is exactly calculated, then the  $u_{eq}$  control input signal can be defined as follows:

$$u_{eq} = F(x, t) - \ddot{x}_d + \beta \alpha^{-1} \dot{e}^{2-\alpha} + K_V s. \quad (\text{B.13})$$

The switching control term is designed as:

$$u_{sw} = (\Xi + \varpi) \operatorname{sgn}(s), \quad (\text{B.14})$$

where  $K_V$  is a diagonal matrix.

We will utilize a neural network to approximate the nonlinear unknown dynamic function of the robotic system  $F(x, t)$ . Accordingly, the controller of Eq. (B.9) becomes

$$u_{in} = -Q^{-1}(x, t) \left( \hat{\theta}^T \Psi(x) - \ddot{x}_d + \beta \frac{1}{\alpha} \dot{e}^{2-\alpha} + K_V s + (\Xi + \varpi) \operatorname{sgn}(s) \right). \quad (\text{B.15})$$



## Chapter 4

# An Adaptive Terminal Sliding Mode Control for Robot Manipulators with Non-singular Terminal Sliding Surface Variables

### 4.1 Introduction

During recent decades, considerable research efforts have been devoted to investigating robot manipulator control systems. To achieve higher-precision tracking performance, numerous control methods have been constructed for motion control of robot manipulators, such as PID controller [93] and CTC [94]. Those mentioned controllers were highlighted as simple and monotonic methods for robot control. Generally, dynamic models of robot manipulators have been challenged with various parametric uncertainties consisting of friction, perturbation, payload parameters, and sensor noise. Unfortunately, those controllers do not exhibit good control performance of highly nonlinear and uncertain control systems. Accordingly, to handle the uncertainty of robotic systems and to improve the control performance, recently, many nonlinear methods have been suggested for robot manipulators such as AC [1,95], FLS [58,96], OC [97], NN [54,98], and SMC [15,16,99,100].

SMC has been a useful and impressive robust control methodology to correct deficiency from any kind of uncertainties or perturbation for both linear and nonlinear systems. The scheme of SMC is to firstly perform a sliding manifold and then build up a control principle that obligates the controlled variables to attain and maintain the sliding surface. Nonetheless, in real systems, the primary weakness of SMC is an undesirable chattering behavior caused by high-frequency switching. Furthermore, this algorithm only stabilizes the system asymptotically in the sliding phase following a linear sliding manifold method-



ology. From this point of view, the controlled variables cannot obtain the desired values within a finite amount of time.

In 1990s, a new category of SMC called as TSMC was originally published by Venkataraman S and Gulati S. [25] and then advanced by Zhihong M et al. [76] and Wu Y et al. [27]. Contrary to linear sliding surfaces, nonlinear sliding hyperplanes have exposed some advanced properties in terms of high robustness, fast transient response, high tracking positional accuracy, and finite-time convergence. Therefore, various uses of the TSMC method have been established (e.g., robot control [28, 76], motor control [29], TSMO [32].) Nonetheless, this control algorithm does not exhibit good convergence when the controlled variables are distant from the desired values. Specifically, the TSMC algorithm has encountered the singularity drawback that causes complex-value, exponent, and a greater control effort. To increase convergence speed once the controlled variables are significantly different from the desired values, Yu X et al. [39] and Yang L and Yang J [85] presented FTSMC. However, both of the above methods still encounter the singularity drawback. So, to deal with this obstacle, several NTSM methods [40, 85] based on TSMC have been established.

In addition, those above-mentioned control algorithms require information regarding the upper bound of the uncertainties in the robot system, eliminating them from control input signals. In general, it is not easy to precisely define the upper bound of the uncertainty. Some control methods, which are based on an integration of AC law, FL control, NN control, or SC into TSMC or NTSMC to overcome above issue, have been presented ([101–107] reference therein). In those papers, adaptive laws were used only to determine unidentified parameters. These methods still required information on the upper bound of the unidentified parameters, but no attention was paid to disturbances and uncertainties. Other approaches [37, 39, 40, 85] utilized TSM manifolds, but also encountered the singularity drawback. To prove convergence in finite-time, those algorithms ordered the approximately large estimated parameters to generate initial values. However, such techniques are not practically possible since the magnitude of the generated control input seems to be not suitable in terms of motor torque saturation during the period of manifold switching, and . Another critical problem is that a chattering phenomenon occurred by applying high-frequency control switching, which reduces the tracking control performance. Some procedures have also used a function, sometimes called a relay function, but those techniques reduce tracking positional accuracy and increase steady-state errors. So, the robustness and performance of the control algorithm will be degraded.

Purposed by the above analysis, the target of our chapter is to propose a novel tracking control algorithm for robot manipulators. The benefits of our control methodology are highlighted as:

- Satisfies updating rules to control the system's controlled variables, attains the sliding manifold, and converges to the balanced point in finite-time, as well as guarantees asymptotic stability of the robot system with a fast transient response rate.
- Not only prevents the singularity problem by presenting a modified NTSM surface, but also avoids the reaching phase issue.
- Eliminates the requirement for prior information about the upper bounds of parametric uncertainties existing in a real robotic system.
- Rejects the effect of chattering behavior in control input.
- Finite time convergence characteristic and asymptotic stability of the robot system are proved by the Lyapunov criterion.

The rest of this chapter is arranged as follows. The problem statements required for the proposed non-singular sliding surface and control are presented in Section 2. The structural procedure of the suggested control algorithm is reported in Section 3. In Section 4, the proposed control algorithm is applied to the joint position tracking control simulation for a 3-DOF PUMA560 robot. Further, the proposed algorithm's trajectory tracking performance is compared with those of the conventional TSMC and conventional SMC. Lastly, several concluding remarks are presented in Section 5. Several symbols are utilized throughout the article,  $\|*\|$  and  $|*|$  correspond to the Euclidean norm and modulus, while  $N$  and  $R$  correspond to the spaces of natural numbers and real numbers, respectively.

## 4.2 Problem Formulations

For an  $n$ -link rigid robotic manipulator, the corresponding dynamic equation can be given as ([40]):

$$M(\theta)\ddot{\theta} + C_m(\theta, \dot{\theta})\dot{\theta} + G(\theta) + F(\dot{\theta}) + \tau_D = \tau \quad (4.1)$$

in which  $\theta, \dot{\theta}, \ddot{\theta} \in R^n$  are defined as the system's state vector.  $M(\theta) \in R^{n \times n}$  is the inertia matrix,  $C_m(\theta, \dot{\theta}) \in R^{n \times 1}$  is defined as the matrix resulting from Coriolis and centrifugal forces,  $G(\theta) \in R^{n \times 1}$  is the gravitational force term,  $F_r(\dot{\theta}) \in R^{n \times 1}$  is the friction matrix,  $\tau \in R^{n \times 1}$  is the torque produced by actuators, and  $\tau_D \in R^{n \times 1}$  is a load disturbance matrix.

From Eq. (4.1), we have:

$$\ddot{\theta} = M^{-1}(\theta) \left[ \tau - C_m(\theta, \dot{\theta})\dot{\theta} - F_r(\dot{\theta}) - G(\theta) - \tau_D \right] \quad (4.2)$$

To simplify the analysis and design in next section, Eq. (4.2) can be given as:

$$\ddot{\theta} = H(\theta, \dot{\theta}) + D(\theta, \dot{\theta}, t) + Q(\theta)\tau \quad (4.3)$$

in which  $H(\theta, \dot{\theta}) = M^{-1}(\theta) [-C_m(\theta, \dot{\theta})\dot{\theta} - G(\theta)]$ ,  $Q(\theta) = M^{-1}(\theta)$ , and  $D(\theta, \dot{\theta}, t) = M^{-1}(\theta) [-F_r(\dot{\theta}) - \tau_D]$ .

Next, we employ  $u(t) = \tau$  as the control input and  $x = [x_1, x_2]^T$  as the state vector in which  $x_1, x_2$  correspond to  $\theta, \dot{\theta} \in R^{n \times 1}$ . The robotic dynamic of Eq. (4.3) can be described in the following state space form as:

$$\begin{cases} \dot{x}_1 = x_2 \\ \dot{x}_2 = H(x, t) + D(x, t) + Q(x, t)u(t) \end{cases}, \quad (4.4)$$

in which  $H(x, t) \in R^{n \times 1}$  and  $Q(x, t) \in R^{n \times n}$  are smooth nonlinear vector fields, and  $D(x, t) \in R^{n \times 1}$  presents the disturbances and uncertainties.

The sliding motion in finite-time can occur with no prior information regarding the upper bounds of undefined parameters (e.g., friction, disturbances, and uncertainties), and the following assumption is necessary for designing a control scheme in the next section.

**Assumption 4.1:** There exists a bounded function of  $D(x, t)$  presenting undefined parameters (e.g., friction, disturbances, and uncertainties), which satisfies the following condition:

$$\|D(x, t)\| \leq \Psi \quad (4.5)$$

where  $\Psi$  is a positive constant.

The control target in our article is to construct a suggested control algorithm such that the system's controlled variables of  $x_1$  attain the desired values of  $x_d$  within a finite amount of time with no prior information about upper bounds of undefined parameters. Accordingly, the tracking positional error is defined as follows:

$$e = x_1 - x_d \quad (4.6)$$

To achieve this target, this chapter presents two main tasks: (1) construct apposite NTSM manifolds including the desirable dynamic features and (2) establish a control algorithm to guarantee the sliding movement and the system's controlled variables to achieve the desired trajectory within a finite-time.

## 4.3 Design Procedure of the Control Algorithm

In this section, a novel control algorithm is proposed for the robot manipulator of Eq. (4.1) and is expressed by following two main tasks.

### 4.3.1 Design of NTSM Surface

First, with the tracking error in Eq. (4.6), the following NTSM surface variables are suggested:

$$s = \dot{e} + \int_0^t (g_0 e^{[\gamma]} + g_1 e + g_2 e^3 + g_3 \dot{e}^{[\beta]}) \quad (4.7)$$

in which  $s = [s_1, s_2, \dots, s_n]^T \in R^{n \times 1}$  is the sliding variable;  $g_0, g_1, g_2, g_3$  are positive coefficients;  $0 < \gamma < 1$ ,  $\beta = \frac{2\gamma}{(1+\gamma)}$ , and  $e = [e_1, e_2, \dots, e_n]^T \in R^{n \times 1}$  are tracking errors; and  $\dot{e} = [\dot{e}_1, \dot{e}_2, \dots, \dot{e}_n]^T \in R^{n \times 1}$  is the time derivative of the tracking error of  $e$ .

In addition,  $e^{[\gamma]}$  and  $\dot{e}^{[\beta]}$  are defined as ([90]):

$$e^{[\gamma]} = |e|^\gamma \text{sign}[e]; \frac{d}{dt} e^{[\beta]} = \beta |e|^{\beta-1} \dot{e} \quad (4.8)$$

$$\text{in which } \gamma > 0, \beta > 0 \text{ and } \text{sign}[e] = \begin{cases} 1 & \text{if } e > 0 \\ -1 & \text{if } e < 0 \\ 0 & \text{if } e = 0 \end{cases}.$$

**Remark 4.1:** The converging speed property of the NTSM variable has been explained in [85]. Once the tracking positional error of  $|e|$  is much greater than 1,  $g_0 e^{[\gamma]} + g_1 e + g_2 e^3$  conveys a fast convergence rate. While the tracking positional error of  $|e|$  is much smaller than 1,  $g_3 \dot{e}^{[\beta]}$  conveys the role of defining finite-time convergence.

According to the SMC principle, when the system's tracking positional error runs in sliding mode, the following equation should be satisfied ([16]):

$$s = 0; \dot{s} = 0 \quad (4.9)$$

Accordingly, from Eq. (4.7) and Eq. (4.9), it is obtained that

$$\ddot{e} + g_0 e^{[\gamma]} + g_1 e + g_2 e^3 + g_3 \dot{e}^{[\beta]} = 0 \quad (4.10)$$

Therefore, the following dynamic system of the sliding mode can be acquired as:

$$\ddot{e} = -g_0 e^{[\gamma]} - g_1 e - g_2 e^3 - g_3 \dot{e}^{[\beta]} \quad (4.11)$$

Consequently, the following theorem is generated to complete the proof of convergence

within a known finite-time.

**Theorem 4.1:** For the following dynamic system of Eq. (4.11), the original points  $e_i = 0, (i = 1, 2, \dots, n)$  are globally balanced points in finite-time.

**Proof:** Defines the following Lyapunov function candidate as:

$$V_1 = \frac{g_0}{\gamma + 1} |e|^{\gamma+1} + \frac{g_1}{2} e^2 + \frac{g_2}{4} e^4 + \frac{1}{2} \dot{e}^2 \quad (4.12)$$

With Eq. (4.11) the time derivative of Eq. (4.12) is derived as:

$$\begin{aligned} \dot{V}_1 &= g_0 |e|^{[\gamma]} \dot{e} + g_1 e \dot{e} + g_2 e^3 \dot{e} + \dot{e} \ddot{e} \\ &= g_0 |e|^{[\gamma]} \dot{e} + g_1 e \dot{e} + g_2 e^3 \dot{e} \\ &\quad + \dot{e} (-g_0 e^{[\gamma]} - g_1 e - g_2 e^3 - g_3 \dot{e}^{[\beta]}) \\ &= -g_2 |\dot{e}|^{1+\beta} \leq 0 \end{aligned} \quad (4.13)$$

As a result, the condition for the Lyapunov stability principle is fulfilled. Next, the original point of the system in Eq. (4.11) is needed to prove a point as globally stable in finite-time.

From the system in Eq. (4.11), this can be given as:

$$\dot{e} = \psi(e) + \hat{\psi}(e) \quad (4.14)$$

with

$$\psi(e) = \begin{pmatrix} \dot{e} \\ -g_0 e^{[\gamma]} - g_2 \dot{e}^{[\beta]} \end{pmatrix}, \hat{\psi}(e) = \begin{pmatrix} \hat{\psi}_1(e) \\ \hat{\psi}_2(e) \end{pmatrix} = \begin{pmatrix} 0 \\ -g_1 e - g_2 e^3 \end{pmatrix} \quad (4.15)$$

when  $\hat{\psi}(e) = 0$ ; the system in Eq. (4.14) becomes the form of the system under the feedback control law (C.6)-(C.7). It is a globally stable solution in finite-time, according to Lemma 4.2 shown in the Appendix C.

Accordingly, using Lemma 4.1 in the Appendix C, the original point of the dynamic system of Eq. (4.14) is a globally balanced point in case Eq. (C.5) that is satisfied with a disturbance vector  $\hat{\psi}(e)$ .

Based on Definition 4.2 shown in the Appendix C, the system of  $\dot{e} = \psi(e)$  is homogeneous of negative degree  $p = \gamma - 1 < 0$  with respect to the dilation  $(r_1, r_2) = (2, 1 + \gamma)$ . It is sure that  $r_1 - r_2 - p > 0$ . Hence,

$$\lim_{\lambda \rightarrow 0} \frac{\hat{\psi}_2(\lambda^{r_1} e, \lambda^{r_2} \dot{e})}{\lambda^{r_2+p}} = \lim_{\lambda \rightarrow 0} \frac{-g_1 \lambda^{r_1} e - g_2 \lambda^{3r_1} e^3}{\lambda^{r_2+p}} = 0, \forall e \neq 0 \quad (4.16)$$

Accordingly,  $\hat{\psi}(e) = 0$  satisfies the condition from Lemma 4.1 shown in the Appendix C; hence, the original point of the dynamic system ( $e = 0$ ) is a locally balanced point in finite-time.

Proof of stability has been fulfilled.

Given the suitable NTSM surfaces have already been selected, the next task is designing a controller such that the sliding mode motion occurs in finite-time.

**Remark 4.2:** The NTSM surfaces proposed in Eq. (4.7) are totally different from the previously proclaimed surfaces referenced by TSM [25,27,76] and Fast TSM [39,85]. Their sliding surfaces are expressed respectively in the form of the following equations:

$$\begin{aligned} s &= \dot{e} + \mu e^{\frac{q}{l}}, \\ s &= \dot{e} + \rho e + \mu e^{\frac{q}{l}}. \end{aligned} \tag{4.17}$$

in which  $\rho$  and  $\mu$  are defined positive coefficients, and  $l, q$  are positive odd integers that satisfy the condition  $1 < \frac{l}{q} < 2$ . It can be clearly observed that, for  $e < 0$ , the fractional power  $\frac{l}{q}$  can cause the component of  $e^{\frac{q}{l}} \notin R$ .

Additionally, the control input in [39] encompasses  $e^{\frac{q}{l}-1}\dot{e}$ , which may cause a singularity in cases  $e_2 \neq 0$  and  $e_1 = 0$ .

To overcome obstacles of the complex-valued problem in Eq. (4.17), Yu et al. [40] suggested another form of TSM surface as:

$$\begin{aligned} s &= \dot{e} + \mu |e|^\gamma \text{sign}(e), \\ s &= \dot{e} + \rho e + \mu |e|^\gamma \text{sign}(e). \end{aligned} \tag{4.18}$$

With the sliding surface of Eq. (4.18), the complex-valued number problem has been solved, but the control input has also encountered the singularity drawback in cases of  $e_2 \neq 0$  and  $e_1 = 0$ .

In recent years, some new forms of NTSM surfaces were proposed to deal with the singularity obstacle [37,40,85]:

$$s = e + \frac{1}{\mu} \dot{e}^{\frac{l}{q}} \tag{4.19}$$

Nonetheless, the restriction of this sliding surface is that  $q$  and  $l$  must be positive odd integers. Accordingly, the proposed NTSM surface in this paper has not encountered the singularity drawback as discussed above.

### 4.3.2 Design of the Proposed Control Algorithm

As mentioned before, the appropriate finite-time NTSM surface in the form of Eq. (4.7) has been selected, and the next task is to construct a control algorithm satisfying the control target in Section 2. Further, to obtain the desired performance for System (4.4) with Assumption 4.1, the following control law is presented in Theorem 4.2.

**Theorem 4.2:** For the dynamic system in state space as shown in Eq. (4.4), if the control input signal is constructed as (4.20)-(4.22), a suitable finite-time NTSM surface is selected as shown in Eq. (4.7), and positive coefficients of  $\Psi$  satisfying Assumption 4.1 exist. This means that the system tracking position  $x_1$  will reach the desired trajectory values  $x_d$  in finite-time. Accordingly, the goal of achieving global stability in finite-time is guaranteed.

The proposed controller based on the NTSM surface variable is designed as:

$$u(t) = -Q(x, t)^+ (u_{eq}(t) + u_s(t)) \quad (4.20)$$

$$u_{eq}(t) = (H(x, t) - \ddot{x}_d + g_0 e^{[\gamma]} + g_1 e + g_2 \dot{e}^{[\beta]} + \Upsilon s) \quad (4.21)$$

$$u_s(t) = (\Psi + \eta) \text{sign}(s) \quad (4.22)$$

where  $Q^+(x, t) = Q^T(x, t) [Q(x, t) Q^T(x, t)]^{-1}$ .  $\Upsilon, \eta$  and  $\Psi$  are positive constants.

**Proof:** With System (4.4),  $\ddot{e}$  is present as:

$$\begin{aligned} \ddot{e} &= \dot{x}_2 - \ddot{x}_d \\ &= H(x, t) + D(x, t) + Q(x, t) u(t) - \ddot{x}_d \end{aligned} \quad (4.23)$$

Inserting (4.23) into the time derivative of the NTSM variable of (4.7) gives:

$$\begin{aligned} \dot{s} &= \ddot{e} + g_0 e^{[\gamma]} + g_1 e + g_2 e^3 + g_3 \dot{e}^{[\beta]} \\ &= H(x, t) + D(x, t) + Q(x, t) u(t) \\ &\quad - \ddot{x}_d + g_0 e^{[\gamma]} + g_1 e + g_2 e^3 + g_3 \dot{e}^{[\beta]} \end{aligned} \quad (4.24)$$

Applying the control law (4.20)-(4.22) to (4.24) obtains:

$$\begin{aligned}
 \dot{s} &= H(x, t) + D(x, t) + g_0 e^{[\gamma]} + g_1 e + g_2 e^3 + g_3 \dot{e}^{[\beta]} \\
 &\quad + Q(x, t) (-Q(x, t)^+ (u_{eq}(t) + u_s(t))) - \ddot{x}_d \\
 &= H(x, t) + D(x, t) - \ddot{x}_d + g_0 e^{[\gamma]} + g_1 e + g_2 e^3 + g_3 \dot{e}^{[\beta]} \\
 &\quad - \left( \left( \begin{array}{c} H(x, t) - \ddot{x}_d + g_0 e^{[\gamma]} + g_1 e \\ + g_2 e^3 + g_3 \dot{e}^{[\beta]} + \Upsilon s \end{array} \right) + (\Psi + \eta) \text{sign}(s) \right) \\
 &= -\Upsilon s + D(x, t) - (\Psi + \eta) \text{sign}(s)
 \end{aligned} \tag{4.25}$$

Let us define the following Lyapunov function candidate as:

$$V_2 = \frac{1}{2} s^T s \tag{4.26}$$

From (4.25), the time derivative of Eq. (4.26) is then derived as:

$$\begin{aligned}
 \dot{V}_2 &= s^T \dot{s} \\
 &= s^T (-\Upsilon s + D(x, t) - (\Psi + \eta) \text{sign}(s)) \\
 &= -\Upsilon s^T s + D(x, t) s - \Psi s - \eta |s|
 \end{aligned} \tag{4.27}$$

Using Assumption 4.1, the following inequality is obtained as:

$$\dot{V}_2 \leq -\Upsilon s^T s - \eta |s| \leq 0 \tag{4.28}$$

According to the Lyapunov stability criterion [90, 108], the stability and convergence of the error variables have been secured despite terrible conditions such as disturbances, dynamic uncertainties, or faults. It also means positive coefficients of  $\Psi$  exist, which satisfying the condition of Eq. (4.5). Hence, Theorem 4.2 has been proved.

In comparison with Theorem 4.2 that is subject to the traditional SMC in terms of chattering behavior, the suggested system has significantly less chattering behavior in the control input. Both methods demand prior information regarding the upper bounds of the uncertainty terms; unfortunately, this prior information is not always accessible in real systems. In an unknown bound case, for (4.27) to be ensured, the design parameters selected in control law should be greater than the upper-bounds uncertainties. One weak point is that greater design parameters yield more serious chattering behavior. To overcome these control performance limitations, our method applies an adaptive technique to approximate the design parameters of the reaching control law and obtain the desired control algorithm.



Therefore, the proposed controller based on the NTSM surface variable and adaptive technique as depicted in Fig. 4.1 is designed as:

$$u(t) = -Q(x, t)^+ (u_{eq}(t) + u_{as}(t)) \quad (4.29)$$

where  $u_{eq}(t)$  is constructed the same as the equivalent control term in Eq. (21), and the adaptive control term is constructed as:

$$u_{as}(t) = \left( \hat{\Psi}_{ad} + \eta \right) \text{sign}(s) \quad (4.30)$$

where  $u_{eq}(t)$  is constructed identically to the equivalent control term in Eq. (21), and the adaptive control term is constructed as:

$$\dot{\hat{\Psi}}_{ad} = \frac{1}{\kappa} |s| \quad (4.31)$$

where  $\kappa > 0$  indicates the adaptive gain.

The following theorem is formulated for the proposed controller to achieve the control objective for the robotic system of Eq. (4.4).

**Theorem 4.3:** For the dynamic system in state space as Eq. (4.4), if the control input signal is constructed (4.29)-(4.30) with its parameter updating law as in Eq. (4.31) and a suitable finite-time NTSM surface is selected as in Eq. (4.7), the estimating value of  $\hat{\Psi}_{ad}$  has an upper limit. It means that there exists a positive coefficient of  $\hat{\Psi}_{ad}$  satisfying the following condition:

$$\hat{\Psi}_{ad} \leq \Psi^* \quad (4.32)$$

Furthermore, this means that the system tracking position  $x_1$  will reach the desired trajectory values  $x_d$  in finite-time. Accordingly, the goal of achieving global stability in finite-time is guaranteed.

**Proof:** Proof of stability will be done according to the following approach.

Firstly, it will be shown there exist positive coefficients  $\Psi^*$  satisfying the condition of Eq. (4.32), which causes the system tracking position  $x_1$  to reach the desired trajectory values  $x_d$ .

The following positive-definite Lyapunov functional is considered:

$$V_3 = \frac{1}{2} s^T s + \frac{1}{2} \kappa \left( \hat{\Psi}_{ad} - \Psi \right)^T \left( \hat{\Psi}_{ad} - \Psi \right) \quad (4.33)$$

where  $\kappa$  is a positive constant. Utilizing the same method employed to obtain (4.25), the

time derivative of Eq. (4.33) is derived as:

$$\begin{aligned}\dot{V}_3 &= s^T \dot{s} + \kappa \left( \hat{\Psi}_{ad} - \Psi \right)^T \dot{\hat{\Psi}}_{ad} \\ &= s^T \begin{pmatrix} -\Upsilon s + D(x, t) \\ -\left( \hat{\Psi}_{ad} + \eta \right) \text{sign}(s) \end{pmatrix} + \kappa \left( \hat{\Psi}_{ad} - \Psi \right)^T \dot{\hat{\Psi}}_{ad}\end{aligned}\quad (4.34)$$

Inserting the adaptive rule (4.31) into (4.34) yields:

$$\begin{aligned}\dot{V}_3 &= -\Upsilon s^T s + D(x, t) s - \hat{\Psi}_{ad} |s| \\ &\quad - \eta |s| + \left( \hat{\Psi}_{ad} - \Psi \right) |s|\end{aligned}\quad (4.35)$$

Applying Assumption 4.1, the following inequality is obtained as:

$$\begin{aligned}\dot{V}_3 &= -\Upsilon s^T s + D(x, t) s - \hat{\Psi}_{ad} |s| - \eta |s| + \left( \hat{\Psi}_{ad} - \Psi \right) |s| \\ &= -\Upsilon s^T s + D(x, t) s - \Psi |s| - \eta |s| \\ &\leq -\Upsilon s^T s - \eta |s| \leq -\eta |s| \leq 0\end{aligned}\quad (4.36)$$

According to the Lyapunov stability criterion [90, 108], the estimating parameter of  $\hat{\Psi}_{ad}$  is limited. It means that there exist positive coefficients of  $\Psi^*$  satisfying the condition of Eq. (32). Thus, Eq. (4.32) is proved.

Then, the method will continue to show that the system of Eq. (4.4) will attain the NTSM surfaces  $s = 0$  in a finite-time.

We use the following proof procedure ([99]).

Consider the following Lyapunov function candidate as:

$$V_4 = \frac{1}{2} s^T s + \frac{1}{2} \nu \tilde{\Psi}^T \tilde{\Psi} \quad (4.37)$$

where  $\nu$  is the positive coefficient,  $\tilde{\Psi} = \hat{\Psi} - \Psi^*$ .

The time derivative of Eq. (4.37) is derived as:

$$\begin{aligned}\dot{V}_4 &= s^T \dot{s} + \nu \tilde{\Psi}^T \dot{\tilde{\Psi}} \\ &= s^T \left( -\Upsilon s + D(x, t) - \left( \hat{\Psi}_{ad} + \eta \right) \text{sign}(s) \right) + \nu \left( \hat{\Psi}_{ad} - \Psi^* \right)^T \dot{\hat{\Psi}}_{ad}\end{aligned}\quad (4.38)$$

Inserting the adaptive rule (4.31) into (4.38) and using (4.32) yields:

$$\begin{aligned}
\dot{V}_4 &= s^T \left( -\Upsilon s + D(x, t) - \left( \hat{\Psi}_{ad} + \eta \right) \text{sign}(s) \right) + v \left( \hat{\Psi}_{ad} - \Psi^* \right) \frac{1}{\kappa} |s| \\
&= -\Upsilon s^T s + D(x, t) s - \hat{\Psi}_{ad} |s| - \eta |s| + \frac{v}{\kappa} \left( \hat{\Psi}_{ad} - \Psi^* \right) |s| \\
&\leq -\Upsilon s^T s + \Psi s - \hat{\Psi}_{ad} |s| - \eta |s| + \frac{v}{\kappa} \left( \hat{\Psi}_{ad} - \Psi^* \right) |s| \\
&\leq \Psi s - \hat{\Psi}_{ad} |s| + \frac{v}{\kappa} \left( \hat{\Psi}_{ad} - \Psi^* \right) |s| + \Psi^* |s| - \Psi^* |s| \\
&= -(\Psi^* - \Psi) |s| + \frac{v}{\kappa} \left( \hat{\Psi}_{ad} - \Psi^* \right) |s| - \left( \hat{\Psi}_{ad} - \Psi^* \right) |s| \\
&= -(\Psi^* - \Psi) |s| - \left( -|s| + \frac{v}{\kappa} |s| \right) \left| \hat{\Psi}_{ad} - \Psi^* \right|
\end{aligned} \tag{4.39}$$

For a simpler description, some symbols are defined as:

$$\begin{cases} \Lambda_0 = (\Psi^* - \Psi) \\ \Lambda_1 = \left( -|s| + \frac{v}{\kappa} |s| \right) \end{cases} \tag{4.40}$$

$\Psi^*$ , and  $\nu$  must be selected to satisfy the conditions that  $\Psi^* > \Psi$  and  $v > \kappa$ . It follows that  $\Lambda_0 > 0$  and  $\Lambda_1 > 0$ .

Therefore, the following result is obtained:

$$\begin{aligned}
\dot{V}_4 &\leq -\Lambda_0 |s| - \Lambda_1 \left| \hat{\Psi}_{ad} - \Psi^* \right| \\
&\leq -\sqrt{2}\Lambda_0 \frac{|s|}{\sqrt{2}} - \Lambda_1 \sqrt{\frac{2}{v}} \sqrt{v} \frac{\left| \hat{\Psi}_{ad} - \Psi^* \right|}{\sqrt{2}} \\
&\leq -\min \left\{ \sqrt{2}\Lambda_0, \Lambda_1 \sqrt{\frac{2}{v}} \right\} \cdot \left( \frac{|s|}{\sqrt{2}} + \sqrt{v} \frac{\left| \hat{\Psi}_{ad} - \Psi^* \right|}{\sqrt{2}} \right)
\end{aligned} \tag{4.41}$$

Using Jensen's inequality of Lemma 5.4 shown in the Appendix C and defining that  $\Lambda = \min \left\{ \sqrt{2}\Lambda_0, \Lambda_1 \sqrt{\frac{2}{v}} \right\}$ , the following results are consequently obtained:

$$\begin{aligned}
\dot{V}_4 &\leq -\Lambda \left( \frac{s^T s}{(\sqrt{2})^2} + (\sqrt{v})^2 \frac{\left( \hat{\Psi}_{ad} - \Psi^* \right)^T \left( \hat{\Psi}_{ad} - \Psi^* \right)}{(\sqrt{2})^2} \right)^{\frac{1}{2}} \\
&\leq -\Lambda V_4^{\frac{1}{2}}
\end{aligned} \tag{4.42}$$

Based on Lemma 4.3 shown in the Appendix C, it is shown that the controlled variables in Eq. (4.4) reach the NTSM variable in a known amount of time  $T \leq \frac{2V_4^{\frac{1}{2}}(0)}{\Lambda}$ .

Furthermore, once the NTSM surface converges to zero, then the tracking error of the robot system will also become zero. This completes the proof of Theorem 4.3.

**Remark 4.3:** In real systems, the parameter drift matter usually occurs under adaptive law (4.31). Therefore, the bounded method is performed to set up the adaptive law as:

$$\dot{\Psi}_{ad} = \begin{cases} 0 & \text{if } |s| \leq v \\ \frac{1}{\kappa} |s| & \text{if } |s| > v \end{cases} \quad (4.43)$$

in which  $v$  is an arbitrary positive value.

Theoretically, the proposed control algorithm contains the discontinuous term  $(\hat{\Psi}_{ad} + \eta) \text{sign}(s)$  that may cause chattering phenomenon from an infinite switching frequency of a discontinuous term. To reject the possible chattering phenomenon, some procedures have been used. For example, the function of  $\frac{s}{(|s| + \varepsilon^*)}$  can be utilized to approximate the function of  $\text{sign}(s)$  (in which  $\varepsilon^*$  is a minor positive coefficient) or another technique is applied in this paper, which is summarized in Remark 4.4.

**Remark 4.4:** [40] The chattering phenomenon can be significantly alleviated by replacing the  $\text{sign}(s)$  function with a saturation function in the control input signal, such as:

$$\text{sat}\left(\frac{s}{\varepsilon^*}\right) = \begin{cases} \text{sign}(s) & \text{if } |s| \geq \varepsilon^* \\ \frac{s}{\varepsilon^*} & \text{if } |s| < \varepsilon^* \end{cases} \quad (4.44)$$

in which  $\varepsilon^*$  is a minor positive coefficient.

## 4.4 Numerical Simulation Results

We consider a 3-DOF PUMA560 robot [72] with the first three joints and the last three joints blocked. Its kinematic illustration is shown in Fig. 4.2. The uncertainties in this simulation are assumed as follows. The friction  $F_r(\dot{\theta})$  and disturbance  $\tau_D$  are assumed to be

$$F_r(\dot{\theta}) + \tau_D = \begin{bmatrix} 2.1\dot{\theta}_1 + 2.02\text{sign}(3\dot{\theta}_1) \\ 4.2\dot{\theta}_2 + 2.2\text{sign}(2\dot{\theta}_2) \\ 1.1\dot{\theta}_3 + 1.15\text{sign}(2\dot{\theta}_3) \end{bmatrix} + \begin{bmatrix} 7.2\sin(\dot{\theta}_1) \\ 6.1\sin(\dot{\theta}_2) \\ 4.15\sin(\dot{\theta}_3) \end{bmatrix} \quad (4.45)$$

The desired joint trajectories are

$$\theta_d = \begin{bmatrix} \cos\left(\frac{t}{5\pi}\right) - 1 & \sin\left(\frac{t}{5\pi} + \frac{\pi}{2}\right) - 1 & \sin\left(\frac{t}{5\pi} + \frac{\pi}{2}\right) - 1 \end{bmatrix}^T \quad (4.46)$$

The parameters for the NTSM surface in Eq. (4.7) and the controlling input (4.29)-

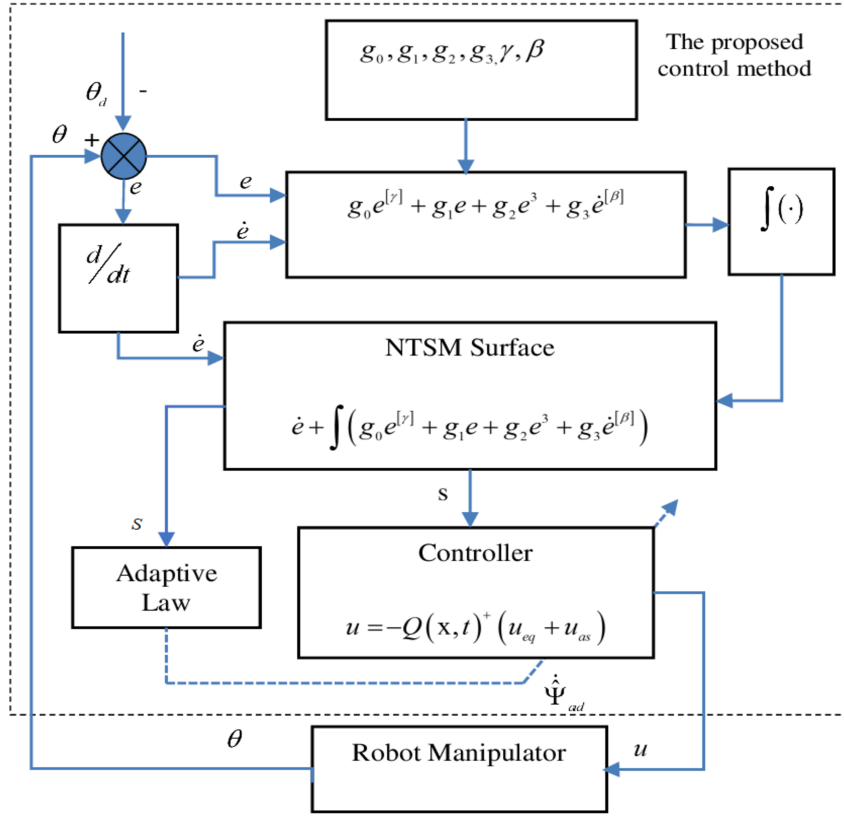


Figure 4.1: Block diagram of the proposed control method.

(4.31) are experimentally selected as  $g_0 = 15$ ,  $g_1 = 6$ ,  $g_2 = 3$ ,  $g_3 = 10$ ,  $\gamma = 0.2$ ,  $\beta = 0.6$ ,  $\Upsilon = 20$ ,  $\kappa = 0.1$ ,  $\varepsilon^* = 0.15$  and  $\eta = 0.2$ . The initial values of the system are chosen as  $\theta_1(0) = -0.5$ ,  $\theta_2(0) = -0.5$ , and  $\theta_3(0) = -0.5$ . The initial value of adaptive control law is selected as  $\hat{\Psi}_{ad}(0) = 0$ .

To show the effectiveness of the proposed control algorithm, its trajectory tracking performances are compared with those of the conventional SMC [15, 16, 99, 100] and the NTSM controller [37, 40, 85]. These control methods for comparison are briefly explained as follows.

The conventional SMC [15] has the control input:

$$u(t) = -Q(x, t)^{-1} [H(x, t) + \varphi(x_2 - \dot{x}_d) - \ddot{x}_d + (\Psi + \eta) \text{sign}(s)] \quad (4.47)$$

in which  $s = \dot{e} + ce$  is the linear sliding surface.

The parameters of the controller in Eq. (4.47) were selected as  $\Psi = 19.8$ ,  $\eta = 0.2$ ,  $c = 2$  and  $\varphi = 2$  to obtain good simulation results.

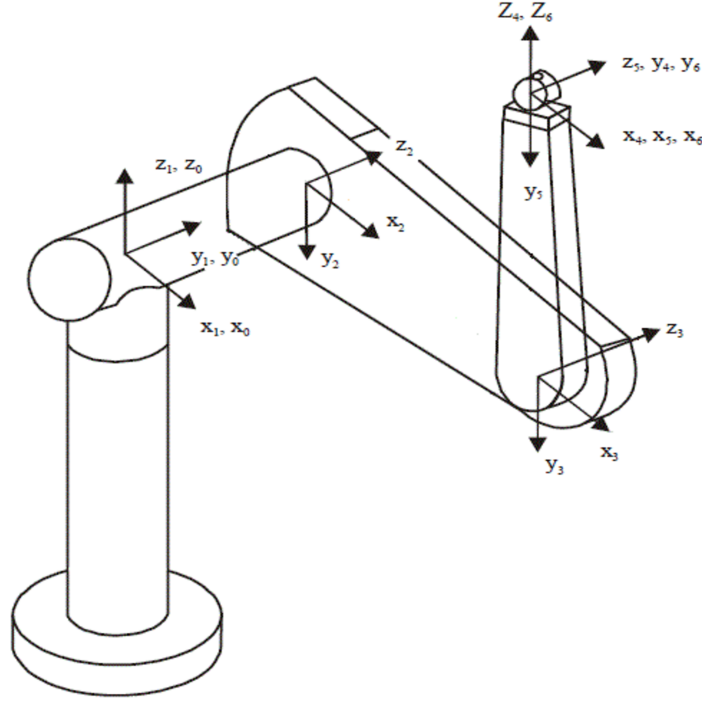


Figure 4.2: 3-DOF PUMA560 robot manipulator.

Further, the NTSM controller [37] has the control input:

$$u(t) = -Q(x, t)^{-1} \left[ H(x, t) + \mu \frac{q}{l} \dot{e}^{2-\frac{l}{q}} - \ddot{x}_d + (\Psi + \eta) \text{sign}(s) \right] \quad (4.48)$$

in which  $s = e + \mu^{-1} \dot{e}^{\frac{l}{q}}$  is a nonlinear sliding surface.

The parameters of the controller in Eq. (4.48) were selected as  $q = 3, l = 5, \eta = 0.2, \Psi = 19.8$  and  $\mu = 2.0$  to obtain good simulation results.

The simulations were carried out in the following two cases to compare the controllers in terms of both positional accuracy and the resulting chattering behaviors in their control inputs.

Case 1: Each of three controllers has the discontinuous term of  $\text{sign}(s)$  in its control input signal.

Case 2: Each of three controllers applied Remark 4.4 in which the discontinuous term of  $\text{sign}(s)$  is replaced with a saturation function in its control input signal.

In Case 1, the tracking positions and tracking errors of the three joints with three control methods are given in Fig. 7.3 and Fig. 7.4, respectively. All three controllers offer similar good trajectory tracking performances. However, the tracking errors of the proposed controller are smaller than those of the other control methods by the order of  $10^{-6}$  rad. The tracking errors of the other control methods are on the order of  $10^{-4} \sim 10^{-5}$

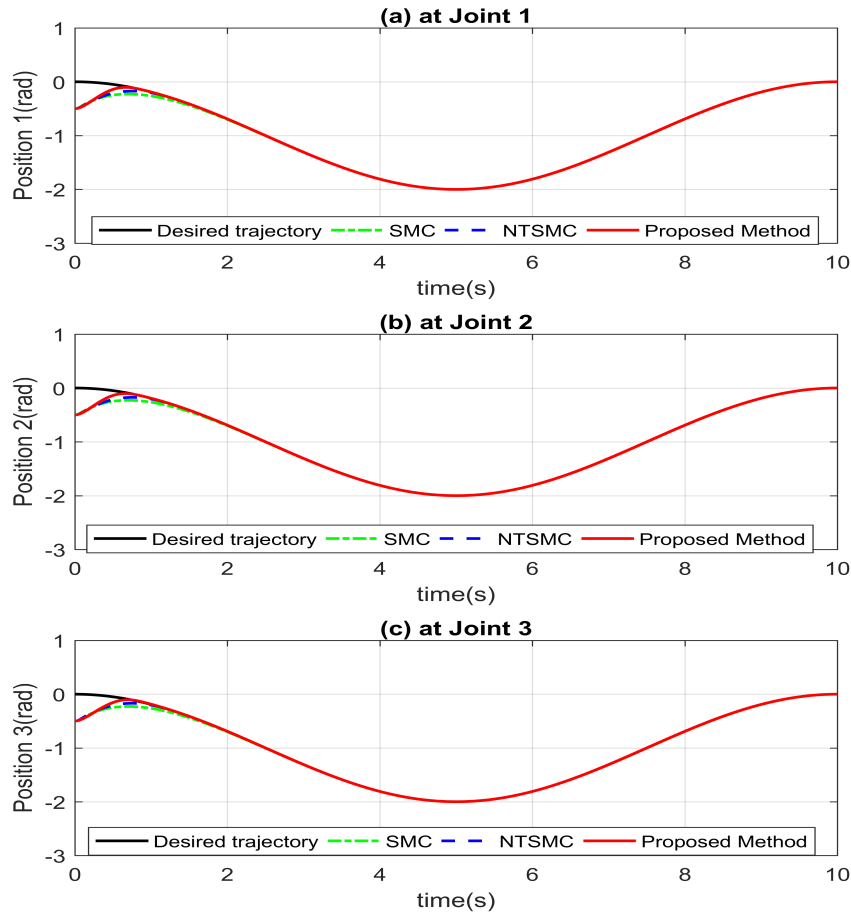


Figure 4.3: Tracking Positions with a sign function: (a) at Joint 1, (b) at Joint 2, and (c) at Joint 3.

rad. The more interesting finding involves comparison of the control inputs in terms of the chattering phenomena, shown in Fig. 7.5. The chattering behavior from the proposed NTSM surface and control law was shown as significantly less than those of the other control methods.

To reduce chattering, the saturation function has been adopted in SMC methods instead of the sign function. In this case, it is easily expected that reducing chattering often reduces positional accuracy. The simulation results of Case 2 confirm the expectant results shown in Figs. 7.6-4.8. Noteworthy is that the degradation of the tracking positional accuracies of the proposed control method is the smallest among the three controllers, while the chattering of the control inputs is in the allowable range. The tracking errors of the proposed controller are on the order of  $10^{-6}$  rad, while those of the other control methods are worse, on the order of  $10^{-3}$  rad. Furthermore, the required initial control

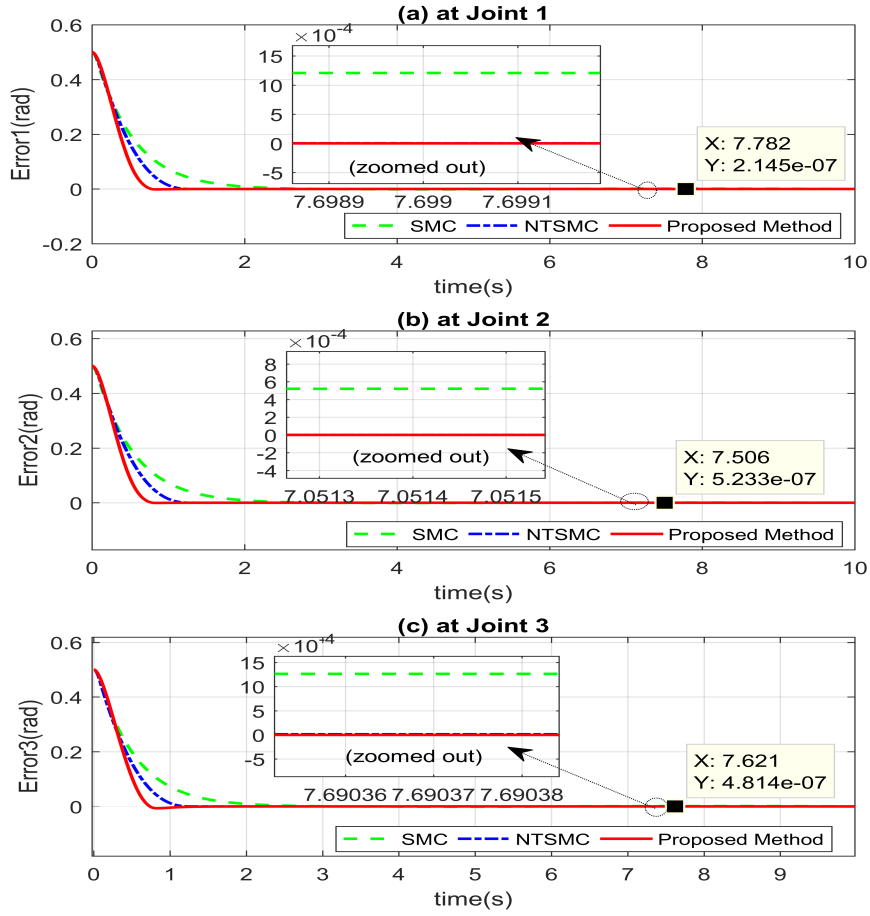


Figure 4.4: Tracking Errors with a sign function: (a) at Joint 1, (b) at Joint 2, and (c) at Joint 3.

input of the proposed control method seems to be an affordable magnitude, while those of the other control method seems to be too high and lead to motor torque saturation as shown in Fig. 4.8.

The response time of the sliding surface in two cases is shown in Figs. 4.9-4.10. It is shown that the proposed NTSM surface allows a faster finite-time convergence trajectory than the old-style SMC and conventional NTSM surfaces. The transient response of the proposed NTSM surface has been improved and quickly responded to the fast variation of influences of the external disturbances or uncertainties.

The variations of the estimated parameter of  $\hat{\Psi}_{ad}$  in two Case are shown in Figs. 4.11-4.12. The parameters are estimated according to the variation of the undefined parameters, and this estimated parameter will reach a constant when the system state variables converge to the non-singular sliding surfaces.



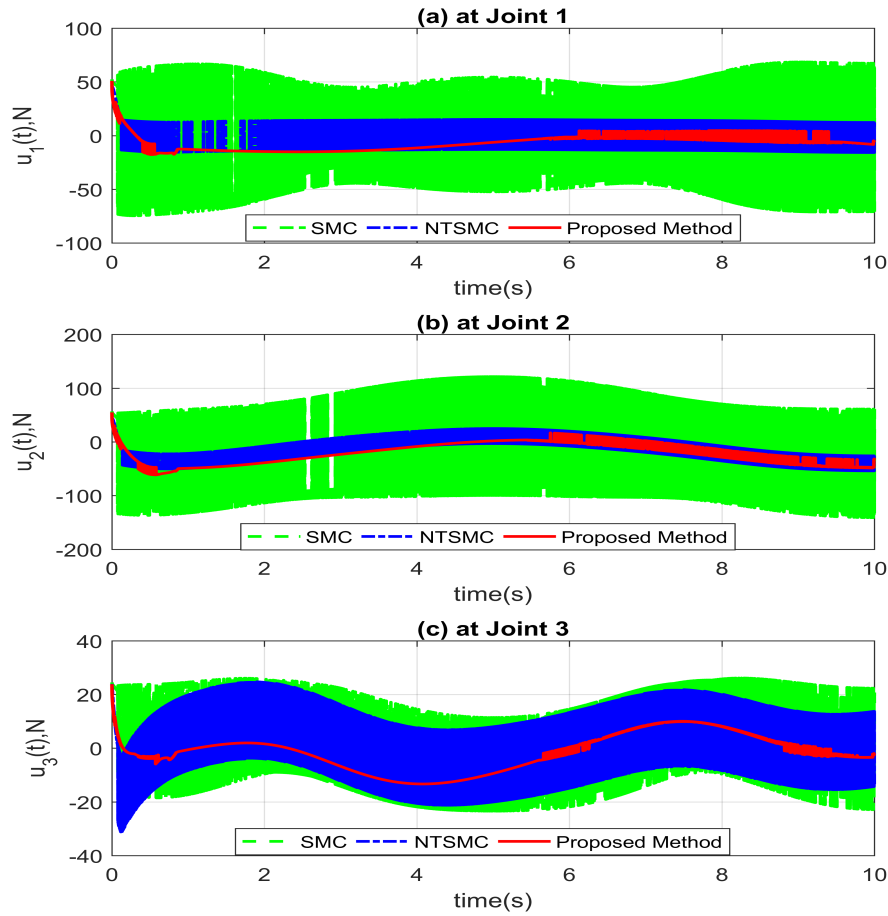


Figure 4.5: Control inputs with a sign function: (a) at Joint 1, (b) at Joint 2, and (c) at Joint 3.

From the simulation results, it can be concluded that the proposed controller shows the best performance among the three in terms of tracking positional accuracy, small steady state error, fast response speed, and weak chattering behavior.

**Remark 5.5 :** The robustness issue and the finite-time convergence of the suggested system are totally confirmed by the Lyapunov stability principle. Through simulation studies and comparison among those of the conventional SMC [15,16,99,100] and the NTSM controller [37,40,85], the experimental results and performance comparison could be expected to show the effectiveness and viability of our proposed scheme for the joint position tracking control of a 3-DOF PUMA560 robot. In the next work, authors will apply the proposed controller to the real robot system and compare with other state-of-the-art controllers to demonstrate the effectiveness of this control method.

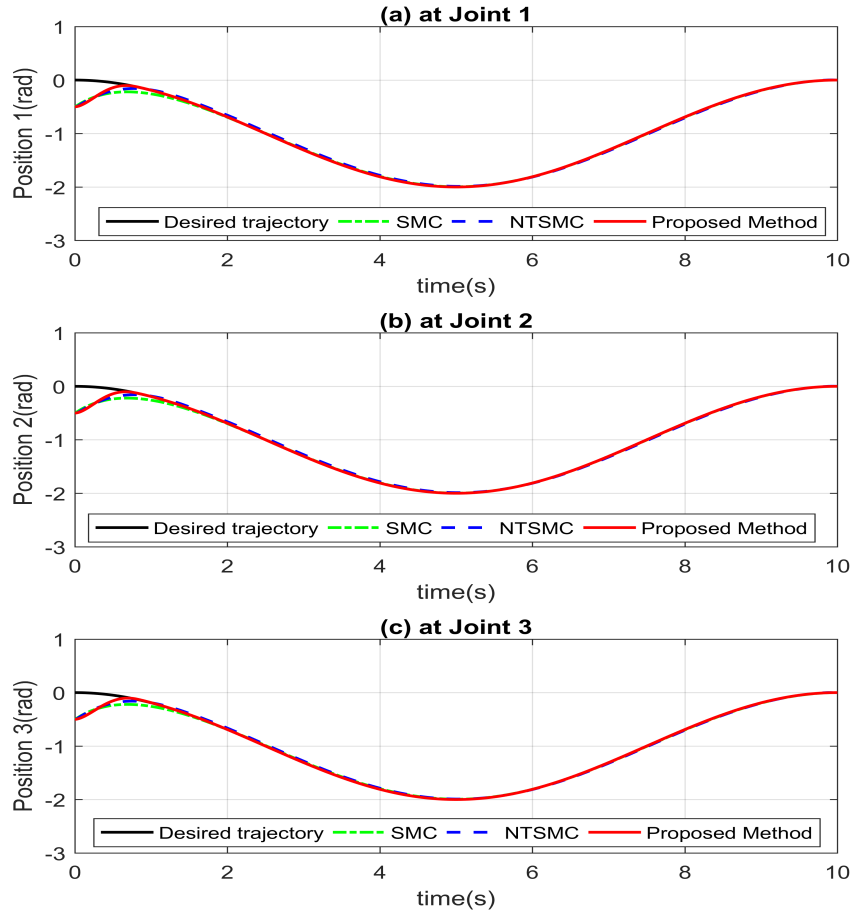


Figure 4.6: Tracking positions with a saturation function: (a) at Joint 1, (b) at Joint 2, and (c) at Joint 3.

## 4.5 Conclusions

In this paper, an adaptive continuous finite-time TSMC algorithm is presented for robot manipulators. From the simulation and performance comparison with two other control methods for a 3-DOF PUMA560 robot, the suggested control method shows the best performance among the three controllers in terms of tracking positional accuracy, small steady state error, fast response speed, and weak chattering behavior. We think that the proposed control algorithm has the following important characteristics: 1) the NTSM surface allows finite-time convergence without singularity, 2) requires no prior information of the upper limits of uncertainties, 3) shows tremendously less chattering behavior, and 4) the magnitude of the generated control input seems to be more suitable in terms of motor torque saturation compared with those of the other control methods.

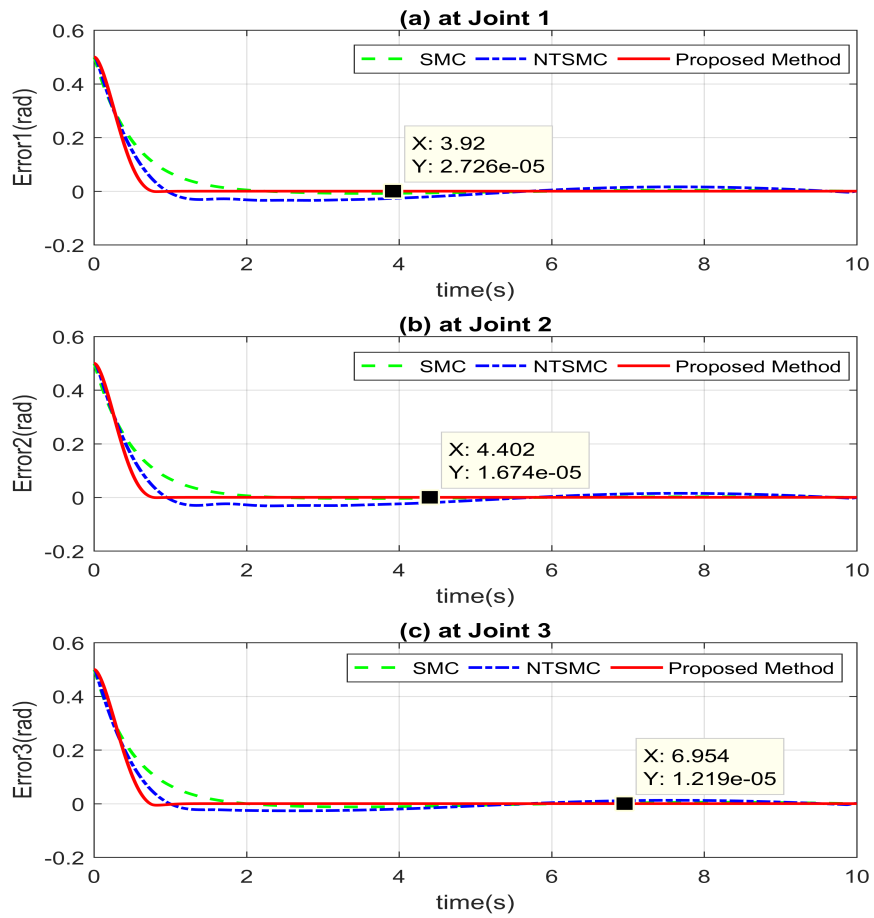


Figure 4.7: Tracking errors with a saturation function: (a) at Joint 1, (b) at Joint 2, and (c) at Joint 3.

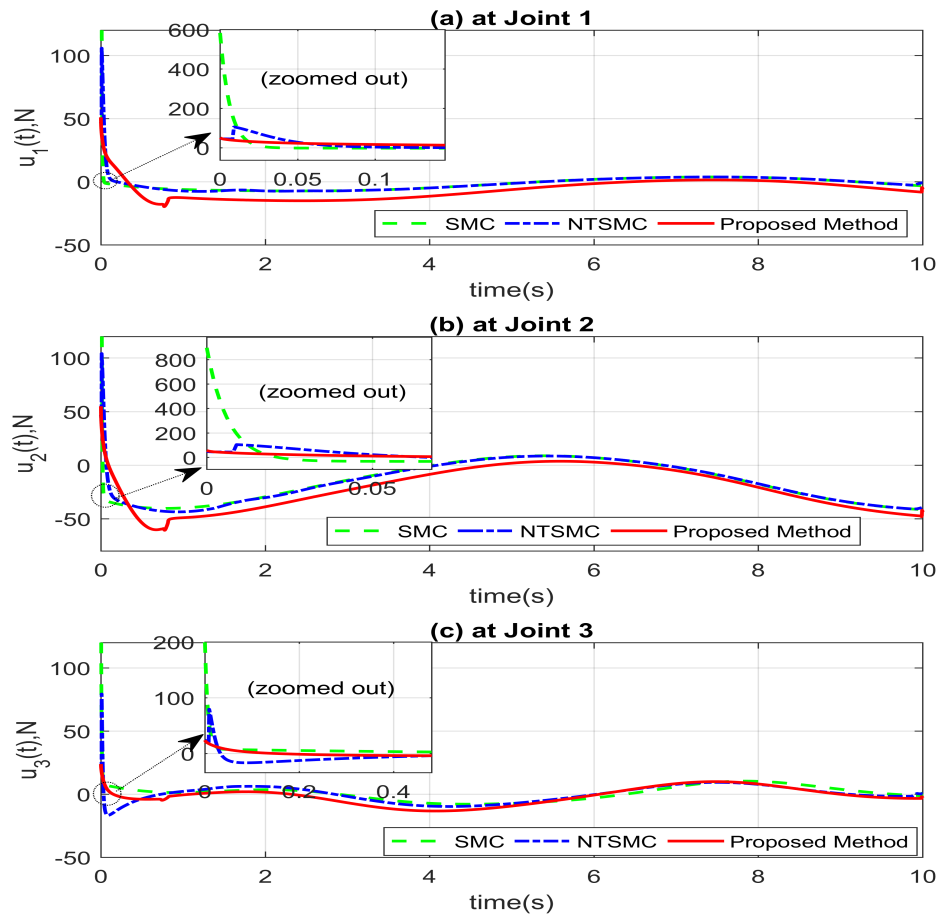


Figure 4.8: Control inputs with a saturation function: (a) at Joint 1, (b) at Joint 2, and (c) at Joint 3.

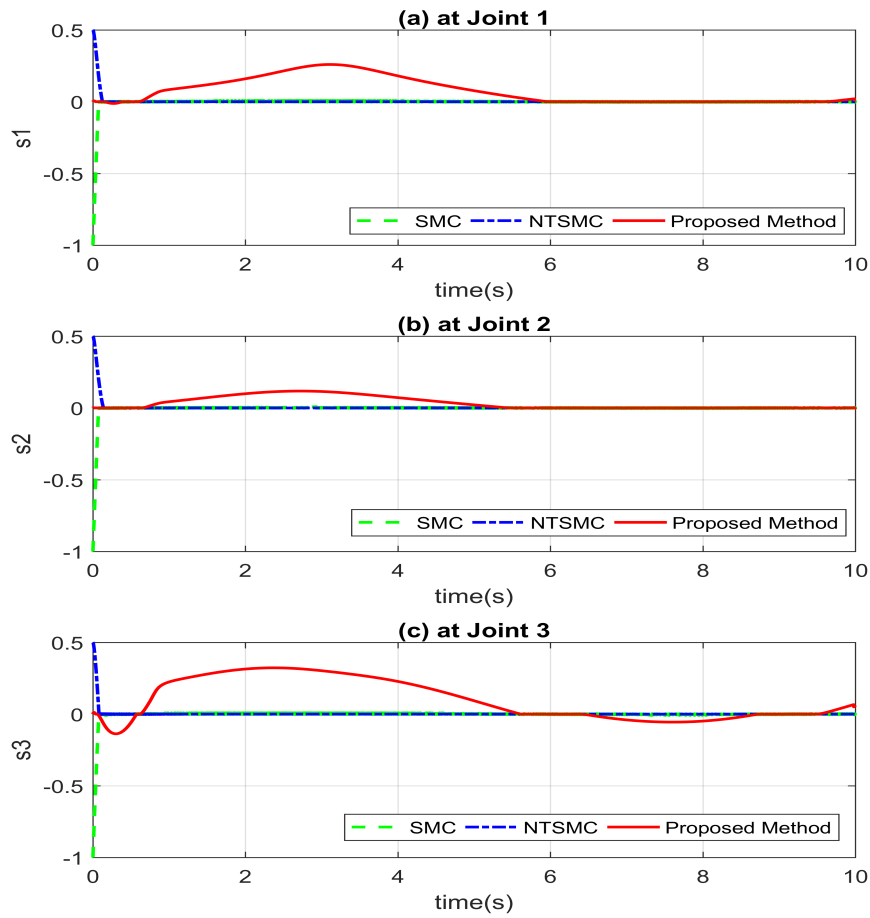


Figure 4.9: Non-singular terminal sliding surfaces with a sign function: (a) at Joint 1, (b) at Joint 2, and (c) at Joint 3.

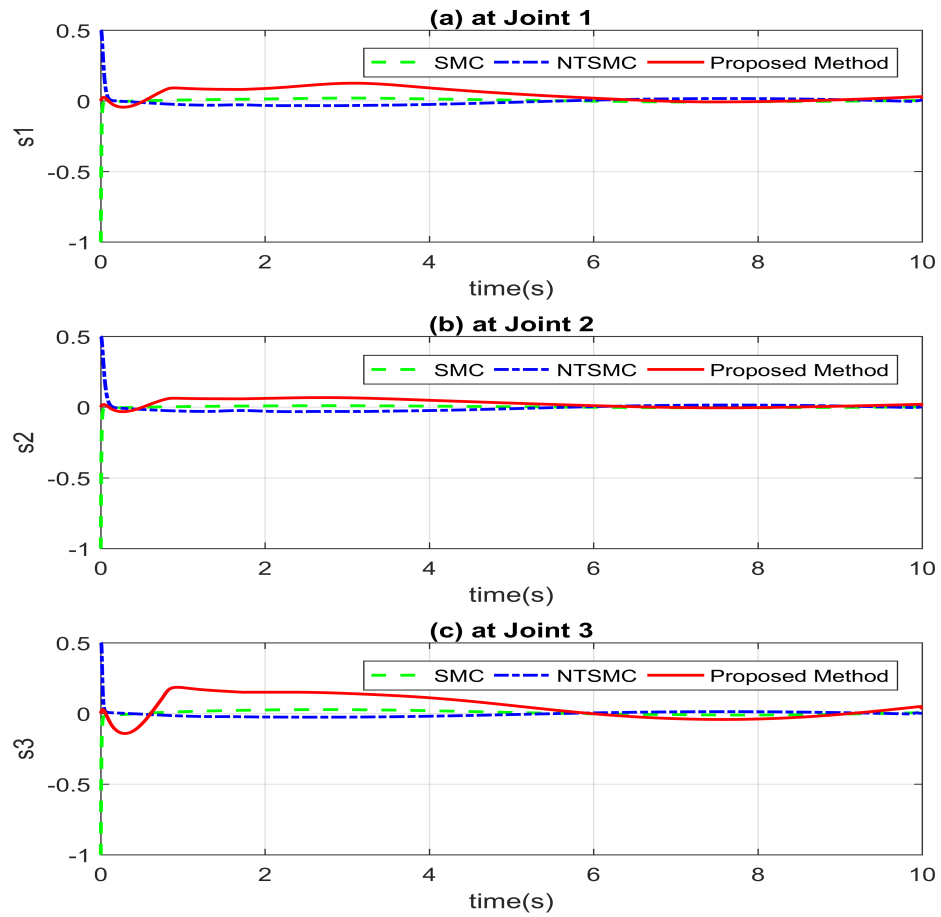


Figure 4.10: Non-singular terminal sliding surfaces with a saturation function: (a) at Joint 1, (b) at Joint 2, and (c) at Joint 3.

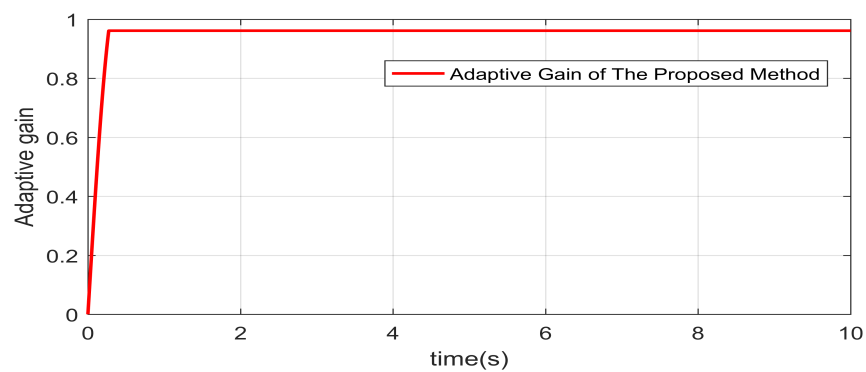


Figure 4.11: The response time of the estimating parameters with a sign function: (a) at Joint 1, (b) at Joint 2, and (c) at Joint 3.

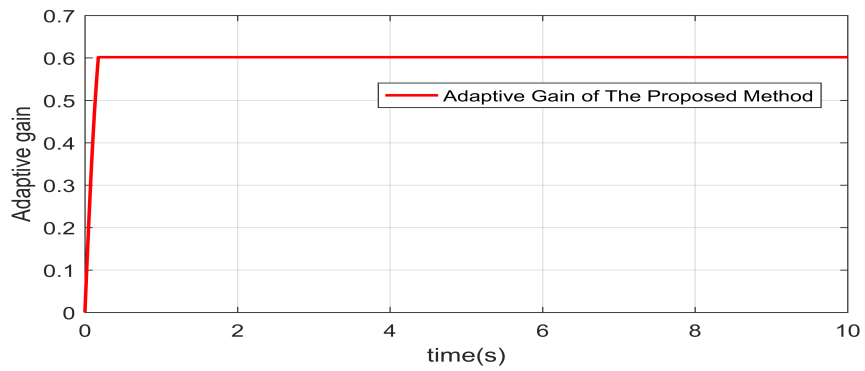


Figure 4.12: The response time of the estimating parameters with a saturation function:  
(a) at Joint 1, (b) at Joint 2, and (c) at Joint 3.

# Appendix C

Some preliminary definitions applied in the progress of the control scheme are introduced in this part.

Consider the following system as

$$\dot{x} = \psi(x); \psi(0) = 0 \quad (\text{C.1})$$

where  $x \in \Omega \subset R^n, x(0) = x_0$ .

**Definition 4.1:** [42] The original point is termed a globally balanced point of the system (C.1) in finite time in the case of an open neighborhood  $N \subseteq \Omega$  of the original point and a function  $T : N \setminus \{0\} \rightarrow (0, \infty)$ , termed the settling time, such that the following criterion holds:

Finite time convergence property: For every  $x_0 \in N \setminus \{0\}$ , every solution  $x(t, x_0)$  is defined for  $t \in [0, T(x_0))$ ,  $x(t, x_0) \in N \setminus \{0\}$ , for  $t \in [0, T(x_0))$  and,  $\lim_{t \rightarrow T(x_0)} x(t, x_0) = 0$ .

The Lyapunov stability criterion: For every open set  $\mathcal{U}_s$  such that  $0 \in \mathcal{U}_s \subseteq N$ , there exists an open set  $\mathcal{U}_\delta$  such that and such that, for every  $x_0 \in \mathcal{U}_\delta \setminus \{0\}$ ,  $x(t, x_0) \in \mathcal{U}_s$  for all  $t \in [0, T(x_0))$ .

The original point is defined as a globally balanced point in finite time in the case that it is a finite-time balanced point and  $\Omega = N = R^n$ .

**Definition 4.2:** A family of dilations  $C_\epsilon^r$  is a mapping that designates to every real  $\lambda > 0$  a diffeomorphism

$$C_\lambda^r(x_1, x_2, \dots, x_n) = (\lambda^{r_1}x_1, \lambda^{r_2}x_2, \dots, \lambda^{r_n}x_n) \quad (\text{C.2})$$

where  $x_1, x_2, \dots, x_n$  are appropriate coordinates on  $R^n$ , and  $r = r_1, r_2, \dots, r_n$  with the dilation coefficients  $r = r_1, r_2, \dots, r_n$  are positive real numbers.

A vector field  $\psi(x) = [\psi_1(x), \psi_2(x), \dots, \psi_n(x)]^T$  is homogeneous to the degree  $p \in R$  with respect to the family of dilations for all  $\lambda > 0$

$$\psi_l(\lambda^{r_1}x_1, \lambda^{r_2}x_2, \dots, \lambda^{r_n}x_n) = \lambda^{p+r_l}\psi_l(x), l = 1, 2, \dots, n \quad (\text{C.3})$$

The system of Eq. (C.1) is named homogeneous in the case its vector field  $\lambda$  is homo-



geneous.

**Lemma 4.1:** [45] The following non-linear system is considered:

$$\dot{x} = \psi(x) + \hat{\psi}(x), x \in R^n \quad (\text{C.4})$$

where  $\psi(x)$  is an  $n$ -dimensional continuous homogeneous vector field of degree  $p < 0$  with dilation  $(r_1, r_2, \dots, r_n)$  satisfying  $\psi(0) = 0$ , and  $\hat{\psi}$  is a continuous vector field satisfying  $\hat{\psi}(0) = 0$ . Assume  $x = 0$  as an asymptotic balanced point of the system  $\dot{x} = \psi(x)$ . Then, the zero solution of Eq. (C.4) is a locally finite time stable result if

$$\frac{\lim_{\lambda \rightarrow 0} \left( \hat{\psi}_l(\lambda^{r_1} x_1, \lambda^{r_2} x_2, \dots, \lambda^{r_n} x_n) \right)}{\lambda^{p+r_l}} = 0 \quad (\text{C.5})$$

$$l = 1, 2, \dots, n, \quad \forall x \neq 0$$

**Lemma 4.2:** [45, 109] The following system is considered as:

$$\begin{cases} \dot{x}_1 = x_2 \\ x_2 = u \end{cases} \quad (\text{C.6})$$

The original point of the system of Eq. (C.6) is a globally balanced point in finite time according to the principle of feedback control:

$$u = -\mu_1 |x_1|^{\vartheta_1} \text{sign}(x_1) - \mu_2 |x_2|^{\vartheta_2} \text{sign}(x_2) \quad (\text{C.7})$$

in which  $\vartheta_1, \vartheta_2$  are positive coefficients, and  $\vartheta_1, \dots, \vartheta_n$  satisfy  $\vartheta_{i-1} = \frac{\vartheta_i \vartheta_{i+1}}{2\vartheta_{i+1} - \vartheta_i}$ ,  $i = 2, \dots, n$ , with  $\vartheta_{i+1} = 1$  and  $\vartheta_i = \vartheta$ .

**Lemma 4.3:** [79] Suppose that a continuous positive-definite function  $\Delta(t)$  satisfies the differential inequality:

$$\dot{\Delta}(t) \leq -\alpha \Delta^\delta(t), \quad \forall t \geq t_0, \quad \Delta(t_0) \geq 0 \quad (\text{C.8})$$

in which  $\delta > 0$ ,  $0 < \delta < 1$  are coefficients. Then, for any given  $t_0, \Delta(t)$ , the following inequality is satisfied:

$$\Delta^{1-\delta}(t) \leq \Delta^{1-\delta}(t_0) - \alpha(1-\delta)(t-t_0), \quad t_0 \leq t \leq t_1 \quad (\text{C.9})$$

with  $\Delta(t) = 0, \forall t \geq t_1$ , where  $t_1$  is calculated by:

$$t_1 = t_0 + \frac{1}{\alpha(1-\delta)} \Delta^{1-\delta}(t_0) \quad (\text{C.10})$$

**Lemma 4.4:** ([73], Jensen's inequality). It has the following form:

$$\left(\sum_{i=1}^m \phi_i^{a_2}\right)^{\frac{1}{a_2}} \leq \left(\sum_{i=1}^m \phi_i^{a_1}\right)^{\frac{1}{a_1}}, \quad 0 < a_1 < a_2 \quad (\text{C.11})$$

with  $\phi_i \geq 0, 1 \leq i \leq m$ .



## Chapter 5

# A New Finite-time Control Solution for Robotic Manipulators Based on Non-singular Fast Terminal Sliding Variables and the Adaptive Super-Twisting Scheme

### 5.1 Introduction

In the literature related to robot manipulators, numerous control algorithms have been designed to achieve good performance and reliability with uncertainties and external noises. Several methods have been proposed to control the motion of robot manipulators, such as using PD controller [110], a nonlinear PD controller [111], an ASL-PD control scheme [112], and a PID controller [4,5]. These controllers are highlighted as simple and monotonic ways to achieve control. However, they cannot always achieve good performance results. Other competitive methods have also been presented to track the motion of robot manipulators, including FLS [113,114] and NN control [91,115,116]; however, these require higher computation costs and the effectiveness of each method is still limited. When designing a control scheme based on the robot dynamic model, the whole dynamics of the robotic system are determined and compensated for explicitly. Some advanced control methods have also been presented, including CTC [6,7], OC [97,117], AC [118], and RC [97,119]. Among these controllers, robust control algorithms have been verified to provide higher robustness, and they are also capable of rejecting uncertainties and perturbations.

SMC is a well-known robust control scheme, which is one of the most powerful method-

ologies for resolving nonlinear systems with external perturbation and uncertainty. SMC has been successfully applied to both serial and parallel robotic manipulators [15, 16]. Conventional SMC, however, still has several main drawbacks. (1) Conventional SMC commonly uses a linear sliding variable, which can only guarantee the asymptotic stability of the system but cannot converge the controlled variables to the desired values in a finite amount of time. (2) The inclusiveness of a discontinuous control input generates large chattering behavior. (3) For bigger perturbations and uncertainties, a large discontinuous control input must be used. Those control gains are determined based on essential knowledge related to the upper bound values of the perturbations and uncertainty, which are too complicated to estimate in a practical system. (4) It may encounter difficulties handling the fast variation effects of perturbations.

Motivated by these issues, research efforts have been implemented to reduce the limitations of SMC. To converge the system states within a finite amount of time on the sliding variable, TSMC based on a nonlinear sliding variable has been presented [120, 121]. However, TSMC has a slower convergence speed than conventional SMC, and TSMC also suffers from a singularity problem. To handle this singularity problem, FTSMC [68, 69] and NTSMC [122, 123] methods have been investigated. Practically, however, methods based on FTSMC or NTSMC have only addressed one limitation, skipping the other issues that limit conventional SMC. Therefore, NFTSMC [47, 48] has been introduced. With NFTSMC, the system states achieve fast finite-time convergence and avoid the singularity problem. Another approach to improve the transient response of conventional SMC is to use ISMC [50, 51]. One of the goals of this research is to achieve both finite-time convergences and fast transient response speed. Therefore, ISMC and TSMC can be combined to establish ITSMC [52, 53]. However, ITSMC still has the drawbacks of conventional SMC because the TSMC scheme is still included in the design of ITSMC.

Chattering behavior is an undesired issue in practical applications that rely on TSMC, FTSMC, NTSMC, or NFTSMC with a high-frequency switching control term. Therefore, some effective algorithms have been developed to handle this issue via the saturation function or hyperbolic and relay function. However, such techniques reduce the robustness and tracking positional accuracy, and they sometimes require too much initial control input. While each limitation of conventional SMC and TSMC has been handled on its own, this paper attempts to solve all of the limitations of SMC and TSMC, including chattering, fast finite-time convergence, and unknown knowledge of the upper bounds of the uncertainty and perturbation, simultaneously.

Thus, the main goal of our paper is to propose a new finite-time tracking control algorithm based on non-singular fast terminal sliding variables and the adaptive super-twisting method for robotic manipulators. The major benefits of the proposed control

solution are given as:

- Inherits the advantages of NFTSMC in terms of its high robustness, fast transient response speed, finite-time convergence, and ability to avoid the singularity drawback.
- The upper limit of the convergence time can be set beforehand.
- Does not demand essential information of the upper limits for perturbations and uncertainties.
- Generates control inputs with smooth and chattering-free behavior.
- Robustness and finite-time stability problem of the robot system have been verified fully by the Lyapunov principle.

The remainder of this chapter is organized as follows. The problem statements required for the proposed nonsingular fast sliding variables and control are presented in the second section. The third section gives the design procedure of the suggested control solution. In the fourth section, the suggested control solution is applied to the joint position tracking control simulation for a 3-DOF PUMA560 robot, and its trajectory tracking performance is compared with those of SMC and TSMC, as shown in [16,37]. Finally, some conclusions are described in the last section.

**Notation:** Several types of notation are utilized in the article.  $\|\cdot\|$  denote the Euclidean norm and modulus, respectively.  $\mathbb{R}$  denotes the space of real numbers.

## 5.2 Problem Statement

For an n-link rigid robotic manipulator, the corresponding dynamic model can be defined in joint space as (see [37,40]):

$$M(q)\ddot{q} + C_m(q, \dot{q})\dot{q} + G(q) + F_r(\dot{q}) = \tau - \tau_p. \quad (5.1)$$

Here,  $q, \dot{q}, \ddot{q} \in R^n$  correspond to the position, velocity, and acceleration of the robot manipulator, respectively, and  $M(q) \in R^{n \times n}$  is the inertia matrix,  $C_m(q, \dot{q}) \in R^{n \times 1}$  is the matrix from the centrifugal force and Coriolis,  $G(q) \in R^{n \times 1}$  is the gravitational force matrix,  $F_r(\dot{q}) \in R^{n \times 1}$  is the matrix resulting from friction,  $\tau \in R^{n \times 1}$  is the control input torque, and  $\tau_p \in R^{n \times 1}$  is a load perturbation matrix.

To simplify the design and analysis in the next part, Eq. (5.1) can be rewritten as:

$$\Xi(q, \dot{q}, \ddot{q}) + \Delta_u(q, \dot{q}, t) = \tau. \quad (5.2)$$

Here,  $\Xi(q, \dot{q}, \ddot{q})$  is the nominal robot system when there are no perturbations or uncertainties.  $\Delta_u(q, \dot{q}, t) = F_r(\dot{q}) + \tau_p$  presents the total components of the perturbations and uncertainties. General robotic manipulators have the following properties.

**Assumption 5.1:** The inertia matrix  $M(q)$  is an invertible, positive definite, and symmetric matrix bounding the following condition:

$$\delta_1 \leq M(q) \leq \delta_2. \quad (5.3)$$

Here,  $\delta_1$  and  $\delta_2$  denote positive coefficients.

To ensure occurrence of the sliding motion in a finite amount of time without essential information related to the upper bounds of elements influencing the robot (e.g. friction, disturbances, and uncertainties), the following assumptions are necessary when designing the control algorithm in the sequel.

**Assumption 5.2:** The perturbations and uncertainties are a limited function satisfying the following relation:

$$\left\| \frac{d}{dt} \Delta_u \right\| \leq \Omega. \quad (5.4)$$

Here,  $\Omega$  is a known positive coefficient that is first-order differentiable.

**Remark 5.1:** The Assumption 5.2 is realistic in real applications. For example, when a cutting tool or an end mill of a CNC machine tool cuts a work-piece, the load torque may change as the cutting thickness changes, but the change rate of the load torque is always limited. In this chapter, the Assumption 5.2 in equation (5.4) might not be satisfied for some conditions when the change of disturbances and uncertainties is very fast. In this situation, the system might be unstable. Fortunately, due to the benefits of the proposed NFTSM variables and ASTA, the system responses against disturbances and uncertainties can stabilize the system very quickly. This is one of the contributions of the chapter, which has been verified in the simulation. The reviewers can refer to [71] for more detail of this Assumption.

The control destination of our paper is that the controlled variables will achieve the desired trajectory in a limited time under the newly designed control method. In this case, essential information related to the upper limits of the perturbations and uncertainties is rejected.

## 5.3 Design Procedure of the Control Scheme

In this section, a new control scheme is suggested for Eq. (5.1), which is described by the two following main tasks.

### 5.3.1 Design of NFTSM Variables

The set  $e_i^p = q_i - q_i^r$  ( $i = 1, 2, \dots, n$ ) is the tracking positional error, where  $q^r$  is defined as the desired trajectory value. According to the design technique of TSMC, a state variable (referred to as the NFTSM variable) is defined beforehand. From the tracking positional error, the novel NFTSM variables are proposed as:

$$s_i = e_i^p + \int_0^t \left( \Gamma_{1i} (e_i^p)^{[2-\vartheta_i]} + \Gamma_{2i} e_i^p + \Gamma_{3i} (e_i^p)^{[\vartheta_i]} \right) d\sigma. \quad (5.5)$$

Here,  $s_i$  is the sliding variable;  $\Gamma_{1i}, \Gamma_{2i}, \Gamma$  are positive coefficients satisfying the relation  $4\Gamma_{1i}\Gamma_{3i} > \Gamma_{2i}^2$ ,  $0 < \vartheta_i < 1$  ( $i = 1, 2, \dots, n$ ); and  $(e_i^p)^{[\vartheta_i]}$  are defined as (see [124]):

$$(e_i^p)^{[\vartheta_i]} = |e_i^p|^{\vartheta_i} \text{sign}[e_i^p]. \quad (5.6)$$

**Remark 5.2:** Once the tracking positional error of  $|e_i^p|$  is much greater than 1,  $\Gamma_{1i} (e_i^p)^{[2-\vartheta_i]} + \Gamma_{2i} e_i^p$  expresses the role of providing a fast convergence speed. Alternatively, when the tracking positional error of  $|e_i^p|$  is much smaller than 1,  $\Gamma_{3i} (e_i^p)^{[\vartheta_i]}$  expresses the role of determining finite-time convergence.

According to the SMC technique, once the tracking positional error runs in the sliding mode, the following relations are approved [16] and [20]:

$$s_i = 0; \dot{s}_i = 0. \quad (5.7)$$

Accordingly, based on Eq. (5.5) and Eq. (5.7), it is determined that

$$e_i^p + \int_0^t \left( \Gamma_{1i} (e_i^p)^{[2-\vartheta_i]} + \Gamma_{2i} e_i^p + \Gamma_{3i} (e_i^p)^{[\vartheta_i]} \right) d\sigma = 0. \quad (5.8)$$

Therefore, the following sliding mode dynamics can be obtained:

$$\dot{e}_i^p = -\Gamma_{1i} (e_i^p)^{[2-\vartheta_i]} - \Gamma_{2i} e_i^p - \Gamma_{3i} (e_i^p)^{[\vartheta_i]}. \quad (5.9)$$

The following theorem establishes that finite-time convergence occurs.

**Theorem 5.1:** Consider the dynamic system of Eq. (5.9). The original point  $e_i^p = 0$  is globally balanced in a finite amount of time and the state variable of the system in Eq. (5.9) converges to zero in a finite amount of time  $T_{e_i^p}^f \leq T_{e_i^p}^f$ .



$T_{e_i^p}^f$  is defined as:

$$T_{e_i^p}^f = \frac{2}{(1 - \vartheta_i)} \left( \frac{\pi}{2} - \tan^{-1} \frac{\Gamma_{2i}}{\sqrt{4\Gamma_{1i}\Gamma_{3i} - \Gamma_{2i}^2}} \right) \frac{1}{\sqrt{4\Gamma_{1i}\Gamma_{3i} - \Gamma_{2i}^2}}. \quad (5.10)$$

**Proof:** From Eq. (5.9), the Lyapunov function candidate is defined as:

$$L_1 = (e_i^p)^2. \quad (5.11)$$

With Eq. (5.9), the time derivative of Eq. (5.11) is derived as:

$$\begin{aligned} \dot{L}_1 &= 2e_i^p \dot{e}_i^p \\ &= 2e_i^p \left( -\Gamma_{1i} (e_i^p)^{[2-\vartheta_i]} - \Gamma_{2i} e_i^p - \Gamma_{3i} (e_i^p)^{[\vartheta_i]} \right) \\ &= 2 \left( -\Gamma_{1i} (e_i^p)^{[3-\vartheta_i]} - \Gamma_{2i} (e_i^p)^2 - \Gamma_{3i} (e_i^p)^{[1+\vartheta_i]} \right) \\ &= 2 \left( -\Gamma_{1i} L_1^{\frac{3-\vartheta_i}{2}} - \Gamma_{2i} L_1 - \Gamma_{3i} L_1^{\frac{\vartheta_i+1}{2}} \right) \end{aligned} \quad (5.12)$$

To give a conclusion from Eq. (5.12), the following Lemma is used.

**Lemma 5.1:** [40] For any real numbers  $z_1 > 0$ ,  $z_2 > 0$ , and  $0 < \varphi < 1$ , an extended Lyapunov function condition of finite-time stability can be given in the form of a fast terminal sliding mode:  $\dot{L}(x) + z_1 L(x) + z_2 L^\varphi(x) \leq 0$ , where the settling time can be estimated by

$$T \leq \frac{1}{z_1(1-\varphi)} \ln \frac{z_1 L^{1-\varphi}(x(0)) + z_2}{z_2}. \quad (5.13)$$

From Eq. (5.12),  $\frac{\vartheta_i+1}{2} < 1$  means  $\dot{L}_1 \leq 0$ . Based on Lemma 5.1, the original point of  $e_i^p = 0$  is a globally balanced point over a finite amount of time. In the next step, it will be proven that the error state variable of the system in (5.9) converges to zero in a finite amount of time.

Eq. (5.12) can be shown as:

$$\dot{L}_1 = 2L_1^{\frac{\vartheta_i+1}{2}} \left( -\Gamma_{1i} L_1^{1-\vartheta_i} - \Gamma_{2i} L_1^{\frac{1-\vartheta_i}{2}} - \Gamma_{3i} \right). \quad (5.14)$$

Additionally, Eq. (5.14) can be expressed as:

$$\begin{aligned}
 dL_1 &= 2L_1^{\frac{\vartheta_i+1}{2}} \left( \Gamma_{1i}L_1^{1-\vartheta_i} + \Gamma_{2i}L_1^{\frac{1-\vartheta_i}{2}} + \Gamma_{3i} \right) dt \\
 \Rightarrow dt &= -\frac{dL_1}{2L_1^{\frac{\vartheta_i+1}{2}} \left( \Gamma_{1i}L_1^{1-\vartheta_i} + \Gamma_{2i}L_1^{\frac{1-\vartheta_i}{2}} + \Gamma_{3i} \right)} \\
 &= -\frac{1}{1-\vartheta_i} \frac{dL_1^{\frac{1-\vartheta_i}{2}}}{\left( \Gamma_{1i}L_1^{1-\vartheta_i} + \Gamma_{2i}L_1^{\frac{1-\vartheta_i}{2}} + \Gamma_{3i} \right)}
 \end{aligned} \tag{5.15}$$

Setting  $L_1(T_{e_i^p}) = 0$  and taking the integral of Eq. (5.15) during the time period of  $0 \rightarrow T_{e_i^p}$  gives:

$$T_{e_i^p} = \frac{2}{(1-\vartheta_i)} \frac{1}{\sqrt{4\Gamma_{1i}\Gamma_{3i} - \Gamma_{2i}^2}} \left( \arctan \frac{2\Gamma_{1i}L_1^{\frac{1-\vartheta_i}{2}}(e_i^p(0))}{\sqrt{4\Gamma_{1i}\Gamma_{3i} - \Gamma_{2i}^2}} - \arctan \frac{\Gamma_{2i}}{\sqrt{4\Gamma_{1i}\Gamma_{3i} - \Gamma_{2i}^2}} \right). \tag{5.16}$$

From Eq. (5.16),  $T_{e_i^p}$  is limited by  $T_{e_i^p}^f = \frac{2}{(1-\vartheta_i)} \left( \frac{\pi}{2} - \arctan \frac{\Gamma_{2i}}{\sqrt{4\Gamma_{1i}\Gamma_{3i} - \Gamma_{2i}^2}} \right) \frac{1}{\sqrt{4\Gamma_{1i}\Gamma_{3i} - \Gamma_{2i}^2}}$ . In fact,  $L_1(T_{e_i^p}) = 0$  means  $e_i^p(T_{e_i^p}) = 0$ . In addition, it can be seen that the upper bound of  $T_{e_i^p}^f$  is depends only on the designing constants  $\Gamma_{1i}, \Gamma_{2i}, \Gamma_{3i}$ , and  $\vartheta_i$ , and the tracking positional error in Eq. (5.9) reaches zero in a finite amount of time. This completes the proof of Theorem 5.1.

The proposed control solution forces the error state variables to reach sliding variables in a finite amount of time. This will be presented in the next step.

### 5.3.2 Design of a New Finite-time Control Solution Based on NFTSM Variables and the ASTA

The following proposed controller is designed according to the designing procedure of sliding mode control:

$$\tau_{SMC} = \tau_{eq} + \tau_{sw}. \tag{5.17}$$

The term of the equivalent control of  $\tau_{eq}$  maintains the trajectory of the error state variables on the sliding variables. To get this result, it is necessary to take the derivative of sliding variables with respect to time. Also,  $\dot{s} = 0$  for a nominal system that does not consider perturbations or uncertainties. The time derivative of sliding variables is

expressed as:

$$\dot{s} = \dot{e}^p + \Gamma_1 (e^p)^{[2-\vartheta_i]} + \Gamma_2 e^p + \Gamma_3 (e^p)^{[\vartheta_i]}. \quad (5.18)$$

With Eq. (5.1),  $\dot{e}^p$  can be presented as:

$$\dot{e}^p = \tau_{SMC} + \Xi^*, \quad (5.19)$$

in which the dynamic function of the robot is shown as:

$$\Xi^* = -M(q)\ddot{q} + (I^{n \times n} - C_m(q, \dot{q}))\dot{q} - G(q) - F_r - \tau_p - \dot{q}^r. \quad (5.20)$$

Substituting Eq. (5.19) into Eq. (5.18) gives:

$$\dot{s} = (\tau_{SMC} + \Xi^*) + \Gamma_1 (e^p)^{[2-\vartheta_i]} + \Gamma_2 e^p + \Gamma_3 (e^p)^{[\vartheta_i]}. \quad (5.21)$$

The equivalent control term can be defined in the case where  $\dot{s} = 0$ , without considering the perturbations and uncertainties, as:

$$\tau_{eq} = -\Xi - \Gamma_1 (e^p)^{[2-\vartheta_i]} - \Gamma_2 e^p - \Gamma_3 (e^p)^{[\vartheta_i]} - \mu s^{[\frac{1}{2}]} - \eta_\mu s. \quad (5.22)$$

Here,  $\mu$  and  $\eta_\mu$  are positive coefficients.

The switching control term is designed as:

$$\tau_{sw} = -\eta_2 \text{sign}(s), \quad (5.23)$$

in which  $\eta_2$  is a positive coefficient.

Therefore, the overall control input becomes

$$\tau_{SMC} = \tau_{eq} + \tau_{sw} = -\Xi - \Gamma_1 (e^p)^{[2-\vartheta_i]} - \Gamma_2 e^p - \Gamma_3 (e^p)^{[\vartheta_i]} - \mu s^{[\frac{1}{2}]} - \eta_\mu s - \eta_2 \text{sign}(s). \quad (5.24)$$

When the design parameters of the switching control term are greater than the uncertainties of the upper bounds, the stability of the system in Eq. (5.17) can be fully proven by the Lyapunov criterion. Unfortunately, robot manipulators have a complicated dynamic model with many parametric uncertainties (e.g., friction, payload, perturbations, and sensor noise). Those may reduce the tracking positional precision. Also, it is not easy to exactly determine the essential information of the uncertainties of upper limits and the robot dynamic function in the equivalent control. To solve those problems, we construct a new finite-time control solution for the robot manipulator with adaptive tuning principles instead of using a fixed gain  $\eta_2$ . Therefore, the sliding motion is guaranteed to take place

in a finite amount of time without requiring the essential information of the upper limits of perturbations and uncertainties. For that reason, the robot control solution of Eq. (5.24) is presented as:

$$\tau_{SMC} = \tau_{eq} + \tau_{asw} = -\Xi - \Gamma_1 (e^p)^{[2-\vartheta_i]} - \Gamma_2 e^p - \Gamma_3 (e^p)^{[\vartheta_i]} - \mu s^{[\frac{1}{2}]} - \eta_\mu s + \rho_a, \quad (5.25)$$

in which  $\tau_{asw}$  is an adaptive control term that replaces the control law  $\tau_{sw}$  in Eq. (5.23). Its adaptive updating rule is given as:

$$\dot{\rho}_a = \eta_\nu s - \nu \text{sign}(s), \quad (5.26)$$

in which  $\nu$  and  $\eta_\nu$  are positive coefficients.

The adaptive updating rule is proposed and referred to as the super-twisting method [124]. To complete the proof, the following Lemma is necessary.

**Lemma 5.2:** [125] The following system is considered:

$$\begin{cases} \dot{\sigma} = -\mu(t) w^{[\frac{1}{2}]} - \eta_\mu(t) w + \varpi \\ \dot{\varpi} = -\eta_\nu(t) w - \nu(t) \text{sign}(w) + \kappa(t) \end{cases}. \quad (5.27)$$

Assume that the term  $\kappa$  is a perturbation that satisfies the following condition:

$$|\kappa(t)| \leq \kappa^*. \quad (5.28)$$

With some unknown coefficients  $\kappa^* > 0$ , the estimating parameters  $\mu, \nu, \eta_\mu$ , and  $\eta_\nu$  are defined as:

$$\begin{cases} \mu(t) = \mu_0 \sqrt{V_0(t)} \\ \nu(t) = \nu_0 V_0(t) \\ \eta_\mu(t) = \eta_{\mu_0} V_0(t) \\ \eta_\nu(t) = \eta_{\nu_0} V_0^2(t) \end{cases}. \quad (5.29)$$

Here, the initial values  $\mu_0, \nu_0, \eta_{\mu_0}$ , and  $\eta_{\nu_0}$  of the estimating parameters  $\mu, \nu, \eta_\mu$ , and  $\eta_\nu$  are positive coefficients and  $V_0(t)$  is a time-varying, positive, scalar function. The adaptive updating rule of the time-varying function  $V_0(t)$  is given as:

$$\dot{V}_0(t) = \begin{cases} \Upsilon, & |w| \neq 0 \\ 0, & \text{otherwise} \end{cases}. \quad (5.30)$$

Here,  $\Upsilon$  is an arbitrary positive constant. The state variables of Eq. (5.26) reach zero within a finite amount of time when the initial values  $\mu_0, \nu_0, \eta_{\mu_0}$ , and  $\eta_{\nu_0}$  satisfy the

following relation:

$$4\nu_0\eta_{\nu_0} \geq (8\nu_0 + 9\mu_0^2) \eta_{\mu_0}^2. \quad (5.31)$$

The control method used to achieve the control goal for the system of Eq. (5.10) is summarized in Theorem 5.2.

**Theorem 5.2:** For the system of Eq. (5.1), if the suitable finite-time NFTSM variables have been selected as shown in Eq. (5.5), the control input signal is constructed as shown in Eq. (5.25) (with its parameter updating rules designed as shown in Eqs. (5.29)-(5.30)), and the corresponding parameters satisfy the conditions of Eq. (5.31), then the sliding variable motion is guaranteed to happen. This means that the error state variables reach sliding variables in a finite amount of time and the system of Eq. (5.9) is globally finite-time stable.

**Proof:** With Eq. (5.1) and the control input of Eq. (5.25), Eq. (5.21) yields:

$$\begin{cases} \dot{s} = -\Xi - \Gamma_1 (e^p)^{[2-\vartheta_i]} - \Gamma_2 e^p - \Gamma_3 (e^p)^{[\vartheta_i]} - \mu s^{[\frac{1}{2}]} \\ \quad - \eta_\mu s + \rho_a + \Xi^* + \Gamma_1 (e^p)^{[2-\vartheta_i]} + \Gamma_2 e^p + \Gamma_3 (e^p)^{[\vartheta_i]} \\ \quad = -\mu s^{[\frac{1}{2}]} - \eta_\mu s + \rho_a + \Delta_u \\ \dot{\rho}_a = -\eta_\nu s - \nu \text{sign}(s) \end{cases}. \quad (5.32)$$

By denoting the new variable as  $\varpi$

$$\varpi = \rho_a + \Delta_u, \quad (5.33)$$

the system of Eq. (5.32) can be rewritten as:

$$\begin{cases} \dot{s} = -\mu s^{[\frac{1}{2}]} - \eta_\mu s + \varpi \\ \dot{\varpi} = -\eta_\nu s - \nu \text{sign}(s) + \frac{d}{dt} \Delta_u \end{cases}. \quad (5.34)$$

According to Assumption 5.2 and Lemma 5.2, the state variables of Eq. (5.32) reach zero in a finite amount of time, which means that the sliding mode motions of  $s = 0$  take place in the finite amount of time,  $T_s$  [125]. Therefore, Theorem 5.2 is totally proven.

**Remark 5.3:** With the proven results of Theorems 5.1 and 5.2, it can be summarized that applying the suggested control method in Eq. (5.25) (with its parameter updating rules designed as shown in Eqs. (5.29)-(5.30), with the corresponding parameters satisfying the conditions of Eq. (5.31), and with the finite-time NFTSM variables selected as shown in Eq. (5.5)) leads the error state variables to reach sliding variables within a finite amount of time  $T \leq \max \{T_s + T_{e_i^p}^f\}$ .

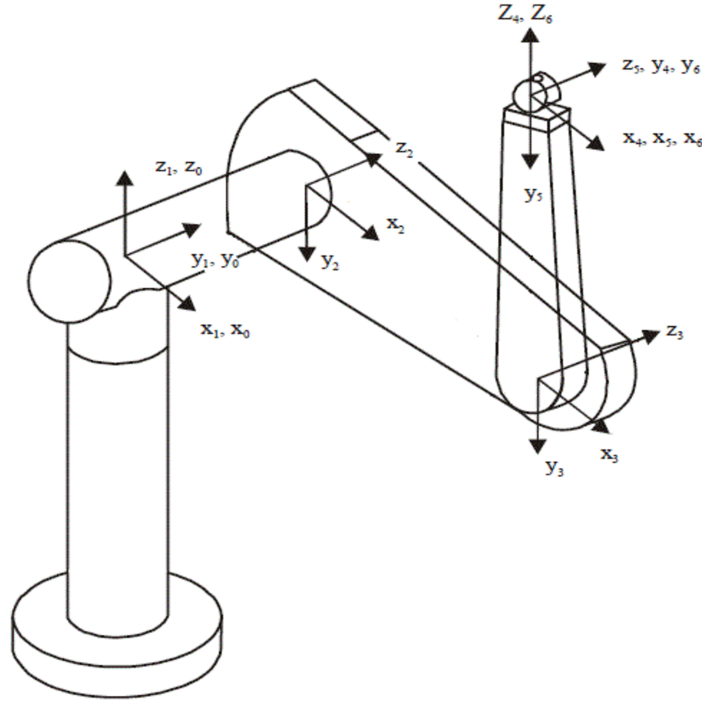


Figure 5.1: 3-DOF PUMA560 robot manipulator.

**Remark 5.4:** In this chapter, the robustness issue and the finite-time convergence of the suggested system are totally confirmed by the Lyapunov stability principle. Through simulation studies, the experimental results could be expected to exhibit the effectiveness and viability of our proposed scheme for joint position tracking control of a 3-DOF PUMA560 robot. In the future, authors will apply the proposed controller to the real robot system to demonstrate the effectiveness of this control method.

## 5.4 Numerical Simulation Studies

The proposed control solution is applied for trajectory tracking control simulation for the first three joints of a PUMA560 manipulator to demonstrate its viability and effectiveness. A dynamic model with essential parameters of the manipulator was utilized in [72]. We used Matlab/Simulink software for all numerical simulation studies, and the sampling time was set to  $10^{-3}$  s.

A 3-DOF PUMA560 robot manipulator with the first three joints and the last three joints locked is considered. Its kinematic representation is shown in Fig. 5.1.

To test the robustness of the control system, a large value of the perturbations and uncertainties are assumed in these simulations, as follows. The friction  $F_r(\dot{\theta})$  and per-

turbation  $\tau_p$  are assumed to be

$$F_r(\dot{\theta}) + \tau_p = \begin{bmatrix} 0.5\dot{q}_1 + 1.0\text{sign}\left(3\dot{\theta}_1\right) \\ 1.3\dot{q}_2 + 1.8\text{sign}\left(2\dot{\theta}_2\right) \\ -1.8\dot{q}_3 + 2.0\text{sign}\left(2\dot{\theta}_3\right) \end{bmatrix} + \begin{bmatrix} 7.2 \sin\left(\dot{\theta}_1\right) \\ 6.1 \sin\left(\dot{\theta}_2\right) \\ 4.15 \sin\left(\dot{\theta}_3\right) \end{bmatrix}. \quad (5.35)$$

Additionally, the desired joint trajectories for the position tracking are

$$q^r = \begin{bmatrix} 0.6 + \cos\left(\frac{t}{6\pi}\right) - 1, & -0.6 + \sin\left(\frac{t}{6\pi} + \frac{\pi}{2}\right), & 0.6 + \sin\left(\frac{t}{6\pi} + \frac{\pi}{2}\right) - 1 \end{bmatrix}^T. \quad (5.36)$$

The parameters for the NFTSM variables of Eq. (5.5) are experimentally selected. They are based on convergence properties stated in Remark 6.2. The parameters for the controlling input signals in Eq. (5.25) (with the adaptive updating rules established in Eqs. (5.29)-(5.30)) were experimentally chosen to make system stable, to obtain the desired performance with fast convergence time (the upper bound of the convergence time is  $T_{e_i^p}^f \approx 0.8\text{s}$  based on the results in Eq. (5.16)) as  $\Gamma_1 = \text{diag}(3, 3, 3)$ ,  $\Gamma_2 = \text{diag}(2, 2, 2)$ , and  $\Gamma_3 = \text{diag}(3, 3, 3)$ , which satisfy conditions mentioned in the article and explained in references [90, 124, 125] as  $4\Gamma_{1i}\Gamma_{3i} > \Gamma_{2i}^2$  and  $\vartheta_i = 0.4$  ( $i = 1, 2, 3$ ) ( $0 < \vartheta < 1$ ). Additionally, we set  $\Upsilon = 8$  and  $V_0(0) = 3$ , which satisfy the relation of Eq. (5.30), and  $\mu_0 = 2$ ,  $\nu_0 = 4$ ,  $\eta_{\mu_0} = 2.5$ , and  $\eta_{\nu_0} = 30$ , which satisfy the relation of Eq. (5.31) and  $\rho_a(0) = 0$ .

To demonstrate the effectiveness of the proposed control solution, its trajectory tracking performances are compared with those of SMC [16] and NTSMC [37, 40]. The control schemes for these comparisons are briefly expressed in the appendix.

The parameters of the controller in Eq. (D.10) were chosen as  $\alpha = 2$  and  $g = 10$  to guarantee stability and obtain good performances (referred to [16]).

Additionally, the parameters of the controller in Eq. (D.18) were chosen as  $l = 5$ ,  $h = 3$ ,  $\beta = 2$ ,  $l_g = 8$ , and  $\xi = 2$  to guarantee stability and obtain the good performances (referred to [37, 40]).

For a fair comparison, the initial control input magnitudes of the control methods are similar and in the allowable range. Simulations were performed to compare the controllers in terms of their positional precision, their fast response speed, and the resulting chattering behaviors in their control inputs.

The averaged tracking errors are calculated according to:  $e_i^p = \sqrt{\frac{1}{n} \sum_{k=1}^n (\|e_i^p\|^2)}$  in which  $i = 1, 2, 3$ , and  $n$  is the number of simulation steps.

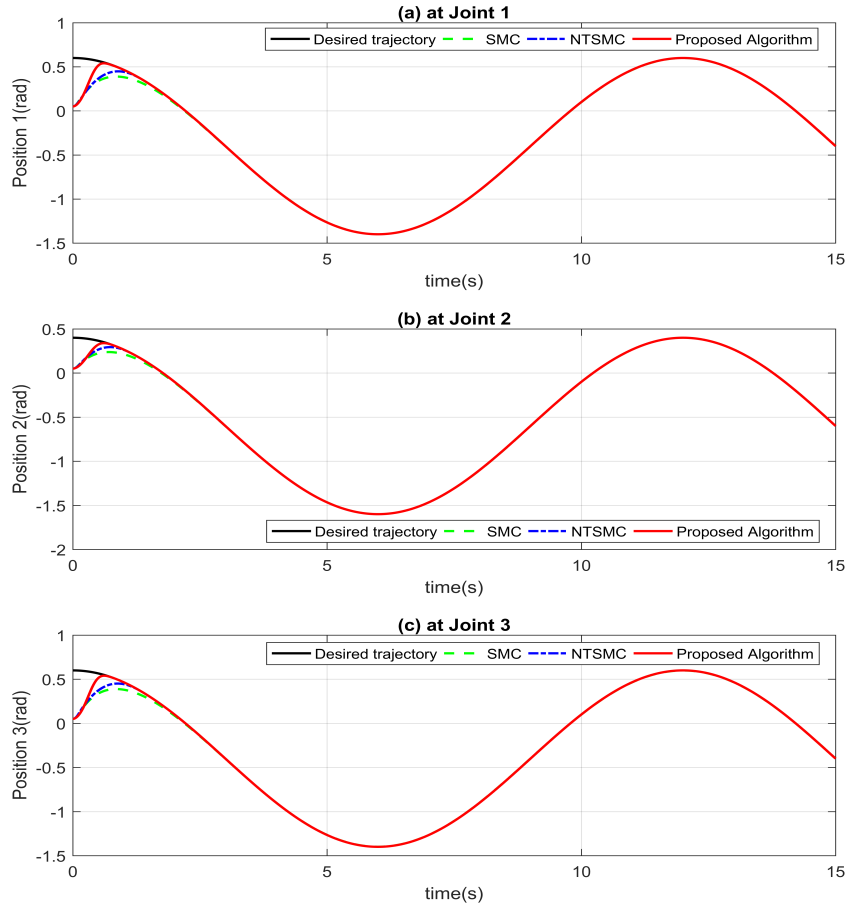


Figure 5.2: Tracking positions: (a) at Joint 1, (b) at Joint 2, and (c) at Joint 3

The tracking positional trajectories and tracking positional errors of the first three joints with the three control schemes are exhibited in Figs. 7.3-7.4. It can be seen that all three of the control schemes seem to have the same good trajectory tracking performance. However, the tracking errors of the suggested control scheme are relatively small compared to those of the other control methods, on the order of  $10^{-7}$  rad, and the convergence times of those errors are faster. The tracking positional errors of the other control schemes are on the order of  $10^{-4} \sim 10^{-5}$  rad, with slower convergence times, as can be observed in Table 5.1. Additionally, the chattering phenomena of our proposed solution were improved, as shown in Fig. 7.5.

The chattering behavior obtained with the suggested NFTSM variable and control principle was much less compared to the other control schemes. The suggested control input system is efficiently smooth and demonstrates chattering-free behavior.



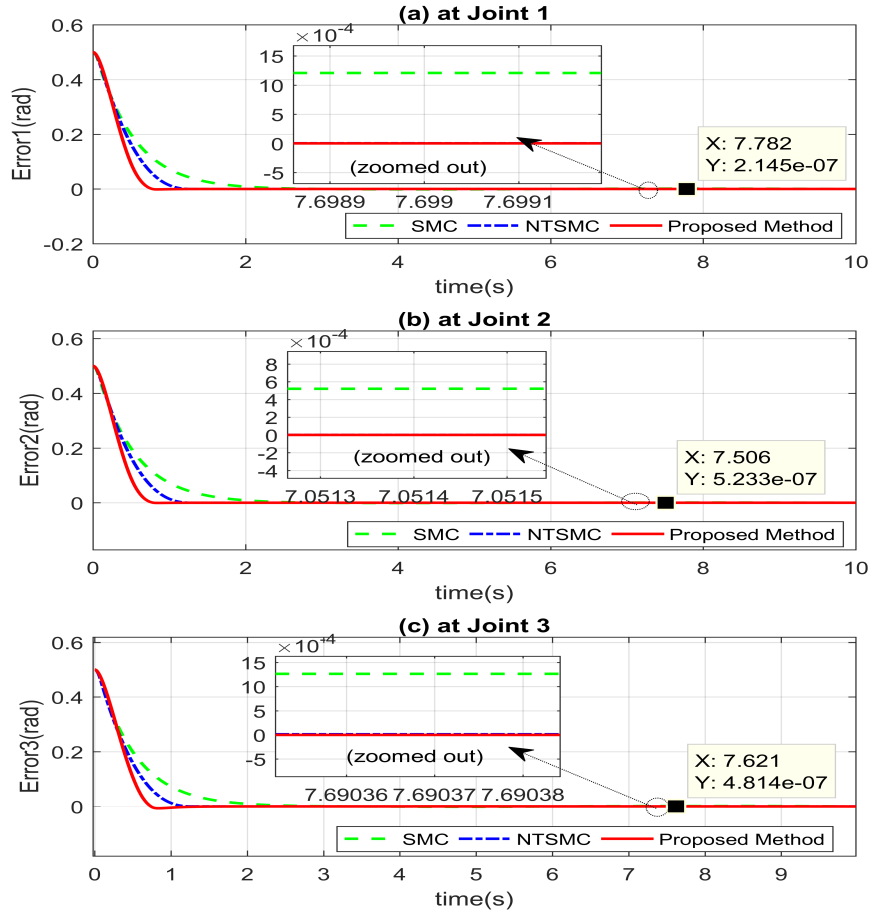


Figure 5.3: Tracking errors: (a) at Joint 1, (b) at Joint 2, and (c) at Joint 3 .

By adjusting the value of  $\dot{V}_0(t)$ , a better transient performance can be obtained. From the response time of the sliding variables in Fig. 7.6, the proposed NFTSM variable shows the best performance for fast finite-time convergence.

## 5.5 Conclusions

In this study, a new trajectory tracking control solution is developed for robot manipulators. Based on numerical simulation results and a performance comparison with two other control schemes for a 3-DOF PUMA560 robot manipulator, our control scheme shows the best performance in terms of tracking positional precision, small steady-state errors, fast response rate, and small chattering behavior. The suggested control solution has the following valuable benefits. 1) It uses new NFTSM variables, which offer a fast transient

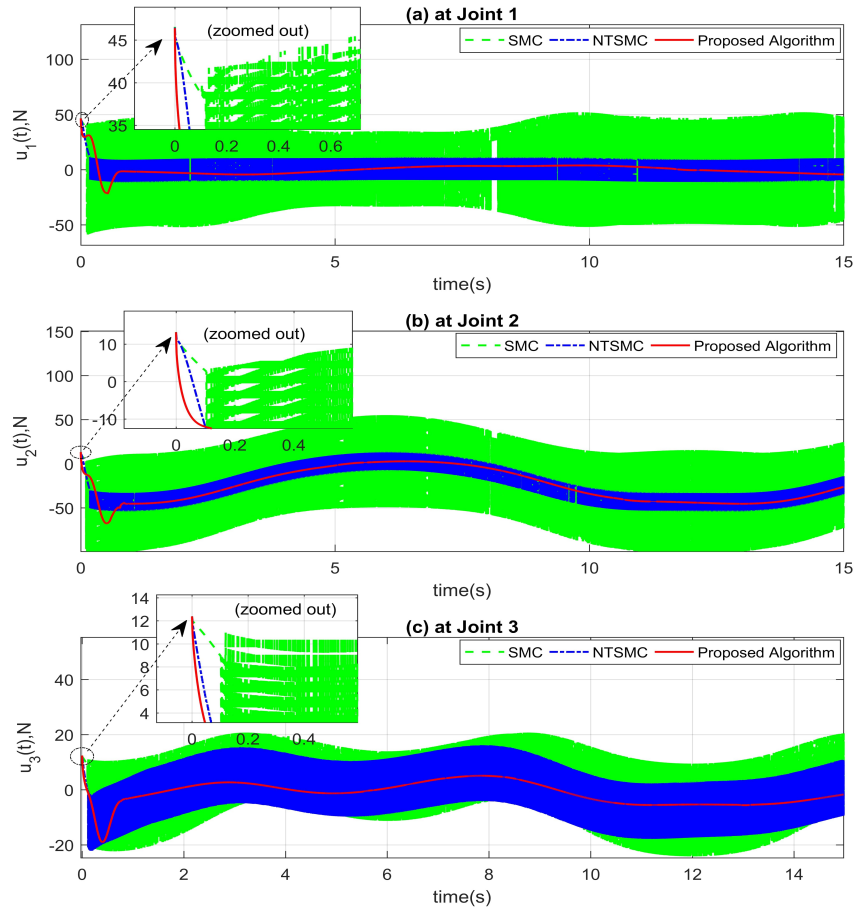


Figure 5.4: Control input signals: (a) at Joint 1, (b) at Joint 2, and (c) at Joint 3 .

response rate and finite-time convergence with no singularity drawback. 2) It requires no essential information regarding the upper limits of the perturbations and uncertainties. 3) The upper limit of the convergence time can be set beforehand. 4) It demonstrates impressively small chattering behavior. 5) The robustness and the finite-time convergence of the system have been guaranteed fully by the Lyapunov stability criterion.

Table 5.1: Averaged tracking errors under the control signals of the control schemes.

Control Method	Error		
	$e_1^p$	$e_2^p$	$e_3^p$
SMC	$1.91 \times 10^{-4}$	$2.71 \times 10^{-4}$	$8.82 \times 10^{-4}$
NTSMC	$1.27 \times 10^{-5}$	$2.17 \times 10^{-5}$	$2.78 \times 10^{-5}$
Proposed Algorithm	$6.76 \times 10^{-7}$	$5.74 \times 10^{-7}$	$7.72 \times 10^{-7}$

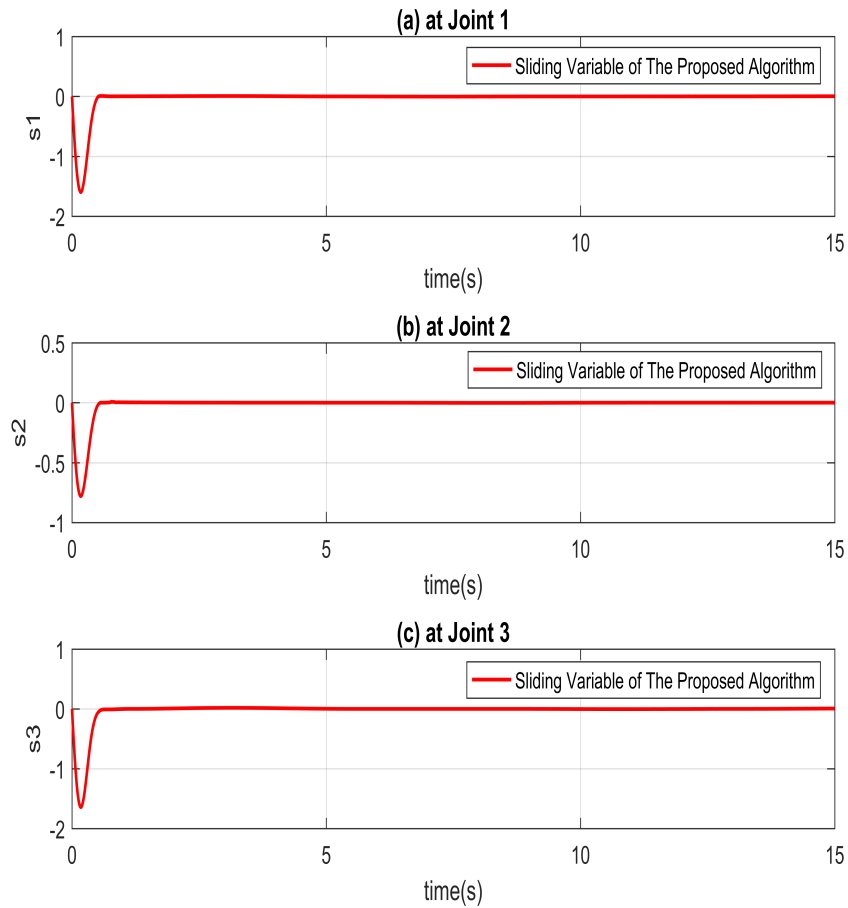


Figure 5.5: Sliding variables: (a) at Joint 1, (b) at Joint 2, and (c) at Joint 3.

# Appendix D

To design SMC [16] and NTSMC [37,40], the dynamic equation of the robotic manipulators in Eq. (5.1) is expressed as:

$$\ddot{q} = M^{-1}(q) [\tau - C_m(q, \dot{q}) \dot{q} - F_r(\dot{q}) - G(q) - \tau_p]. \quad (D.1)$$

To simplify the designing procedure and analysis in the sequel, Eq. (D.1) can be expressed as:

$$\ddot{q} = \Phi(q, \dot{q}) + H(q) \tau + \Delta(q, \dot{q}, t), \quad (D.2)$$

where  $\Phi(q, \dot{q}) = M^{-1}(q) [-C_m(q, \dot{q}) \dot{q} - G(q)]$  and  $H(q) = M^{-1}(q)$  are smooth nonlinear vector fields and  $\Delta(q, \dot{q}, t) = M^{-1}(q) [-F_r(\dot{q}) - \tau_p]$  presents the total components of the perturbations and uncertainties.

## The design procedure of SMC

Set  $e^p = q - q^r$  as the tracking positional error and define  $q^r$  as the desired trajectory values.

Then, define the following sliding variable as:

$$s = \dot{e}^p + \alpha e^p, \quad (D.3)$$

in which  $\alpha$  is a positive coefficient.

Using Eq. (D.2), Eq. (D.3) then gives:

$$\begin{aligned} \dot{s} &= \ddot{e}^p + \alpha \dot{e}^p \\ &= \ddot{q} - \ddot{q}^r + \alpha (\dot{q} - \dot{q}^r) \\ &= \Phi(q, \dot{q}) + H(q) \tau + \Delta(q, \dot{q}, t) - \ddot{q}^r + \alpha (\dot{q} - \dot{q}^r) \end{aligned} \quad (D.4)$$

To guarantee that the controlled variables of Eq. (D.1) converge to sliding variables,

the following relation must be satisfied:

$$s = 0; \dot{s} = 0. \quad (\text{D.5})$$

The following proposed controller is designed according to the sliding mode design procedure:

$$\tau_{SMC} = \tau_{eq} + \tau_{sw}. \quad (\text{D.6})$$

The term of the equivalent control of  $\tau_{eq}$  maintains the trajectory of the error state variables on the sliding variables. To get this result, it is necessary to take the derivative of sliding variables with respect to time. Additionally,  $\dot{s} = 0$  for the nominal system that does not consider perturbations and uncertainties. The time derivative of sliding variables is expressed as:

$$\Phi(q, \dot{q}) + H(q) \tau_{eq} - \ddot{q}^r + \alpha(\dot{q} - \dot{q}^r) = 0, \quad (\text{D.7})$$

and Eq. (D.7) yields:

$$\tau_{eq} = -H^{-1}(q) (\Phi(q, \dot{q}) + \alpha(\dot{q} - \dot{q}^r) - \ddot{q}^r). \quad (\text{D.8})$$

The switching control term is designed as:

$$\tau_{sw} = -H^{-1}(q) g \text{sign}(s), \quad (\text{D.9})$$

in which  $g$  is a positive coefficient.

Therefore, the control input of SMC is

$$\tau_{SMC} = -H^{-1}(q) (\Phi(q, \dot{q}) + \alpha(\dot{q} - \dot{q}^r) - \ddot{q}^r + g \text{sign}(s)). \quad (\text{D.10})$$

## The design procedure of NTSMC

Set  $e^p = q - q^r$  as the tracking positional error and define  $q^r$  as the desired trajectory values.

Then, define the following sliding variable as:

$$s = e^p + \frac{1}{\beta} (\dot{e}^p)^{\frac{l}{h}}, \quad (\text{D.11})$$

in which  $\beta$  is a positive coefficient,  $l$  and  $h$  are positive odd integers satisfying condition

$1 < \frac{l}{h} < 2$ :

$$\dot{s} = \dot{e}^p + \frac{1}{\beta} \frac{l}{h} (\dot{e}^p)^{\frac{l}{h}-1} \ddot{e}^p. \quad (D.12)$$

To guarantee that the controlled variables of Eq. (D.1) converge to sliding variables, the following relations must be satisfied:

$$s = 0; \dot{s} = 0. \quad (D.13)$$

The following proposed controller is designed according to the sliding mode design procedure:

$$\tau_{SMC} = \tau_{eq} + \tau_{sw}. \quad (D.14)$$

The term of the equivalent control of  $\tau_{eq}$  maintains the trajectory of the error state variables on the sliding variables. To get this result, it is necessary to take the derivative of sliding variables with respect to time. Additionally,  $\dot{s} = 0$  for the nominal system that does not consider perturbations and uncertainties. The time derivative of sliding variables is expressed as:

$$\begin{aligned} \dot{s} &= \dot{e}^p + \frac{1}{\beta} \frac{l}{h} (\dot{e}^p)^{\frac{l}{h}-1} \ddot{e}^p \\ &= \dot{q} - \ddot{q}^r + \frac{1}{\beta} \frac{l}{h} (\dot{e}^p)^{\frac{l}{h}-1} (\Phi(q, \dot{q}) - \ddot{q}^r + H(q) \tau_{eq}), \end{aligned} \quad (D.15)$$

and Eq. (D.15) yields:

$$\tau_{eq} = -H^{-1}(q) \left( \Phi(q, \dot{q}) - \ddot{q}^r + \beta \frac{h}{l} (\dot{e}^p)^{2-\frac{l}{h}} \right). \quad (D.16)$$

The switching control term is designed as:

$$\tau_{sw} = -H^{-1}(q) (l_g + \xi) \text{sign}(s), \quad (D.17)$$

in which  $l_g$  and  $\xi$  are positive coefficients.

Therefore, the control input of the NTSM controller is

$$\tau_{SMC} = -H^{-1}(q) \left( \Phi(q, \dot{q}) - \ddot{q}^r + \beta \frac{h}{l} (\dot{e}^p)^{2-\frac{l}{h}} + (l_g + \xi) \text{sign}(s) \right). \quad (D.18)$$



## Chapter 6

# An Adaptive Neural Non-Singular Fast-Terminal Sliding-Mode Control for Industrial Robotic Manipulators

### 6.1 Introduction

Literature regarding robotic manipulators has introduced many control systems focused on achieving high performance against various uncertainties, including external noise. These control methods were derived to fundamentally control the motion of robot manipulators, and include PD controller [110], nonlinear PD controller [111], and PID controller [4, 93]. The advantages of the cited control systems were to provide a simple and basic approach to implementation, as they do not require an exact dynamic model. However, these systems could not obtain the desired performance in the presence of disturbances and dynamic uncertainties. Several advanced control approaches have been proposed to advance system performance, such as FLS controller [28, 58] and NN controller [54, 98, 126], but they demand complicated calculations, and the effectiveness of each solution still has several limitations. The control scheme design strategy is based on the robot dynamic model, where the whole dynamic model is computed and compensated explicitly to achieve the desired performance. Therefore, other enhanced methods were suggested to improve the motion tracking for robot manipulators, including CTC [7], AC [101, 127], and SMC [15, 16]. Among those controllers, SMC has been confirmed to offer high robustness against uncertainties and disturbances for nonlinear systems. Therefore, the SMC has been widely applied in real applications [15, 16]. However, the traditional SMC still possesses drawbacks such as requiring an exact dynamic model, singularity problems, a chattering phenomenon, and finite-time convergence. Some research efforts have focused on overcoming these disadvantages. For the system states to approach the sliding



variable within a finite-time, the use of TSMC, based on the nonlinear sliding surface, has been reported in the literature [27, 79, 101]. Nonetheless, the TSMC convergence time is slow when compared to the conventional SMC, and still contains a singularity glitch. To solve convergence time and singularity issues, several FTSMC [39, 68] and NTSMC [80, 122, 128] approaches have been proposed. Practically, private algorithms, such as FTSMC or NTSMC, have only treated an individual weakness or failed to solve the other disadvantages of the classical SMC. Consequently, NFTSMC has been introduced [47, 85, 129–131]. Here, NFTSMC can solve many disadvantages of the classical SMC or other control algorithms based on TSMC. However, chattering behavior has not been removed by applying a high-frequency switching control law to the control input of the above methods, which include TSMC, FTSMC, NTSMC, and NFTSMC. Therefore, some effective techniques have been introduced to handle this topic by application of the saturation function (refer to [64]), FOSMC [71, 132], or HOSMC [64, 65].

One of the main tasks in the design of a control method based on SMC or TSMC is to develop an exact dynamic model of the robot manipulator, which one does not readily know in advance for real robot systems. To estimate this unknown dynamic model, several computing approaches have been proposed such as NNs [55, 133] and FLSs [134, 135] due to their universal approximation capabilities.

While each disadvantage of the classical SMC and TSMC has been treated individually, this report focuses on simultaneous resolution of the disadvantages of SMC and TSMC, including the requirement for an exact dynamic model, as well as the presence of a singularity problem, chattering phenomenon, and finite-time convergence.

Consequently, the goal of this research is to develop a robust control strategy for robotic manipulators based on an ANNFTSMC scheme. The main advantages of the suggested control strategy include:

- The inheritance of NFTSMC advantages in terms of non-singularity, finite-time convergence, fast transient response, low steady-state errors, and high position tracking accuracy.
- The achievement of smooth control inputs with chattering behavior elimination.
- The removal of demand for an exact dynamic model by applying an adaptive radial basis function neural network to approximate an unknown robot function.
- Better tracking performance and less impact by disturbances and uncertainties compared to classic SMC and other control methods based on TSMC.
- Improved robustness and stability of the robot system, as demonstrated by Lyapunov theory.

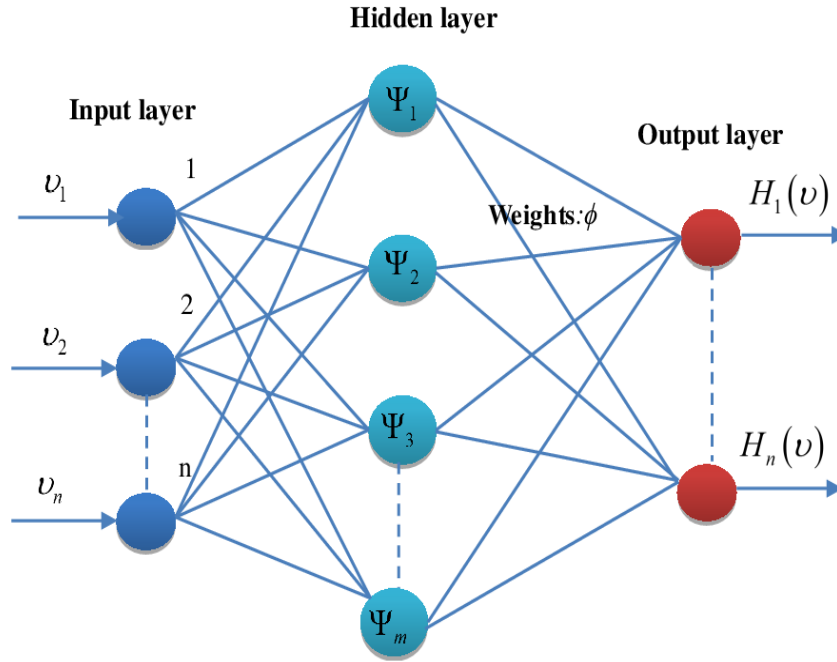


Figure 6.1: Structure of radial basis function neural network.

The remainder of this chapter is structured as follows. Following the introduction, the problem statements are presented, succeeded by the design approach for the proposed control strategy, where the proposed strategy is utilized to allow joint position tracking control simulation for a 3-DOF robot manipulator. Here, its tracking performance is compared with SMC and TSMC to analyze the effectiveness of the proposed control strategy. Finally, conclusions are presented.

## 6.2 Problem Statements

### 6.2.1 Radial Basis Function Neural Network

Previous research on the universal approximation theory proved that any nonlinear function over a compact set with arbitrary accuracy can be approximated by an RBFNN. Here, RBFNNs have several advantages, including ease of design, good generalization, strong tolerance to input noise, and online learning ability. Compared with a multilayer neural network, an RBFNN is simpler and converges faster. An RBFNN includes three layers: the input layer, hidden layer, and output layer, all of which are expressed in Figure 6.1.

The output of the RBFNN can be computed as:

$$H(v) = \phi^T \Psi(v) + \xi(v), \quad (6.1)$$

where  $v \in R^n$  and  $H(v)$  are the neural network input and output, respectively. Here,  $\phi^T \in R^{n \times n}$  is the weight matrix connecting the hidden layer and the output layer,  $\Psi(v)$  is the nonlinear function of the hidden nodes, and  $\xi(v) \in R^n$  is an approximation error of NN.

A Gaussian fit is selected for the nonlinear function as follows:

$$\Psi(v) = \exp\left(\frac{-(v - \mu_l)^T (v - \mu_l)}{\delta_l^2}\right), l = 1, 2, \dots, \quad (6.2)$$

where  $\delta$  and  $\mu$  correspond to the width and center of the Gaussian function, respectively.

## 6.2.2 Dynamic Model of the Robot Manipulator

For an n-link rigid robotic manipulator, the dynamic model can be described as (refer to [75, 94]):

$$M(q) \ddot{q} + C_m(q, \dot{q}) \dot{q} + G(q) + F_r(\dot{q}) + \tau_d(t) = \tau, \quad (6.3)$$

where  $q, \dot{q}, \ddot{q} \in R^n$  correspond to the position, velocity, and acceleration of the robot manipulator, respectively. Additionally,  $M(q) \in R^{n \times n}$  is the invertible inertia matrix,  $C_m(q, \dot{q}) \in R^{n \times 1}$  is the matrix from the centrifugal force and Coriolis,  $G(q) \in R^{n \times 1}$  is the gravitational force matrix,  $F_r(\dot{q}) \in R^{n \times 1}$  denotes the friction matrix,  $\tau \in R^{n \times 1}$  is the designed actuation input of actuators, and  $\tau_d \in R^{n \times 1}$  is a load disturbance matrix.

To simplify the approach and analysis, Eq. (6.3) is given as:

$$\ddot{q} = \Xi(q, \dot{q}) + B(q) \tau(t) + \Delta_u(q, \dot{q}, t), \quad (6.4)$$

where  $\Xi(q, \dot{q}) = M^{-1}(q) [-C_m(q, \dot{q}) \dot{q} - G(q)]$  is the nominal dynamic model of the robot manipulator without perturbations and uncertainties,  $\Delta_u(q, \dot{q}, t) = M^{-1}(q) [-F_r(\dot{q}) - \tau_d(t)]$  represents the unknown perturbation and uncertainty terms, and  $B(q) = M^{-1}(q)$ .

The hypothesis here is that the control variables will follow the desired trajectory, with high performance, in finite-time under a robust control strategy. In this case, the proposed system does not need an exact robotic model.

The following assumptions are crucial for the design approach.

**Assumption 6.1:** The inertia matrix  $M(q)$  is an invertible, positive definite, and sym-

metric matrix that adheres to the bounded condition:

$$\theta_1 \leq M(q) \leq \theta_2, \quad (6.5)$$

where  $\theta_1$  and  $\theta_2$  represent positive constants.

**Assumption 6.2:** The unknown perturbations, uncertainties, and approximation errors of NN have an upper-bound satisfying the following relation:

$$\|\Delta_u(q, \dot{q}, t)\| \leq \Omega, \quad (6.6)$$

where  $\Omega$  is an unknown positive constant.

## 6.3 Design Procedure of the Control Strategy

In this section, a new control strategy is suggested for a robot manipulator using Eq. (6.3), which is described by the two following main tasks.

### 6.3.1 Design of NFTSM Variable

Based on the TSMC design approach, a state variable termed as NFTSM variable was previously designed, where the novel NFTSM variables are proposed from the tracking positional error as:

$$s_i = \dot{\varsigma}_i + h_{1i} \text{sign}[\varsigma_i] + h_{2i} \varsigma_i^{[\alpha_i]}, \quad (6.7)$$

where  $h_{1i}, h_{2i}$  are positive values,  $\alpha_i > 1$ , and the variable  $\varsigma_i$  is selected as:

$$\varsigma_i = e_i + \int_0^t \left( \Gamma_{1i} (e_i)^{[2-\vartheta_i]} + \Gamma_{2i} e_i + \Gamma_{3i} (e_i)^{[\vartheta_i]} \right) d\sigma, \quad (6.8)$$

where  $e_i = q_i - q_{ir}$  ( $i = 1, 2, \dots, n$ ) is the tracking positional error,  $q_{ir}$  is described as the desired path value,  $\varsigma_i$  is the sliding surface variable,  $\Gamma_{1i}, \Gamma_{2i}, \Gamma_{3i}$  are positive coefficients satisfying the relation  $4\Gamma_{1i}\Gamma_{3i} > \Gamma_{2i}^2$ ,  $0 < \vartheta_i < 1$  ( $i = 1, 2, \dots, n$ ) and  $e_i^{[\vartheta_i]}$  is as described in [90]:

$$e_i^{[\vartheta_i]} = |e_i|^{\vartheta_i} \text{sign}[e_i]. \quad (6.9)$$

**Remark 6.1:** Once the tracking positional error  $|e_i|$  is much greater than 1,  $\Gamma_{1i} (e_i)^{[2-\vartheta_i]} + \Gamma_{2i} e_i$  contributes to the task by offering a fast convergence. While the tracking positional error  $|e_i|$  is much smaller than 1,  $\Gamma_{3i} (e_i)^{[\vartheta_i]}$  contributes by producing finite-time convergence.

According to the SMC manner, once the state variable proceeds in sliding mode, the following constraints are imposed (refer to [15, 16, 136–138]):

$$s_i = 0; \dot{s}_i = 0, \quad (6.10)$$

$$\varsigma_i = 0; \dot{\varsigma}_i = 0. \quad (6.11)$$

Combining Eq. (6.10) constraints with Eq. (6.7) yields:

$$\dot{\varsigma}_i = -h_{1i} \text{sign}[\varsigma_i] - h_{2i} \varsigma_i^{[\alpha_i]}, \quad (6.12)$$

and combining Eq. (6.11) constraints with Eq. (6.8) gives:

$$\dot{e}_i = -\Gamma_{1i} e_i^{[2-\vartheta_i]} - \Gamma_{2i} e_i - \Gamma_{3i} e_i^{[\vartheta_i]}. \quad (6.13)$$

It must be proved that once the second-order sliding motion takes place, i.e.,  $s_i = 0$ , the first-order sliding motion takes place in finite-time, i.e.,  $\varsigma_i = 0$ , and the state variable system of Eq. (6.13) reaches zero in finite-time. The following theorems have been established for this proof.

**Theorem 6.1:** Consider the dynamic system shown in Eq. (6.12). The original point  $\varsigma_i = 0$  is globally balanced in finite-time and the state variable of the system (6.10) converges to zero in finite-time  $T_{s_i} \leq \frac{\varsigma_i^2(0)}{\sqrt{2}h_{1i}}$ .

**Proof:** The positive-definite Lyapunov functional is investigated as:

$$V_1 = \frac{\varsigma_i^2}{2}. \quad (6.14)$$

With Eq. (6.12), the time derivative of Eq. (6.14) is computed as:

$$\begin{aligned} \dot{V}_1 &= \varsigma_i \left( -h_{1i} \text{sign}[\varsigma_i] - h_{2i} \varsigma_i^{[\alpha_i]} \right) \\ &= -h_{1i} |\varsigma_i| - h_{2i} \varsigma_i^{[\alpha_i+1]} \\ &\leq -h_{1i} |\varsigma_i| \\ &= -\sqrt{2} h_{1i} V_1^{\frac{1}{2}} \end{aligned} \quad (6.15)$$

It can be seen that (6.15) has the form  $\dot{V}_1 + \sqrt{2} h_{1i} V_1^{\frac{1}{2}} \leq 0$ . Therefore, the defined finite-time is given by [41]:

$$T_{s_i} \leq \frac{\varsigma_i^2(0)}{\sqrt{2} h_{1i}}. \quad (6.16)$$

This completes the proof.

**Theorem 6.2:** Consider the dynamic system (6.13). The original point  $e_i = 0$  consists of globally balanced points in finite-time and the state variable of the system (6.13) as it converges to zero in finite-time  $T_{e_i} \leq T_{e_i}^f$ .  $T_{e_i}^f$  is defined as:

$$T_{e_i}^f = \frac{2}{(1 - \vartheta_i)} \left( \frac{\pi}{2} - \arctan \frac{\Gamma_{2i}}{\sqrt{4\Gamma_{1i}\Gamma_{3i} - \Gamma_{2i}^2}} \right) \frac{1}{\sqrt{4\Gamma_{1i}\Gamma_{3i} - \Gamma_{2i}^2}}. \quad (6.17)$$

**Proof:** The Lyapunov function candidate is investigated as:

$$V_2 = e_i^2. \quad (6.18)$$

With Eq. (6.13), the time derivative of Eq. (6.18) is calculated as:

$$\begin{aligned} \dot{V}_2 &= 2e_i \dot{e}_i \\ &= 2e_i \left( -\Gamma_{1i} e_i^{[2-\vartheta_i]} - \Gamma_{2i} e_i - \Gamma_{3i} e_i^{[\vartheta_i]} \right) \\ &= 2 \left( -\Gamma_{1i} e_i^{[3-\vartheta_i]} - \Gamma_{2i} e_i^2 - \Gamma_{3i} e_i^{[1+\vartheta_i]} \right) \\ &= 2 \left( -\Gamma_{1i} V_2^{\frac{(3-\vartheta_i)}{2}} - \Gamma_{2i} V_2 - \Gamma_{3i} V_2^{\frac{(\vartheta_i+1)}{2}} \right) \end{aligned} \quad (6.19)$$

To arrive at a conclusion from Eq. (6.19), the following Lemma is used.

**Lemma 6.1:** [40] For any real numbers  $z_1 > 0$ ,  $z_2 > 0$ , and  $0 < \varphi < 1$ , an extended Lyapunov function condition of finite-time stability can be given in the form of a FTSM as  $\dot{L}(x) + z_1 L(x) + z_2 L^\varphi(x) \leq 0$ , where the settling time can be estimated by:

$$T \leq \frac{1}{z_1(1-\varphi)} \ln \frac{z_1 L^{1-\varphi}(x(0)) + z_2}{z_2}. \quad (6.20)$$

From Eq. (6.19),  $\frac{\vartheta_i+1}{2} < 1$  indicates that  $\dot{V}_2 \leq 0$ . Based on Lemma 7.1, the original point  $e_i = 0$  is a globally balanced point in finite-time. In the next step, proof that the error state variable of the system (6.13) converges to zero in finite-time will be given.

Eq. (6.19) can be shown as:

$$\dot{V}_2 = 2V_2^{\frac{\vartheta_i+1}{2}} \left( -\Gamma_{1i} V_2^{1-\vartheta_i} - \Gamma_{2i} V_2^{\frac{1-\vartheta_i}{2}} - \Gamma_{3i} \right). \quad (6.21)$$

Eq. (6.21) can be expressed as:

$$\begin{aligned}
 dV_2 &= 2V_2^{\frac{\vartheta_i+1}{2}} \left( \Gamma_{1i}V_2^{1-\vartheta_i} + \Gamma_{2i}V_2^{\frac{1-\vartheta_i}{2}} + \Gamma_{3i} \right) dt \\
 \Rightarrow dt &= -\frac{dV_2}{2L_1^{\frac{\vartheta_i+1}{2}} \left( \Gamma_{1i}V_2^{1-\vartheta_i} + \Gamma_{2i}V_2^{\frac{1-\vartheta_i}{2}} + \Gamma_{3i} \right)} \\
 &= -\frac{1}{1-\vartheta_i} \frac{dV_2^{\frac{1-\vartheta_i}{2}}}{\left( \Gamma_{1i}V_2^{1-\vartheta_i} + \Gamma_{2i}V_2^{\frac{1-\vartheta_i}{2}} + \Gamma_{3i} \right)}
 \end{aligned} \tag{6.22}$$

Setting  $V_2(T_{e_i}) = 0$  and taking the integral of Eq. (6.22) during the time period where  $0 \rightarrow T_{e_i}$  gives:

$$T_{e_i} = \frac{2}{(1-\vartheta_i)} \frac{1}{\sqrt{4\Gamma_{1i}\Gamma_{3i} - \Gamma_{2i}^2}} \left( \arctan \frac{2\Gamma_{1i}V_2^{\frac{1-\vartheta_i}{2}}(e_i(0))}{\sqrt{4\Gamma_{1i}\Gamma_{3i} - \Gamma_{2i}^2}} - \arctan \frac{\Gamma_{2i}}{\sqrt{4\Gamma_{1i}\Gamma_{3i} - \Gamma_{2i}^2}} \right). \tag{6.23}$$

It can be seen that  $T_{e_i}$  is limited by  $T_{e_i}^f = \frac{2}{(1-\vartheta_i)} \left( \frac{\pi}{2} - \arctan \frac{\Gamma_{2i}}{\sqrt{4\Gamma_{1i}\Gamma_{3i} - \Gamma_{2i}^2}} \right) \frac{1}{\sqrt{4\Gamma_{1i}\Gamma_{3i} - \Gamma_{2i}^2}}$ . In fact,  $V_2(T_{e_i}) = 0$  means  $e_i(T_{e_i}) = 0$ . In addition, it can be seen that the upper-bound of  $T_{e_i}^f$  is only dependent on the design constants, as  $\Gamma_{1i}, \Gamma_{2i}, \Gamma_{3i}, \vartheta_i$  and the tracking positional error in Eq. (6.13) approach zero in finite-time. Therefore, the proof of Theorem 7.2 is complete.

The proposed control strategy forces the error state variables to reach sliding variables in finite-time, as will be presented next.

### 6.3.2 Design an ANNFTSMC for Robotic Manipulators

To achieve the desired control performance for the system in Eq. (6.3), the control method is performed as follow:

Substituting Eq. (6.8) into Eq. (6.7) provides:

$$s = \dot{e} + \Gamma_1 e^{[2I_n - \vartheta]} + \Gamma_2 e + \Gamma_3 e^{[\vartheta]} + h_1 \text{sign}[\varsigma] + h_2 \varsigma^{[\alpha]}, \tag{6.24}$$

where  $s = [s_1, \dots, s_n]^T$ ,  $I_n$  is the unit matrix,  $\vartheta = \text{diag}(\vartheta_1, \dots, \vartheta_n)$ ,  $\alpha = \text{diag}(\alpha_1, \dots, \alpha_n)$ ,  $\Gamma_1 = \text{diag}(\Gamma_{11}, \dots, \Gamma_{1n})$ ,  $\Gamma_2 = \text{diag}(\Gamma_{21}, \dots, \Gamma_{2n})$ ,  $\Gamma_3 = \text{diag}(\Gamma_{31}, \dots, \Gamma_{3n})$ ,  $h_1 = \text{diag}(h_{11}, \dots, h_{1n})$ ,  $h_2 = \text{diag}(h_{21}, \dots, h_{2n})$ ,  $\text{sign}[\varsigma] = [\text{sign}[\varsigma_1], \dots, \text{sign}[\varsigma_n]]^T$ ,  $e = [e_1, \dots, e_n]^T$ .  $e^{[2I_n - \vartheta]}$ ,  $e^{[\vartheta]}$

and  $\varsigma^{[\alpha]}$  are vectors defined as:

$$e^{[\vartheta]} = \text{diag}(\text{sign}[e]) \cdot |e|^{\vartheta} = \begin{bmatrix} e_1^{[\vartheta_1]}, & e_2^{[\vartheta_2]}, & \dots, & e_n^{[\vartheta_n]} \end{bmatrix}^T. \quad (6.25)$$

To simplify the analysis, the following notion is applied as:

$$\frac{de^{[\vartheta]}}{dt} = \vartheta \text{diag}(|e|^{\vartheta-I_n}) \cdot \dot{e}. \quad (6.26)$$

Using Eq. (6.26), the time derivative of Eq. (6.24) is derived as:

$$\dot{s} = \ddot{e} + \Gamma_1 (2I_n - \vartheta) \text{diag}(|e|^{I_n-\vartheta}) \dot{e} + \Gamma_2 \dot{e} + \Gamma_3 \vartheta \text{diag}(|e|^{\vartheta-I_n}) \dot{e} + h_2 \alpha \text{diag}(|\varsigma|^{\alpha-I_n}) \dot{\varsigma}. \quad (6.27)$$

From Eq. (6.4),  $\ddot{e}$  is presented as:

$$\begin{aligned} \ddot{e} &= \ddot{q} - \ddot{q}_d \\ &= \Xi(q, \dot{q}) + B(q) \tau(t) + \Delta_u(q, \dot{q}, t) - \ddot{q}_d \end{aligned} \quad (6.28)$$

Substituting Eq. (6.28) into Eq. (6.27) gives:

$$\dot{s} = \Xi(q, \dot{q}) + B(q) \tau(t) + \Delta_u(q, \dot{q}, t) - \ddot{q}_d + \Pi(e, \varsigma), \quad (6.29)$$

where  $\Pi(e, \varsigma) = \Gamma_1 (2I_n - \vartheta) \text{diag}(|e|^{I_n-\vartheta}) \dot{e} + \Gamma_2 \dot{e} + \Gamma_3 \vartheta \text{diag}(|e|^{\vartheta-I_n}) \dot{e} + h_2 \alpha \text{diag}(|\varsigma|^{\alpha-I_n}) \dot{\varsigma}$ .

To obtain the desired performance, the proposed control algorithm is designed for system (6.3) as:

$$\tau(t) = B^+(q) (\tau_{eq}(t) + \tau_s(t)), \quad (6.30)$$

where  $B^+(q) = B^T(q) [B(q) B^T(q)]^{-1}$ , the equivalent control law is constructed as:

$$\tau_{eq}(t) = -(\Xi(q, \dot{q}) + \Pi(e, \varsigma) - \ddot{q}_d) \quad (6.31)$$

and the switching control term is designed as:

$$\tau_s = -(\Omega + \rho_1) \text{sign}(s), \quad (6.32)$$

in which  $\Omega$  and  $\rho_1$  are positive constants.

Substituting control laws (6.30)–(6.32) into Eq. (6.29) provides:

$$\dot{s} = -(\Omega + \rho_1) \text{sign}(s) + \Delta_u(q, \dot{q}, t). \quad (6.33)$$



The positive-definite Lyapunov functional is selected as:

$$V_3 = \frac{1}{2} s^T s. \quad (6.34)$$

With Eq. (6.33), the time derivative of Eq. (6.34) is derived as:

$$\begin{aligned} \dot{V}_3 &= s^T \dot{s} \\ &= s^T (-(\Omega + \rho_1) \text{sign}(s) + \Delta_u(q, \dot{q}, t)) \quad . \\ &= -\Omega |s| - \rho_1 |s| + \Delta_u(q, \dot{q}, t) s \leq -\rho_1 |s| \end{aligned} \quad (6.35)$$

Accordingly, based on the Lyapunov criterion [90], it can be verified that the stability of the tracking error is secured under control laws (6.30)–(6.32) despite the presence of external disturbances and system uncertainties.

Unfortunately, robot manipulators have complicated dynamic models with many parametric uncertainties (e.g., friction, sensor noise, payload, perturbations). Therefore, it is not trivial to precisely calculate the uncertainty upper-bounds and provide an exact robot dynamic function in the equivalent control law. To overcome these difficulties, a robust control strategy will be constructed for robotic manipulators based on an ANNFTSMC. Here, an ARBFNN will be utilized to approximate an unknown robot function, while an adaptive law will be used to estimate the uncertainty upper bounds and estimated error of the NN. In this report, RBFNN is used to approximate the dynamic robot model as follows:

$$f(x) = \Xi(q, \dot{q}), \quad (6.36)$$

where  $x = [x_1, x_2]^T$ , assign  $x_1 = q$ , and  $x_2 = \dot{q}$ .

Define  $\hat{f}(x)$  as an approximated function of  $f(x)$ ,  $\hat{f}(x)$  can be described by an NN, as follows:

$$\hat{f}(x) = \hat{\phi}^T \Psi(x). \quad (6.37)$$

Here,  $\hat{\phi}$  is the adaptable parameter vector.

The optimal parameter  $\phi^*$  can be described, as follows:

$$\phi_H^* = \arg \min \left\{ \sup_{x \in \Theta_x} \left| f(x) - \hat{f}(x, \hat{\phi}) \right| \right\}. \quad (6.38)$$

Accordingly, RBFNN (6.37) can exactly approximate the arbitrary value of  $f(x)$  which is given by the following Lemma.

**Lemma 6.2:** For any given real continuous function  $f(X)$  on the compact set  $\Theta_X \in R^n$  and arbitrary positive coefficient  $\xi > 0$ , there is a neural approximator existence  $\hat{f}(X)$

that possesses a similar form as Eq. (6.37), such that

$$\sup_{X \in \Theta_X} \left| f(X) - \hat{f}(X, \hat{\phi}) \right| < \xi. \quad (6.39)$$

Therefore, the robot dynamic model can be described as:

$$\ddot{q} = \phi^{*T} \Psi(x) + B(q) \tau(t) + W, \quad (6.40)$$

where  $W = \Delta_u(q, \dot{q}, t) + \xi$  is the lumped uncertainty, including disturbances, dynamic uncertainties, and NN approximation error. In this step, the lumped uncertainty is assumed to be bounded by an unknown positive constant,  $|W| \leq \Phi$ .

The proposed control law as depicted in Figure 6.2 is designed as follows:

$$\tau(t) = B^+(q) (\tau_{eq}(t) + \tau_{as}(t)). \quad (6.41)$$

Here, the equivalent control law is constructed as:

$$\tau_{eq}(t) = - \left( \hat{\phi}^T \Psi(x) + \Pi(e, \varsigma) - \ddot{q}_d \right), \quad (6.42)$$

and  $\tau_{as}(t)$  is an adaptive control term for replacing the control law  $\tau_s(t)$  in Eq. (6.32), describing  $\tau_{as}(t)$  as:

$$\tau_{as} = - \left( \hat{\Phi} + \rho_1 \right) \text{sign}(s), \quad (6.43)$$

and the adaptive updating rules are given as:

$$\dot{\hat{\Phi}} = \frac{1}{\gamma} |s|, \quad (6.44)$$

$$\dot{\hat{\phi}} = \frac{1}{\omega} s \Psi(x), \quad (6.45)$$

where  $\hat{\Phi}$  is the estimated value of the design parameter  $\Phi$ ,  $\rho_1$  is a positive constant, and  $\gamma, \omega$  indicate the adaptive gains.

The control design approach for the robot system is summarized in Theorem 3 below.

**Theorem 6.3:** For the system (6.3), if the suitable NFTSM variables have been selected as (6.7) and (6.8) and the control input signal is constructed as (6.41)–(6.43) with its parameter updating rules designed as (6.44) and (6.45), then the sliding variable motion is a certainty, and the tracking error variables converge to zero.

**Proof:** Define the adaptive estimation error and NN weight approximation error, respec-

tively, as follows:

$$\tilde{\Phi} = \hat{\Phi} - \Phi, \quad (6.46)$$

$$\tilde{\phi} = \phi^* - \hat{\phi}. \quad (6.47)$$

The time derivative of the sliding surface in Eq. (6.29) is rewritten as:

$$\dot{s} = \phi^* \Psi(x) + B(q) \tau(t) + W - \ddot{q}_d + \Pi(e, \varsigma). \quad (6.48)$$

Substituting control laws (6.41)–(6.43) into Eq. (6.48) provides:

$$\dot{s} = \tilde{\phi}^T \Psi(x) - \left( \hat{\Phi} + \rho_1 \right) \text{sign}(s) + W. \quad (6.49)$$

The positive-definite Lyapunov functional is selected as:

$$V_4 = \frac{s^T s}{2} + \frac{\gamma \tilde{\Phi}^T \tilde{\Phi}}{2} + \frac{\omega \tilde{\phi}^T \tilde{\phi}}{2}. \quad (6.50)$$

With the result of Eq. (6.49), the time derivative of Eq. (6.50) is derived as:

$$\begin{aligned} \dot{V}_4 &= s^T \dot{s} + \gamma \tilde{\Phi}^T \dot{\tilde{\Phi}} - \omega \tilde{\phi}^T \dot{\tilde{\phi}} \\ &= s^T \left( \tilde{\phi}^T \Psi(x) - \left( \hat{\Phi} + \rho_1 \right) \text{sign}(s) + W \right) + \gamma \left( \hat{\Phi} - \Phi \right) \dot{\tilde{\Phi}} - \omega \tilde{\phi}^T \dot{\tilde{\phi}}. \\ &= s^T \tilde{\phi}^T \Psi(x) - \hat{\Phi} |s| - \rho_1 |s| + W s + \gamma \left( \hat{\Phi} - \Phi \right) \dot{\tilde{\Phi}} - \omega \tilde{\phi}^T \dot{\tilde{\phi}} \end{aligned} \quad (6.51)$$

Applying the updating laws (6.41)–(6.43) to (6.51) yields:

$$\begin{aligned} \dot{V}_4 &= -\hat{\Phi} |s| - \rho_1 |s| + \Phi s + \left( \hat{\Phi} - \Phi \right) |s| \\ &= -\rho_1 |s| + W s - \Phi |s| \\ &\leq -\rho_1 |s| \end{aligned} \quad (6.52)$$

If the parameter  $\rho_1$  is selected to be greater than zero,  $\dot{V}_4$  will be negative-definite. Based on the Lyapunov principle [90],  $\dot{V}_4$  becoming negative-definite indicates that  $s$  and  $\tilde{\Phi}$  reach zero. Therefore, the tracking error variables converge to the sliding variables. Therefore, Theorem 7.3 is proven.

**Remark 6.2:** In practical systems, the parameter drift problem typically occurs under the adaptive control rule (6.44). Consequently, the bounded approach is implemented to set up the adaptive estimator as:

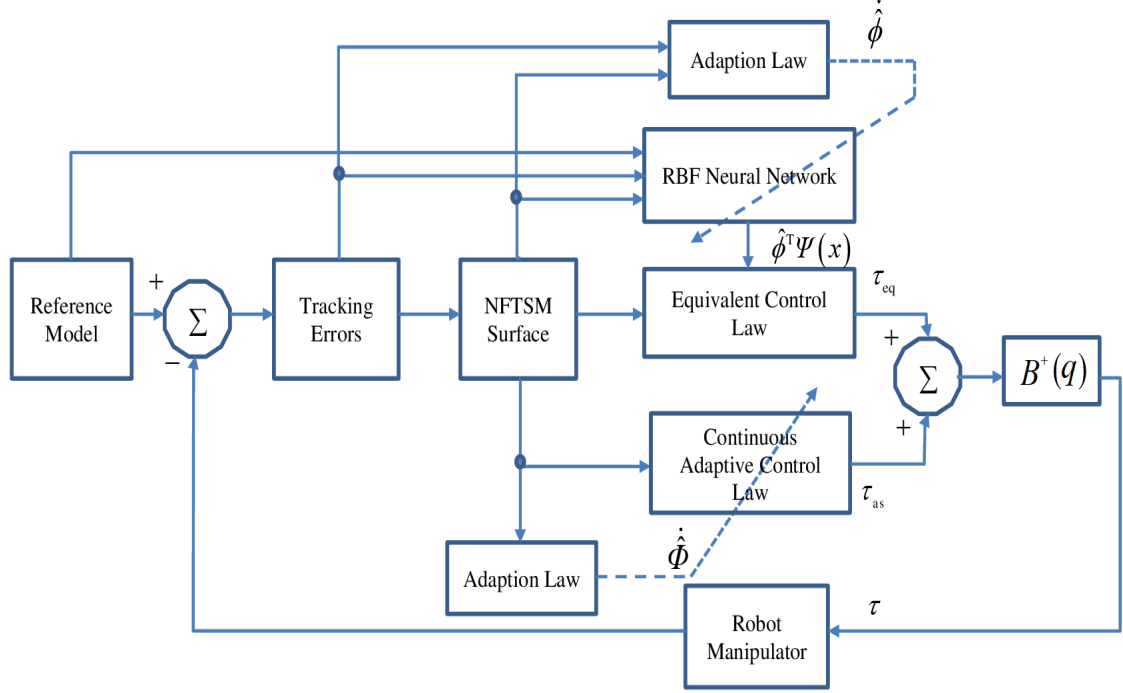


Figure 6.2: Block diagram of the proposed control method.

$$\dot{\hat{\Phi}} = \begin{cases} 0 & \text{if } |s| \leq \varpi \\ \frac{1}{\gamma} |s| & \text{if } |s| > \varpi \end{cases}, \quad (6.53)$$

in which  $\varpi > 0$  is an arbitrary positive value.

**Remark 6.3:** [64] The chattering phenomenon can be significantly alleviated by replacing the  $sign(\cdot)$  function with a saturation function in the control input signal, such as:

$$\text{sat}\left(\frac{s}{\varepsilon^*}\right) = \begin{cases} sign(s) & \text{if } |s| \geq (\varepsilon^*)^2 \\ \frac{s}{\varepsilon^*} & \text{if } |s| < \varepsilon^* \end{cases}, \quad (6.54)$$

in which  $0 < \varepsilon^* < 1$  is a minor positive coefficient called boundary layer thickness, and  $\varepsilon^* = 0.1$ .

## 6.4 Numerical Simulation Studies

To demonstrate the effectiveness of the proposed control strategy, the strategy was applied to a pathway tracking control for the first three joints of a PUMA560 manipulator, and its tracking performance was compared with those of a classical SMC [15, 16] and

NFTSMC [37, 40]. The dynamic model with the crucial parameters found in a 3-DOF PUMA560 robot manipulator was explained by Armstrong et al. [72]. We utilized the MATLAB/Simulink environment for all simulation analysis with the sampling rate set to  $10^{-3}s$ . In this work, only the first three joints of a robot manipulator were investigated (the last three joints were blocked). The simulations were implemented to compare the controllers in terms of their positional accuracy, response speed, and the resulting chattering phenomenon in their control inputs.

To ascertain the robustness of all control methods, we evaluated the system performance in three operation stages, where disturbances and uncertainties were modeled as follows:

$$F_r(\dot{q}) + \tau_d(t) = \begin{bmatrix} 0.9\dot{q}_1 + 1.0\text{sign}(3\dot{q}_1) \\ 1.8\dot{q}_2 + 1.85\text{sign}(2\dot{q}_2) \\ -2.1\dot{q}_3 + 2.5\text{sign}(2\dot{q}_3) \end{bmatrix} + \begin{bmatrix} 7.2 \sin(\dot{q}_1) \\ 1.65 \sin(\dot{q}_2) \\ 0.57 \sin(\dot{q}_3) \end{bmatrix}. \quad (6.55)$$

Stage 1: Robot system was assumed to run under normal operation from time 0s to 15s.

Stage 2: Robot system was assumed to run under operation condition, but there was an external disturbance impacting the first joint between 15s and 50s. This external disturbance had a value defined as  $(15 \sin(q_1 q_2) + 1.5 \cos(\dot{q}_1 q_2) + 5.5 \cos(\dot{q}_1 \dot{q}_2))$ .

Stage 3: Robot system was assumed to run under operation condition, but there was a partial loss (75%) of control input effectiveness at the second joint between 25s and 50s.

The desired joint pathways for the position tracking were

$$q_r = \left[ \cos\left(\frac{t}{5\pi}\right) - 1, \quad \sin\left(\frac{t}{5\pi} + \frac{\pi}{2}\right), \quad \sin\left(\frac{t}{5\pi} + \frac{\pi}{2}\right) - 1 \right]^T. \quad (6.56)$$

The RBFNN architecture consisted of seven nodes, the initial weight matrix of the network was selected as 0, the width and center of the Gaussian function was set as  $\delta = 0.2$ , and the center of the Gaussian function  $\mu$  was selected in range  $(-1.5 \div 1.5)$  with  $\mu_l = 0.5$ . The matrix used in an adaptive law of RBFNN was selected as  $\omega = 15I_7$ , and the NN input was selected as  $v = \begin{bmatrix} e & \dot{e} & q_r & \dot{q}_r & \ddot{q}_r \end{bmatrix}$ .

The SMC control input was set as:

$$\tau(t) = -B^{-1}(q) (\Xi(q, \dot{q}) + \eta(\dot{q} - \dot{q}_r) - \ddot{q}_r + (\Phi_2 + \rho_2) \text{sign}(s)). \quad (6.57)$$

Here,  $\eta, \Phi_2, \rho_2$  are positive constants,  $s$  is a linear sliding function, and  $q_r$  is defined as a desired trajectory value.

Table 6.1: The control parameter selection for the varying control strategies.

Control Strategy	Control Parameters	Control Parameter Values
Classical SMC	$\eta, \Phi_2, \rho_2$	2, 9.9, 1
NFTSMC	$d, h, \beta$	5, 3, 2
	$\Phi_3, \rho_3, \nu$	9.9, 1, 0.1
ANNFTSMC	$h_1, h_2$	20, 7, 0.5, 0.6
	$\Gamma_1, \Gamma_2, \Gamma_3$	$diag(10, 10, 10), diag(6, 6, 6)$
	$\vartheta, \alpha$	$diag(3, 3, 3), diag(3, 3, 3), diag(2, 2, 2)$
	$\gamma, \rho_1, \varpi, \varepsilon^*$	0.5, 0.1, 0.01, 0.1

Table 6.2: Averaged tracking errors under the control signals of the control schemes.

Control Method	Error		
	$E_1^{av}$	$E_2^{av}$	$E_3^{av}$
SMC	0.1943	0.8708	0.0060
NFTSMC	0.1542	0.1218	0.0038
ANNFTSMC	0.0031	0.0031	0.0029

The NFTSMC control input was set as:

$$\tau(t) = -B^{-1}(q) \left( \Xi(q, \dot{q}) - \ddot{q}_r + \beta \frac{h}{d} (\dot{e})^{2-\frac{d}{h}} + (\Phi_3 + \rho_3) \frac{s}{\|s\| + \nu} \right). \quad (6.58)$$

Here,  $\beta, \Phi_3, \rho_3$  are positive constants,  $s$  is a nonlinear sliding function,  $\nu$  is a small positive scalar,  $q_r$  is defined as a desired trajectory value, and  $d, h$  are positive odd integers satisfying the condition  $1 < \frac{d}{h} < 2$ .

The control parameter selection for the varying control strategies, including classical SMC, NTSMC, and the proposed control strategy is shown in Table 6.1.

The averaged tracking errors were calculated according to the following equation:  $E_i^{av} = \sqrt{\frac{1}{n} \sum_{k=1}^n (\|e_i\|^2)}$  in which  $i = 1, 2, 3$ , and  $n$  is the number of simulation steps.

The trajectory tracking performances, including tracking positions and tracking errors at each of the first three joints with three controllers, are illustrated in Figures 6.3 and 6.4. In Stage 1 (from 0s to 15s), three of the control systems give similar good path tracking performance. In Stage 2 (from time greater than 15s) and in Stage 3 (from time greater

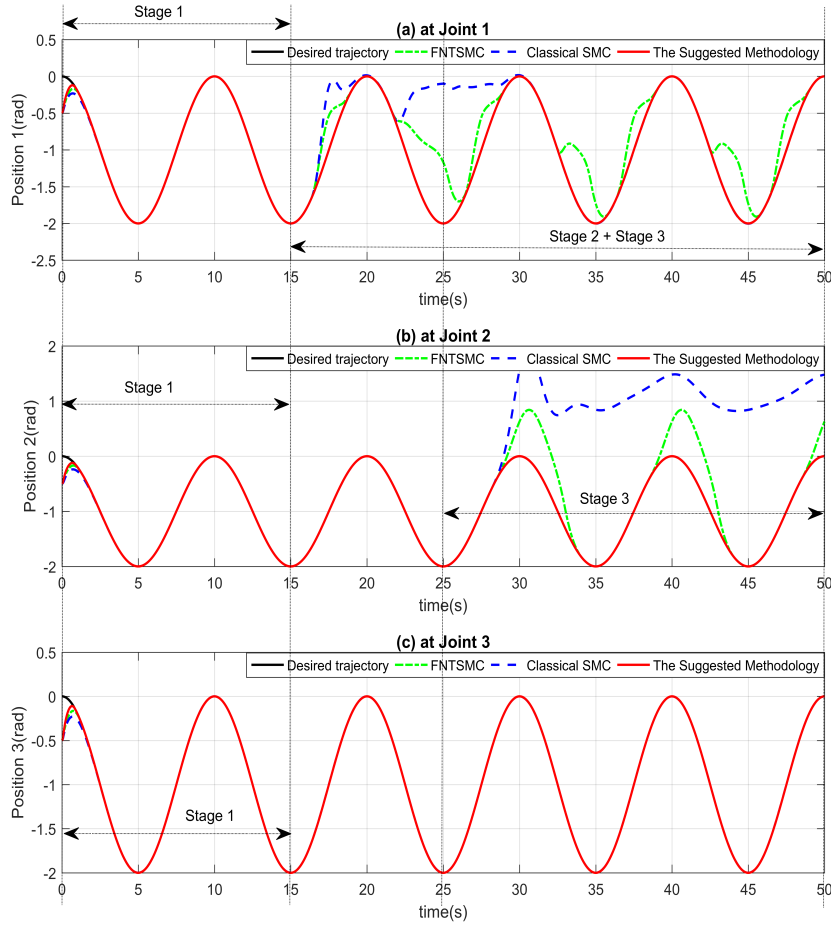


Figure 6.3: Trajectory tracking positions: (a) at Joint 1, (b) at Joint 2, and (c) at Joint 3.

than  $25s$ ), it is clear that the classical SMC provides the poorest path tracking performance, where robot operation becomes unstable when a large disturbance or uncertainty is applied. From Table 6.2 and Figure 6.4, it is observed that NFTSMC provides less path tracking error and faster transient response than classical SMC. However, tracking performance is also diminished upon application of a large disturbance. It is noteworthy that the proposed sliding surface is designed based on the sliding function integral in Eq. (6.8), and this integral portion has a significant role in providing fast transient response and robustness against uncertainty and disturbances. Therefore, the proposed control strategy gives the best path tracking performance and fastest transient response among the compared control strategies, due to the role of the proposed surfaces, an adaptive compensator, and a main contribution of the proposed controller.

The control input signals for all control types, including classical SMC, NFTSMC, and

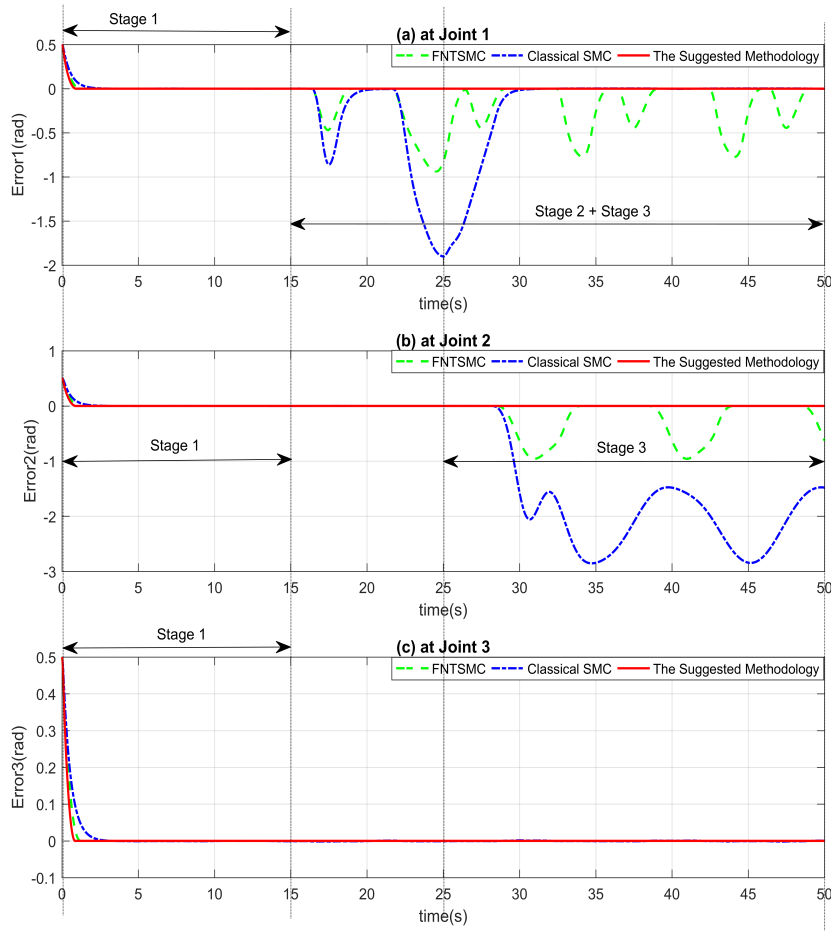


Figure 6.4: Trajectory tracking errors: (a) at Joint 1, (b) at Joint 2, and (c) at Joint 3.

the suggested system are shown in Figure 6.5. In Figure 6.5a, it is clear that the NFTSMC offers a continuous control signal by using a boundary technique [64]. However, the weakness of this technique is that a choice must be made between chattering phenomenon removal and path tracking precision. Consequently, this technique decreases the robustness of the system while also increasing the tracking error. In Figure 6.5b, the SMC offers a discontinuous control signal with serious chattering behavior. On the contrary, the suggested system offers a continuous control signal for the robot manipulator without the loss of its effectiveness, as shown in Figure 6.5c.

The adaptations of the estimated parameters are shown in Figure 6.6. These adaptive gains are estimated according to the variation of the influences of disturbances and uncertainties, and they will attain a constant value once the error variables converge to the sliding surface in a stable phase.



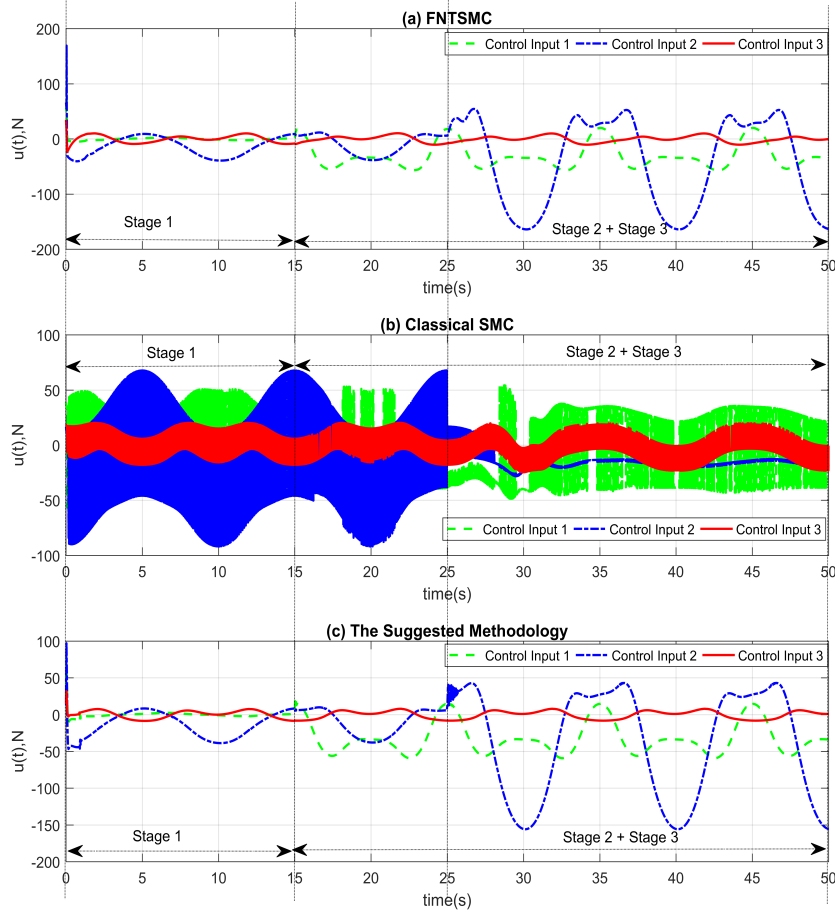


Figure 6.5: Control input signals: (a) FNTSMC, (b) classical SMC, and (c) the suggested control methodology.

From the simulation performance, we conclude that the proposed controller gives the best performance compared to a classical SMC and NFTSMC in terms of tracking precision, transient response, chattering deletion, and small steady state error.

## 6.5 Conclusions

In this report, a robust trajectory tracking control strategy was developed for robot manipulators. From the simulation results and performance comparison with two other control strategies for a 3-DOF PUMA560 robot manipulator, our control strategy offered the best performance in terms of tracking positional accuracy, small steady-state errors, fast convergence, and chattering phenomenon rejection. The suggested control solution has the following benefits: (1) inherits the advantages of the NFTSMC, including non-

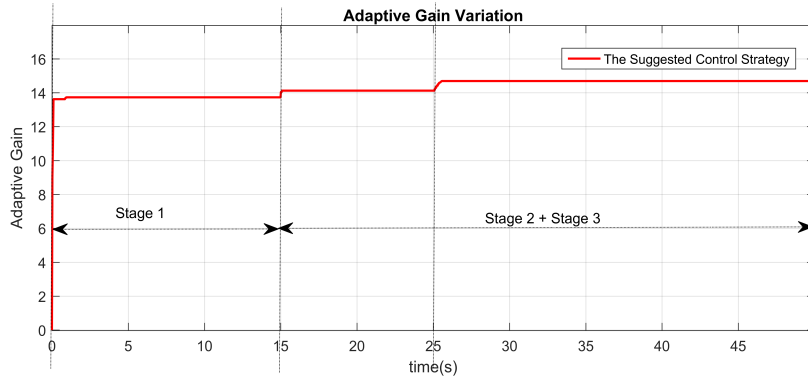


Figure 6.6: Time history of adaptive gain.

singularity, finite-time convergence, fast transient response, low steady-state errors, and high position tracking accuracy; (2) achieves smoothness with elimination of chattering behavior; (3) does not demand an exact dynamic model for the robot manipulator by applying an adaptive radial basis function neural network to approximate an unknown robot function; (4) compared to the classical SMC and another control methods based on TSMC, the proposed control strategy offers better tracking performance and stronger resistance against disturbances and uncertainties; (5) robustness and stability of the robot system was demonstrated fully by Lyapunov theory.



## Chapter 7

# Neural Integral Non-singular Fast Terminal Synchronous Sliding Mode Control for Uncertain 3-DOF Parallel Robotic Manipulators

### 7.1 Introduction

Parallel robotic manipulators have become increasingly popular and play an important role in industrial production systems, applied science fields, and the broader research community. The highlighted benefits of parallel robotic manipulators include a low motion inertia, high movement speeds, high mechanical stiffness, high-precision positioning, and a large load-carrying capability. Therefore, research involving parallel robotic manipulators has received highly significant attention from a lot of scientists in the field of robotics. In real applications, parallel robotic manipulators have been widely applied in applications, such as laser cutting machines, precise manufacturing, flight simulators, medical science, automobile simulators, 3D printers, humanoid robots, and space exploration equipment. Nonetheless, parallel robotic manipulators have constrained workspace and a complicated dynamic model in comparison with serial manipulators. Furthermore, they are attached high nonlinear behavior, the forward kinematic matter, and singularities. Hence, specific experiments are required to completely handle the above problems.

As published in the literature, numerous control approaches, based on model-free control algorithms, have been proposed to drive both parallel and serial robotic manipulators. The highlighted methods, including PID scheme [139], PD synchronized control algorithm [140], or the approach in [112] have been published to control the movement of robotic manipulators. However, these control approaches almost always offer low track-

ing performance or experience degradation in their effectiveness owing to the existence of high nonlinear behavior, uncertainties, or exterior disturbances. Likewise, some model-based control solutions have been introduced to increase the tracking accuracy of robot systems, including CTC [6, 7, 141], adaptive control techniques [142, 143], and robust controllers [8, 15, 58, 66, 75, 83, 137, 144, 145]. However, the tracking accuracy of these algorithms tremendously depends on the exact model of the robot, which is difficult to characterize in real or generalized applications. Moreover, these algorithms include general properties, such as the state-variables of each joint responding to the control closed-loop of each respective actuator, exclusive of the response data from the remaining joints. Accordingly, the control closed-loop of every individual joint will only tune state errors which generated from uncertain terms by its corresponding closed-loop control, the remaining errors were not considered. Furthermore, the end-effector of parallel robotic manipulators follows a certain path, which is synchronously controlled by all active joints. And so, we should synchronously control all active joints of these robot systems to achieve higher trajectory tracking precision.

In recent years, research attention on the SC of parallel robotic systems has steadily increased. In the SC methods, the relation of the kinematic coupling among all active actuators was considered. As a result, the precision of the trajectory tracking has been expressively improved. The first SC algorithm used for this purpose was introduced in [146]. Subsequently, this controller was extensively improved in [147, 148], and gradually became popular in the tracking control for parallel robots [149–151]. An analysis of the comparative performance among the SC schemes stated in [149] pointed out that the SC methods based on a dynamic model provide a better tracking accuracy than other controllers without such a dynamic model. Nonetheless, the model-based synchronization controllers have additional complexity relative to the model-free ones because of the inherent complexity in the dynamic model.

NFTSMC methods suitably minimize the effects of high uncertainties and exterior disturbances for uncertain nonlinear systems. These methods mostly overcome the limitations of both classic SMC and normal TSMC, including slow convergence rate, undefined time convergence, and singularity glitch. And, they have been effectively used for the robotic field and in other real applications [8, 49, 86, 87]. With the use of NFTSMC, the state variables of the system not only quickly converge, but also overcome the possibility of a singularity glitch. However, like the conventional SMC and conventional TSMC schemes, the NFTSMC approaches still have a slow transient response. And, these approaches also skip the relation of the kinematic coupling among the active joints of a parallel robotic manipulator while the approach is designed; further, the torque signals still suffer from chattering as a result of using a discontinuous control law in the reaching phase. Further-

more, the NFTSMC model requires knowledge of the upper bound of uncertain terms in the system, which is difficult to precisely calculate for all uncertain terms. First, to obtain a faster transient response, ITSMC approach was proposed in [52, 53], which preserves the role of the integral term in the PID control method [86, 152]. Secondly, to reduce chattering, numerous useful techniques have been published. These include BLT [64, 153], HOSMC [100, 154], FOSMC [71, 88], and Fuzzy-SMC (F-SMC) [155–157]. Third, several control methodologies based on a combination of Adaptive Control (AC), Fuzzy logic System (FLS), or NN have been combined into TSMC or NFTSMC algorithms to overcome the upper bound problem, as respectively discussed in [103, 106, 158]. In those published papers, due to their approximation ability, NN, FLS, or AC schemes were adopted to approximate unknown elements in the system. These methods only required data regarding output error variables, but no attention was paid to the upper bound of uncertain terms. In [159], an adaptive control system has been introduced for robotic manipulators utilizing the NN-based friction compensator. The friction components between the gear or shaft with the bearing usually degrade control performance at low velocities in motion, and these components have been fully estimated and compensated for. Nonetheless, this controller missed the compensation for any perturbations and approximated errors in the robotic system. Otherwise, the neural-sliding mode controller has built for robotic systems [160] in which the control algorithm applied two equivalent NNs. The first one for learning the system behaviors of the nominal control component and the second one for approximating high-frequency control term. Though the control system behaviors could learn or estimate thoroughly. However, stability analyses of the closed-loop control system have not guaranteed yet. Besides, it also raises a new drawback to applying in real applications, since the large size NNs has a complex structure and a large calculation requirement. In another solution [92], a controller has been developed for 2-DOF parallel robotic manipulators where disturbances and uncertainties are compensated by using a combination of FNN with an error estimator. With this method, the controller can offer continuous control torque and the desired control performance for 2-DOF parallel robot manipulators. Nonetheless, the FNN design only uses a standard linear filter, so, the convergence speed of the tracking errors is normal.

The central motivation in our paper is to develop an enhanced path tracking controller for 3-DOF parallel robot manipulators with uncertain components, while offering the following benefits: (1) the designed method contains the benefits of the INFTSMC, SC, and FNN regarding faster error convergence, a faster transient response, approximation ability, singularity rejection, robustness, and high tracking accuracy; (2) all types of errors in the robotic system are synchronously considered to obtain a better tracking accuracy; (3) the control torque system is smooth with minimized chattering; (4) it removes the

constraint for prior information about the upper bounds of uncertain terms that exist in the robotic system; (5) unlike the current NN or fuzzy algorithms, the proposed algorithm sufficiently compensates for the lumped uncertain dynamics, considers the estimated errors, and high-order components of Taylor's series extension. Moreover, the novelty of the proposed control system in comparison with a normal FNN is that the proposed FNN applies the NFTSM filter replacing for a normal linear filter. Therefore, they adapt better to variations of uncertainties and external disturbances with faster convergence speed.

The remaining of this chapter is arranged in the following outline. In Section 2, the problem formulations and definitions are discussed. In Section 3, the designed control method synthesis is stated with the stability analysis. The designed NINFTSSMC applied for a 3-DOF parallel robot manipulator in Section 4. Then, the path tracking performance of the designed controller is discussed with those of SMC, Synchronization SMC (SSMC), and NFTSMC. Several highlighted conclusions are summarized in Section 5. The control methods for comparison are briefly explained in the Appendix.

## 7.2 Problem Formulations and Preliminaries

### 7.2.1 Dynamic Model Description of 3-DOF parallel robot manipulators

Let us consider the parallel robotic manipulators with the corresponding dynamic model as in [116, 161] and its kinematic illustration as in Fig. 7.1:

$$M_a(q_a) \ddot{q}_a + C_a(q_a, \dot{q}_a) \dot{q}_a + F_a(\dot{q}) + D_a = \tau_a \quad (7.1)$$

where  $q_a = [q_{a1} \ q_{a2} \ q_{a3}]^T$ ,  $\dot{q}_a = [\dot{q}_{a1} \ \dot{q}_{a2} \ \dot{q}_{a3}]^T$ , and  $\ddot{q}_a = [\ddot{q}_{a1} \ \ddot{q}_{a2} \ \ddot{q}_{a3}]^T$  represent the system state vectors at active joints. The components of  $M_a(q_a)$ ,  $C_a(q_a, \dot{q}_a)$ ,  $F_a(\dot{q})$ , and  $D_a$  have been highlighted in [65].  $M_a(q_a) = \hat{M}_a(q_a) + \delta M_a(q_a) \in R^{3 \times 3}$  denotes the actual inertia matrix and  $C_a(q_a, \dot{q}_a) = \hat{C}_a(q_a, \dot{q}_a) + \delta C_a(q_a, \dot{q}_a) \in R^{3 \times 3}$  denotes the actual Coriolis and centrifugal force matrix.  $\hat{M}_a(q_a) \in R^{3 \times 3}$  denotes the approximated inertia matrix and  $\hat{C}_a \in R^{3 \times 3}$  denotes the approximated Coriolis and centrifugal force matrix.  $F(\dot{q})_a = [F_{a1}(\dot{q}) \ F_{a2}(\dot{q}) \ F_{a3}(\dot{q})]^T$  and  $D_a = [D_{a1} \ D_{a2} \ D_{a3}]^T$  are the frictions and load disturbances at active joints, respectively.  $\delta M_a(q_a) \in R^{3 \times 3}$  and  $\delta C_a(q_a, \dot{q}_a) \in R^{3 \times 3}$  represent errors of the actual dynamic model, and  $\tau_a = [\tau_{a1} \ \tau_{a2} \ \tau_{a3}]^T$  are the control input signals.

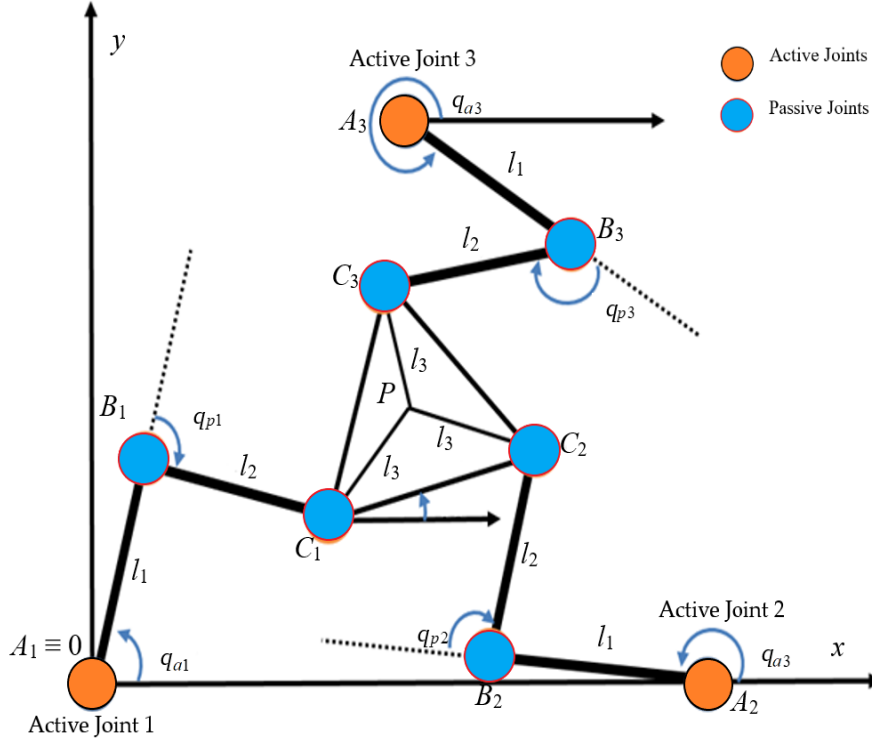


Figure 7.1: The kinematic illustration of the 3-DOF planar parallel robot manipulators.

The actual dynamic equation of the parallel manipulator can be given as follows:

$$\hat{M}_a(q) \ddot{q}_a + \hat{C}_a(q_a, \dot{q}_a) \dot{q}_a + \delta\tau_a = \tau_a \quad (7.2)$$

The vector of uncertain terms  $\delta\tau_a$  in Eq. (7.2) is described as the following expression:

$$\delta\tau_a = \delta M_a(q_a) \ddot{q}_a + \delta C_a(q_a, \dot{q}_a) \dot{q}_a + F_a(\dot{q}_a) + D_a \quad (7.3)$$

To minimize both analysis and design, the dynamic (1) can be expressed in shorter form as:

$$\ddot{q}_a = \Phi(q_a, \dot{q}_a) - \Delta(q_a, \tau_a) \quad (7.4)$$

where  $\Delta(q_a, \tau_a) = \hat{M}^{-1}(q_a) \delta\tau_a$  and  $\Phi(q_a, \dot{q}_a) = \hat{M}^{-1}(q_a) [\tau_a - \hat{C}_a(q_a, \dot{q}_a) \dot{q}_a]$ .

The following assumption is crucial for the design approach.

**Assumption 7.1:** The lumped uncertain terms are a bounded function satisfying the below constraint:

$$\|\Delta(q_a, \tau_a)\| \leq \Lambda \quad (7.5)$$

where  $\Lambda$  is a positive constant that needs to be known in advance.

The main motivation for developing this controller is to further improve the accuracy in



the trajectory tracking control for uncertain 3-DOF parallel robotic manipulators. Here, the coupling position error is utilized to build a synchronous nonlinear sliding surface and develop the control loop. Additionally, an FNN is applied to estimate uncertain dynamics. Therefore, synchronization errors and position errors can synchronously converge to zero and maintain stability for the control system with the presence of uncertain components.

### 7.2.2 Error Definitions in Synchronization Control

Define  $e_{aj} = q_{da j} - q_{aj}$  with  $j = 1, 2, 3$  as the position tracking errors at each active joint, where  $q_{ida}$  indicates the angle of the collated position of the  $j^{th}$  active joint.

With SC methods, the positional error of  $e_{aj}$  not only reaches zero, but also adjusts the relationship of the movement among multiple active joints throughout the tracking process, such that  $e_1 = e_2 = e_3$ .

When a 3-DOF parallel robotic manipulator has three active joints, the synchronization errors are computed as follows:

$$E = \begin{bmatrix} e_1 - e_2, & e_2 - e_3, & e_3 - e_1 \end{bmatrix}^T = \begin{bmatrix} E_1, & E_2, & E_3 \end{bmatrix}^T \quad (7.6)$$

where  $E$  represents the vector of synchronization errors.

As a result, the aim is to ensure that the position errors and synchronization errors quickly converge to zero, which is guaranteed to occur at the same time if  $E_j = 0$  for all active joints.

In SC methods, the coupling position error is described with the following expression:

$$\begin{cases} E_{1a}^* = e_{1a} + \kappa \int_0^\phi \delta E_{13} d\phi \\ E_{2a}^* = e_{2a} + \kappa \int_0^\phi \delta E_{21} d\phi \\ E_{3a}^* = e_{3a} + \kappa \int_0^\phi \delta E_{32} d\phi \end{cases} \quad (7.7)$$

where  $\phi$  is a temporal variable starting time zero,  $\kappa$  is a positive constant.  $\delta E_{13} = E_1 - E_3$ ,  $\delta E_{21} = E_2 - E_1$ , and  $\delta E_{32} = E_3 - E_2$  are defined as the cross-coupling errors.

Denote  $E_a^* = \begin{bmatrix} E_{1a}^*, & E_{2a}^*, & E_{3a}^* \end{bmatrix}^T$  as the vector of coupling position errors,  $\delta E = \begin{bmatrix} \delta E_{13}, & \delta E_{21}, & \delta E_{32} \end{bmatrix}^T$ , and its time derivative  $\dot{\delta E} = \begin{bmatrix} \dot{\delta E}_{13}, & \dot{\delta E}_{21}, & \dot{\delta E}_{32} \end{bmatrix}^T$ .

According to Eq. (7.7), the coupling position error has first-order and second-order derivatives as follows:

$$\dot{E}_a^* = \dot{e}_a + \kappa \delta E \quad (7.8)$$

and

$$\ddot{E}_a^* = \ddot{e}_a + \kappa \dot{\delta} E \quad (7.9)$$

## 7.3 Proposed NINFTSSMC Design

### 7.3.1 Design of SINFTSM Surface

In this section, a novel NINFTSSMC is devised for uncertain 3-DOF parallel robotic manipulators as follows.

From the coupling position errors in Eqs. (7.7) - (7.9), the SINFTSM surfaces are built according to [109]:

$$\sigma = \dot{E}_a^* + \int_0^t \left( W_1 |E_a^*|^{\alpha_1} \text{sign}(E_a^*) + W_2 \left| \dot{E}_a^* \right|^{\alpha_2} \text{sign}(\dot{E}_a^*) \right) dt \quad (7.10)$$

where  $\sigma = \begin{bmatrix} \sigma_1 & \sigma_2 & \sigma_3 \end{bmatrix}^T \in R^{3 \times 1}$  are the sliding manifold variables,  $\alpha_1, \alpha_2, W_1$ , and  $W_2$  are positive constants, which are assigned in the same manner as in [109].  $W_1$  and  $W_2$  can be assigned such that the polynomial  $\rho^2 + W_2\rho + W_1$  is Hurwitz.  $\alpha_1$  and  $\alpha_2$  can be defined according to the constraints:  $0 < \alpha_1 < 1$ , and  $\alpha_2 = \frac{2\alpha_1}{1+\alpha_1}$ .

Taking the first derivative of the SINFTSM surface (7.10) with respect to time, we obtain:

$$\dot{\sigma} = \ddot{E}_a^* + W_1 |E_a^*|^{\alpha_1} \text{sign}(E_a^*) + W_2 \left| \dot{E}_a^* \right|^{\alpha_2} \text{sign}(\dot{E}_a^*) \quad (7.11)$$

From Eq. (7.9), the dynamic of Eq. (7.11) gives:

$$\dot{\sigma} = \ddot{e}_a + \kappa \dot{\delta} E + W_1 |E_a^*|^{\alpha_1} \text{sign}(E_a^*) + W_2 \left| \dot{E}_a^* \right|^{\alpha_2} \text{sign}(\dot{E}_a^*) \quad (7.12)$$

Inserting the robotic system (7.4) into Eq. (7.12), Eq. (7.12) gives:

$$\begin{aligned} \dot{\sigma} = & \ddot{q}_{da} - \hat{M}^{-1}(q_a) \tau_a + \hat{M}^{-1}(q_a) \hat{C}_a(q_a, \dot{q}_a) \dot{q}_a \\ & + \Delta(q_a, \tau_a) + \kappa \dot{\delta} E + W_1 |E_a^*|^{\alpha_1} \text{sign}(E_a^*) \\ & + W_2 \left| \dot{E}_a^* \right|^{\alpha_2} \text{sign}(\dot{E}_a^*) \end{aligned} \quad (7.13)$$

### 7.3.2 Design of the proposed NINFTSSMC

The following control action is now designed to control the end-effector of the robot system, which is tracked over the trajectory profile with the desired performance:

$$\tau_a = \hat{M}(q_a)(\tau_{eq} + \tau_{sw}) \quad (7.14)$$

The equivalent control action is designed as follows:

$$\begin{aligned} \tau_{eq} = & \ddot{q}_{da} + \hat{M}^{-1}(q_a) \hat{C}_a(q_a, \dot{q}_a) \dot{q}_a + \kappa \dot{\delta} E \\ & + W_1 |E_a^*|^{\alpha_1} \text{sign}(E_a^*) + W_2 \left| \dot{E}_a^* \right|^{\alpha_2} \text{sign}(\dot{E}_a^*) \end{aligned} \quad (7.15)$$

and, the switching control action is selected as follows:

$$\tau_{sw} = (\Lambda + \xi) \text{sign}(\sigma) \quad (7.16)$$

where  $\xi$  is positive constant, and  $\Lambda$  is chosen according to Assumption 1.

Applying the control input (7.14)-(7.16) to Eq. (7.13), Eq. (7.13) gives:

$$\dot{\sigma} = -\tau_{sw} + \Delta(q_a, \tau_a) \quad (7.17)$$

**Proof:** Define  $\sigma_j$ , and  $\Delta_j(q_a, \tau_a)$  as the  $j^{th}$  sliding manifold variable and the  $j^{th}$  lumped uncertain term, respectively, and  $\tau_{jsw} = (\Lambda + \xi) \text{sign}(\sigma_j)$  as the  $j^{th}$  switching control torque with  $j = 1, 2, 3$ . Therefore,

$$\dot{\sigma}_j = -\tau_{jsw} + \Delta_j(q_a, \tau_a) \quad (7.18)$$

In order to prove the correctness of the designed control action in Eqs. (7.14)-(7.16), the following Lyapunov function is defined as follows:

$$V_1 = 0.5 \sum_{j=1}^3 \sigma_j^T \sigma_j \quad (7.19)$$

The time derivative of Eq. (7.19) employing the result of Eq. (7.18) is

$$\begin{aligned}
 \dot{V}_1 &= \sum_{j=1}^3 \sigma_j^T \dot{\sigma}_j \\
 &= \sum_{j=1}^3 \sigma_j^T (-\tau_{jsw} + \Delta_j(q_a, \tau_a)) \\
 &= \sum_{j=1}^3 \sigma_j^T (-(\Lambda + \xi) \text{sign}(\sigma_j) + \Delta_j(q_a, \tau_a)) \\
 &= \sum_{j=1}^3 (-\Lambda |\sigma_j| + \Delta_j(q_a, \tau_a) \sigma_j) - \sum_{j=1}^3 \xi |\sigma_j| \\
 &\leq - \sum_{j=1}^3 \xi |\sigma_j|
 \end{aligned} \tag{7.20}$$

Since  $\xi > 0$ , the synchronization errors and position errors can be synchronously converged to zero and maintained stability under control commands (7.14)-(7.16) for the robot system with the presence of uncertain components. However, the switching control term in Eq. (7.16) is designed according to Assumption 1. That means uncertain dynamics, external disturbances, the mathematical models cannot obtain an exact computation. To overcome this dependence, we use FNN to approximate the lumped uncertain dynamics. The novelty of the proposed approach compared to a classic FNN is that the proposed FNN utilizes a NFTSM filter replacing for a classic filter. Thanks to this procedure, the lumped uncertain dynamics are compensated more quickly and more accurately, thus, the malfunction in the reaching phase of state variables approaching the sliding surface is handled thoroughly.

### 7.3.3 Feed Forward Neural Network Structural Design

The structure of FNN with multiple inputs and multiple outputs is exhibited in Fig. 7.2

The structural design of FNN has three layers including the layer of neural inputs, the layer of hidden nodes, and the layer of neural outputs. In this paper, we design an FNN including 3 outputs corresponding the 3 active actuators of the 3-DOF parallel robot manipulators. The FNN outputs are expressed by the following equation:

$$f(x) = W^T G(x, V) + \varepsilon \tag{7.21}$$

with  $G_i = \frac{1}{\sum_{j=1}^{N_i} v_{ij} x_j}$ ,  $i = 1, \dots, N_h$ . Here,  $x$  is network state input,  $N_i$  is network

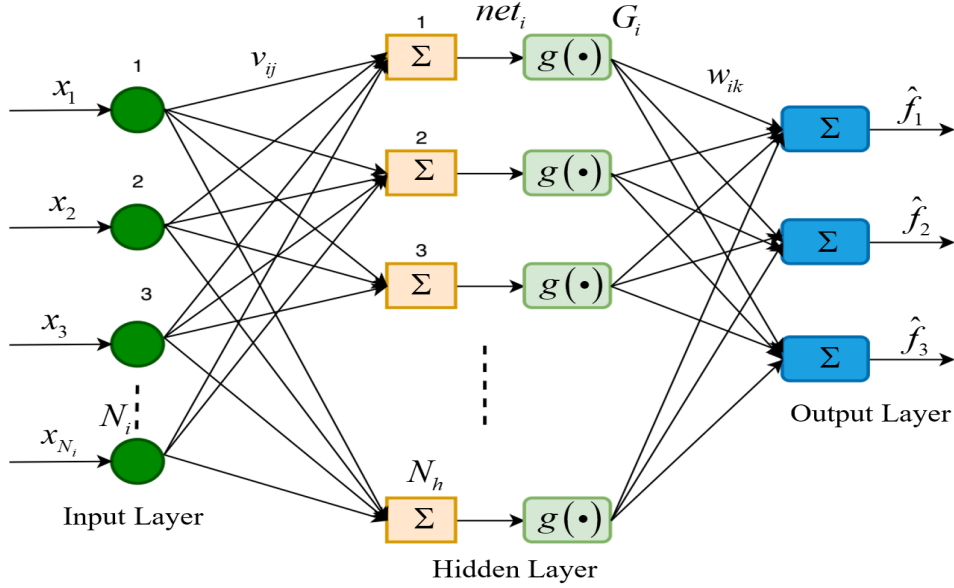


Figure 7.2: The architecture of the FNN.

input number,  $N_h$  is the node number in the hidden layer of neural network.  $G = [G_1, G_2, \dots, G_{N_h}]^T$  represents the sigmoid function output,  $V, W$  are NN weights and the approximation error  $\varepsilon$  of NN bounded on a compact set by  $\|\varepsilon\| < \varepsilon_B$ .

In the layer of NN inputs, the input vector is defined as:

$$x = [x_1, x_2, \dots, x_{N_i}]^T = [E_{a1}^*, \dot{E}_{a1}^*, E_{a2}^*, \dot{E}_{a2}^*, E_{a3}^*, \dot{E}_{a3}^*]^T \quad (7.22)$$

In the layer of the hidden nodes, we denote the NN numbers in this layer as  $N_h$ , the input and hidden layers are connected by the weight matrix and described as follows:

$$\hat{V} = [v_1, v_2, \dots, v_{N_h}] \in R^{6 \times N_h} \quad (7.23)$$

with  $v_i = [v_{i1}, v_{i2}, v_{i3}, v_{i4}, v_{i5}, v_{i6}]^T \in R^{6 \times 1}, i = 1, 2, \dots, N_h$ .

In the layer of the hidden nodes, their inputs and outputs are stated, respectively.

$$net_i = \sum_{j=1}^{N_i} v_{ij} x_j \quad (7.24)$$

$$\hat{G}_i = g(net_i), i = 1, 2, \dots, N_h \quad (7.25)$$

The following sigmoid function is selected to become the transfer function in the layer of the hidden nodes

$$g(z) = \frac{1}{1 - e^{-z}} \quad (7.26)$$

In the layer of the NN outputs, the hidden and output layers are linked by the following weight matrices:

$$\begin{aligned}\hat{W} &= [w_1, w_2, \dots, w_{N_h}]^T \in R^{N_h \times 3} \\ w_i &= [w_{i1}, w_{i2}, w_{i3}] \in R^{3 \times 1}, i = 1, 2, \dots, N_h\end{aligned}\tag{7.27}$$

Defining  $\hat{f}(x)$  as the approximated function of  $f(x)$ .  $\hat{f}(x)$  is afterward described by the FNN, as follows:

$$\hat{f}(x) = \hat{W}^T \hat{G}(x, \hat{V}) \in R^{3 \times 1}\tag{7.28}$$

in which  $\hat{G} = [\hat{G}_1, \hat{G}_2, \dots, \hat{G}_{N_h}]^T \in R^{N_h \times 1}$  and the  $k^{th}$  element of  $\hat{f}(x)$  is described as  $\hat{f}_k = \sum_{i=1}^{N_h} w_{ik} G_i, k = 1, 2, 3$ .

In this work, the FNN is used to approximate the lumped uncertain dynamics  $\Delta(q_a, \tau_a)$ . Therefore, the approximation error is defined as follows:

$$\Delta(q_a, \tau_a) - f(x) = W^{*T} G(x, V^*) - \hat{W}^T G(x, \hat{V}) + \varepsilon_B\tag{7.29}$$

Here, the weight matrices  $W$  and  $V$  have the corresponding optimal parameters  $W^* \in R^{N_h \times 3}$  and  $V^* \in R^{6 \times N_h}$ ;  $\hat{W} \in R^{N_h \times 3}$  and  $\hat{V} \in R^{6 \times N_h}$  are the estimated parameters of the optimal weight matrices.

We define  $\tilde{W} = W^* - \hat{W} \in R^{N_h \times 3}$ ,  $\tilde{V} = V^* - \hat{V} \in R^{6 \times N_h}$  as weight estimation errors and  $\tilde{G} = G^* - \hat{G} \in R^{N_h}$  as the hidden-layer output error in which  $G^* \equiv G(x, V^*) \in R^{N_h}$  and  $\hat{G} \equiv G(x, \hat{V}) \in R^{N_h}$ . Then, Eq. (7.29) is rewritten as:

$$\Delta(q_a, \tau_a) - f(x) = W^{*T} \tilde{G} - \tilde{W}^T \hat{G} + \varepsilon_B\tag{7.30}$$

With a given  $x$ , the Taylor series expansion of  $\tilde{G}(x)$  has the following statement:

$$\begin{aligned}\tilde{G} &= \begin{bmatrix} \tilde{G}_1 \\ \vdots \\ \tilde{G}_{N_h} \end{bmatrix} \Big|_{V=\hat{V}} + \begin{bmatrix} \frac{\partial \tilde{G}_1}{\partial V^T} \\ \vdots \\ \frac{\partial \tilde{G}_{N_h}}{\partial V^T} \end{bmatrix} \Big|_{V=\hat{V}} (V^* - \hat{V}) \\ &\quad + O(\hat{V}^T x) \\ &= G_V \tilde{V}^T x + O(\hat{V}^T x)\end{aligned}\tag{7.31}$$

where  $G_V = \left[ \frac{\partial \tilde{G}_1}{\partial V^T x}, \dots, \frac{\partial \tilde{G}_{N_h}}{\partial V^T x} \right]^T \Big|_{V=\hat{V}} \in R^{N_h \times N_h}$ ,  $\tilde{V} = V^* - \hat{V} \in R^{6 \times N_h}$ , and  $O(\hat{V}^T x) \in R^{N_h}$  is a vector of high-order components and these components are assumed to be bounded.

Adding Eq. (7.31) to Eq. (7.30) gives:

$$\begin{aligned}\Delta(q_a, \tau_a) - f(x) &= W^{*T} G_V \tilde{V}^T x + \tilde{W}^T \hat{G} + W^{*T} O(\hat{V}^T x) + \varepsilon_B \\ &= \hat{W}^T G_V \tilde{V}^T x + \tilde{W}^T \hat{G} + v\end{aligned}\quad (7.32)$$

in which  $v = \tilde{W}^T G_V \tilde{V}^T x + W^{*T} O(\hat{V}^T x) + \varepsilon_B \in R^{3 \times 1}$  is called as error vector and it is assumed to be bounded  $\|v\| \leq \xi$ .

Because the lumped uncertain dynamics  $\Delta(q_a, \tau_a)$  is approximated by the FNN, hence, the dynamic (7.13) becomes:

$$\begin{aligned}\dot{\sigma} &= \ddot{q}_{da} - \hat{M}^{-1}(q_a) \tau_a + \hat{M}^{-1}(q_a) \hat{C}_a(q_a, \dot{q}_a) \dot{q}_a + f(x) \\ &\quad + \kappa \dot{\delta} E + W_1 |E_a^*|^{\alpha_1} \text{sign}(E_a^*) + W_2 \left| \dot{E}_a^* \right|^{\alpha_2} \text{sign}(\dot{E}_a^*)\end{aligned}\quad (7.33)$$

**Theorem 7.1:** Consider the robot system (7.1), if the torque inputs are proposed as

$$\tau_a = \hat{M}(q_a) (\tau_{eq} + \tau_{sw}) \quad (7.34)$$

$$\begin{aligned}\tau_{eq} &= \ddot{q}_{da} + \hat{M}^{-1}(q_a) \hat{C}_a(q_a, \dot{q}_a) \dot{q}_a \\ &\quad + \kappa \dot{\delta} E + \hat{W}^T \hat{G}(x, \hat{V}) \\ &\quad + W_1 |E_a^*|^{\alpha_1} \text{sign}(E_a^*) + W_2 \left| \dot{E}_a^* \right|^{\alpha_2} \text{sign}(\dot{E}_a^*)\end{aligned}\quad (7.35)$$

the switching control term is proposed as:

$$\tau_{sw} = \xi \text{sign}(\sigma) \quad (7.36)$$

and the update laws of the FNN are proposed as:

$$\dot{\hat{W}} = K_W \hat{G} \sigma^T \quad (7.37)$$

$$\dot{\hat{V}} = K_V x \left( G_V^T \hat{W} \sigma \right)^T \quad (7.38)$$

where  $K_W \in R^{N_h \times N_h}$  and  $K_V \in R^{6 \times 6}$  are diagonal matrices. The FNN uses the NFTSM error filter as (7.10). When these conditions hold then the closed-loop system is stable.

**Remark 7.1:** From Eqs. (7.37) - (7.38), it is seen that the updating laws of FNN use the NFTSM surface to make error filter. Therefore, it achieves a faster convergence speed than a normal error filter.

Block Diagram of the designed control system is illustrated in Fig. 7.3.

To confirm the correctness of Theorem 1, the following proof is given.

**Proof:** Applying the designed control inputs (7.34) - (7.36) to dynamic (7.33) and using result in Eq. (7.32), we have:

$$\dot{\sigma} = -\tau_{sw} + \hat{W}^T G_V \tilde{V}^T x + \tilde{W}^T \hat{G} + v \quad (7.39)$$

The control performance is confirmed employing the following Lyapunov function:

$$\begin{aligned} V_2 = & 0.5\sigma^T \sigma + 0.5tr \left\{ \tilde{V}^T K_V^{-1} \tilde{V} \right\} \\ & + 0.5tr \left\{ \tilde{W}^T K_W^{-1} \tilde{W} \right\} \end{aligned} \quad (7.40)$$

Using the result of Eq. (7.39), the time derivative of Eq. (7.40) gives:

$$\begin{aligned} \dot{V}_2 = & \sigma^T \left( -\xi \text{sign}(\sigma) + \hat{W}^T G_V \tilde{V}^T x + \tilde{W}^T \hat{G} + v \right) \\ & + tr \left( \tilde{V}^T K_V^{-1} \dot{\tilde{V}} \right) + tr \left( \tilde{W}^T K_W^{-1} \dot{\tilde{W}} \right) \\ = & \sigma^T \left( -\xi \text{sign}(\sigma) + \hat{W}^T G_V \tilde{V}^T x + \tilde{W}^T \hat{G} + v \right) \\ & - tr \left( \tilde{V}^T K_V^{-1} \dot{\tilde{V}} \right) - tr \left( \tilde{W}^T K_W^{-1} \dot{\tilde{W}} \right) \\ = & -\xi |\sigma| + \sigma^T v + tr \left( \tilde{V}^T \left( -K_V^{-1} \dot{\tilde{V}} + x \sigma^T \hat{W}^T G_V \right) \right) \\ & + tr \left( \tilde{W}^T \left( -K_W^{-1} \dot{\tilde{W}} + \hat{G} \sigma^T \right) \right) \end{aligned} \quad (7.41)$$

Substituting the update laws (7.37) and (7.38) into (7.41) obtains:

$$\begin{aligned} \dot{V}_2 = & -\xi |\sigma| + \sigma^T v \\ \leq & 0 \end{aligned} \quad (7.42)$$

## 7.4 Numerical Simulation Studies

Firstly, the 3-DOF parallel robotic manipulator was designed in SOLIDWORKS and the SimMechanics package of MATLAB. Then, this robot system is used as the testing system for all simulated validation to investigate the effectiveness of the designed NINFTSSMC. Specifically, we used the SOLIDWORKS software to build the 3-D computer-aided design (CAD) of the robot system in which each robotic component was individually formed and jointly connected using the appropriate joints. An XML file of the 3-D computer-aided design was afterward exported by the SimMechanics link plug-in and this file was put into Simulink environment. For that reason, in SimMechanics, the assembly model of the robot is geometry files. The sensors measured position and velocity, and actuators



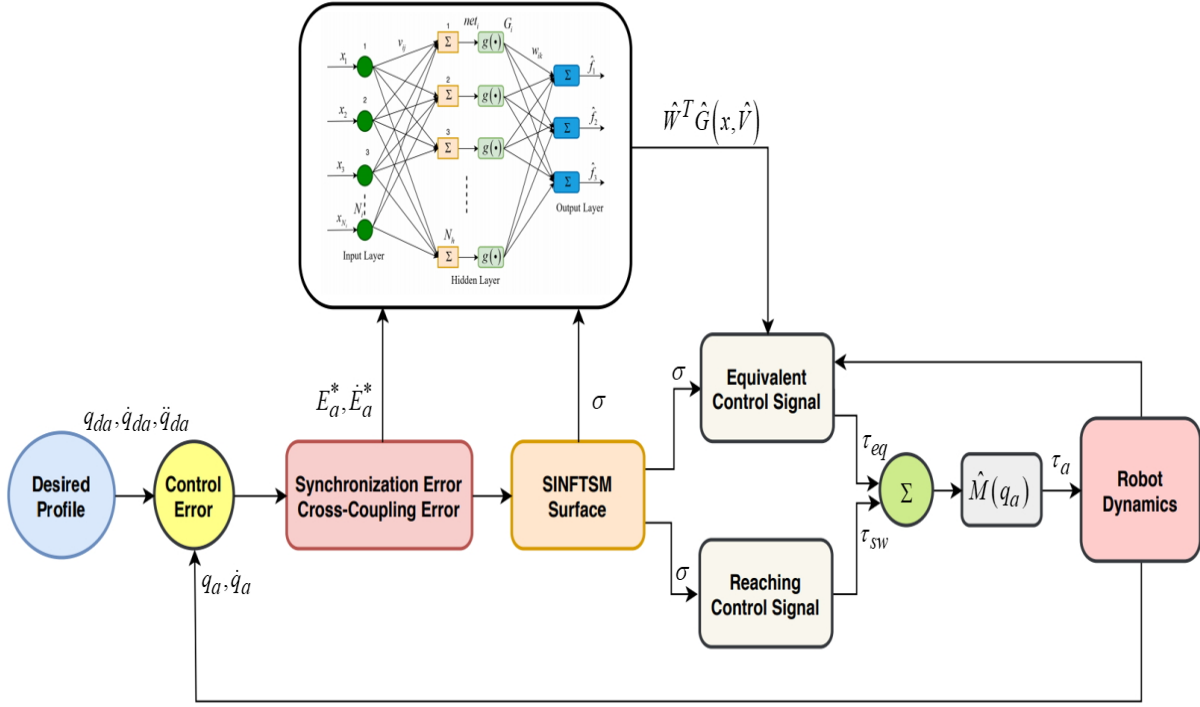


Figure 7.3: Diagram of the proposed control system.

were also set up on the robot system. exterior disturbances and uncertain frictions were modelled to add to the system when the properties of the proposed NINFTSSMC are investigated. Finally, the designed NINFTSSMC were performed for the above testing system. The 3D CAD model of the manipulator is shown in Fig. 7.4. The parameters of the robotic system are given in Table 7.1.

The selected parameters of four different control systems: SMC, SSMC, NFTSMC, and NINFTSSMC are stated in Table 7.2. The FNN had six neurons in the input layer, eleven neurons in the hidden layer, and three neurons in the output layer. The weight matrices of the FNN are initialized with values  $W(0) = 0.05 \times rand(N_h, 3)$ ,  $V(0) = 0.05 \times rand(N_h, N_i)$ .

The designed NINFTSSMC was applied to a specified path tracking control of a 3-DOF parallel robotic manipulator. Then, its path tracking performance was compared with those of the SMC, the SSMC, and NFTSMC. Furthermore, to investigate the properties of the proposed NINFTSSMC, a large value of uncertain dynamics and exterior disturbances were assumed in the simulated examples, as follows. The following friction forces at each active joint were modelled:

Table 7.1: The parameters of the robotic system

Parameters	Depiction	Value
$m_{i1}$	Mass of each lower Link	$5.12kg$
$m_{i1}$	Mass of each upper Link	$7.39kg$
$m_p$	Mass of the motion Platform	$3.84kg$
$l_p$	Inertia moment of the motion Platform	$65 \times 10^{-3}kg.m^2$
$l_1$	The lower part length of each Link	$0.4m$
$l_2$	The upper part length of each Link	$0.6m$
$l_3$	The dimension of the motion Platform	$0.2m$
$l_{c1}$	Distance from the Joint to the mass center of each lower Link	$0.3m$
$l_{c2}$	Distance from the Joint to the mass center of each upper Link	$0.3m$
$l_{i1}$	Inertia moment of the lower of ith Link	$91 \times 10^{-3}kg.m^2$
$l_{i2}$	Inertia moment of the upper of ith Link	$267 \times 10^{-3}kg.m^2$

$$F_a = \begin{bmatrix} F_{a1} \\ F_{a2} \\ F_{a3} \end{bmatrix} = \begin{bmatrix} 0.5sign(\dot{q}_{a1}) + 2.5\dot{q}_{a1} \\ 0.5sign(\dot{q}_{a2}) + 2.5\dot{q}_{a2} \\ 0.5sign(\dot{q}_{a3}) + 2.5\dot{q}_{a3} \end{bmatrix} \quad (7.43)$$

The end-effector of the parallel robotic manipulator is controlled to track the prescribed path as follows:

$$P = \begin{bmatrix} x_P \\ y_P \\ \beta_P \end{bmatrix} = \begin{bmatrix} 0.49 + 0.03 \cos\left(\frac{\pi t}{3}\right) \\ 0.37 + 0.03 \sin\left(\frac{\pi t}{3}\right) \\ \frac{\pi}{2} \end{bmatrix} \quad (7.44)$$

Fig. 7.5 exhibits the prescribed path and actual path of end-effector under four different control schemes, including SMC, SSMC, NFTSMC, and the proposed NINFTSSMC. The end-effector of the robotic system is controlled to follow a circular path with the starting position as  $XY(0.5284, 0.3681)$ . As seen in Fig. 7.5, there is the largest discrepancy between the tracking circular path from SMC and the desired circular profile; it provides the worst tracking performance among the four control methodologies. Fig. 7.6, Fig. 7.7, and Fig. 7.8 exhibit the tracking errors of the end-effector in the X- axis, Y- axis, and the error of rotary angle, respectively. The tracking error comparison under all

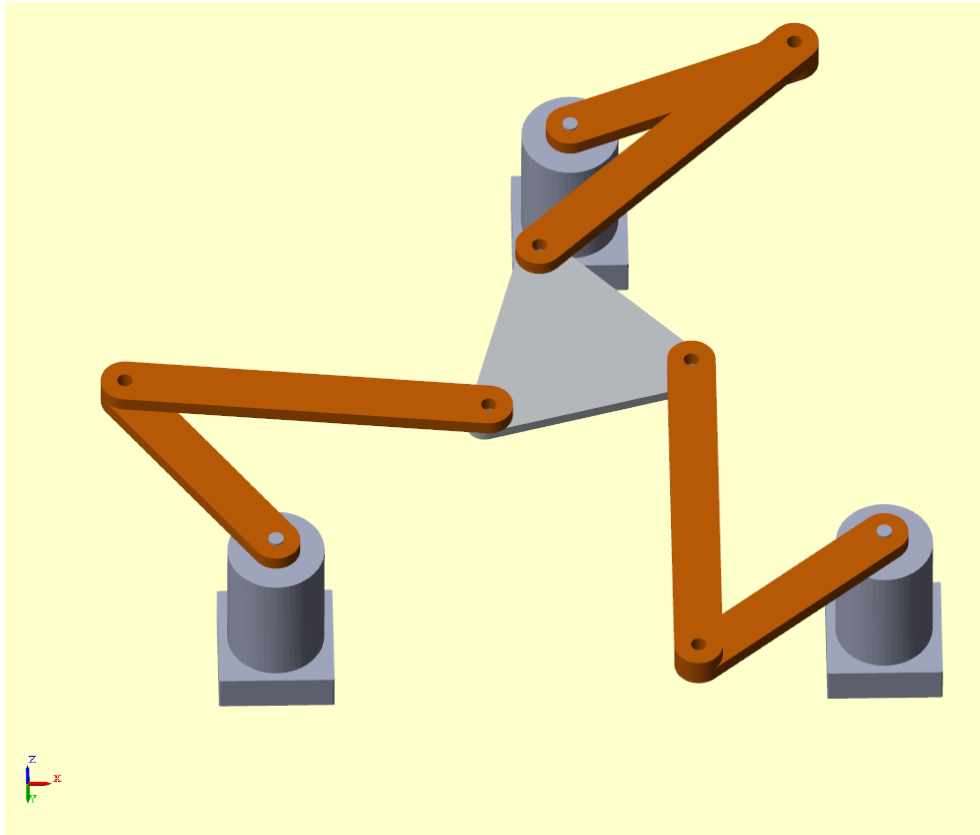


Figure 7.4: 3-D computer-aided design of the 3-DOF planar parallel robot manipulator.

control methods and synchronization errors and cross-coupling errors at active joints are corresponding in Fig. 7.9 and Fig. 7.10. The SSMC and the NFTSMC approaches produce better tracking performance than SMC. Nonetheless, the NFTSMC offers a better tracking precision and a faster reaching time for the errors than SSMC. It is notable that the proposed NINFTSSMC is formed based on the integration of synchronization control, the NFTSMC and the FNN. Accordingly, the actual tracking circular path generated by the designed NINFTSSMC has the smallest discrepancy in comparison with the desired trajectory profile, and the fastest convergence time to the prescribed circular path among the four control methodologies. From Fig. 7.6, Fig. 7.7, Fig. 7.8, and Fig. 7.9, it is seen that the tracking errors produced by SSMC are smaller than the tracking errors offered by SMC. However, SSMC offers a worse tracking error than NFTSMC. Specifically, the proposed NINFTSSMC offers the smallest tracking errors compared with SMC, SSMC, and NFTSMC. By using the proposed NINFTSSMC, the control precision is most increased compared with SMC, SSMC and NFTSMC.

The control input actions for all control approaches, including SMC, SSMC, NFTSMC, and the proposed NINFTSSMC are exhibited in Fig. 7.11. From Fig. 7.11, it is clear that

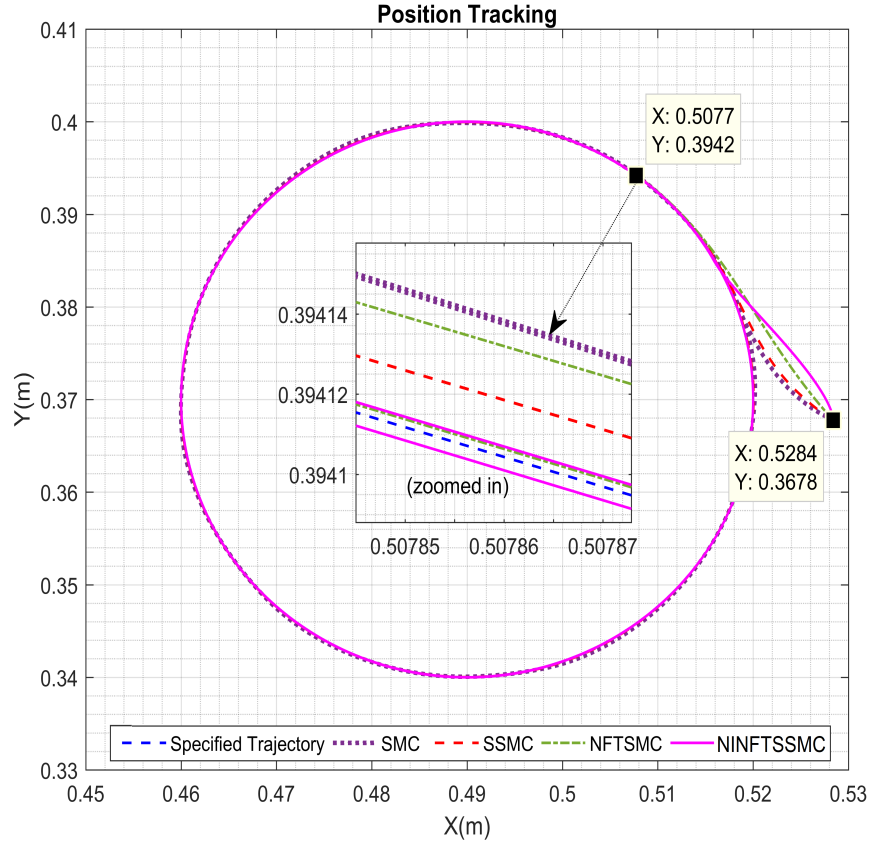


Figure 7.5: The prescribed path and actual path of the end-effector under the four different control methods.

all control schemes produce a continuous control torque. All those controllers including SMC, SSMC, NFTSMC use the BLT to reject high frequency control signals, which is known as chattering. However, the application of the BLT leads to a decrease in powerful properties and precision of the control action in several situations. While the proposed control system applies the FNN with the NFTSM filter to compensate for the lumped uncertain dynamics. It was found that under the combination of SC, INFTSMC, and FNN, the trajectory tracking precision produced by the proposed NINFTSSMC was very high without the chattering phenomenon in the control signal. This is because these lumped uncertain dynamics have been compensated for by the proposed FNN and the faster transient response of the integral term in synchronization nonlinear sliding surface. Consequently, the designed NINFTSSMC is extremely useful for trajectory tracking control of 3-DOF parallel robot manipulators. By using the suggested NINFTSSMC, the influences of high nonlinear terms, exterior disturbances, uncertain dynamics have been thoroughly compensated for, and does not require prior information about the upper bounds of these

Table 7.2: Parameters the different control systems

Parameters	SMC	SSMC	NFTSMC	NINFTSSMC
$z$	20	20	—	—
$\Lambda$	10	10	10	—
$\xi$	0.01	0.01	0.01	0.01
$\varepsilon$	0.7	0.7	0.7	—
$\kappa$	—	0.9	—	0.9
$K_W$	—	—	—	$0.01 \times I_{11 \times 11}$
$K_V$	—	—	—	$0.01 \times I_{4 \times 6}$
$\Upsilon$	20	20	—	—
$W_1$	—	—	10	16
$W_2$	—	—	5	6.5
$\alpha_1$	—	—	1.4	0.5
$\alpha_2$	—	—	1.28	0.5

uncertain terms.

## 7.5 Conclusions

This chapter proposed NINFTSSMC for 3-DOF parallel robotic manipulators with uncertain dynamics using synchronous nonlinear sliding surface, where this sliding surface is formed based on the integration of SC and INFTSMC. Accordingly, position errors and synchronization errors quickly converge to the SINFTSM surface at the same time. Next, the FNN is applied to estimate uncertain dynamics, in which the novelty of the proposed approach compared to a classic FNN is that the proposed NN utilizes the NFTSM error filter replacing for a classic error filter. Finally, the control approach was designed for the robotic system to achieve the performance described in this paper, such as rapid error convergence, robustness with uncertain dynamics, minimum chattering, synchronization, and high precision. The stability of the control loop has been secured according to the Lyapunov criteria. The powerful properties and effectiveness of the proposed NINFTSSMC were confirmed by computer simulations and performance comparisons for a 3-DOF parallel robotic manipulator. Through control performance comparison, it is concluded that the NINFTSSMC is extremely efficient for trajectory tracking control of uncertain 3-DOF parallel robotic manipulators.

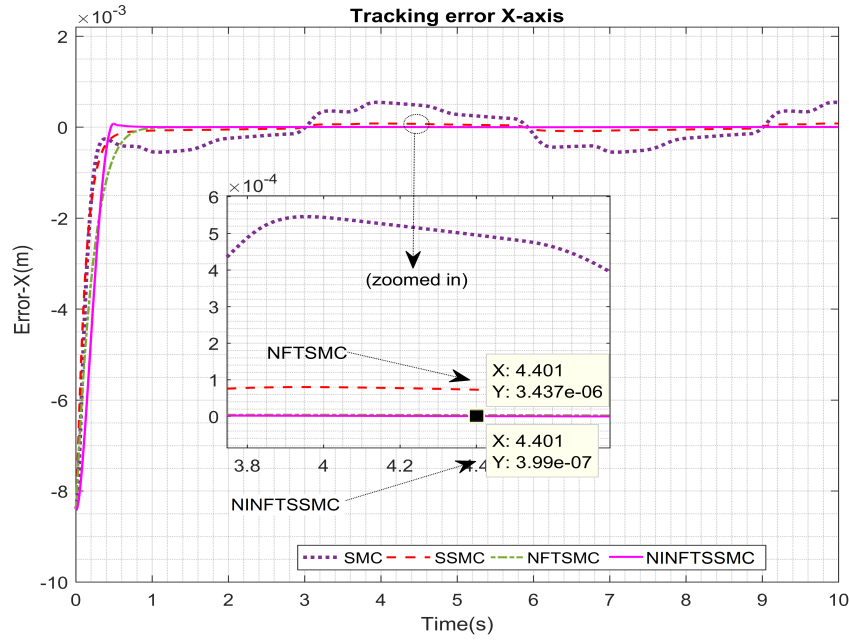


Figure 7.6: The response time of the end-effector in control error comparison (X-axis).

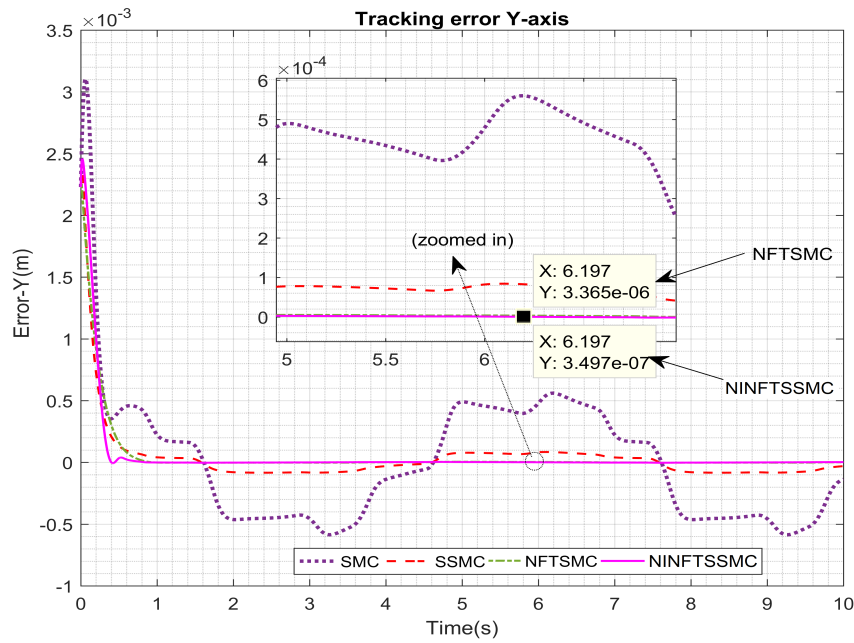


Figure 7.7: Response time of the end-effector in control error comparison (Y-axis).

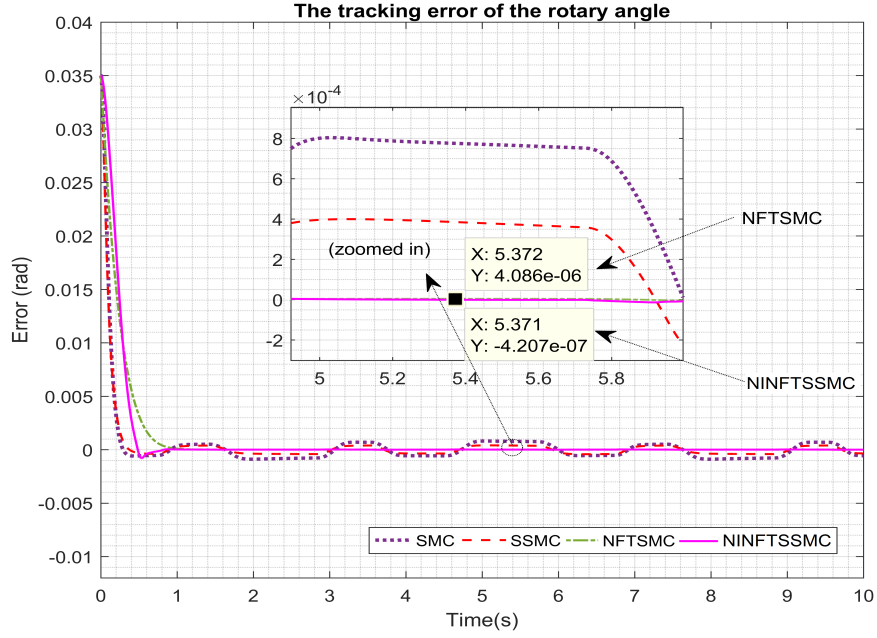


Figure 7.8: Response time of the rotary angle in control error comparison.

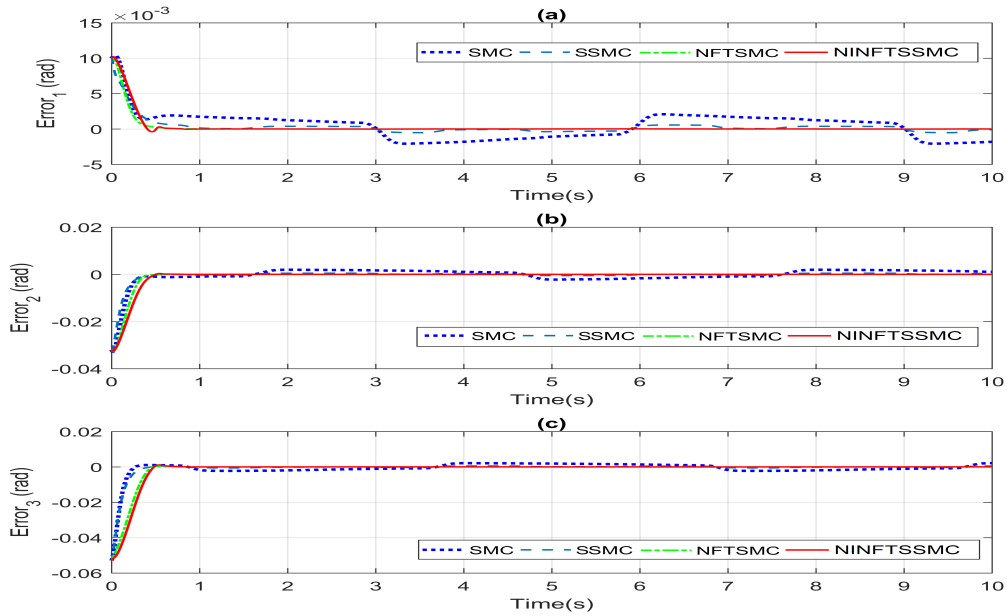


Figure 7.9: Control errors of Joints (a) at Joint 1, (b) at Joint 2, and (c) at Joint 3.

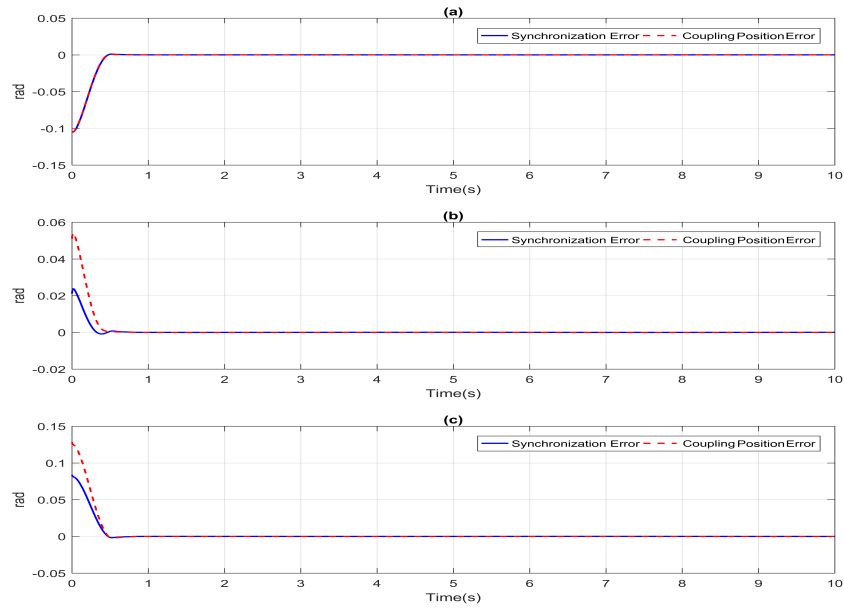


Figure 7.10: Synchronization Error and Coupling Position Error of Joints (a) at Joint 1, (b) at Joint 2, and (c) at Joint 3.

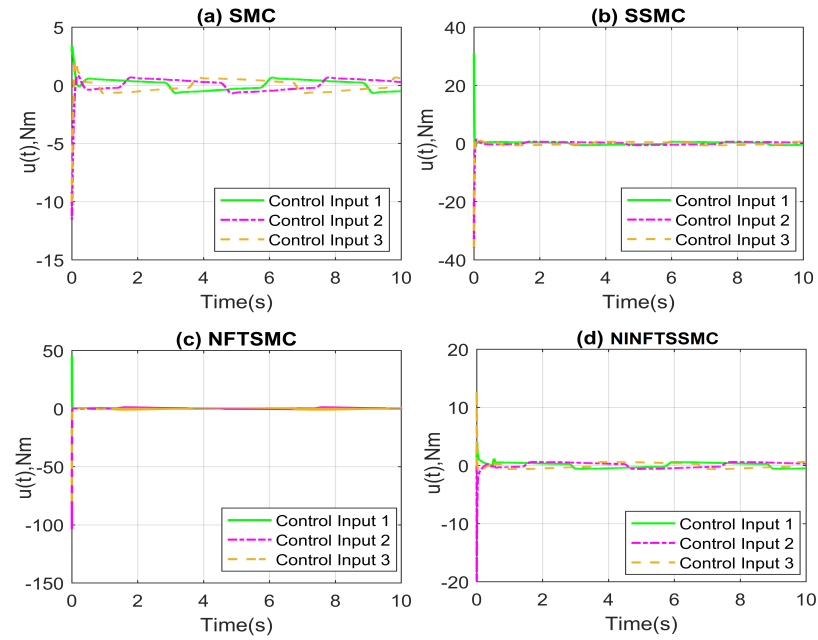


Figure 7.11: Control input actions: (a) SMC, (b) SSMC, (c) NFTSMC, and (d) NINFTSSMC.





# Appendix E

## Design of the SMC

In [1, 92], the SMC scheme was designed with the following approach:

Firstly, the sliding manifold was selected and then taken its first derivative with respect to time, we can gain:

$$\begin{aligned}\sigma &= \dot{e}_a + ze_a = \dot{q}_a - \dot{q}_{ra}; \\ \dot{\sigma} &= \ddot{e}_a + z\dot{e}_a = \ddot{q}_a - \ddot{q}_{ra}\end{aligned}\tag{E.1}$$

where  $z$  is a positive constant,  $e_a = q_a - q_{da}$  are the path tracking errors,  $q_{da}$  are the prescribed trajectories,  $\dot{q}_{ra} = \dot{q}_{da} - ze_a$  is the vector of reference velocity, and  $\ddot{q}_{ra} = \ddot{q}_{da} - z\dot{e}_a$  represents the vector of reference acceleration.

The time derivative of the dynamic system (E.1) along the robot dynamic model (7.4) is given as

$$\dot{\sigma} = \hat{M}^{-1} \left[ \tau_a - \hat{C}_a \dot{q}_a \right] - \Delta(q_a, \tau_a) - \ddot{q}_{ra}\tag{E.2}$$

The torque command was then proposed as in [1, 92] to provide the required control performance for the system (7.1):

$$\tau_a = \hat{M}\ddot{q}_{ra}(t) + \hat{C}_a\dot{q}_{ra} - (\Lambda + \xi) \operatorname{sgn}(\sigma)\tag{E.3}$$

To disregard the chattering in the torque signal during the control process, the BLT was performed. Consequently, the torque action of Eq. (E.3) becomes

$$\tau_a = \hat{M}\ddot{q}_{ra} + \hat{C}_a\dot{q}_{ra} - (\Lambda + \xi) \operatorname{sat}(\sigma/\varepsilon)\tag{E.4}$$

where  $\Lambda, \xi$  are positive constants,  $\varepsilon$  is the boundary layer thicknesses, and  $\operatorname{sat}(\sigma/\varepsilon)$  is a saturation vector [1].

## Design of the SSMC

The synchronization sliding mode surface was first proposed and then taken its first derivative with respect to time, the result was

$$\begin{aligned}\sigma &= E_a^* + z\dot{E}_a^* = \dot{q}_a - \dot{q}_{ra}; \\ \dot{\sigma} &= \dot{E}_a^* + z\ddot{E}_a^* = \ddot{q}_a - \ddot{q}_{ra}\end{aligned}\tag{E.5}$$

where  $z$  is a positive constant,  $E_a^*$  is defined in Eq. (7.9) as the cross-coupling error,  $q_{da}$  is the prescribed trajectory,  $\dot{q}_{ra} = \dot{q}_{da} - \delta E$  represents the vector of reference velocity, and  $\ddot{q}_{ra} = \ddot{q}_{da} - \dot{\delta}E$  denotes the vector of reference acceleration.  $\delta E$  and  $\dot{\delta}E$  are also described in Eq. (7.9).

Inserting the robotic from Eq. (7.4) into Eq. (E.5), yields:

$$\dot{\sigma} = \hat{M}^{-1} \left[ \tau_a - \hat{C}_a \dot{q}_a \right] - \Delta(q_a, \tau_a) - \ddot{q}_{ra}\tag{E.6}$$

The following torque command is constructed as in [162] to obtain the desired tracking performance for robotic manipulator of Eq. (7.1):

$$\tau_a = \hat{M}\ddot{q}_{ra}(t) + \hat{C}_a\dot{q}_{ra} - \Upsilon\sigma - (\Lambda + \xi) \operatorname{sgn}(\sigma)\tag{E.7}$$

The BLT was performed to substitute the discontinuous component in the torque action. Therefore, the torque command of Eq. (E.7) becomes

$$\tau_a = \hat{M}\ddot{q}_{ra} + \hat{C}_a\dot{q}_{ra} - \Upsilon\sigma - (\Lambda + \xi) \operatorname{sat}(\sigma/\varepsilon)\tag{E.8}$$

where  $\Lambda$ ,  $\xi$ ,  $\Upsilon$  are positive constants,  $\varepsilon$  is the boundary layer thicknesses, and  $\operatorname{sat}(\sigma/\varepsilon)$  is a saturation vector [1].

## Design of the NFTSMC

Select the NFTSMC surface, as in [85]:

$$\sigma = \dot{e}_a + W_1 e_a^{[\alpha_1]} + W_2 e_a^{[\alpha_2]}\tag{E.9}$$

where  $\sigma = \begin{bmatrix} \sigma_1 & \dots & \sigma_3 \end{bmatrix}^T \in R^{3 \times 1}$  are the sliding variables,  $e_a = q_{da} - q_a$  are the position tracking errors,  $W_1, W_2, \alpha_1, \alpha_2$  are positive constants and  $1 < \alpha_1 < 2, \alpha_2 > \alpha_1$ , which are chosen as in [85]. In addition,  $e_a^{[\alpha_1]}$  and  $e_a^{[\alpha_2]}$  are defined as:

$$e_a^{[\alpha_i]} = |e_a|^{\alpha_i} \operatorname{sgn}[e_a]; \frac{d}{dt} e_a^{[\alpha_i]} = \alpha_i |e_a|^{\alpha_i-1} \dot{e}_a \quad (E.10)$$

$$i = 1, 2$$

in which  $\operatorname{sgn}[e_a] = \begin{cases} 1 & \text{if } e_a > 0 \\ -1 & \text{if } e_a < 0 \\ 0 & \text{if } e_a = 0 \end{cases}$ .

Taking the first derivative of Eq. (E.9) with respect to time, yields:

$$\dot{\sigma} = \ddot{e}_a + \Gamma_1 \alpha_1 |e_a|^{\alpha_1-1} \dot{e}_a + \Gamma_2 \alpha_2 |e_a|^{\alpha_2-1} \dot{e}_a \quad (E.11)$$

The time derivative of the dynamic system (E.11) along the robot dynamic model (7.4) is given as

$$\dot{\sigma} = \ddot{q}_{da} - \hat{M}^{-1} [\tau_a - \hat{C}_a \dot{q}_a] + \Delta(q_a, \tau_a) + \Gamma_1 \alpha_1 |e_a|^{\alpha_1-1} \dot{e}_a + \Gamma_2 \alpha_2 |e_a|^{\alpha_2-1} \dot{e}_a \quad (E.12)$$

The following torque command is constructed to get the desired tracking performance for robotic manipulator of Eq. (7.1):

$$\tau_a = \hat{M} (\tau_{eq} + \tau_{sw}) \quad (E.13)$$

the equivalent control action is designed as follows:

$$\tau_{eq} = \ddot{q}_{da} + \hat{M}^{-1} \hat{C}_a \dot{q}_a + \Gamma_1 \alpha_1 |e_a|^{\alpha_1-1} \dot{e}_a + \Gamma_2 \alpha_2 |e_a|^{\alpha_2-1} \dot{e}_a \quad (E.14)$$

and, the switching control action is chosen as follows:

$$\tau_{sw} = (\Lambda + \xi) \operatorname{sgn}(\sigma) \quad (E.15)$$

The BLT was employed to ignore the chattering in the control action. Thus, the torque command of Eq. (E.13) becomes

$$\tau_a = \hat{M} \left( \ddot{q}_{da} + \hat{M}^{-1} \hat{C}_a \dot{q}_a + \Gamma_1 \alpha_1 |e_a|^{\alpha_1-1} \dot{e}_a + \Gamma_2 \alpha_2 |e_a|^{\alpha_2-1} \dot{e}_a + (\Lambda + \xi) \operatorname{sat}(\sigma/\varepsilon) \right) \quad (E.16)$$

where  $\Lambda, \xi$  are positive constants,  $\varepsilon$  is the boundary layer thicknesses, and  $\operatorname{sat}(\sigma/\varepsilon)$  is a saturation vector [1].



## Chapter 8

# A Novel Fault-Tolerant Control Method for Robot Manipulators Based on Non-Singular Fast Terminal Sliding Mode Control and Disturbance Observer

### 8.1 Introduction

Robots are essential for manufacturing, human life, and performing complex tasks nowadays and in the future. With the need for high-quality products, the robot is more widely used. To achieve quality products with high productivity, the robot system must be operated smoothly, reliably, and safely. Unfortunately, Robotic manipulators unavoidably face many complicated uncertainties caused by unmodeled and unknown dynamic models, nonlinear frictional forces, exterior disturbances, or faults. Consequently, this leads to obstacles for the control design process and precise control of robot manipulators. The tracking control of robotic manipulators has concerned many scientists in studying its potential capability. The tracking control method of robotic systems that require a high degree of precision, safety, and stability during operation has been an important subject in both theoretical and practical applications [163,164]. Developing solutions to enhance the tracking performance and fast response of robotic systems, specifically with respect to uncertainty, external disturbances, and possible faults, continues to present a challenge in robotics research. To enhance the reliability, tracking performance, and safety of robotic systems in all cases, FTTCM has been recommended [165–168], however, it is difficult to apply fault-tolerant controls in robotic systems due to high nonlinearities, external distur-

bances, and dynamic uncertainties. Furthermore, the time delay implicit in mechanical systems is also a concern for the performance of FTCM. FTCMs can be categorized as either passive FTCM or active FTCM [169].

In the passive FTCM, a control system is constructed without fault detection process for both standard and fault conditions. Therefore, the performance of the control system is depended on the robust properties to handle external disturbances or uncertainties. As published in the literature, several FTCs have been successfully adopted to control uncertain nonlinear systems. Noteworthy examples such as sliding mode FTC [170–172] or adaptive FTC [173]. The remarkable characteristics of the passive FTCM are fast response with external disturbances, uncertainties or fault occurrence. However, this method needs partial information about possible system faults and capability solves high magnitude faults. Consequently, it is limited in applying to the real robot system.

Different from the passive FTCM, In the active FTCM, the output signal of the controller is constantly adjusted according to a fault approximation response, which is estimated by a fault diagnosis observer (FDO) [138,174]. As a result, the control performance of the active FTCM depends on the fault information accuracy. The active FTCM with the exact fault information will provide performance better than that of a passive FTCM and therefore it is more suitable for real robot applications. On the other hand, wrong fault information leading to the robot system runs loss stability and damage. Therefore, designing an active FTCM based on the exact fault observation is really challenges for the researchers. In controlling robot manipulators, active FTCM offers a control performance better than passive FTCM due to compensation from online control reconfiguration.

In the literature, several control methods, which can be adapted for use in the FTCM design, have been successful in controlling robot systems in real-world applications with uncertainties, disturbances, or faults. The successful control methods employed in these studies include CTC [174], PID controllers [4,5], SC [13,14], intelligent controllers [9,10,58], a predictive controller [175], AC [12,176], and SMC [17,78]. Among these mentioned control methods, SMC has a simple design, a robust control algorithm, and a proven ability to solve perturbations, uncertainties, or system faults. SMC has attracted a great deal of attention in control system as well as in FTCM [170–172]. Unfortunately, the classical SMC is not an optimal solution for all robot control problems because of its limitations, which include chattering behavior, singularity phenomena, and the requirement to know the upper limit values of disturbances, uncertainties, and faults in advance. Recently, several studies have proposed enhanced control algorithms to handle the SMC control obstacles [40,76,177]; these control schemes applied a nonlinear sliding variable for the improvement of the transient performance, called as TSMC.

Generally, the conventional TSMC can be used solve the problems associated with

classical SMC, but issues persist with the singularity phenomenon, and convergence speeds can be slower for TSMC than for SMC. Hence, to remove the singularity phenomenon issue and improve convergence speed at the same time, NFTSMC have been developed [8, 48, 83, 85].

Despite their advantages, it is important to note that serious chattering phenomena will occur whenever using one of the above control schemes in real robotic systems (e.g., SMC, TSMC, and FNTSMC) with a large sliding gain value in the switching control law. Consequently, the chattering can compromise the robustness behavior of the control system and significantly weaken its performance. As such, researchers have focused a lot of effort to develop methods that eliminate chattering, including BLT [64, 153], HOSMC [64, 65, 178], STA [124], or FOTSMC [179–181]. However, these methods using BL to eliminate chattering come with tradeoffs and require selection between weakening the chattering phenomenon or the path tracking precision. On the contrary, HOSMC, STA, or FOTSMC offers both higher tracking precision and chattering dismissal. Therefore, in this study, we develop a novel, robust FTCM with STRCL to achieve the control target with smooth control input signals.

As mentioned, the active FTCM will provide control performance better than that of a passive FTCM when the exact fault information is used. Therefore, to precisely estimate the effects of the uncertainties, disturbances, or faults acting on the robot system, a simple resolution is to design observers. Researching this trend, numerous observers based on control schemes have been established [182–184]. With those control algorithms, firstly, a disturbance observer is constructed to estimate external disturbance and uncertainty terms. Then, these estimated values are supported for feedforward control technique to compensate for disturbances and uncertainties in the system. Noteworthy is that, according to the stable condition of the SMC, the sliding gain values must assign greater than the boundary values of disturbances and uncertainties in the system [15]. However, the large sliding gain values will cause serious chattering. For this reason, a simple resolution reduced the chattering in control input is that the effects of disturbances and uncertainties must cut down on the system. According to the mentioned solution, DO has been added into the SMC to compensate for the effects of disturbances and uncertainties to reject the chattering behavior [185, 186].

For all control methods based on SMC, TSMC, NFTSMC, or FOTSMC, the two greatest challenges are to achieve an exact value of the upper bounds for the lumped uncertain terms and an exact robot model in the design procedure of the control system. To overcome these challenges, many types of SMC and TSMC have been suggested based on ACs because they can automatically adapt the control parameters to reject the influences of environmental disturbances, uncertainties, or faults [59, 61]. And, to approximate unknown



nonlinear functions, several computing attempts have been suggested, such as NNs [55,56] and FLS [187], due to their approximation capabilities. However, using NNs or FLSs to approximate unknown nonlinear functions lead to increases the complex calculations for the control system.

Purposed by the above analysis, the aim of this report is to design a novel FTCM for robot manipulators based on the combination of NFTSMC, DO, and STRCL that solves several important problems: 1) speedy transient performance; 2) convergence in a short time; 3) rejection of the chattering phenomenon; (4) highly effective for trajectory tracking control with the presence of exterior disturbances, uncertainties, component or actuator faults; 5) rejects the requirement for prior information about upper bound values of exterior disturbances, uncertainties, or faults.

The remainder of this report is outlined as follows: The problem statement is given in section 2. Section 3 describes the design process of the proposed FTCM. In section 4, the proposed FTCM is applied to a robotic system [72], and its simulation tracks the prescribed pathway and compares it to control schemes based on conventional SMC [15] and TSMC [40] to inspect positional errors, fast transient performance, and chattering phenomenon rejection. Finally, section 5 summarizes the notable conclusions of this work. **Notations:** Several symbols are utilized throughout this paper,  $\|\cdot\|$  and  $|\cdot|$  correspond to the Euclidean norm and modulus, while  $N$  and  $R$  correspond to the spaces of natural numbers and real numbers, respectively.  $\{\cdot\}^{-1}$  and  $\{\cdot\}^T$  correspond to inverse of and matrix transpose of, respectively.

## 8.2 Statement of the Problem

### 8.2.1 The Problem Statement

Consider the robotic dynamic equation explained by:

$$\begin{aligned} \ddot{\theta} = M^{-1}(\theta) \left( \tau - V_m(\theta, \dot{\theta}) \dot{\theta} - F_r(\dot{\theta}) - G(\theta) - \tau_d \right) \\ + \psi(t - T_f) \omega(\theta, \dot{\theta}, \tau) \end{aligned} \quad (8.1)$$

where  $\theta(t), \dot{\theta}(t), \ddot{\theta}(t) \in R^n$  represent the position, velocity and acceleration at each joint of the robot system, respectively,  $M(\theta) \in R^{n \times n}$  is the inertia matrix,  $V_m(\theta, \dot{\theta}) \in R^{n \times 1}$  indicates the Coriolis and centrifugal forces,  $G(\theta) \in R^{n \times 1}$  is the gravitational force term,  $\tau(t) \in R^{n \times 1}$  represents the control input torque,  $\tau_d(t) \in R^{n \times 1}$  indicates anonymous disturbances,  $\psi(t - T_f) \omega(\theta, \dot{\theta}, \tau)$  is the unexpected fault terms that affect the robotic system,  $T_f$  indicates the time instant that a fault occurs, the  $\psi(t - T_f)$  function gives

the time profile of a fault that occurs at some unknown time  $T_f$ , and  $\omega(\theta, \dot{\theta}, \tau)$  is the bounded but uncontrollable term of the controlled system output.

The following fundamental property satisfies the robot dynamic model (1):

**Property 1:** The inertia matrix is a positive definite matrix and limited as follows:

$$\begin{aligned} 0 < \lambda_{\min} \{M(\theta)\} \leq \|M\| \leq \lambda_{\max} \{M(\theta)\} \leq \Upsilon, \\ \Upsilon > 0 \end{aligned} \quad (8.2)$$

where  $\lambda_{\min} \{M(\theta)\}$  and  $\lambda_{\max} \{M(\theta)\}$  correspond to the minimum and maximum eigenvalues of the inertia matrix.

The  $\psi(t - T_f)$  function is defined as a diagonal matrix with the following form:

$$\psi(t - T_f) = \text{diag} \left\{ \psi_1(t - T_f), \dots, \psi_n(t - T_f) \right\} \quad (8.3)$$

In the literature, there are two types of faults that have been identified, including abrupt and incipient faults, according to the following formula:

$$\psi(t - T_f) = \begin{cases} 0, & t \leq T_f \\ 1 - e^{-\nu(t - T_f)}, & t > T_f \end{cases} \quad (8.4)$$

where  $\nu > 0$  indicates the unknown fault evolution rate.

When the value of  $\nu$  is small, it characterizes incipient faults. While  $\nu$  is large, the formula characterizes abrupt faults.

To simplify the analysis and design in the control system, the robot dynamic model (8.1) can be rearranged:

$$\begin{aligned} \ddot{\theta} = M^{-1}(\theta) \tau + M^{-1}(\theta) \left( V_m(\theta, \dot{\theta}) \dot{\theta} + G(\theta) \right) \\ + M^{-1}(\theta) \left( F_r(\dot{\theta}) + \tau_d \right) + \psi(t - T_f) \omega(\theta, \dot{\theta}, \tau) \end{aligned} \quad (8.5)$$

Here, we assign  $x_1 = \theta, x_2 = \dot{\theta}, x = [x_1, x_2]^T$  and  $u = \tau$ ; thus, the dynamic model (5) can be described according to the following expression:

$$\begin{cases} \dot{x}_1 = x_2 \\ \dot{x}_2 = q(x)u - H(x) - \Delta \end{cases} \quad (8.6)$$

where  $H(x) = M^{-1}(\theta) \left( V_m(\theta, \dot{\theta}) \dot{\theta} + G(\theta) \right)$  indicates the known element,  $q(x) = M^{-1}(\theta)$  represents a smooth nonlinear function, and  $\Delta = M^{-1}(\theta) \left( F_r(\dot{\theta}) + \tau_d \right) - \psi(t - T_f) \omega(\theta, \dot{\theta}, \tau)$  gives the anonymous element in the system dynamics.

Our goal is to propose a robust, active FTCM such that this control algorithm can

provide the prescribed performance regardless of disturbances, uncertainties, and faults.

The following constraint is assumed for the control design approach.

**Assumption:** The modelling uncertainty is bounded such that

$$\|\Delta\| \leq \Lambda \quad (8.7)$$

where  $\Lambda$  are arbitrary positive constants.

## 8.3 FTCM for Robot Manipulators based on NFTSMC, DO, and STRCL

This section presents FTCM for robot manipulators based on the combination of NFTSMC, DO, and STRCL, which secures the stabilization of the system and obtains the prescribed tracking performance.

### 8.3.1 Design of the new FTSMS

To overcome singularity glitch and to enhance convergence time of conventional TSMC, the new FTSMS is constructed as:

$$\begin{aligned} \sigma_i = \dot{e}_i + \frac{2\gamma_1}{1 + E^{-\mu_1(|e_i|-\phi)}} e_i \\ + \frac{2\gamma_2}{1 + E^{\mu_2(|e_i|-\phi)}} |e_i|^\alpha \text{sign}(e_i) \end{aligned} \quad (8.8)$$

where  $\sigma \in R^n$  is the FTSMS,  $E$  defines as exponential function. Likewise,  $e_i = x_{1i} - x_{ri}$  represents the positional control error, and  $\dot{e}_i = \dot{x}_{1i} - \dot{x}_{ri}$  represents the velocity control error  $x_r \in R^n$  is the prescribed reference path. Furthermore,  $\gamma_1, \gamma_2, \mu_1, \mu_2$  are the positive constants,  $0 < \alpha < 1$ , and  $\phi = \left(\frac{\gamma_2}{\gamma_1}\right)^{\frac{1}{1-\alpha}}$ .

Based on the SMC, the following terms must be satisfied when the control errors run in the sliding mode:

$$\begin{aligned} \sigma_i &= 0; \\ \dot{\sigma}_i &= 0 \end{aligned} \quad (8.9)$$

Combining dynamic (8.8) with terms (8.9) gives:

$$\begin{aligned} \dot{e}_i = -\frac{2\gamma_1}{1+E^{-\mu_1(|e_i|-\phi)}} e_i \\ -\frac{2\gamma_2}{1+E^{\mu_2(|e_i|-\phi)}} |e_i|^\alpha \text{sign}(e_i) \end{aligned} \quad (8.10)$$

To prove that  $e_i = 0$  is an equilibrium point, and it will converge to zero in finite-time, the following Lyapunov function is considered:

$$V_1 = 0.5e_i^2 \quad (8.11)$$

Calculating time derivation of Lyapunov function (8.11) and noting (8.10), we can yield as:

$$\begin{aligned} \dot{V}_1 &= e_i \dot{e}_i \\ &= -\frac{2\gamma_1}{1+E^{-\mu_1}(|e_i|-\phi)} e_i^2 - \frac{2\gamma_2}{1+E^{\mu_2}(|e_i|-\phi)} |e_i|^{\alpha+1} \\ &< 0 \end{aligned} \quad (8.12)$$

The inequality (8.12) confirms  $e_i = 0$  in finite-time according to Lyapunov criterion.

Once  $|e_i(0)| > \phi$ , the sliding motion includes two phases:

The first phase:  $e_i(0) \rightarrow |e_i| = \phi$ , the first part of Eq. (10) offers the role of providing a rapid convergence speed and the second part plays a secondary role.

$$\begin{aligned} \int_0^{t_1} dt &= \int_{\phi}^{e_i(0)} \frac{1}{\frac{2\gamma_1}{1+E^{-\mu_1}(|e_i|-\phi)} e_i + \frac{2\gamma_2}{1+E^{\mu_2}(|e_i|-\phi)} |e_i|^{\alpha}} d(|e_i|) \\ &< \int_{\phi}^{e_i(0)} \frac{1}{\gamma_1 |e_i|} d(|e_i|) = \frac{\ln(|e_i(0)|) - \ln(\phi)}{\gamma_1} \end{aligned} \quad (8.13)$$

The second phase:  $|e_i| = \phi \rightarrow e_i = 0$ , the second component of Eq. (8.10) offers the role greater than the first one.

$$\begin{aligned} \int_0^{t_2} dt &= \int_0^{\phi} \frac{1}{\frac{2\gamma_1}{1+E^{-\mu_1}(|e_i|-\phi)} e_i + \frac{2\gamma_2}{1+E^{\mu_2}(|e_i|-\phi)} |e_i|^{\alpha}} d(|e_i|) \\ &< \int_0^{\phi} \frac{1}{\gamma_1 |e_i|^{\alpha}} d(|e_i|) = \frac{1}{\gamma_2(1-\alpha)} |\phi|^{1-\alpha} \end{aligned} \quad (8.14)$$

The time total of the sliding motion phase is defined as:

$$\begin{aligned} T_s &= t_1 + t_2 \\ &< \frac{\ln(|e_i(0)|) - \ln(\phi)}{\gamma_1} + \frac{1}{\gamma_2(1-\alpha)} |\phi|^{1-\alpha} \end{aligned} \quad (8.15)$$

The state variable of the dynamic (8.10) converge to sliding manifold ( $\sigma(0) \rightarrow 0$ ) within the defined time  $T_r$ , which was point out in [16]. Therefore, the time total for stability on the sliding manifold is computed as:  $T \leq T_r + T_s$ .

### 8.3.2 Design of NFTSMC

With system (8.6),  $\ddot{e}$  is described as follows:

$$\ddot{e} = q(x)u - H(x) - \Delta - \ddot{x}_r \quad (8.16)$$

Let us take the time derivation of Eq. (8.8):

$$\begin{aligned} \dot{\sigma} = \ddot{e} &+ \frac{2\gamma_1}{1+E^{-\mu_1(|e|-\phi)}}\dot{e} + \frac{2\gamma_1\mu_1\dot{e}\text{sign}(e)E^{-\mu_1(|e|-\phi)}}{(1+E^{-\mu_1(|e|-\phi)})^2}e \\ &+ \frac{2\gamma_2\alpha}{1+E^{\mu_2(|e|-\phi)}}|e|^{\alpha-1}\dot{e} - \frac{2\gamma_2\mu_2\dot{e}E^{\mu_2(|e|-\phi)}}{(1+E^{\mu_2(|e|-\phi)})^2}|e|^\alpha \end{aligned} \quad (8.17)$$

Noting result (8.16), therefore, Eq. (8.17) becomes:

$$\begin{aligned} \dot{\sigma} = q(x)u - H(x) - \Delta - \ddot{x}_r &+ \frac{2\gamma_1}{1+E^{-\mu_1(|e|-\phi)}}\dot{e} \\ &+ \frac{2\gamma_1\mu_1\dot{e}\text{sign}(e)E^{-\mu_1(|e|-\phi)}}{(1+E^{-\mu_1(|e|-\phi)})^2}e \\ &+ \frac{2\gamma_2\alpha}{1+E^{\mu_2(|e|-\phi)}}|e|^{\alpha-1}\dot{e} - \frac{2\gamma_2\mu_2\dot{e}E^{\mu_2(|e|-\phi)}}{(1+E^{\mu_2(|e|-\phi)})^2}|e|^\alpha \end{aligned} \quad (8.18)$$

In order to reach the prescribed tracking performance, the following control method is designed for the robotic system (8.1):

$$u = -q^{-1}(x)(u_n + u_r) \quad (8.19)$$

where the term of the nominal control,  $u_n$ , holds the path of the control errors on the FTSMS (8.8).  $u_n$  is defined as follows:

$$\begin{aligned} u_n = -H(x) - \ddot{x}_r &+ \frac{2\gamma_1}{1+E^{-\mu_1(|e|-\phi)}}\dot{e} \\ &+ \frac{2\gamma_1\mu_1\dot{e}\text{sign}(e)E^{-\mu_1(|e|-\phi)}}{(1+E^{-\mu_1(|e|-\phi)})^2}e \\ &+ \frac{2\gamma_2\alpha}{1+E^{\mu_2(|e|-\phi)}}|e|^{\alpha-1}\dot{e} - \frac{2\gamma_2\mu_2\dot{e}E^{\mu_2(|e|-\phi)}}{(1+E^{\mu_2(|e|-\phi)})^2}|e|^\alpha \end{aligned} \quad (8.20)$$

In order to combat the influences of the lumped anonymous elements on dynamics of the robot manipulator, a reaching control law is proposed according to the following expression:

$$u_r = (\Lambda + \rho) \text{sign}(\sigma) \quad (8.21)$$

where  $\rho$  is a minor positive constant.

**Remark 8.1:** The convergence condition of sliding mode only guarantees that the initial motion point at any position in the state space can approach the sliding surface within a defined time, and there is no limitation on the prescribed pathway of the reaching motion. The reaching law enhances faster convergence time of reaching motion.

### 8.3.3 Stability Analysis of NFTSMC

Applying control input signals (8.19)-(8.21) to Eq. (8.18) gives:

$$\dot{\sigma} = -u_r - \Delta \quad (8.22)$$

To confirm the correctness of the control commands (8.19)-(8.21), the Lyapunov function is defined as:

$$V_2 = 0.5\sigma^T \sigma \quad (8.23)$$

Therefore, the time derivative of Eq. (8.23) is given as:

$$\dot{V}_2 = \sigma^T \dot{\sigma} \quad (8.24)$$

Now, substituting Eq. (8.22) into Eq. (8.24), we can yield the following inequality:

$$\begin{aligned} \dot{V}_2 &= \sigma^T (-u_r - \Delta) \\ &= \sigma^T (-(\Lambda + \rho) \text{sign}(\sigma) - \Delta) \\ &= (-\Lambda |\sigma| - \Delta \sigma) - \rho |\sigma| \\ &\leq -\rho |\sigma| \end{aligned} \quad (8.25)$$

From inequality (8.25), it is apparent that the robotic system of Eq. (8.1) is globally stable under the control law (8.19)-(8.21), and the control errors will approach zero in a short time regardless of disturbances, uncertainties, and faults. However, the main challenge in scheming an FTSMC based on SMC, TSMC, or NFTSMC is serious chattering. To overcome the above challenge, proposed FTSMC for robot manipulators is developed and clearly stated below.

### 8.3.4 Design of DO

The lumped uncertain component can be described according to estimation, as follows:

$$\Delta = \hat{\Delta} + \tilde{\Delta} \quad (8.26)$$

where  $\hat{\Delta}$  is the estimated value of the lumped uncertainty of  $\Delta$ , it is used to compensate the effects of the lumped uncertain term, and  $\tilde{\Delta}$  is the estimated error of disturbances,  $\tilde{\Delta} = [\tilde{\Delta}_1, \dots, \tilde{\Delta}_n]$ , this estimated error is assumed to be bounded by an unknown positive constant,  $\|\tilde{\Delta}_i\| \leq \Pi_i |\sigma_i|^{0.5}; i = 1, \dots, n$  with  $\Pi_i > 0$ .

We design an observer to estimate the lumped uncertain term for the system (8.6) with

time-varying disturbance as:

$$\begin{aligned}\dot{\hat{\Delta}} &= k_1 (\hat{\omega} - \dot{x}_1) \\ \dot{\hat{\omega}} &= q(x)u - H(x) - \hat{\Delta} - k_2 (\hat{\omega} - \dot{x}_1)\end{aligned}\tag{8.27}$$

where  $\hat{\Delta}$  is the estimated value of  $\Delta$ , and  $\hat{\omega}$  is the estimated value of  $x_2$ ,  $k_1 > 0$ ,  $k_2 > 0$ .

### 8.3.5 Stability Analysis of DO

Let us select the Lyapunov function for DO (8.27) as:

$$V_3 = 0.5 \frac{1}{k_1} \tilde{\Delta}^2 + 0.5 \tilde{\omega}^2 \tag{8.28}$$

where  $\tilde{\Delta} = \Delta - \hat{\Delta}$  is the estimated error of disturbances,  $\tilde{\omega} = x_2 - \hat{\omega}$  is the estimated error of the state variable  $x_2$ .

Taking time derivative of Eq. (8.28), we have:

$$\begin{aligned}\dot{V}_3 &= \frac{1}{k_1} \tilde{\Delta} \dot{\tilde{\Delta}} + \tilde{\omega} \dot{\tilde{\omega}} \\ &= \frac{1}{k_1} \tilde{\Delta} (\dot{\Delta} - \dot{\hat{\Delta}}) + \tilde{\omega} (\dot{x}_2 - \dot{\hat{\omega}}) \\ &= \frac{1}{k_1} \tilde{\Delta} \dot{\Delta} - \frac{1}{k_1} \tilde{\Delta} \dot{\hat{\Delta}} + \tilde{\omega} (\dot{x}_2 - \dot{\hat{\omega}})\end{aligned}\tag{8.29}$$

Substituting Eqs. (8.26) and (8.27) into Eq. (8.29) gives:

$$\begin{aligned}\dot{V}_3 &= \frac{1}{k_1} \tilde{\Delta} \dot{\Delta} + \tilde{\Delta} \tilde{\omega} + \tilde{\omega} (-\Delta + \hat{\Delta} + k_2 (\hat{\omega} - \dot{x}_1)) \\ &= \frac{1}{k_1} \tilde{\Delta} \dot{\Delta} - k_2 \tilde{\omega}^2 \leq 0\end{aligned}\tag{8.30}$$

When  $k_1$  is selected as a relative large value, we have  $\frac{1}{k_1} \dot{\Delta} \approx 0$ . Obviously, the lumped uncertainty can be estimated by this DO, and the compensation of the lumped uncertain term will be realized in the designed controller.

### 8.3.6 Design of the proposed FTSM

In this paper, the FTSM is proposed for robot manipulators to achieve high performance with no significant chattering as follow:

$$u = -q^{-1}(x)(u_n + u_r) \tag{8.31}$$

Where, the  $u_n$  is designed based on novel FTSM and DO as follows:

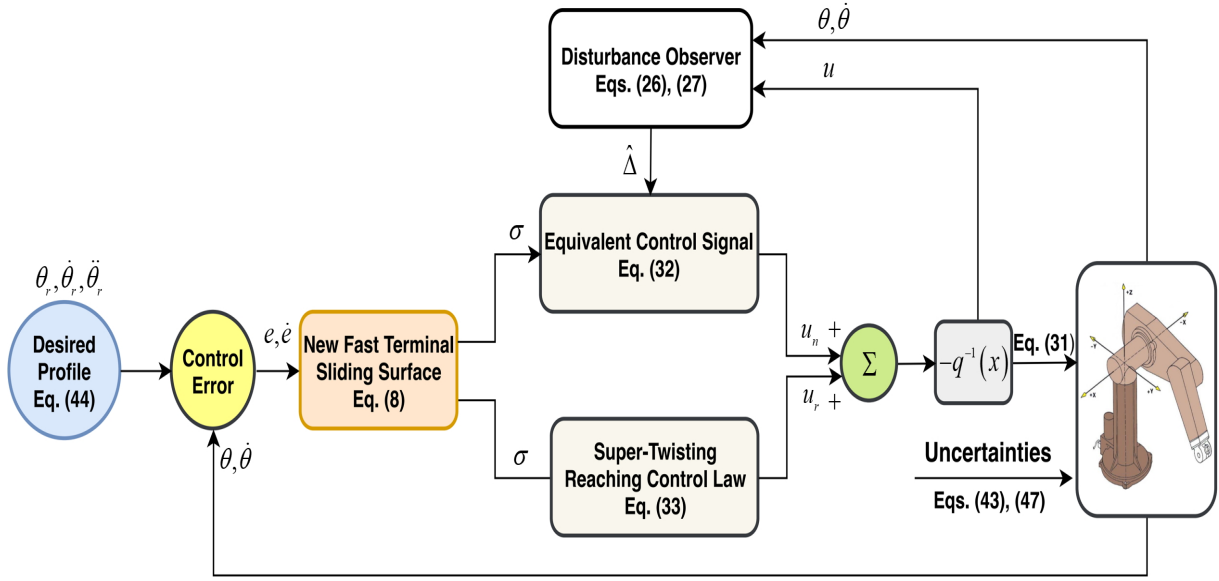


Figure 8.1: Diagram of the proposed FTCM.

$$\begin{aligned}
 u_n = & -H(x) - \hat{\Delta} - \ddot{x}_r + \frac{2\gamma_1}{1+E^{-\mu_1(|e|-\phi)}} \dot{e} \\
 & + \frac{2\gamma_1\mu_1 \dot{e} \text{sign}(e) E^{-\mu_1(|e|-\phi)}}{(1+E^{-\mu_1(|e|-\phi)})^2} e \\
 & + \frac{2\gamma_2\alpha}{1+E^{\mu_2(|e|-\phi)}} |e|^{\alpha-1} \dot{e} - \frac{2\gamma_2\mu_2 \dot{e} E^{\mu_2(|e|-\phi)}}{(1+E^{\mu_2(|e|-\phi)})^2} |e|^\alpha
 \end{aligned} \tag{8.32}$$

and STRCL of  $u_r$  is designed as

$$\begin{aligned}
 u_r &= \Upsilon_1 |\sigma|^{0.5} \text{sign}(\sigma) + \eta \\
 \dot{\eta} &= -\Upsilon_2 \text{sign}(\sigma)
 \end{aligned} \tag{8.33}$$

where  $\Upsilon_1 = \text{diag}(\Upsilon_{11}, \dots, \Upsilon_{1n})$  and  $\Upsilon_2 = \text{diag}(\Upsilon_{21}, \dots, \Upsilon_{2n})$ .  $\Upsilon_{1i}$  and  $\Upsilon_{2i}$  are assigned to satisfy the following relationship [188]:

$$\begin{cases} \Upsilon_{1i} > 2\Pi_i \\ \Upsilon_{2i} > \Upsilon_{1i} \frac{5\Pi_i \Upsilon_{1i} + 4\Pi_i^2}{2(\Upsilon_{1i} - 2\Pi_i)} \end{cases} ; i = 1, 2, \dots, n \tag{8.34}$$

Block Diagram of the designed control system is illustrated in Fig. 8.1.

### 8.3.7 Stability Analysis of The Proposed FTCM

To verify correctness of the proposed system (8.31)-(8.33), the following procedure:

Applying control commands (8.31)-(8.33) to Eq. (8.18) gains:



$$\begin{cases} \dot{\sigma} = \tilde{\Delta} - \Upsilon_1 |\sigma|^{0.5} \text{sign}(\sigma) - K \\ \dot{K} = -\Upsilon_2 \text{sign}(\sigma) \end{cases} \quad (8.35)$$

Now, using one of the elements in Eq. (8.35) as follows:

$$\begin{cases} \dot{\sigma}_i = \tilde{\Delta}_i - \Upsilon_{1i} |\sigma_i|^{0.5} \text{sign}(\sigma_i) - K_i \\ \dot{K}_i = -\Upsilon_{2i} \text{sign}(\sigma_i) \end{cases} \quad (8.36)$$

Let us consider the following Lyapunov function for dynamic (8.36):

$$V_4 = \kappa^T Q \kappa \quad (8.37)$$

Here,  $\kappa = [\sigma_i^{0.5}, \lambda_i]^T$ ,  $Q = \frac{1}{2} \begin{bmatrix} 4\Upsilon_{2i} + \Upsilon_{1i}^2 & -\Upsilon_{1i} \\ -\Upsilon_{1i} & 2 \end{bmatrix}$ . If  $\Upsilon_{2i} > 0$ , so, according to Rayleigh's inequality:

$$\lambda_{\min}(Q) \|\kappa\|^2 \leq V_4 \leq \lambda_{\max}(Q) \|\kappa\|^2 \quad (8.38)$$

with  $\|\kappa\|^2 = |\sigma_i| + \eta_i^2$ .

Taking the time derivation of Eq. (8.37), we can yield:

$$\dot{V}_4 = -\frac{1}{|\sigma_i|^{0.5}} \kappa^T P \kappa + \frac{1}{|\sigma_i|^{0.5}} [\tilde{\Delta}_i, 0] Q \kappa \quad (8.39)$$

with  $P = \frac{\Upsilon_{1i}}{2} \begin{bmatrix} 2\Upsilon_{2i} + \Upsilon_{1i}^2 & -\Upsilon_{1i} \\ -\Upsilon_{1i} & 1 \end{bmatrix}$ .

With Assumption  $\|\tilde{\Delta}_i\| \leq \Pi_i |\sigma_i|^{0.5}; i = 1, \dots, n$ , it can gain:

$$\begin{aligned} \dot{V}_4 &\leq -\frac{1}{|\sigma_i|^{0.5}} \kappa^T \tilde{P} \kappa \\ &\leq -\frac{1}{|\sigma_i|^{0.5}} \lambda_{\min}(\tilde{P}) \|\kappa\|^2 \end{aligned} \quad (8.40)$$

where

$$\tilde{P} = \frac{\Upsilon_{1i}}{2} \begin{bmatrix} \left( 2\Upsilon_{2i} + \Upsilon_{1i}^2 \right) & -(\Upsilon_{1i} + 2\Pi_i) \\ - (4\Upsilon_{2i} + \Upsilon_{1i}) \Pi_i & 1 \end{bmatrix}.$$

We select  $\tilde{P} > 0$ . So,  $\dot{V}_4 < 0$ .

Employing inequality (8.38) obtains:

$$|\sigma_i|^{0.5} \leq \|\kappa\| \quad (8.41)$$

It follows that

$$\dot{V}_4 \leq vV_4^{0.5} \quad (8.42)$$

with  $v = \frac{\lambda_{\min}(\tilde{P})}{\lambda_{\max}^{0.5}(Q)}$ .

Refer to [16],  $\sigma_i = 0$  and  $\dot{\sigma}_i = 0$  in finite-time ( $t_{ri} = 2V_4^{0.5}(t=0)/v$ ). Therefore,  $\sigma = 0$  and  $\dot{\sigma} = 0$  in finite-time ( $T_r = \max_{i=1,\dots,n} \{t_{ri}\}$ ) and  $e_i, \dot{e}_i$  also stabilize to zero in finite-time ( $T \leq T_r + T_s$ ) under the control commands (8.31)-(8.33).

## 8.4 Simulation Results and Discussion

To exhibit the tracking performance of the suggested control method, position tracking computer simulations were performed for a PUMA 560 robot [72]. For convenience in the analysis, in this work, we only consider a robot manipulator with the first three joints (the remainder three joints were locked). The kinematic and dynamic model with the crucial parameters found in a 3-DOF PUMA560 robot manipulator has been previously described in detail [72].

The friction and disturbance term at each joint are modelled as follows:

$$F_r(\theta, \dot{\theta}) + \tau_d = \begin{cases} 1.5 \sin((t-2)\dot{\theta}_1) + 1.2\theta_1^3 \\ 1.3 \sin((t-2)\dot{\theta}_2) + 1.1\theta_2^3 \\ 2.5 \sin((t-2)\dot{\theta}_3) + 1.3\theta_3^3 \end{cases} \quad (8.43)$$

The reference joint paths for the position tracking at each joint are designed according to the following expression:

$$x_r = \begin{bmatrix} 0.5 + \cos\left(\frac{t}{5\pi}\right) - 1 \\ -0.5 + \sin\left(\frac{t}{5\pi} + \frac{\pi}{2}\right) \\ 0.5 + \sin\left(\frac{t}{5\pi} + \frac{\pi}{2}\right) - 1 \end{bmatrix} \quad (8.44)$$

The initial position trajectories for the robotic system were indicated as  $\theta_1(0) = 0$ ,  $\theta_2(0) = 0$ ,  $\theta_3(0) = 0$ ,  $\dot{\theta}_1(0) = 0$ ,  $\dot{\theta}_2(0) = 0$ , and  $\dot{\theta}_3(0) = 0$ .

MATLAB/Simulink software was used to perform all simulations with a fixed-step size of  $10^{-3}s$ .

In order to exhibit the improvements in the tracking performance gained by using the suggested control algorithm, its reference path performances were compared with other control algorithms, including the normal SMC [15] and NFTSMC [37, 47, 48]. The details of SMC and NFTSMC design are briefly described as follow:

The normal SMC [15] has the following control torque:

Table 8.1: Control parameter selection of control algorithms

Control Algorithm	Control Parameters	Control Parameter Values
SMC	$c, \xi, \Sigma$	2, 0.01, 20
NFTSMC	$l, q, \varpi, \xi, \Sigma$	5, 3, 2, 0.01, 20
Proposed Control Algorithm-DO	$\gamma_1, \gamma_2, \mu_1, \mu_2$	2.0, 2.0, 1.2, 1.4
	$\phi, \alpha, \Upsilon_1, \Upsilon_2$	1, 0.6, 16, 20
	$k_1, k_2$	20000, 200

Table 8.2: The average control errors are provided by control systems

	$E_1$	$E_2$	$E_3$
SMC	0.008021	0.007490	0.154244
NFTSMC	0.019966	0.005121	0.004845
Proposed Controller	0.002819	0.002807	0.002785

$$u = -q^{-1}(x) \begin{bmatrix} H(x) + c(x_2 - \dot{x}_r) - \ddot{x}_r \\ + (\Sigma + \xi) \text{sign}(\sigma) \end{bmatrix} \quad (8.45)$$

where  $\sigma = \dot{e} + ce$  is the linear sliding manifold,  $c$  is a positive constant.

Further, the NFTSMC [37] has the following control torque:

$$u = -q^{-1}(x) \begin{bmatrix} H(x) + \varpi \frac{q}{l} \dot{e}^{2-\frac{l}{q}} - \ddot{x}_r \\ + (\Sigma + \xi) \text{sign}(\sigma) \end{bmatrix} \quad (8.46)$$

where  $\sigma = e + \varpi^{-1} \dot{e}^{\frac{l}{q}}$  is a nonlinear sliding manifold.

The control parameters that were selected for use in the algorithms are depicted in Table 8.1. The performance simulations were carried out in cases of both normal and fault operations to compare the controllers under expressions of positional accuracy, transient response, steady-state error, and the resulting chattering phenomenon in their control inputs. For situation 1, the system was controlled in normal operating condition with the assumed disturbances and uncertainties. For situation 2, the system was controlled in fault operating conditions with the assumed disturbances, uncertainties, and faults.

In Situation 1 at times where  $0s < t < 10s$ , we first consider the robot working in normal operation. The effectiveness of DO is analyzed. The target of DO in this condition is to precisely approximate the assumed value of disturbances and uncertainties. The

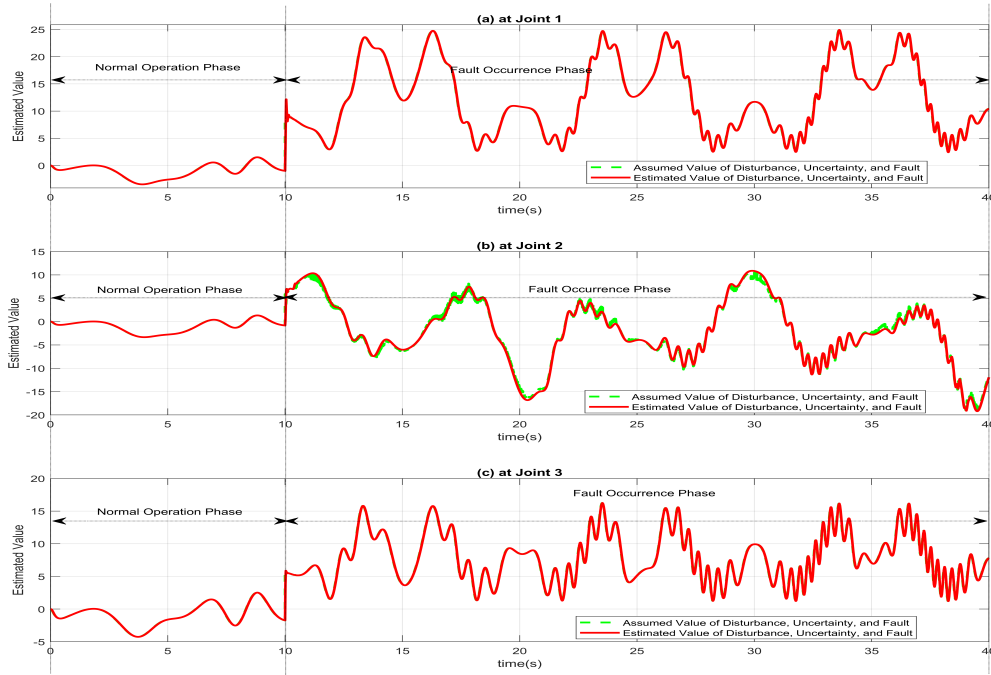


Figure 8.2: Assumed and estimated value of disturbance, uncertainty, and fault: (a) at the first Joint, (b) at the second Joint, and (c) at the third Joint.

time history of the assumed disturbances and uncertainties, and the outputs of DO are illustrated in Fig. 8.2. From Fig. 8.2, it is seen that DO has estimated the assumed value of disturbances and uncertainties with high precision, thus, DO provides exact information for the control loop in this phase. The tracking positions, positional control errors, and velocity control errors of the three joints for all three of the tested control algorithms are shown in Figs. 8.3, 8.4, and 8.5, respectively. Table 8.2 states the average control errors which are provided by SMC, NFTSMC, and proposed controller. From the simulation results in Figs. 8.3, 8.4, and 8.5, we observed that each control algorithm offered good tracking performance when the assumed disturbances and uncertainties were applied to the robotic dynamic system. SMC, NFTSMC, and proposed controller are based on the SMC to design a control approach. Therefore, those controllers preserve the robust ability of SMC in mitigating disturbances and uncertainties, as well as the ability to obtain high position tracking accuracy. It is noteworthy that the controller suggested in this study has the best performance compared to the other tested control algorithms because it preserves the low steady-state error and the fast-transient response properties of the NFTSMC, exact information from DO, and STRCL. The reader can see the results reported in Table 8.2.

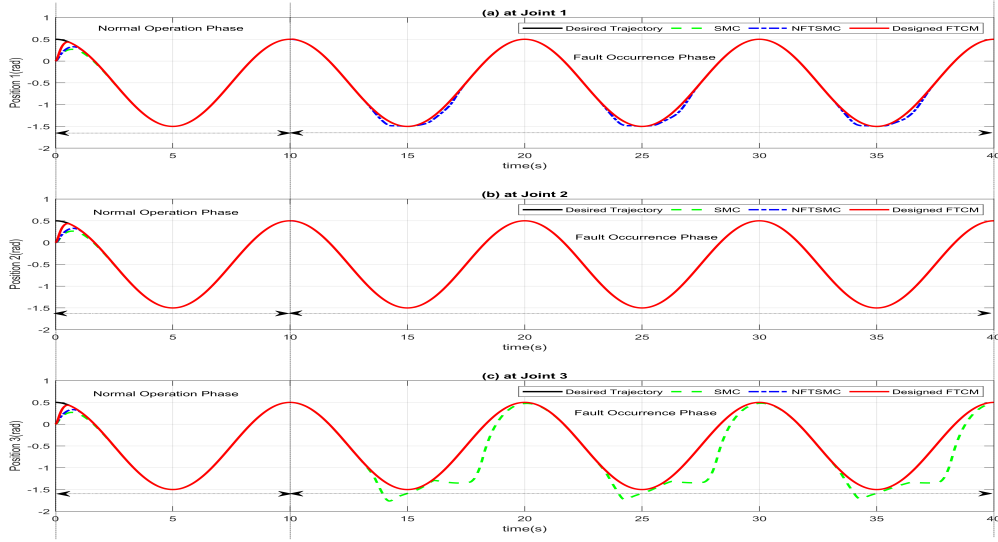


Figure 8.3: Tracking positions are provided by SMC, NFTSMC, and proposed controller: (a) at the first Joint, (b) at the second Joint, and (c) at the third Joint.

$$\omega(\theta, \dot{\theta}, \tau) = \begin{bmatrix} \begin{pmatrix} 25 \sin(\theta_1 \theta_2) + 1.5 \cos(\dot{\theta}_1 \theta_2) \\ +2.5 \cos(\dot{\theta}_1 \dot{\theta}_2) \end{pmatrix} \\ 0.3 \sin(t) u_2 \\ \begin{pmatrix} 15 \sin(\theta_3 \theta_1) + 1.2 \cos(\dot{\theta}_2 \theta_2) \\ +2.5 \cos(\dot{\theta}_2 \dot{\theta}_3) \end{pmatrix} \end{bmatrix} \quad (8.47)$$

$$T_f \geq 10s$$

From Eq. (8.47), an abrupt fault,  $25 \sin(\theta_1 \theta_2) + 1.5 \cos(\dot{\theta}_1 \theta_2) + 2.5 \cos(\dot{\theta}_1 \dot{\theta}_2)$ , was assumed to appear in the first joint at times where  $t \geq 10s$ , the effectiveness of the control input at the second joint was assumed to be damaged by  $0.3 \sin(t) u_2$  once the time reached  $t \geq 10s$ , and an abrupt fault,  $25 \sin(\theta_1 \theta_2) + 1.5 \cos(\dot{\theta}_1 \theta_2) + 2.5 \cos(\dot{\theta}_1 \dot{\theta}_2)$ , was assumed to appear in the third joint at times where  $t \geq 10s$ , during the simulation. The effectiveness of DO is also investigated. The goal of DO in the second phase is to precisely approximate the assumed disturbances, uncertainties, faults. From Fig. 8.2, it is observed that DO also has the ability to estimate the assumed value of disturbances, uncertainties, and faults with high accuracy, thus, DO exactly provides information of these lumped uncertain components for designed control loop in fault occurrence phase.

From Figs. 8.3, 8.4, 8.5, and Table 8.2, we observed that SMC offers the poorest path tracking performance, where the operation of the robotic manipulator becomes unstable,

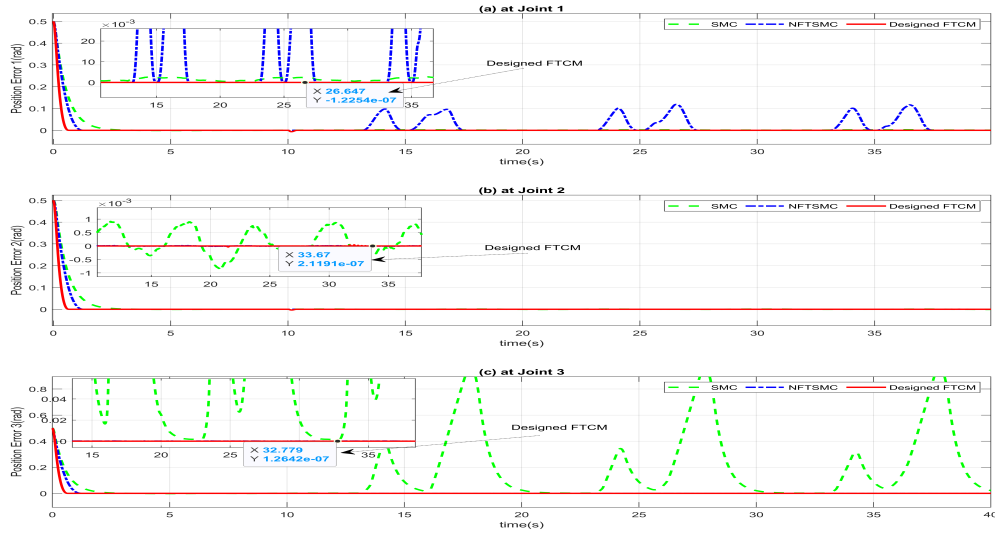


Figure 8.4: Positional control errors are provided by SMC, NFTSMC, and proposed controller: (a) at the first Joint, (b) at the second Joint, and (c) at the third Joint.

especially, at the third joint, during the presence of a fault. Although SMC gives good tracking performance for the robotic system in cases of disturbances and uncertainties, once faults appear, the system loses stability instantaneously. NFTSMC has better tracking performance than SMC, but its accuracy is low, especially, at the first joint. While the proposed control algorithm provides a faster transient response and smaller trajectory tracking error compared to SMC and NFTSMC. The proposed control algorithm offered the best performance with respect to tracking errors among the compared control algorithms because of the combination of NFTSMC, DO, and STRCL.

Throughout the simulation process in both situations, the proposed control scheme improves the tracking position accuracy at the three joints, respectively in comparison with SMC, as follows: the first joint (64.85%), the second joint (62.52%), and third joint (98.11%). And. the proposed scheme also enhances the tracking position precision at the three joints, respectively in comparison with NFTSMC, as follows: the first joint (85.88%), the second joint (45.18%), and third joint (42.51%).

The control input signals of the controllers, including SMC, NFTSMC, and suggested control methodology, are depicted in Fig. 8.7. The results in Fig. 8.7 indicates that suggested control methodology seems to offer a continuous control signal with minor chattering. Because disturbances, uncertainties, faults were estimated by DO. Moreover, the remaining of the estimated errors also were handled by STRCL. While SMC and NFTSMC offer discontinuous control efforts when both methods applied a large gain in

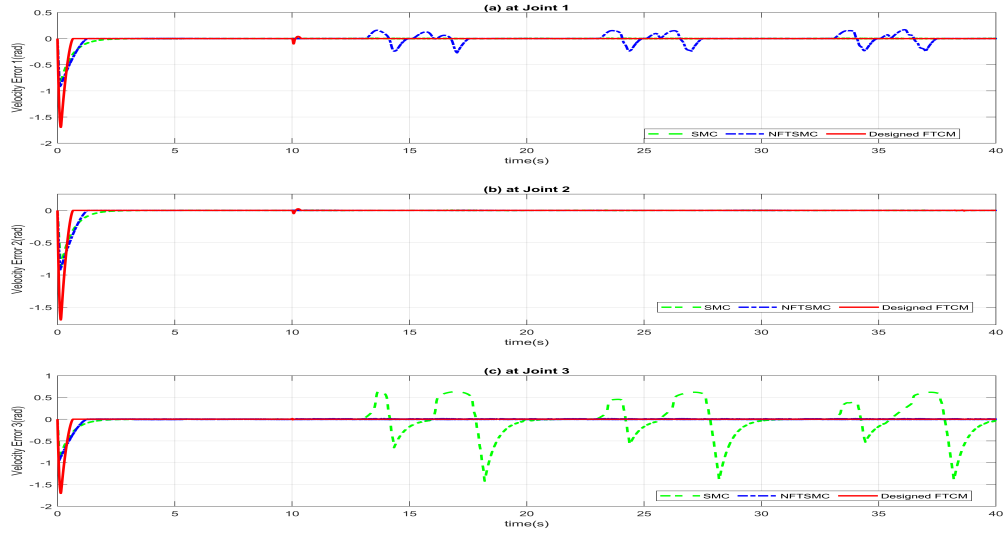


Figure 8.5: Velocity control errors are provided by SMC, NFTSMC, and proposed controller: (a) at the first Joint, (b) at the second Joint, and (c) at the third Joint.

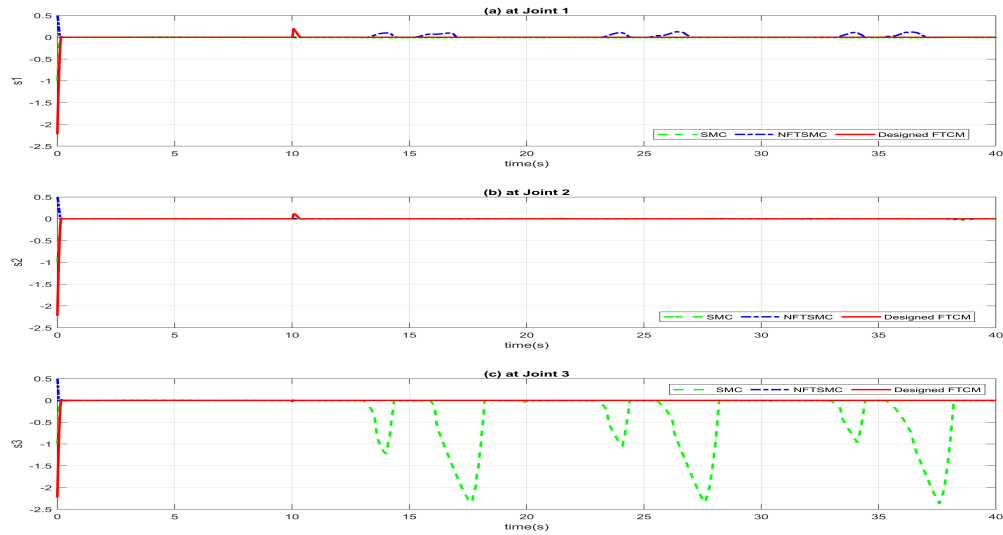


Figure 8.6: Response time of the sliding mode manifolds: (a) at the first Joint, (b) at the second Joint, and (c) at the third Joint.

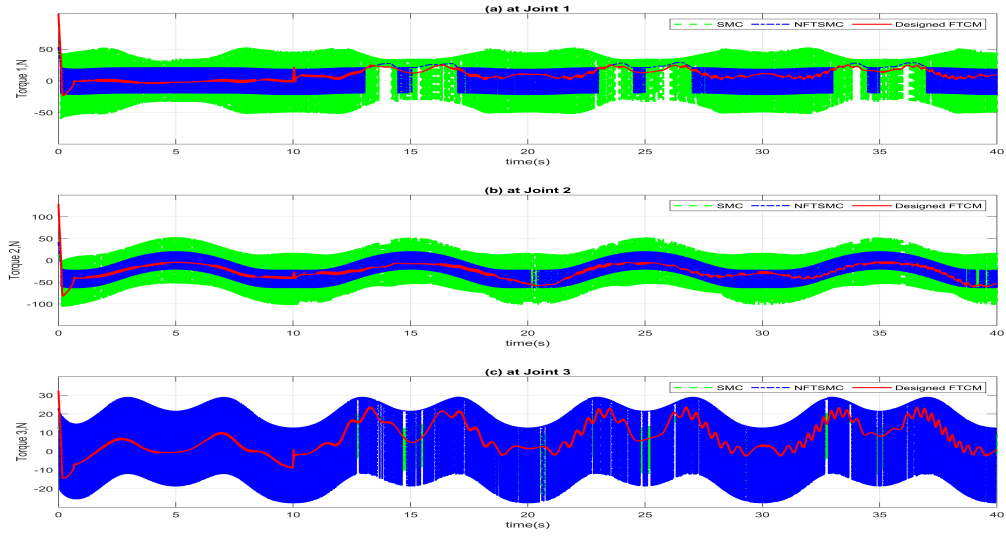


Figure 8.7: Control input signals are provided by SMC, NFTSMC, and proposed controller: (a) at the first Joint, (b) at the second Joint, and (c) at the third Joint.

high-frequency control to combat the effects of those lumped uncertain components.

From trajectory tracking performance and its performance comparison, we observed that suggested control algorithm offers the best performance compared to the other control methods, including SMC and NFTSMC, under expressions of the pathway tracking precision, speedy transient response, small steady state error, and chattering removal.

**Remark 8.2:** The parameters for SMC, NFTSMC, and proposed sliding surface were experimentally selected and based on their convergence properties. For example,  $\gamma_1, \gamma_2, \mu_1, \mu_2$  are the positive constants,  $0 < \alpha < 1$ , and  $\phi = \left(\frac{\gamma_2}{\gamma_1}\right)^{\frac{1}{1-\alpha}}$ . The parameters for the proposed control input with DO and STRCL were experimentally chosen to make system stable, to obtain the desired performance with a fast convergence time, and to satisfy the conditions, which were mentioned in the study and have been explained in greater detail by previous researchers [48, 70, 85]. The parameters of the controllers, including SMC and NFTSMC were chosen to guarantee stability and obtain the good performance (refer to SMC [15], and NFTSMC [47, 48]).

**Remark 8.3:** In this work, we only simulated abrupt faults, as their influences are larger than incipient faults in a robotic system. Therefore, since the suggested control scheme can effectively manage abrupt faults entirely, it is also able to resolve the influences from incipient faults.

**Remark 8.4:** In order to confirm the effectiveness of the suggested control system from a technical viewpoint, it would be more convincing to demonstrate experimental results



on real systems. Nonetheless, experimenting with various fault types in a real system is difficult and presents dangerous challenges and possible damage to the robotic system. Accordingly, in literature related to fault-tolerant control systems, almost every strategy, including this report, has adopted simulation performance to prove the usefulness of controllers [133, 134, 189]. However, verifying the effectiveness of the suggested control methodology in experimental patterns by implementing suitable methods without destroying a robotic system is an important goal and will be considered in future study. The parameters of the robotic system are given in Table 8.1.

**Remark 8.5:** It should be noted that the control parameters are chosen by performing repetitive testing and control error checking. In this condition how to choose these parameters is a remarkable issue. Future research is to select the optimal control parameters by applying optimization algorithms.

## 8.5 Conclusion

In this chapter, a novel FTTCM is developed for robot manipulators. According to theoretical proof, simulation performance, and a comparison with both SMC and NFTSMC, the proposed control strategy has some contributions, as follows: (1) the proposed strategy is easy in implementation, which provides finite-time convergence, and faster transient performance without singularity obstacle in controlling; (2) the proposed strategy inherits the advantages of the NFTSMC, STRCL, and estimation ability of DO in the features of robustness towards the existing uncertainties; (3) a new FTSMC was introduced, and evidence of finite-time convergence was sufficiently confirmed; (4) the accuracy of the proposed strategy was further enhanced in the trajectory tracking control; (5) the proposed strategy displayed the smoother control torque actions with lesser oscillation.

# Chapter 9

## Conclusions and Future Works

### 9.1 Conclusions

The study reported in this thesis develops TSMCs for uncertain nonlinear systems and their applications to robotic manipulators that plays a very critical role in modern control technology. The central motivation of this thesis is to significantly improve trajectory tracking precision and to overcome the limitations of SMC-based methods and TSMC-based methods for several classes of uncertain nonlinear systems in presence of external disturbances and uncertain dynamics, or even undesired faults. These proposed control methodologies are developed based on SMC, SC, TSMC, NFTSMC, FLS, STA, NNs, observer-based controllers, and AC. The fundamental theoretical procedure is the foundation of the asymptotic stability based Lyapunov theory underpinned by the Lipschitz condition in the ordinary differential equations and finite time control method. The main applications of the proposed control methodologies are to apply to uncertain mechanical systems and robotic systems, in which external disturbances and uncertain dynamics are required to be bounded and to satisfy the suitable condition.

The proposed control algorithms are designed to achieve the following major advantages such as simple design, fast transient response, defined time convergence, robustness against uncertainties, high tracking accuracy, and stabilization with small steady-state errors. These proposed control algorithms can reject some/all of the limitations in conventional SMC or TSMC such as reaching phase glitch and the singularity problem. They can also avoid/ eliminate/ attenuate the effects of chattering behavior and the requirement for prior information about the upper bound of external disturbances and uncertain dynamics as well as the necessity for an exact mathematical model. Especially, some the designed controllers have estimate ability and fault tolerance.

The proposed control algorithms were applied for trajectory tracking control and FTC of parallel and serial robotic manipulators, or synchronization problem in motion control-

ling. The computer numerical simulation and experiment results are performed for 2-DOF planar parallel manipulator, 3-DOF planar parallel manipulator, 2-DOF serial robotic manipulator, and 3-DOF Puma560 robot manipulator to demonstrate the effectiveness and applicability of the proposed systems and to validate the theoretical derivation. Moreover, the designed control methodologies can be extended their applications to uncertain high-order MIMO systems.

Chapter 2 developed a chattering-free, adaptive, robust tracking control algorithm for a class of second-order nonlinear systems. In our algorithm, a novel sliding function, termed as a PID-NFTSM function, is proposed to incorporate the good features of both the PID and the NFTSM approaches. Our proposed sliding function inherits some approaches in the field such as PID, NTSMC, and FTSMC to achieve non-singularity, fast response, defined time convergence, and stability with small steady-state error. To obtain a chattering-free behavior, a continuous method (with an integral of a switching term and adaptive updating law) have been applied to compensate for all of the anonymous uncertain components in the control system, such as disturbances, unmodeled dynamics, nonlinearities, and unmeasurable noise. Accordingly, the suggested method does not need prior information about the bound values of those anonymous components, along with chattering-free behavior, compared to other controllers. The experimental results for a PUMA560 robot manipulator confirm that the suggested methodology has more capability to adapt to many uncertain nonlinear systems with high accuracy.

Chapter 3 developed the design of the control system for the class of general nonlinear second-order systems. The suggested system has the following major advantages: 1) it receives the advantages of both RBFNN and IFOSMC, including good performance with minimum position errors, robustness against uncertainties, and work with a precise dynamic model; 2) it consists of a control input system with chattering reduction; 3) ARBFNN-IFOSMC provides better performance and stronger resistance against disturbances and uncertainties compared to RBFNN-SMC and RBFNN-TSMC; and 4) stability and tracking error convergence of the class of general nonlinear second-order systems was fully confirmed by the Lyapunov benchmark.

Chapter 4 presented an adaptive continuous finite-time TSMC algorithm for robot manipulators. From the simulation and performance comparison with two other control methods for a 3-DOF PUMA560 robot, the suggested control method shows the best performance among the three controllers in terms of tracking positional accuracy, small steady state error, fast response speed, and weak chattering behavior. We think that the proposed control algorithm has the following important characteristics: 1) the NTSM surface allows finite-time convergence without singularity, 2) requires no prior information of the upper limits of uncertainties, 3) shows tremendously less chattering behavior, and

4) the magnitude of the generated control input seems to be more suitable in terms of motor torque saturation compared with those of the other control methods.

Chapter 5 developed a new trajectory tracking control solution for robot manipulators. Based on numerical simulation results and a performance comparison with two other control schemes for a 3-DOF PUMA560 robot manipulator, our control scheme shows the best performance in terms of tracking positional precision, small steady-state errors, fast response rate, and small chattering behavior. The suggested control solution has the following valuable benefits. 1) It uses new NFTSM variables, which offer a fast transient response rate and finite-time convergence with no singularity drawback. 2) It requires no essential information regarding the upper limits of the perturbations and uncertainties. 3) The upper limit of the convergence time can be set beforehand. 4) It demonstrates impressively small chattering behavior. 5) The robustness and the finite-time convergence of the system have been guaranteed fully by the Lyapunov stability criterion.

Chapter 6 developed a robust trajectory tracking control strategy for robot manipulators. From the simulation results and performance comparison with two other control strategies for a 3-DOF PUMA560 robot manipulator, our control strategy offered the best performance in terms of tracking positional accuracy, small steady-state errors, fast convergence, and chattering phenomenon rejection. The suggested control solution has the following benefits: (1) inherits the advantages of the NFTSMC, including non-singularity, finite-time convergence, fast transient response, low steady-state errors, and high position tracking accuracy; (2) achieves smoothness with elimination of chattering behavior; (3) does not demand an exact dynamic model for the robot manipulator by applying an adaptive radial basis function neural network to approximate an unknown robot function; (4) compared to the classical SMC and another control methods based on TSMC, the proposed control strategy offers better tracking performance and stronger resistance against disturbances and uncertainties; (5) robustness and stability of the robot system was demonstrated fully by Lyapunov theory.

Chapter 7 proposed NINFTSSMC for 3-DOF parallel robotic manipulators with uncertain dynamics using synchronous nonlinear sliding surface, where this sliding surface is formed based on the integration of SC and INFTSMC. Accordingly, position errors and synchronization errors quickly converge to the SINFTSM surface at the same time. Next, the FNN is applied to estimate uncertain dynamics, in which the novelty of the proposed approach compared to a classic FNN is that the proposed NN utilizes the NFTSM error filter replacing for a classic error filter. Finally, the control approach was designed for the robotic system to achieve the performance described in this paper, such as rapid error convergence, robustness with uncertain dynamics, minimum chattering, synchronization, and high precision. The stability of the control loop has been secured according to the Lya-

punov criteria. The powerful properties and effectiveness of the proposed NINFTSSMC were confirmed by computer simulations and performance comparisons for a 3-DOF parallel robotic manipulator. Through control performance comparison, it is concluded that the NINFTSSMC is extremely efficient for trajectory tracking control of uncertain 3-DOF parallel robotic manipulators.

Chapter 8 focused on the analysis and design of a novel FTSM for robot manipulators. According to theoretical proof, simulation performance, and a comparison with both SMC and NFTSMC, the proposed control strategy has some contributions, as follows: (1) the proposed strategy is easy in implementation, which provides finite-time convergence, and faster transient performance without singularity obstacle in controlling; (2) the proposed strategy inherits the advantages of the NFTSMC, STRCL, and estimation ability of DO in the features of robustness towards the existing uncertainties; (3) a new FTSM was introduced, and evidence of finite-time convergence was sufficiently confirmed; (4) the accuracy of the proposed strategy was further enhanced in the trajectory tracking control; (5) the proposed strategy displayed the smoother control torque actions with lesser oscillation.

From design procedure of the control theory and obtained results, the proposed control method stated in chapter 8 seems to be the best controller among my proposed control methods due to some advantages as follows.

- An improved non-singular fast terminal sliding surface with the dynamic coefficients is proposed, which can make the system states arrive at a stable point with a fast convergence rate.
- The dynamic coefficients can adapt according to the change of the control errors. The proposed controller not only handles disturbances and uncertainties but also overcomes the effects of faults occurring in the robot.
- The control design is more suitable for real applications due to its simplicity when a disturbance observer is applied to approximate the lumped uncertain terms instead of using a compensator like a neural network or fuzzy logic system.
- Also provides high tracking performance with a smooth control input.
- According to my opinion, each controller in the thesis is suitable for specific applications. The proposed controllers are also suitable for each development stage of TSMC theory.

## 9.2 Future works

The advanced control methods or FTC are very important for the application of the robotic system. This thesis has developed some valuable tracking control schemes to improve control performance and the capacity of condition monitoring for the robot system. However, the proposed control schemes in this thesis are almost model-based. Therefore, the control performance depends on the exact mathematical models of the robot system. Moreover, due to the system complexities and fault diagnosis observer scheme, the diagnosis of robotic faults have still to face a number of practical challenges in designing such system such as: early detection and diagnosis, real time fault diagnosis or multiple fault accommodation. Thus, fault diagnosis, FTC, and the advanced control schemes for robotic system still attracts many researchers. Some possible future studies are listed as follows.

- Applying all proposed controllers to real systems such as magnetic levitation systems, inverted pendulum, or robotic manipulators.
- TSMC method for fault-tolerant tracking control of magnetic levitation systems.
- Almost the methods developed in this thesis are based on the assumption that the output measurement is accurate and no-fault occurs in sensors. However, sensor faults sometimes exist in real systems. Thus, the effective fault diagnosis methods for sensor faults should be carefully studied in future work.
- In this thesis, most of the developed controls are based on the passive method. Although the passive method usually provides faster response and convergence compared to the active method, it provides lower tracking accuracy. Hence, to enhance both the tracking accuracy and system response, a combining scheme that takes the benefits of both active and passive methods should be studied.
- Developing some control algorithms that apply reinforcement learning or intelligent controls to eliminate dependence on the accuracy of mathematical models and assumptions.



# Publications

## SCI (E) Journals

1. Vo, A. T., & Kang, H. J. (2018). An adaptive neural non-singular fast-terminal sliding-mode control for industrial robotic manipulators. *Applied Sciences*, 8(12), 2562.
2. Vo, A. T., & Kang, H. J. (2019). An Adaptive Terminal Sliding Mode Control for Robot Manipulators With Non-Singular Terminal Sliding Surface Variables. *IEEE Access*, 7, 8701-8712.
3. Tuan, V. A., & Kang, H. J. (2019). A New Finite Time Control Solution for Robotic Manipulators Based on Nonsingular Fast Terminal Sliding Variables and the Adaptive Super-Twisting Scheme. *Journal of Computational and Nonlinear Dynamics*, 14(3), 031002.
4. Vo, A. T., & Kang, H. J. (2019). Adaptive Neural Integral Full-Order Terminal Sliding Mode Control for an Uncertain Nonlinear System. *IEEE Access*, 7, 42238-42246.
5. Vo, A. T., & Kang, H. J. (2019). A Chattering-Free, Adaptive, Robust Tracking Control Scheme for Nonlinear Systems With Uncertain Dynamics. *IEEE Access*, 7, 10457-10466.
6. Doan, Q. V., Vo, A. T., Le, T. D., Kang, H. J., & Nguyen, N. H. A. (2020). A Novel Fast Terminal Sliding Mode Tracking Control Methodology for Robot Manipulators. *Applied Sciences*, 10(9), 3010.
7. Nguyen, V. C., Vo, A. T., & Kang, H. J. (2020). A Non-singular Fast Terminal Sliding Mode Control Based on Third-Order Sliding Mode Observer for a Class of Second-Order Uncertain Nonlinear Systems and Its Application to Robot Manipulators. *IEEE Access*.



8. Vo, A. T., & Kang, H. J. (2020). Neural Integral Non-Singular Fast Terminal Synchronous Sliding Mode Control for Uncertain 3-DOF Parallel Robotic Manipulators. *IEEE Access*, 8, 65383-65394.
9. A. T. Vo and H. Kang, "A Novel Fault-Tolerant Control Method for Robot Manipulators Based on Non-Singular Fast Terminal Sliding Mode Control and Disturbance Observer," in *IEEE Access*, vol. 8, pp. 109388-109400, 2020, doi: 10.1109/ACCESS.2020.3001391.
10. T. N. Truong, A. T. Vo and H. -J. Kang, "Implementation of an Adaptive Neural Terminal Sliding Mode for Tracking Control of Magnetic Levitation Systems," in *IEEE Access*, doi: 10.1109/ACCESS.2020.3036010.

## International Conference

1. Vo, A. T., Kang, H. J. & Tien Dung Le. (2017, June). Adaptive Tracking Control of Robot Manipulators Using Neural Network for Friction and Uncertainties Compensation. In 2017 12th International Forum on Strategic Technology (IFOST) (pp. 25-29).
2. Vo, A. T., Kang, H. J., & Nguyen, V. C. (2017, July). An output feedback tracking control based on neural sliding mode and high order sliding mode observer. In 2017 10th International Conference on Human System Interactions (HSI) (pp. 161-165). IEEE.
3. Vo, A. T., Kang, H. J., & Tien Dung Le. (2017, October). Novel Quasi-Continuous Nonsingular Terminal Sliding Mode Controller for Output Feedback Tracking Control of Robot Manipulators. In 2017 21st International Conference on Mechatronics Technology (ICMT) (pp. 50-55).
4. Nguyen, V. C., Vo, A. T., & Kang, H. J. (2017, October). A Fault Tolerant Control for Robot Manipulators Using a Neural Network Observer and a Third-Order Sliding Mode Observer. In 2017 21st International Conference on Mechatronics Technology (ICMT) (pp. 56-61).
5. Vo, A. T., Kang, H. J., & Le, T. D. (2018, August). An adaptive fuzzy terminal sliding mode control methodology for uncertain nonlinear second-order systems. In *International Conference on Intelligent Computing* (pp. 123-135). Springer, Cham.

6. Vo, A. T., Kang, H. J. & Nguyen Ngoc Hoai An (2018, October). A Robust Tracking Control Method for Uncertain Nonlinear Systems with Chattering-free Terminal Sliding Mode Control. In 2018 22st International Conference on Mechatronics Technology (ICMT) (pp. 30).
7. Vo, A. T., Kang, H. J., & Le, T. D. (2019, August). Full-Order Sliding Mode Control Algorithm for Robot Manipulators Using an Adaptive Radial Basis Function Neural Network. In International Conference on Intelligent Computing (pp. 155-166). Springer, Cham.
8. Nguyen, V. C., Vo, A. T., & Kang, H. J. (2019, August). Continuous PID Sliding Mode Control Based on Neural Third Order Sliding Mode Observer for Robotic Manipulators. In International Conference on Intelligent Computing (pp. 167-178). Springer, Cham.
9. Vo, A. T., Kang, H. J., & Le, T. D. (2019, September). An Adaptive Integral Sliding Mode Tracking Control for Robotic Manipulators. In Proceedings of the 2019 3rd International Symposium on Computer Science and Intelligent Control (pp. 1-6).
10. Vo, A. T., Kang, H. J., & Truong, T. N. (2020, October). A Fast Terminal Sliding Mode Control Strategy for Trajectory Tracking Control of Robotic Manipulators. In International Conference on Intelligent Computing (pp. 177-189). Springer, Cham.
11. Truong, T. N., Kang, H. J., & Vo, A. T. (2020, October). An Active Disturbance Rejection Control Method for Robot Manipulators. In International Conference on Intelligent Computing (pp. 190-201). Springer, Cham.



# Bibliography

- [1] Jean-Jacques E Slotine, Weiping Li, and Others, *Applied nonlinear control*, vol. 199, Prentice hall Englewood Cliffs, NJ, 1991.
- [2] Alberto Isidori, *Nonlinear control systems: an introduction*, Springer Science & Business Media, 2013.
- [3] Hassan K Khalil, “Nonlinear systems”, *Upper Saddle River*, 2002.
- [4] Yuxin Su, Peter C Müller, and Chunhong Zheng, “Global Asymptotic Saturated PID Control for Robot Manipulators”, *IEEE Transactions on Control Systems Technology*, vol. 18, no. 6, pp. 1280–1288, 2010.
- [5] Wen Yu and Jacob Rosen, “Neural PID control of robot manipulators with application to an upper limb exoskeleton”, *IEEE Transactions on cybernetics*, vol. 43, no. 2, pp. 673–684, 2013.
- [6] Tien Dung Le, Hee-Jun Kang, Young-Soo Suh, and Young-Shick Ro, “An online self-gain tuning method using neural networks for nonlinear PD computed torque controller of a 2-dof parallel manipulator”, *Neurocomputing*, vol. 116, pp. 53–61, 2013.
- [7] Weiwei Shang and Shuang Cong, “Nonlinear computed torque control for a high-speed planar parallel manipulator”, *Mechatronics*, vol. 19, no. 6, pp. 987–992, 2009.
- [8] Anh Tuan Vo and Hee-Jun Kang, “An Adaptive Neural Non-Singular Fast-Terminal Sliding-Mode Control for Industrial Robotic Manipulators”, *Applied Sciences*, vol. 8, no. 12, pp. 2562, 2018.
- [9] Abdelhamid Tayebi, S Abdul, M B Zaremba, and Y Ye, “Robust iterative learning control design: application to a robot manipulator”, *IEEE/ASME Transactions on mechatronics*, vol. 13, no. 5, pp. 608–613, 2008.
- [10] M. Wang and A. Yang, “Dynamic Learning from Adaptive Neural Control of Robot Manipulators with Prescribed Performance”, *IEEE Transactions on Systems, Man, and Cybernetics: Systems*, vol. 47, no. 8, pp. 2244–2255, 2017.

- [11] Jing Zhou, Changyun Wen, and Ying Zhang, “Adaptive backstepping control of a class of uncertain nonlinear systems with unknown backlash-like hysteresis”, *IEEE transactions on Automatic Control*, vol. 49, no. 10, pp. 1751–1759, 2004.
- [12] Farhad Aghili, “Adaptive control of manipulators forming closed kinematic chain with inaccurate kinematic model”, *IEEE/ASME Transactions on Mechatronics*, vol. 18, no. 5, pp. 1544–1554, 2013.
- [13] Weiwei Shang, Shuang Cong, Yaoxin Zhang, and Yanyang Liang, “Active joint synchronization control for a 2-DOF redundantly actuated parallel manipulator”, *IEEE Transactions on Control Systems Technology*, vol. 17, no. 2, pp. 416–423, 2009.
- [14] Yuxin Su, Dong Sun, Lu Ren, and James K Mills, “Integration of saturated PI synchronous control and PD feedback for control of parallel manipulators”, *IEEE Transactions on Robotics*, vol. 22, no. 1, pp. 202–207, 2006.
- [15] Christopher Edwards and Sarah Spurgeon, *Sliding mode control: theory and applications*, Crc Press, 1998.
- [16] Vadim I Utkin, *Sliding modes in control and optimization*, Springer Science & Business Media, 2013.
- [17] Antonella Ferrara and Gian Paolo Incremona, “Design of an integral suboptimal second-order sliding mode controller for the robust motion control of robot manipulators”, *IEEE Transactions on Control Systems Technology*, vol. 23, no. 6, pp. 2316–2325, 2015.
- [18] Asif Sabanovic, “Variable structure systems with sliding modes in motion control—A survey”, *IEEE Transactions on Industrial Informatics*, vol. 7, no. 2, pp. 212–223, 2011.
- [19] Alessandro Pisano and Elio Usai, “Sliding mode control: A survey with applications in math”, *Mathematics and Computers in Simulation*, vol. 81, no. 5, pp. 954–979, 2011.
- [20] John Y Hung, Weibing Gao, and James C Hung, “Variable structure control: A survey”, *IEEE transactions on industrial electronics*, vol. 40, no. 1, pp. 2–22, 1993.
- [21] V Utkin and J Y Gulder, “Shi j.,“, *Sliding Mode Control in Electromechanical Systems*, Teylor & Francis, 1999.

- [22] Elbrous M Jafarov and Ramazan Tasaltin, “Robust sliding-mode control for the uncertain MIMO aircraft model F-18”, *IEEE Transactions on Aerospace and Electronic Systems*, vol. 36, no. 4, pp. 1127–1141, 2000.
- [23] Abdelaziz Benallegue, Abdellah Mokhtari, and Leonid Fridman, “High-order sliding-mode observer for a quadrotor UAV”, *International Journal of Robust and Nonlinear Control: IFAC-Affiliated Journal*, vol. 18, no. 4-5, pp. 427–440, 2008.
- [24] Giorgio Bartolini, Alessandro Pisano, Elisabetta Punta, and Elio Usai, “A survey of applications of second-order sliding mode control to mechanical systems”, *International Journal of control*, vol. 76, no. 9-10, pp. 875–892, 2003.
- [25] S T Venkataraman and S Gulati, “Control of Nonlinear Systems Using Terminal Sliding Modes”, *Journal of Dynamic Systems, Measurement, and Control*, vol. 115, no. 3, pp. 554–560, 1993.
- [26] Man Zhihong, Andrew P Paplinski, and Hong Ren Wu, “A robust MIMO terminal sliding mode control scheme for rigid robotic manipulators”, *IEEE transactions on automatic control*, vol. 39, no. 12, pp. 2464–2469, 1994.
- [27] Yuqiang Wu, Xinghuo Yu, and Zhihong Man, “Terminal sliding mode control design for uncertain dynamic systems”, *Systems & Control Letters*, vol. 34, no. 5, pp. 281–287, 1998.
- [28] Xuan-Toa Tran and Hee-Jun Kang, “TS fuzzy model-based robust finite time control for uncertain nonlinear systems”, *Proceedings of the Institution of Mechanical Engineers, Part C: Journal of Mechanical Engineering Science*, vol. 229, no. 12, pp. 2174–2186, 2015.
- [29] Yong Feng, Jianfei Zheng, Xinghuo Yu, and Nguyen Vu Truong, “Hybrid terminal sliding-mode observer design method for a permanent-magnet synchronous motor control system”, *IEEE Transactions on Industrial Electronics*, vol. 56, no. 9, pp. 3424–3431, 2009.
- [30] E-C Chang, T-J Liang, J-F Chen, and F-J Chang, “Real-time implementation of grey fuzzy terminal sliding mode control for PWM DC–AC converters”, *IET Power Electronics*, vol. 1, no. 2, pp. 235–244, 2008.
- [31] Liu Hui and Junfeng Li, “Terminal sliding mode control for spacecraft formation flying”, *IEEE Transactions on Aerospace and Electronic Systems*, vol. 45, no. 3, pp. 835–846, 2009.

- [32] Chee Pin Tan, Xinghuo Yu, and Zhihong Man, “Terminal sliding mode observers for a class of nonlinear systems”, *Automatica*, vol. 46, no. 8, pp. 1401–1404, 2010.
- [33] Arie Levant, “Principles of 2-sliding mode design”, *automatica*, vol. 43, no. 4, pp. 576–586, 2007.
- [34] Andrey Polyakov and Alex Poznyak, “Reaching time estimation for “super-twisting” second order sliding mode controller via Lyapunov function designing”, *IEEE Transactions on Automatic Control*, vol. 54, no. 8, pp. 1951–1955, 2009.
- [35] Michael Defoort, Frederic Nollet, Thierry Floquet, and Wilfrid Perruquetti, “A third-order sliding-mode controller for a stepper motor”, *IEEE Transactions on Industrial Electronics*, vol. 56, no. 9, pp. 3337–3346, 2009.
- [36] Liang Yang and Jianying Yang, “Nonsingular fast terminal sliding-mode control for nonlinear dynamical systems”, *International Journal of Robust and Nonlinear Control*, vol. 21, no. 16, pp. 1865–1879, 2011.
- [37] Yong Feng, Xinghuo Yu, and Zhihong Man, “Non-singular terminal sliding mode control of rigid manipulators”, *Automatica*, vol. 38, no. 12, pp. 2159–2167, 2002.
- [38] Kang-Bark Park and Teruo Tsuji, “Terminal sliding mode control of second-order nonlinear uncertain systems”, *International Journal of Robust and Nonlinear Control: IFAC-Affiliated Journal*, vol. 9, no. 11, pp. 769–780, 1999.
- [39] X Yu and M Zhihong, “Fast terminal sliding-mode control design for nonlinear dynamical systems”, *Circuits and Systems I: Fundamental Theory . . .*, vol. 49, no. 2, pp. 261–264, 2002.
- [40] S Yu, X Yu, B Shirinzadeh, and Z Man, “Continuous finite-time control for robotic manipulators with terminal sliding mode”, *Automatica*, vol. 41, no. 11, pp. 1957–1964, 2005.
- [41] Sanjay P Bhat and Dennis S Bernstein, “Finite-time stability of continuous autonomous systems”, *SIAM Journal on Control and Optimization*, vol. 38, no. 3, pp. 751–766, 2000.
- [42] Sanjay P Bhat and Dennis S Bernstein, “Continuous finite-time stabilization of the translational and rotational double integrators”, *IEEE Transactions on automatic control*, vol. 43, no. 5, pp. 678–682, 1998.

- [43] Mohammad Pourmahmood Aghababa and Hasan Pourmahmood Aghababa, “Finite-time stabilization of a non-autonomous chaotic rotating mechanical system”, *Journal of the Franklin Institute*, vol. 349, no. 9, pp. 2875–2888, 2012.
- [44] Mohammad Pourmahmood Aghababa and Hasan Pourmahmood Aghababa, “A general nonlinear adaptive control scheme for finite-time synchronization of chaotic systems with uncertain parameters and nonlinear inputs”, *Nonlinear Dynamics*, vol. 69, no. 4, pp. 1903–1914, 2012.
- [45] Sanjay P Bhat and Dennis S Bernstein, “Geometric homogeneity with applications to finite-time stability”, *Mathematics of Control, Signals and Systems*, vol. 17, no. 2, pp. 101–127, 2005.
- [46] Yiguang Hong, “Finite-time stabilization and stabilizability of a class of controllable systems”, *Systems & control letters*, vol. 46, no. 4, pp. 231–236, 2002.
- [47] Sendren Sheng-Dong Xu, Chih-Chiang Chen, and Zheng-Lun Wu, “Study of non-singular fast terminal sliding-mode fault-tolerant control”, *IEEE Transactions on Industrial Electronics*, vol. 62, no. 6, pp. 3906–3913, 2015.
- [48] Jinchuan Zheng, Hai Wang, Zhihong Man, Jiong Jin, and Minyue Fu, “Robust motion control of a linear motor positioner using fast nonsingular terminal sliding mode”, *IEEE/ASME Transactions on Mechatronics*, vol. 20, no. 4, pp. 1743–1752, 2015.
- [49] Mien Van, Shuzhi Sam Ge, and Hongliang Ren, “Finite time fault tolerant control for robot manipulators using time delay estimation and continuous nonsingular fast terminal sliding mode control”, *IEEE transactions on cybernetics*, vol. 47, no. 7, pp. 1681–1693, 2017.
- [50] Yongping Pan, Chenguang Yang, Lin Pan, and Haoyong Yu, “Integral sliding mode control: performance, modification, and improvement”, *IEEE Transactions on Industrial Informatics*, vol. 14, no. 7, pp. 3087–3096, 2018.
- [51] Jiahu Qin, Qichao Ma, Huijun Gao, and Wei Xing Zheng, “Fault-tolerant cooperative tracking control via integral sliding mode control technique”, *IEEE/ASME Transactions on Mechatronics*, vol. 23, no. 1, pp. 342–351, 2018.
- [52] Qingsong Xu, “Continuous integral terminal third-order sliding mode motion control for piezoelectric nanopositioning system”, *IEEE/ASME Transactions on Mechatronics*, vol. 22, no. 4, pp. 1828–1838, 2017.



- [53] Qingsong Xu, “Digital integral terminal sliding mode predictive control of piezoelectric-driven motion system”, *IEEE Transactions on Industrial Electronics*, vol. 63, no. 6, pp. 3976–3984, 2016.
- [54] Anh Tuan Vo, Hee-Jun Kang, and Van-Cuong Nguyen, “An output feedback tracking control based on neural sliding mode and high order sliding mode observer”, in *Human System Interactions (HSI), 2017 10th International Conference on*. IEEE, 2017, pp. 161–165.
- [55] Ran Sun, Jihe Wang, Dexin Zhang, and Xiaowei Shao, “Neural network-based sliding mode control for atmospheric-actuated spacecraft formation using switching strategy”, *Advances in Space Research*, vol. 61, no. 3, pp. 914–926, feb 2018.
- [56] Jinkun Liu and Xinhua Wang, *Advanced sliding mode control for mechanical systems: design, analysis and MATLAB simulation*, Springer Science & Business Media, 2012.
- [57] Shuzhi Sam Ge and Cong Wang, “Adaptive neural control of uncertain MIMO nonlinear systems”, *IEEE Transactions on Neural Networks*, vol. 15, no. 3, pp. 674–692, 2004.
- [58] Anh Tuan Vo, Hee-Jun Kang, and Tien Dung Le, “An Adaptive Fuzzy Terminal Sliding Mode Control Methodology for Uncertain Nonlinear Second-Order Systems”, in *International Conference on Intelligent Computing*. Springer, 2018, pp. 123–135.
- [59] Bo Liang, Yuqing Zhu, Yuren Li, Pengju He, and Weilin Li, “Adaptive Nonsingular Fast Terminal Sliding Mode Control for Braking Systems with Electro-Mechanical Actuators Based on Radial Basis Function”, *Energies*, vol. 10, no. 10, pp. 1637, 2017.
- [60] Bo Liang, Yuqing Zhu, Yuren Li, Pengju He, and Weilin Li, “Adaptive Nonsingular Fast Terminal Sliding Mode Control for Braking Systems with Electro-Mechanical”, *International Journal of Systems Science*, vol. 44, no. 3, pp. 401–415, 2017.
- [61] Sanjoy Mondal and Chitrakleha Mahanta, “Adaptive second order terminal sliding mode controller for robotic manipulators”, *Journal of the Franklin Institute*, vol. 351, no. 4, pp. 2356–2377, 2014.
- [62] Vadim Utkin, Jürgen Guldner, and Jingxin Shi, *Sliding mode control in electro-mechanical systems*, CRC press, 2009.

- [63] Arie Levant, “Chattering analysis”, *IEEE transactions on automatic control*, vol. 55, no. 6, pp. 1380–1389, 2010.
- [64] Vadim Utkin, “Discussion aspects of high-order sliding mode control”, *IEEE Transactions on automatic control*, vol. 61, no. 3, pp. 829–833, 2016.
- [65] Guillermo Rubio-Astorga, Juan Diego Sánchez-Torres, José Cañedo, and Alexander G Loukianov, “High-order sliding mode block control of single-phase induction motor”, *IEEE Transactions on Control Systems Technology*, vol. 22, no. 5, pp. 1828–1836, 2014.
- [66] Jun Yang, Shihua Li, and Xinghuo Yu, “Sliding-mode control for systems with mismatched uncertainties via a disturbance observer”, *IEEE Transactions on industrial electronics*, vol. 60, no. 1, pp. 160–169, 2013.
- [67] Hua Wang, Zheng-Zhi Han, Qi-Yue Xie, and Wei Zhang, “Finite-time chaos control via nonsingular terminal sliding mode control”, *Communications in Nonlinear Science and Numerical Simulation*, vol. 14, no. 6, pp. 2728–2733, 2009.
- [68] Saleh Mobayen, “Fast terminal sliding mode controller design for nonlinear second-order systems with time-varying uncertainties”, *Complexity*, vol. 21, no. 2, pp. 239–244, 2015.
- [69] Tarek Madani, Boubaker Daachi, and Karim Djouani, “Modular-controller-design-based fast terminal sliding mode for articulated exoskeleton systems”, *IEEE Transactions on Control Systems Technology*, vol. 25, no. 3, pp. 1133–1140, 2017.
- [70] Zhenxin He, Chuntong Liu, Ying Zhan, Hongcai Li, Xianxiang Huang, and Zhili Zhang, “Nonsingular fast terminal sliding mode control with extended state observer and tracking differentiator for uncertain nonlinear systems”, *Mathematical Problems in Engineering*, vol. 2014, 2014.
- [71] Yong Feng, Fengling Han, and Xinghuo Yu, “Chattering free full-order sliding-mode control”, *Automatica*, vol. 50, no. 4, pp. 1310–1314, 2014.
- [72] Brian Armstrong, Oussama Khatib, and Joel Burdick, “The explicit dynamic model and inertial parameters of the PUMA 560 arm”, in *Robotics and Automation. Proceedings. 1986 IEEE International Conference on*. IEEE, 1986, vol. 3, pp. 510–518.
- [73] E M Fels, “Beckenbach, EF, and Bellman R.: Inequalities, Springer Verlag, Berlin-Göttingen-Heidelberg, 1961.([Hungarian Language Ignored]) 276 Seiten, Preis 1 r. 9 k”, *Biometrical Journal*, vol. 8, no. 4, pp. 279, 1966.

- [74] Gregor Edelbaher, Karel Jezernik, and Evgen Urlep, “Low-speed sensorless control of induction machine”, *IEEE Transactions on industrial electronics*, vol. 53, no. 1, pp. 120–129, 2006.
- [75] Shafiqul Islam and Xiaoping P Liu, “Robust sliding mode control for robot manipulators”, *IEEE Transactions on Industrial Electronics*, vol. 58, no. 6, pp. 2444–2453, 2011.
- [76] Man Zhihong, A.P. Paplinski, and H.R. Wu, “A robust MIMO terminal sliding mode control scheme for rigid robotic manipulators”, *IEEE Transactions on Automatic Control*, vol. 39, no. 12, pp. 2464–2469, 1994.
- [77] Yaote Chang, “Adaptive sliding mode control of multi-input nonlinear systems with perturbations to achieve asymptotical stability”, *IEEE Transactions on automatic control*, vol. 54, no. 12, pp. 2863–2869, 2009.
- [78] Qiang Meng, Tao Zhang, Xiang Gao, and Jing-yan Song, “Adaptive sliding mode fault-tolerant control of the uncertain stewart platform based on offline multibody dynamics”, *IEEE/ASME Transactions on mechatronics*, vol. 19, no. 3, pp. 882–894, 2014.
- [79] Yu Tang, “Terminal sliding mode control for rigid robots”, *Automatica*, vol. 34, no. 1, pp. 51–56, 1998.
- [80] Samira Eshghi and Renuganth Varatharajoo, “Nonsingular terminal sliding mode control technique for attitude tracking problem of a small satellite with combined energy and attitude control system (CEACS)”, *Aerospace Science and Technology*, vol. 76, pp. 14–26, may 2018.
- [81] Xuan-Toa Tran and Hee-Jun Kang, “Arbitrary finite-time tracking control for magnetic levitation systems”, *International Journal of Advanced Robotic Systems*, vol. 11, no. 10, pp. 157, 2014.
- [82] Mohammad Pourmahmood Aghababa, “Finite-time chaos control and synchronization of fractional-order nonautonomous chaotic (hyperchaotic) systems using fractional nonsingular terminal sliding mode technique”, *Nonlinear Dynamics*, vol. 69, no. 1-2, pp. 247–261, 2012.
- [83] Vo Anh Tuan and Hee-Jun Kang, “A New Finite-time Control Solution to The Robotic Manipulators Based on The Nonsingular Fast Terminal Sliding Variables

- and Adaptive Super-Twisting Scheme”, *Journal of Computational and Nonlinear Dynamics*, 2018.
- [84] Mien Van, Michalis Mavrovouniotis, and Shuzhi Sam Ge, “An Adaptive Backstepping Nonsingular Fast Terminal Sliding Mode Control for Robust Fault Tolerant Control of Robot Manipulators”, *IEEE Transactions on Systems, Man, and Cybernetics: Systems*, 2018.
- [85] Liang Yang Yang and Jianying, “Nonsingular fast terminal sliding-mode control for nonlinear dynamical systems”, *International Journal of Robust and Nonlinear Control*, vol. 18, no. October 2014, pp. 557–569, 2010.
- [86] A T Vo and H Kang, “A Chattering-Free, Adaptive, Robust Tracking Control Scheme for Nonlinear Systems with Uncertain Dynamics”, *IEEE Access*, p. 1, 2019.
- [87] A T Vo and H Kang, “An Adaptive Terminal Sliding Mode Control for Robot Manipulators with Non-singular Terminal Sliding Surface Variables”, *IEEE Access*, p. 1, 2018.
- [88] Yong Feng, Minghao Zhou, Xuemei Zheng, Fengling Han, and Xinghuo Yu, “Full-order terminal sliding-mode control of MIMO systems with unmatched uncertainties”, *Journal of the Franklin Institute*, vol. 355, no. 2, pp. 653–674, jan 2018.
- [89] Asif Chalanga, Shyam Kamal, Leonid M Fridman, Bijnan Bandyopadhyay, and Jaime A Moreno, “Implementation of super-twisting control: Super-twisting and higher order sliding-mode observer-based approaches”, *IEEE Transactions on Industrial Electronics*, vol. 63, no. 6, pp. 3677–3685, 2016.
- [90] Andrey Polyakov and Leonid Fridman, “Stability notions and Lyapunov functions for sliding mode control systems”, *Journal of the Franklin Institute*, vol. 351, no. 4, pp. 1831–1865, 2014.
- [91] Tianping Chen and Hong Chen, “Approximation capability to functions of several variables, nonlinear functionals, and operators by radial basis function neural networks”, *IEEE Transactions on Neural Networks*, vol. 6, no. 4, pp. 904–910, 1995.
- [92] Tien Dung Le, Hee-Jun Kang, and Young-Soo Suh, “Chattering-free neuro-sliding mode control of 2-DOF planar parallel manipulators”, *International Journal of Advanced Robotic Systems*, vol. 10, no. 1, pp. 22, 2013.

- [93] Suguru Arimoto, “Stability and robustness of PID feedback control for robot manipulators of sensory capability”, in *Robotics Research: First Int. Symp.* MIT Press, Cambridge, Massachusetts, 1984, pp. 783–799.
- [94] M W Spong and M Vidyasagar, “Robot Dynamics and Control (New-York: John Willey & Sons)”, 1989.
- [95] Kye Lim and Mansour Eslami, “Robust adaptive controller designs for robot manipulator systems”, *IEEE Journal on robotics and automation*, vol. 3, no. 1, pp. 54–66, 1987.
- [96] Yuzheng Guo and Peng-Yung Woo, “An adaptive fuzzy sliding mode controller for robotic manipulators”, *IEEE Transactions on Systems, Man, and Cybernetics-Part A: Systems and Humans*, vol. 33, no. 2, pp. 149–159, 2003.
- [97] Feng Lin and Robert D Brandt, “An optimal control approach to robust control of robot manipulators”, *IEEE Transactions on Robotics and Automation*, vol. 14, no. 1, pp. 69–77, 1998.
- [98] Tien C Hsia and Seul Jung, “A simple alternative to neural network control scheme for robot manipulators”, *IEEE Transactions on Industrial Electronics*, vol. 42, no. 4, pp. 414–416, 1995.
- [99] Franck Plestan, Yuri Shtessel, Vincent Bregeault, and Alex Poznyak, “New methodologies for adaptive sliding mode control”, *International journal of control*, vol. 83, no. 9, pp. 1907–1919, 2010.
- [100] Arie Levant, “Higher-order sliding modes, differentiation and output-feedback control”, *International journal of Control*, vol. 76, no. 9-10, pp. 924–941, 2003.
- [101] Man Zhihong, Mike O’day, and Xinghuo Yu, “A robust adaptive terminal sliding mode control for rigid robotic manipulators”, *Journal of Intelligent and Robotic systems*, vol. 24, no. 1, pp. 23–41, 1999.
- [102] Mezghani Ben Romdhane Neila and Damak Tarak, “Adaptive terminal sliding mode control for rigid robotic manipulators”, *International Journal of Automation and Computing*, vol. 8, no. 2, pp. 215–220, 2011.
- [103] Liangyong Wang, Tianyou Chai, and Lianfei Zhai, “Neural-network-based terminal sliding-mode control of robotic manipulators including actuator dynamics”, *IEEE Transactions on Industrial Electronics*, vol. 56, no. 9, pp. 3296–3304, 2009.

- [104] Lei Qiao and Weidong Zhang, “Adaptive non-singular integral terminal sliding mode tracking control for autonomous underwater vehicles”, *IET Control Theory & Applications*, vol. 11, no. 8, pp. 1293–1306, 2017.
- [105] Ranjith Ravindranathan Nair and Laxmidhar Behera, “Robust adaptive gain non-singular fast terminal sliding mode control for spacecraft formation flying”, in *Decision and Control (CDC), 2015 IEEE 54th Annual Conference on*. IEEE, 2015, pp. 5314–5319.
- [106] Junwei Sun, Yi Shen, Xiaoping Wang, and Jie Chen, “Finite-time combination-combination synchronization of four different chaotic systems with unknown parameters via sliding mode control”, *Nonlinear Dynamics*, vol. 76, no. 1, pp. 383–397, 2014.
- [107] Mohammad Pourmahmood Aghababa and Hasan Pourmahmood Aghababa, “Adaptive finite-time synchronization of non-autonomous chaotic systems with uncertainty”, *Journal of Computational and Nonlinear Dynamics*, vol. 8, no. 3, pp. 31006, 2013.
- [108] Yigwruang Hong, Jie Huang, and Yangsheng Xu, “On an output feedback finite-time stabilization problem”, *IEEE Transactions on Automatic Control*, vol. 46, no. 2, pp. 305–309, 2001.
- [109] Xuan-Toa Tran and Hee-Jun Kang, “A novel adaptive finite-time control method for a class of uncertain nonlinear systems”, *International Journal of Precision Engineering and Manufacturing*, vol. 16, no. 13, pp. 2647–2654, 2015.
- [110] Chifu Yang, Qitao Huang, Hongzhou Jiang, O Ogbobe Peter, and Junwei Han, “PD control with gravity compensation for hydraulic 6-DOF parallel manipulator”, *Mechanism and Machine theory*, vol. 45, no. 4, pp. 666–677, 2010.
- [111] Puren R Ouyang, Wen-Jun Zhang, and Fang-Xiang Wu, “Nonlinear PD control for trajectory tracking with consideration of the design for control methodology”, in *Robotics and Automation, 2002. Proceedings. ICRA’02. IEEE International Conference on*. IEEE, 2002, vol. 4, pp. 4126–4131.
- [112] P R Ouyang, W J Zhang, and Madan M Gupta, “An adaptive switching learning control method for trajectory tracking of robot manipulators”, *Mechatronics*, vol. 16, no. 1, pp. 51–61, 2006.

- [113] Min Wang, Bing Chen, Xiaoping Liu, and Peng Shi, “Adaptive fuzzy tracking control for a class of perturbed strict-feedback nonlinear time-delay systems”, *Fuzzy Sets and Systems*, vol. 159, no. 8, pp. 949–967, 2008.
- [114] Hua O Wang, Kazuo Tanaka, and Michael F Griffin, “An approach to fuzzy control of nonlinear systems: Stability and design issues”, *IEEE transactions on fuzzy systems*, vol. 4, no. 1, pp. 14–23, 1996.
- [115] Young Ho Kim and Frank L Lewis, “Neural network output feedback control of robot manipulators”, *IEEE Transactions on robotics and automation*, vol. 15, no. 2, pp. 301–309, 1999.
- [116] Quang Vinh Doan, Tien Dung Le, Quang Dan Le, and Hee-Jun Kang, “A neural network-based synchronized computed torque controller for three degree-of-freedom planar parallel manipulators with uncertainties compensation”, *International Journal of Advanced Robotic Systems*, vol. 15, no. 2, pp. 1729881418767307, 2018.
- [117] Kenji Fujimoto and Toshiharu Sugie, “Iterative learning control of Hamiltonian systems: I/O based optimal control approach”, *IEEE Transactions on Automatic Control*, vol. 48, no. 10, pp. 1756–1761, 2003.
- [118] Jean-Jacques E Slotine and Weiping Li, “On the adaptive control of robot manipulators”, *The international journal of robotics research*, vol. 6, no. 3, pp. 49–59, 1987.
- [119] M. Dansoko, H. Nkwawo, F. Floret, R. Goma, B. Diourté, A. Arzandé, and J.C. Vannier, “Marine turbine system directly connected to electrical grid: Experimental implementations using a nonlinear and robust control”, *Ocean Engineering*, vol. 149, pp. 260–267, feb 2018.
- [120] Hai Wang, Zhihong Man, Huifang Kong, Yong Zhao, Ming Yu, Zhenwei Cao, Jinchuan Zheng, and Manh Tuan Do, “Design and Implementation of Adaptive Terminal Sliding-Mode Control on a Steer-by-Wire Equipped Road Vehicle”, *IEEE Transactions on Industrial Electronics*, vol. 63, no. 9, pp. 5774–5785, 2016.
- [121] Gang Chen, Yongduan Song, and Yanfeng Guan, “Terminal sliding mode-based consensus tracking control for networked uncertain mechanical systems on digraphs”, *IEEE transactions on neural networks and learning systems*, vol. 29, no. 3, pp. 749–756, 2016.

- [122] Chuan-Kai Lin, “Nonsingular terminal sliding mode control of robot manipulators using fuzzy wavelet networks”, *IEEE Transactions on Fuzzy Systems*, vol. 14, no. 6, pp. 849–859, 2006.
- [123] Syuan-Yi Chen and Faa-Jeng Lin, “Robust nonsingular terminal sliding-mode control for nonlinear magnetic bearing system”, *IEEE Transactions on Control Systems Technology*, vol. 19, no. 3, pp. 636–643, 2010.
- [124] Jaime A Moreno and Marisol Osorio, “Strict Lyapunov functions for the super-twisting algorithm”, *IEEE transactions on automatic control*, vol. 57, no. 4, pp. 1035–1040, 2012.
- [125] Salah Laghrouche, Jianxing Liu, Fayez Shakil Ahmed, Mohamed Harmouche, and Maxime Wack, “Adaptive second-order sliding mode observer-based fault reconstruction for pem fuel cell air-feed system”, *IEEE Transactions on Control Systems Technology*, vol. 23, no. 3, pp. 1098–1109, 2014.
- [126] Terence D Sanger, “Neural network learning control of robot manipulators using gradually increasing task difficulty”, *IEEE transactions on Robotics and Automation*, vol. 10, no. 3, pp. 323–333, 1994.
- [127] Jaime A. Moreno, Daniel Y. Negrete, Victor Torres-González, and Leonid Fridman, “Adaptive continuous twisting algorithm”, *International Journal of Control*, 2016.
- [128] Alireza Safa, Reza Yazdanpanah Abdolmalaki, Saeed Shafiee, and Behzad Sadeghi, “Adaptive nonsingular terminal sliding mode controller for micro/nanopositioning systems driven by linear piezoelectric ceramic motors”, *ISA Transactions*, apr 2018.
- [129] Yuxin Su, Chunhong Zheng, and Paolo Mercorelli, “Global finite-time stabilization of planar linear systems with actuator saturation”, *IEEE Transactions on Circuits and Systems II: Express Briefs*, vol. 64, no. 8, pp. 947–951, 2017.
- [130] Yuxin Su and Chunhong Zheng, “Robust finite-time output feedback control of perturbed double integrator”, *Automatica*, vol. 60, pp. 86–91, 2015.
- [131] Gang Chen, Bo Jin, and Ying Chen, “Nonsingular fast terminal sliding mode posture control for six-legged walking robots with redundant actuation”, *Mechatronics*, vol. 50, pp. 1–15, apr 2018.
- [132] Yong Feng, Minghao Zhou, Xuemei Zheng, Fengling Han, and Xinghuo Yu, “Full-order terminal sliding-mode control of MIMO systems with unmatched uncertainties”, *Journal of the Franklin Institute*, vol. 355, no. 2, pp. 653–674, jan 2018.



- [133] Xiao-Jian Li and Guang-Hong Yang, “Neural-network-based adaptive decentralized fault-tolerant control for a class of interconnected nonlinear systems”, *IEEE transactions on neural networks and learning systems*, vol. 29, no. 1, pp. 144–155, 2018.
- [134] Baoyu Huo, Yuanqing Xia, Lijian Yin, and Mengyin Fu, “Fuzzy adaptive fault-tolerant output feedback attitude-tracking control of rigid spacecraft”, *IEEE Transactions on Systems, Man, and Cybernetics: Systems*, vol. 47, no. 8, pp. 1898–1908, 2017.
- [135] Shun-Yuan Wang, Foun-Yuan Liu, and Jen-Hsiang Chou, “Adaptive TSK fuzzy sliding mode control design for switched reluctance motor DTC drive systems with torque sensorless strategy”, *Applied Soft Computing*, vol. 66, pp. 278–291, may 2018.
- [136] Ilyas Eker, “Sliding mode control with PID sliding surface and experimental application to an electromechanical plant”, *ISA transactions*, vol. 45, no. 1, pp. 109–118, 2006.
- [137] Shyam Kamal, Jaime A. Moreno, Asif Chalanga, Bijnan Bandyopadhyay, and Leonid M. Fridman, “Continuous terminal sliding-mode controller”, *Automatica*, 2016.
- [138] Bing Xiao, Qinglei Hu, and Youmin Zhang, “Adaptive sliding mode fault tolerant attitude tracking control for flexible spacecraft under actuator saturation”, *IEEE Transactions on Control Systems Technology*, vol. 20, no. 6, pp. 1605–1612, 2012.
- [139] Chifu Yang, Junwei Han, O Ogbobe Peter, and Qitao Huang, “PID control with gravity compensation for hydraulic 6-DOF parallel manipulator”, in *PID Control, Implementation and Tuning*. InTech, 2011.
- [140] Y X Su, Dong Sun, Lu Ren, Xiaoyun Wang, and James K Mills, “Nonlinear PD synchronized control for parallel manipulators”, in *Robotics and Automation, 2005. ICRA 2005. Proceedings of the 2005 IEEE International Conference on*. IEEE, 2005, pp. 1374–1379.
- [141] Zhiyong Yang, Jiang Wu, and Jiangping Mei, “Motor-mechanism dynamic model based neural network optimized computed torque control of a high speed parallel manipulator”, *Mechatronics*, vol. 17, no. 7, pp. 381–390, 2007.
- [142] Xiaocong Zhu, Guoliang Tao, Bin Yao, and Jian Cao, “Adaptive robust posture control of parallel manipulator driven by pneumatic muscles with redundancy”, *IEEE/ASME Transactions on Mechatronics*, vol. 13, no. 4, pp. 441–450, 2008.

- [143] Jee-Hwan Ryu, Jinil Song, and Dong-Soo Kwon, “A nonlinear friction compensation method using adaptive control and its practical application to an in-parallel actuated 6-DOF manipulator”, *Control Engineering Practice*, vol. 9, no. 2, pp. 159–167, 2001.
- [144] Zhen Qi, John E McInroy, and Farhad Jafari, “Trajectory tracking with parallel robots using low chattering, fuzzy sliding mode controller”, *Journal of Intelligent and Robotic Systems*, vol. 48, no. 3, pp. 333–356, 2007.
- [145] Hongbo Guo, YongGuang Liu, GuiRong Liu, and HongRen Li, “Cascade control of a hydraulically driven 6-DOF parallel robot manipulator based on a sliding mode”, *Control Engineering Practice*, vol. 16, no. 9, pp. 1055–1068, 2008.
- [146] Yoram Koren, “Cross-coupled biaxial computer control for manufacturing systems”, *Journal of Dynamic Systems, Measurement, and Control*, vol. 102, no. 4, pp. 265–272, 1980.
- [147] Yunhua Li, Qi Zheng, and Liman Yang, “Design of robust sliding mode control with disturbance observer for multi-axis coordinated traveling system”, *Computers & Mathematics with Applications*, vol. 64, no. 5, pp. 759–765, 2012.
- [148] Marvin H Cheng, Yue Juan Li, and Ezzat G Bakhoun, “Controller synthesis of tracking and synchronization for multiaxis motion system”, *IEEE Transactions on Control Systems Technology*, vol. 22, no. 1, pp. 378–386, 2014.
- [149] Lu Ren, James K Mills, and Dong Sun, “Experimental comparison of control approaches on trajectory tracking control of a 3-DOF parallel robot”, *IEEE Transactions on Control Systems Technology*, vol. 15, no. 5, pp. 982–988, 2007.
- [150] Lu Ren, James K Mills, and Dong Sun, “Trajectory tracking control for a 3-DOF planar parallel manipulator using the convex synchronized control method”, *IEEE Transactions on Control Systems Technology*, vol. 16, no. 4, pp. 613–623, 2008.
- [151] Dong Sun, R Lu, James K Mills, and C Wang, “Synchronous tracking control of parallel manipulators using cross-coupling approach”, *The International Journal of Robotics Research*, vol. 25, no. 11, pp. 1137–1147, 2006.
- [152] Mien Van, Shuzhi Sam Ge, and Hongliang Ren, “Robust fault-tolerant control for a class of second-order nonlinear systems using an adaptive third-order sliding mode control”, *IEEE Transactions on Systems, Man, and Cybernetics: Systems*, vol. 47, no. 2, pp. 221–228, 2017.

- [153] Hao Li, Lihua Dou, and Zhong Su, “Adaptive nonsingular fast terminal sliding mode control for electromechanical actuator”, *International Journal of Systems Science*, vol. 44, no. 3, pp. 401–415, 2013.
- [154] Mien Van, Pasquale Franciosa, and Dariusz Ceglarek, “Fault diagnosis and fault-tolerant control of uncertain robot manipulators using high-order sliding mode”, *Mathematical Problems in Engineering*, vol. 2016, 2016.
- [155] M Roopaei and M Zolghadri Jahromi, “Chattering-free fuzzy sliding mode control in MIMO uncertain systems”, *Nonlinear Analysis: Theory, Methods & Applications*, vol. 71, no. 10, pp. 4430–4437, 2009.
- [156] Mien Van, “An Enhanced Robust Fault Tolerant Control Based on an Adaptive Fuzzy PID-Nonsingular Fast Terminal Sliding Mode Control for Uncertain Nonlinear Systems”, *IEEE/ASME Transactions on Mechatronics*, 2018.
- [157] Tran Minh Duc, Ngo Van Hoa, and Thanh-Phong Dao, “Adaptive fuzzy fractional-order nonsingular terminal sliding mode control for a class of second-order nonlinear systems”, *Journal of Computational and Nonlinear Dynamics*, vol. 13, no. 3, pp. 31004, 2018.
- [158] Lei Qiao and Weidong Zhang, “Double-Loop Integral Terminal Sliding Mode Tracking Control for UUVs With Adaptive Dynamic Compensation of Uncertainties and Disturbances”, *IEEE Journal of Oceanic Engineering*, , no. 99, pp. 1–25, 2018.
- [159] M Kemal Ciliz, “Adaptive control of robot manipulators with neural network based compensation of frictional uncertainties”, *Robotica*, vol. 23, no. 2, pp. 159–167, 2005.
- [160] Meliksah Ertugrul and Okyay Kaynak, “Neuro sliding mode control of robotic manipulators”, *Mechatronics*, vol. 10, no. 1-2, pp. 239–263, 2000.
- [161] Tien Dung Le and Hee-Jun Kang, “An adaptive tracking controller for parallel robotic manipulators based on fully tuned radial basic function networks”, *Neurocomputing*, vol. 137, pp. 12–23, 2014.
- [162] Tien Dung Le and Quang Vinh Doan, “Fuzzy Adaptive Synchronized Sliding Mode Control Of Parallel Manipulators”, in *Proceedings of the 2018 4th International Conference on Mechatronics and Robotics Engineering*. ACM, 2018, pp. 102–107.
- [163] Ka Chun Lau, Esther Yun Yee Leung, Philip Wai Yan Chiu, Yeung Yam, James Yun Wong Lau, and Carmen Chung Yan Poon, “A flexible surgical robotic system

- for removal of early-stage gastrointestinal cancers by endoscopic submucosal dissection”, *IEEE Transactions on Industrial Informatics*, vol. 12, no. 6, pp. 2365–2374, 2016.
- [164] Francesca Lunardini, Claudia Casellato, Andrea d’Avella, Terence D Sanger, and Alessandra Pedrocchi, “Robustness and reliability of synergy-based myocontrol of a multiple degree of freedom robotic arm”, *IEEE Transactions on Neural Systems and Rehabilitation Engineering*, vol. 24, no. 9, pp. 940–950, 2015.
- [165] Khaled M Ben-Gharbia, Anthony A Maciejewski, and Rodney G Roberts, “A kinematic analysis and evaluation of planar robots designed from optimally fault-tolerant Jacobians”, *IEEE Transactions on Robotics*, vol. 30, no. 2, pp. 516–524, 2014.
- [166] Randy C Hoover, Rodney G Roberts, Anthony A Maciejewski, Priya S Naik, and Khaled M Ben-Gharbia, “Designing a failure-tolerant workspace for kinematically redundant robots”, *IEEE Transactions on Automation Science and Engineering*, vol. 12, no. 4, pp. 1421–1432, 2015.
- [167] Gang Chen, Yongduan Song, and Frank L Lewis, “Distributed fault-tolerant control of networked uncertain Euler–Lagrange systems under actuator faults”, *IEEE transactions on cybernetics*, vol. 47, no. 7, pp. 1706–1718, 2017.
- [168] Yuxin Su, Chunhong Zheng, and Paolo Corelli, “Nonlinear pd fault-tolerant control for dynamic positioning of ships with actuator constraints”, *IEEE/ASME Transactions on Mechatronics*, vol. 22, no. 3, pp. 1132–1142, 2016.
- [169] Jin Jiang and Xiang Yu, “Fault-tolerant control systems: A comparative study between active and passive approaches”, *Annual Reviews in control*, vol. 36, no. 1, pp. 60–72, 2012.
- [170] Qiang Meng, Tao Zhang, Jing-feng He, and Jing-yan Song, “Adaptive vector sliding mode fault-tolerant control of the uncertain Stewart platform based on position measurements only”, *Robotica*, vol. 34, no. 6, pp. 1297–1321, 2016.
- [171] Mien Van, Xuan Phu Do, and Michalis Mavrovouniotis, “Self-tuning fuzzy pid-nonsingular fast terminal sliding mode control for robust fault tolerant control of robot manipulators”, *ISA transactions*, vol. 96, pp. 60–68, 2020.
- [172] Tao Wang, Wenfang Xie, and Youmin Zhang, “Sliding mode fault tolerant control dealing with modeling uncertainties and actuator faults”, *ISA transactions*, vol. 51, no. 3, pp. 386–392, 2012.

- [173] Gang Tao, Shuhao Chen, and Suresh M Joshi, “An adaptive actuator failure compensation controller using output feedback”, *IEEE Transactions on Automatic Control*, vol. 47, no. 3, pp. 506–511, 2002.
- [174] Mien Van, Hee-Jun Kang, Young-Soo Suh, and Kyoo-Sik Shin, “A robust fault diagnosis and accommodation scheme for robot manipulators”, *International Journal of Control, Automation and Systems*, vol. 11, no. 2, pp. 377–388, 2013.
- [175] Ph Poignet and Maxime Gautier, “Nonlinear model predictive control of a robot manipulator”, in *6th International Workshop on Advanced Motion Control. Proceedings (Cat. No. 00TH8494)*. IEEE, 2000, pp. 401–406.
- [176] Luis Angel Castañeda, Alberto Luviano-Juárez, and Isaac Chairez, “Robust trajectory tracking of a delta robot through adaptive active disturbance rejection control”, *IEEE Transactions on Control Systems Technology*, vol. 23, no. 4, pp. 1387–1398, 2015.
- [177] Sliding-mode Strategy and Qingsong Xu, “Piezoelectric Nanopositioning Control Using”, *IEEE Transactions on Industrial Electronics*, vol. 62, no. 12, pp. 7738–7748, 2015.
- [178] Jorge Davila, Leonid Fridman, and Arie Levant, “Second-order sliding-mode observer for mechanical systems”, *IEEE transactions on automatic control*, vol. 50, no. 11, pp. 1785–1789, 2005.
- [179] A T Vo and H Kang, “Adaptive Neural Integral Full-Order Terminal Sliding Mode Control for an Uncertain Nonlinear System”, *IEEE Access*, p. 1, 2019.
- [180] Zhuoyue Song, Chao Duan, Jianan Wang, and Qinghe Wu, “Chattering-free full-order recursive sliding mode control for finite-time attitude synchronization of rigid spacecraft”, *Journal of the Franklin Institute*, mar 2018.
- [181] Xianbo Xiang, Chao Liu, Housheng Su, and Qin Zhang, “On decentralized adaptive full-order sliding mode control of multiple UAVs”, *ISA transactions*, vol. 71, pp. 196–205, 2017.
- [182] Wen-Hua Chen, Jun Yang, Lei Guo, and Shihua Li, “Disturbance-observer-based control and related methods—An overview”, *IEEE Transactions on Industrial Electronics*, vol. 63, no. 2, pp. 1083–1095, 2015.

- [183] Bing Xiao, Xuebo Yang, and Xing Huo, “A novel disturbance estimation scheme for formation control of ocean surface vessels”, *IEEE Transactions on Industrial Electronics*, vol. 64, no. 6, pp. 4994–5003, 2016.
- [184] Wei He, Zichen Yan, Changyin Sun, and Yunan Chen, “Adaptive neural network control of a flapping wing micro aerial vehicle with disturbance observer”, *IEEE transactions on cybernetics*, vol. 47, no. 10, pp. 3452–3465, 2017.
- [185] Jianxing Liu, Yabin Gao, Xiaojie Su, Maxime Wack, and Ligang Wu, “Disturbance-observer-based control for air management of PEM fuel cell systems via sliding mode technique”, *IEEE Transactions on Control Systems Technology*, vol. 27, no. 3, pp. 1129–1138, 2018.
- [186] Y Cao and X B Chen, “Disturbance-observer-based sliding-mode control for a 3-DOF nanopositioning stage”, *IEEE/ASME Transactions on mechatronics*, vol. 19, no. 3, pp. 924–931, 2013.
- [187] Qikun Shen, Bin Jiang, and Vincent Cocquempot, “Adaptive fuzzy observer-based active fault-tolerant dynamic surface control for a class of nonlinear systems with actuator faults”, *IEEE Transactions on Fuzzy Systems*, vol. 22, no. 2, pp. 338–349, 2014.
- [188] Jaime A Moreno and Marisol Osorio, “A lyapunov approach to second-order sliding mode controllers and observers”, in *2008 47th IEEE conference on decision and control*. IEEE, 2008, pp. 2856–2861.
- [189] Lei Liu, Zhansan Wang, and Huaguang Zhang, “Data-based adaptive fault estimation and fault tolerant control for MIMO model-free systems using generalized fuzzy hyperbolic model”, *IEEE Transactions on Fuzzy Systems*, 2017.